Mast cell secretory granules serve as endogenous c-type lectin receptor ligands skewing dendritic cell function towards T_H2/T_H17 response

Thesis

for the degree of

doctor rerum naturalium

(Dr. rer. nat.)

approved by the Faculty of Natural Sciences

of Otto-von-Guericke-University Magdeburg

by M. Sc. Johanna Kotrba

born on 19.03.1991 in Burg (b. Magdeburg).

Examiner: Prof. Dr. rer. nat. Anne Dudeck

Prof. Dr. rer. nat. Stefan F. Martin

Submitted on: 20.12.2022

Defended on: 05.07.2023

Table of Contents

List of Figures

List of Tables

Abbreviations

AA	Amino acid
ACD	Allergic contact dermatitis
AD	Atopic dermatitis
AF488/AF647	Alexa Fluor™ 488/647
AP-1	Activator protein-1
AP2	Adaptor protein 2
APC	Antigen-presenting cell
ATP	Adenosine triphosphate
BCL-10	B-cell lymphoma/leukemia 10
Bcl6	B-cell lymphoma 6
BHR	Bronchial hyperreactivity
BM	Bone marrow
BMCP	Bifunctional basophil-MC lineage progenitor
BMDC	Bone marrow-derived dendritic cell
BMMC	Bone marrow-derived mast cell
bp	Base pair
B_{reg} cell	Regulatory B cell
BSA	Bovine serum albumin
Card9	Caspase recruitment domain-containing protein 9
CBM complex	Protein complex containing Card, BCL-10 and MALT1
CCL	CC motif chemokine ligand
CCP	Clathrin-coated pit
CCR	CC motif chemokine receptor
CCV	Clathrin-coated vesicles
CD	Cluster of differentiation
CD40L	CD40 ligand
cDC	Classical/conventional dendritic cell
Cdc42	Cell division cycle 42
cDNA	Complementary deoxyribonucleic acid
CDP	Common dendritic cell progenitor
CFSE	Carboxyfluorescein succinimidyl ester
CHS	Contact hypersensitivity
CIE	Clathrin-/caveolae-independent endocytosis
Clec(4d)	C-type lectin domain family (4 member d)
Clecsf(8)	C-type lectin superfamily (member 8)
CLP	Common lymphoid progenitor

CLR	C-type lectin receptor
CME	Clathrin-mediated endocytosis
CMP	Common myeloid progenitor
CRD	Carbohydrate recognition domain
CSE	Cigarette smoke extract
Csf-1R	Colony stimulating factor 1 receptor
CTL	C-type lectin
CTLD	C-type lectin-like domain
CTMC	Connective tissue mast cell
DAMP	Damage-associated molecular pattern
DAP10/12	DNAX activating protein of 10/12 kDa
DAPI	4',6-Diamidino-2-phenylindo
DC	Dendritic cell
DCAR2	Dendritic cell activating receptor 2
DC-SIGN	Dendritic cell-specific intercellular adhesion molecule-3 grabbing non-integrin
Dectin-1/2/3	Dendritic cell-associated C-type lectin-1/2/3
Der p 1	*Dermatophagoides. pteronyssinus* peptidase 1
Df	*Dermatophagoides farinae*
DNase I	Deoxyribonuclease I
dLN	Draining lymph node
DMA	5-(N,N-dimethyl)amiloride hydrochloride
DMDC	Dimethyl dicarbonate
DNA	Deoxyribonucleic acid
DNase I	Deoxyribonuclease I
DNFB	1-fluoro-2,4-dinitrobenzene
DNGR-1	Dendritic cell natural killer lectin group receptor-1
DP	Double positive
EpC	Epithelial cell
ELISA	Enzyme-linked immunosorbent assay
ER	Endoplasmatic reticulum
ERK	Extracellular signal-regulated kinase
EV	Extracellular vesicle
FACS	Fluorescence-activated cell sorting
FC	Flow cytometry
FC tube	Flow cytometry tube (Polystyrene Round-Bottom Tube)
FcRγ	Fc receptor gamma-chain
FcγRI	Fc-gamma receptor I
FcεRI	Fc-epsilon receptor I
FITC	Fluorescein isothiocyanate

Flt3L	FMS-like tyrosine kinase 3 ligand
FMO	Fluorescence minus one
FoxP3	Forkhead box protein P3
GAG	Glycosaminoglycan
GATA3	GATA-binding protein 3
GFP	Green fluorescent protein
GI	Gastrointestinal
GM-CSF	Granulocyte-macrophage colony-stimulating factor
GMP	Granulocyte monocyte progenitor
GOI	Gene of interest
GPCR	G-protein-coupled receptor
GTP	Guanosine triphosphate
hDC-SIGN	Human dendritic cell-specific intercellular adhesion molecule-3 grabbing non-integrin
HDM	House dust mite
HE	Haematoxylin and eosin
HSC	Hematopoietic stem cell
i.d.	Intradermal
i.n.	Intranasal
i.p.	Intraperitoneal
ICOSL	Inducible T cell co-stimulatory ligand
IFN-γ	Interferon-gamma
IgG1	Immunoglobulin G1
IgE	Immunoglobulin E
IL	Interleukin
IL-4Rα	Interleukin-4 receptor alpha chain
ILC1/2/3	Type 1/2/3 innate lymphoid cell
imDC	Immature dendritic cell
IRF3	Interferon regulatory factor 3
ITAM	Immunoreceptor tyrosine-based activation motif
ITIM	Immunoreceptor tyrosine-based inhibition motif
JNK	c-Jun N-terminal kinase
KC	Keratinocyte
LAT	Linker of activation of T cells
LC	Langerhans cell
LEC	Lymphatic endothelial cell
LMPP	Lymphoid-primed multipotent progenitor
LN	Lymph node
LNm	Lymph node-migratory
LNr	Lymph node-resident

loxP	locus of x-over, P1
LP	Long pass filter
LT	Lymphoid tissue
LTB_4/LTC_4	Leukotriene B_4/C_4
MAIR-II	Myeloid-associated immunoglobulin-like receptor II
MAL	Myeloid differentiation primary response gene 88-adaptor-like
MALT1	Mucosa-associated lymphoid tissue 1
matDC	Mature dendritic cell
MC	Mast cell
MCAS	Mast cell activation syndrome
MCG	Mast cell granules
MCL	Macrophage-(restricted) C-type lectin
MCp	Mast cell progenitor
$MC_{T/C/TC}$	Mast cell containing tryptase/chymase/both
MDP	Macrophage dendritic cell progenitor
MELC	Multi-epitope ligand cartography
MERTK	MER receptor tyrosine kinase
MFI	Median fluorescence intensity
MHC	Major histocompatibility complex
MHCI/MHCII	Major histocompatibility complex class I/II
migDC	tissue-migratory classical dendritic cell
Mincle	Macrophage inducible C-type lectin
MMC	Mucosal mast cell
mMCP	Murine mast cell protease
MMRRC	Mutant Mouse Resource & Research Centers
moDC	Monocyte-derived dendritic cell
Mph	Macrophage
MPP	Multipotent progenitor
MR	Mannose receptor
MV	Microvesicle
MyD88	Myeloid differentiation primary response gene 88
NADPH	Nicotinamide adenine dinucleotide phosphate
NFAT	Nuclear factor of activated T cell
NFκB	Nuclear factor ‘kappa-light-chain-enhancer’ of activated B cells
NK cell	Natural killer cell
NKT cell	Natural killer T cell
NLR	Nucleotide-binding and oligomerization domain-like receptor
NLRP3	Nucleotide-binding and oligomerization domain-like receptor family pyrin domain containing 3
NLT	Non-lymphoid tissue

NOD	Nucleotide-binding and oligomerization domain
nos	Nonsense
NOX2	Nicotinamide adenine dinucleotide phosphate oxidase 2
Nph	Neutrophil
ns	Not significant (p value > 0.10)
NTAL	Non-T cell activation linker
OSCAR	Osteoclast-associated immunoglobulin-like receptor
OVA	Ovalbumin
PAMP	Pathogen-associated molecular pattern
PCMC	Peritoneal cultured mast cell
PCR	Polymerase chain reaction
pDC	Plasmacytoid dendritic cell
PD-L1/2	Programmed cell death-ligand 1/2
PGD_2/PGE_2	Prostaglandin D_2/E_2
$PI(4,5)P_2$	Phosphatidylinositol-4,5-biphosphate
pre-cDC	Pre-classical dendritic cells
PRR	Pattern recognition receptor
qPCR	Quantitative Real Time – polymerase chain reaction
RIG	Retinoic acid-inducible gene
RLR	Retinoic acid-inducible gene-I-like receptor
RNA	Ribonucleic acid
RNAi	Ribonucleic acid interference
ROI	Region of interest
RORγt	RAR-Related Orphan Nuclear Receptor Variant 2
ROS	Reactive oxygen specie
RT	Room temperature
SAP130	Spliceosome-associated protein 130
SA-PE	Streptavidin-phycoerythrin
SCF	Stem cell factor
SIGNR3	Specific intercellular adhesion molecule-3 grabbing non-integrin homolog-related 3
siRNA	Small interfering ribonucleic acid
SIRPα	Signal-regulator protein α
SMOC	Supramolecular organizing center
Syk	Spleen tyrosine kinase
T-bet	T-box expressed in T cells
Tbp	TATA box binding protein
T_c cell	Cytotoxic T cell
TCR	T cell receptor
TDM	Trehalose-6,6'-dimycolate

T_{eff} cell	Effector T cell
T_{fh} cell	Follicular T helper cell
TGF- β	Transforming growth factor β
T_H cell	T helper cell
T_H1/2/9/17 cell	Type 1/2/9/17 T helper cell
TICAM2	Toll/interleukin-1 receptor domain-containing adaptor inducing interferon-beta-related adaptor molecule 2
TIR	Toll/interleukin-1 receptor domain
TIRAP	Toll/interleukin-1 receptor domain-containing adaptor protein
TLR	Toll-like receptor
TNBS	Trinitrobenzene sulfonic acid
TNCB	Trinitrochlorobenzene
TNF	Tumor necrosis factor α
TNFR2	Tumor necrosis factor receptor 2
TNFSF4	Tumor necrosis factor superfamily member 4
TNF-β	Tumor necrosis factor β
TNP	Trinitrophenyl
TR	TexasRed
TRAF3/6	Tumor necrosis factor receptor associated factor 3/6
TRAM	Toll/interleukin-1 receptor domain-containing adaptor molecule
T_{reg} cell	Regulatory T cell
TREM1	Receptor expressed in myeloid cells 1
TRIF	Toll/interleukin-1 receptor domain-containing adaptor inducing interferon-beta
TSLP	Thymic stromal lymphopoietin
wt	C57BL/6JRj mouse
XCR1	XC-chemokine receptor 1

Abstract

Mast cells (MCs) are best known as key effector cells of type I allergic reaction. However, there is increasing evidence that, beyond IgE-driven responses, they are multifunctional cells and serve as linker between innate and adaptive immunity. In this line, our group reported that dermal dendritic cells (DCs) engulf intact MC granules (MCG), which were released by MCs during skin inflammation. As a consequence, MCG-bearing DCs display an enhanced migratory behavior and maturation and boosted T cell priming capacity compared to MCG-negative DCs. Thereby, peripheral, tissue-resident MCs have remote effects on lymph node-borne adaptive immune responses by modulating DC functions [1].

Based on this study, the aim of this thesis was to decipher the underlying mechanisms mediating the MCG uptake by DCs and the resulting consequences for subsequent immune responses. In the first part of my work, the underlying mechanisms were studied mainly by means of *in vitro* and additional *ex vivo*/*in vivo* methods. The MCG uptake was identified to be restricted to immature DCs and to involve macropinocytosis. The exclusive engulfment of peritoneal cultured MC (PCMC)-derived MCG and the dependency of the MCG uptake on a Syk-/Card9-dependent signaling *in vitro* further suggested the involvement of the induced form of macropinocytosis. *In vivo*, a disrupted Card9-dependent signaling resulted in a reduced inflammatory response. Questioning the DC receptors that sense MCG leading to their uptake, the c-type lectin receptors (CLRs) MCL and SIGNR3 were identified binding specifically to PCMC-derived MCG. Additionally, they were found to be together responsible *in vitro* for an entire uptake of MCG. The second part of this thesis analyzed the resulting consequences of the MCG uptake by imDCs. It was found by using *in vitro* DC-T cell co-culture experiments that the MCG uptake by imDCs modulated the T cell priming capacity of DC towards T_H2- and T_H17-mediated responses. A Card9 deficiency further led to a defect in T cell priming during contact hypersensitivity, especially of T_H2 and T_H17 cells. Additionally, *MCL*$^{-/-}$ *SIGNR3*$^{-/-}$ mice showed a reduced T_H2-driven allergic airway inflammation together with reduced numbers of cDC2s and cells producing T_H2 cytokines.

Collectively, the data gained within this thesis indicate that MCG serve as endogenous CLR ligands that have the ability to convert MC degranulation inducing signals in the periphery into adjuvant effects that promote and modulate the adaptive immune response within the LNs. Detailed knowledge about the MCG uptake mechanism by DCs may be helpful for developing therapeutic strategies that either aim to dampen excessive inflammatory immune responses or to trigger adaptive immunity in a targeted manner.

Zusammenfassung

Mastzellen (MZs) sind vor allem für ihre Rolle als Effektorzellen der Typ I Allergie bekannt. Darüber hinaus wurden ihnen zahlreiche weitere Funktionen zugeschrieben. MZs können u.a. als Bindeglied zwischen der angeborenen und adaptiven Immunität wirken. Unsere Arbeitsgruppe konnte zeigen, dass dermale dendritische Zellen (DZs) Mastzellgranula (MZG) aufnehmen, welche zuvor von MZs als Antwort auf eine Hautentzündung freigesetzt wurden. MZG-tragende DZs wiesen eine erhöhte Migration und Reifung, sowie eine verstärkte Kapazität zur Aktivierung von T-Zellen im Vergleich zu MZG-negativen DZs auf. Diese Art der interzellulären Kommunikation ermöglicht peripheren, gewebsständigen MZs durch Modulierung von DZ-Funktionen Einfluss auf die Induktion einer adaptiven Immunantwort im Lymphknoten zu nehmen [1].

Das Ziel dieser Arbeit war, zugrundeliegende Mechanismen der MZG Aufnahme durch DZs, sowie die daraus resultierenden Konsequenzen für die Immunantwort zu untersuchen. Im ersten Teil dieser Arbeit konnte gezeigt werden, dass die Makropinozytose in die MZG Aufnahme involviert war und sich dabei auf unreife DZs beschränkte. Die ausschließliche Aufnahme von MZG aus peritonealen MZs sowie die Abhängigkeit einer Syk-/Card9-vermittelten Signalkaskade *in vitro* wiesen auf eine Beteiligung der induzierten Makropinozytose hin. *In vivo* resultierte eine Card9-Defizienz weiterhin in einer reduzierten Entzündungsreaktion. Darüber hinaus wurden die c-Typ Lektinrezeptoren (CLRs) MCL und SIGNR3 als DZ-Rezeptoren identifiziert, welche zusammen an der MCZ Aufnahme beteiligt sind. Der zweite Teil dieser Arbeit analysierte die Konsequenzen der MZG Aufnahme für das Immunsystem. *In vitro* DZ-T-Zell Kokultivierungsversuche zeigten, dass die MZG Aufnahme durch DZs deren Kapazität zur T-Zell-Aktivierung in Richtung einer T_H2- und T_H17- vermittelten Antwort förderte. In einem Hautentzündungsmodell wiesen *Card9*$^{-/-}$ Mäuse dabei ebenfalls eine eingeschränkte Aktivierung von T_H2 und T_H17 Zellen auf. Weiterhin zeigten MCL/SIGNR3 defiziente Mäuse eine reduzierte allergische Atemwegsentzündung, vor allem gekennzeichnet durch eine reduzierte Anzahl an Typ 2 DZs und T_H2-Zytokin produzierenden Zellen.

Zusammenfassend deuten die generierten Daten daraufhin, dass MZG als endogene CLR Liganden fungieren und somit Signale, welche die MZ Degranulation induzieren, in adjuvante Effekte übersetzen, welche die adaptive Immunität beeinflussen. Kenntnisse über zugrunde liegende Mechanismen könnten zukünftig helfen, therapeutische Strategien zu entwickeln, die zum Einen überschießende Entzündungsreaktionen reduzieren oder zum Anderen gezielte adaptive Immunantwort auslösen könnten.

1 Introduction

1.1 Biology of classical dendritic cells (cDCs)

1.1.1 Development of cDCs and their sub-classification

Dendritic cells (DCs) represent a heterogeneous group of antigen-presenting cells (APCs), that are known to initiate and regulate innate and adaptive immune responses [2,3]. They were first discovered in 1972 by Ralph M. Steinman and Zanvil A. Cohn [4,5], who termed these cells as DCs due to their “treelike” morphology (from the Greek “dendron” or “dendreon” for tree) [4].

DCs are derived from hematopoietic stem cells (HSCs) in the bone marrow (BM) and differentiate from distinct progenitor cells into immature DCs (imDCs) that are recruited to peripheral lymphoid and non-lymphoid tissues [3,6,7]. DCs can be grouped into pDCs, cDCs and monocyte-derived DCs (moDCs) [8]. Under steady-state conditions, pDCs and moDCs are not present in peripheral tissues, like the skin, or lymphoid organs [8,9]. Therefore, this thesis will focus on the biology of cDCs.

In the BM, HSCs develop to common myeloid progenitors (CMPs) via several intermediate steps [9]. CMPs can differentiate into monocytes, macrophages (Mphs), granulocytes, megakaryocytes and erythrocytes [10]. Further development will decide for the mononuclear lineage, which will give rise to monocytes, Mphs and DCs [9,11]. The presence of FMS-like tyrosine kinase 3 ligand (Flt3L) will decide for the subsequent development to common dendritic cell progenitors (CDPs), which are identified as first dedicated DC progenitors that will contribute to the development of both pDCs and cDCs [6,10]. In terms of cDCs, CDPs will subsequently differentiate to pre-classical dendritic cells (pre-cDCs), which are defined by their CD11c expression and the lack of major histocompatibility complex (MHC) II ($CD11c^+$ $MHCII^-$). Pre-cDCs will solely develop to cDCs, but lose the ability to differentiate into pDCs or Mphs [12,13]. They migrate from the BM and populate all peripheral organs and finally differentiate into cDCs [6,9].

Differentiated cDCs occur in two different subtypes: cDC1 and cDC2 [6,14,15]. Both cDC subsets are defined by their cell surface expression of the hematopoietic markers CD45, CD11c and MHCII while they lack the expression of T cell, NK cell, B cell, granulocyte and erythrocyte lineage markers [6,9,15]. Since also moDCs and Mphs express different amounts of CD11c and MHCII, they can be distinguished from cDCs by additional markers like F4/80 (also known as EMR4), MER receptor tyrosine kinase (MERTK),

Ly6C, CD64 (Fc-gamma receptor I, FcγRI), CD68, lysozyme M (also known as LYZ2), Csf-1R or Flt3 [2,6,8,16].

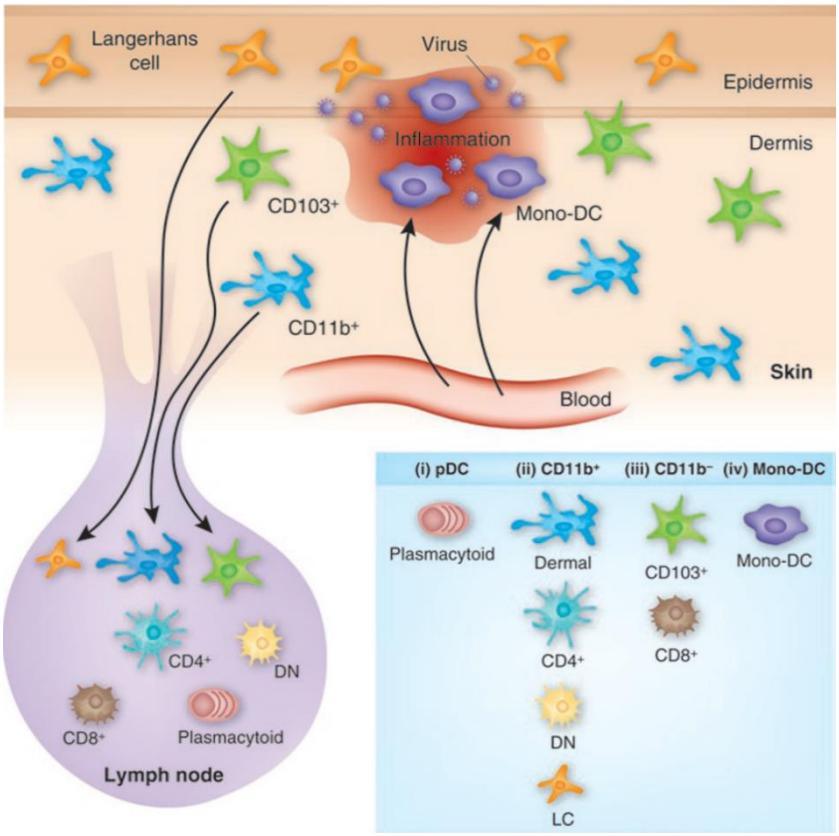

Figure 1.1: Overview of DC subsets. Summary of DC subsets located in the skin and skin-draining LNs. The skin harbors several subsets of DCs – LCs located in the epidermis and cDC1s and cDC2s in the dermis, which all can migrate to the LNs upon activation. Additionally, LN consist of several resident, LT-derived DC subsets. Under inflammatory conditions, pDCs and moDCs can additionally contribute to the immune response. Figure adapted from Heath and Carbone (2009) [17]. $CD103^+$ – NLT cDC1s, $CD11b^+$ – NLT cDC2s, $CD4^+$ – LT cDC2s, $CD8^+$ – LT cDC1s, DN – double negative DCs, pDC – plasmacytoid DCs, mono-DC – monocyte-derived DC (moDC), LC – Langerhans cell.

In general, murine cDCs can be classified by their surface expression of the integrin CD11b into a $CD11b^-$ and $CD11b^+$ compartment (Figure 1.1) [2,8]. Within peripheral non-lymphoid tissues (NLT), for instance the dermis of the skin, cDC1s are found within the $CD11b^-$ subgroup and characterized by their expression of the XC-chemokine receptor 1 (XCR1) and the integrin CD103, while cDC2s completely lack XCR1 and express CD11b. cDC2s can be further distinguished from cDC1s by their expression of the marker signal-regulatory protein α (SIRPα, CD172a) [6,9,17,18]. $CD11b^+$ cDC2s represent the most abundant subset within murine and human dermis, while $CD103^+$ cDC1s occur in a minor fraction [2,6,8,16]. This classification into $CD103^+$ cDC1s and

CD11b$^+$ cDC2s does not count only for DCs localized in the skin. Instead, they are widely distributed and also found in numerous other NLT, such as lung, intestine, liver and kidney [6,17]. Despite similarities between DC subsets within different tissues, some organ-specific DC subsets were found. In the CD11b$^-$ DC subset, an additional subset exists only in the skin. This subset was identified to additionally lack XCR1 and CD103. To date, it was only described in the murine skin, but its function remains unclear [8,16]. Additionally, a double positive (DP) DC subset that expresses CD11b and CD103, was described for the intestine and in some studies for the skin [1,6,17].

The general classification of cDCs into cDC1 and cDC2 cannot only be found in NLT (Figure 1.1). Instead, lymphoid tissues (LTs), such as spleen, lymph nodes (LNs) and thymus, exhibit a similar CD11b-based grouping of DC subsets that also share many similarities with their NLT counterparts. While CD103 is only expressed by NLT-derived DCs, LT-derived DCs are additionally characterized by the expression of CD8α. Therefore, cDC1c of LTs can be described as CD8α$^+$ CD11b$^-$ DCs and LT-derived cDC2 as CD8α$^-$ CD11b$^+$ DCs [6,17].

In respect of DC subsets, LNs are unique. As LTs, they exhibit the classical LT-derived DC subsets based on the expression of CD11b and CD8α. Additionally, tissue-migratory cDCs (migDCs) that refer to the NLT DCs and migrated from peripheral tissues through the lymphatics can be found within LNs in a minor fraction even under steady state conditions. In non-activated state, LN-resident DCs (LNr DCs) can be separated from migDCs by a higher CD11c expression and a lower expression of MHCII [6,19,20].

In summary, DCs represent quite a complex group of APCs that can be subcategorized into distinct organ-specific subsets. De Winde *et al.* recently summarized that each DC subset populates a distinct niche within the body and fulfills specific roles during immune responses [21]. DC functions and activation pathways in regard of different DC subsets will be described in the following sections.

1.1.2 cDCs – capacity of linking innate to adaptive immunity

DCs populate almost all peripheral tissues where they form a close network and express a wide variety of pattern recognition receptors (PRRs) [22]. Due to their strategic location and ability to sense invading pathogens, they are described as peripheral sentinels [23].

Merad *et al.* summarized key attributes of cDCs that mediate their unique functions [6]:

1. In the steady state, DCs are located at host-environmental interfaces, where they constantly sample tissue and blood antigens.
2. DCs possess highly efficient antigen processing and presenting capacities.
3. In the steady state and the in inflamed state, DCs loaded with tissue antigens exhibit the ability to migrate to the T cell zone within the draining LNs (dLNs).
4. DCs are highly efficient in activating and priming naïve T cell responses leading to T cell proliferation and differentiation.

Due to these characteristics, DCs are able to induce either tolerance against self-antigens or immunity against non-self-antigens and therefore act as bridges between the innate and adaptive immune system [2,6,22]. In the following sections, the mechanisms leading to antigen uptake and processing, DC maturation, T cell priming and finally to tolerance or immunity will be described in more detail.

1.1.2.1 Antigen sensing by PRRs

In addition to anatomical barriers, the innate immune system is one of the first defense mechanisms that protect against invading pathogens and contribute to acute inflammation in response to tissue damage and microbial infections [24,25].
First, it is important to detect invading pathogens and their associated products to induce an appropriate immune response. PRRs are germline-encoded receptors that are expressed by cells of the innate immune system, like DCs or Mphs [26]. They are essential for the sensing of microorganisms by specifically targeting pathogen-associated molecular patterns (PAMPs, conserved microbial structures). In addition, they were reported to be responsible for detecting endogenous molecules that are released from damaged host cells, so-called damage-associated molecular patterns (DAMPs) [24,27]. Upon activation, PRRs induce specific signaling pathways that lead to activation of anti-microbial immune responses [28].
To date, PRRs can be divided into four families: Toll-like receptors (TLRs), c-type lectin receptors (CLRs), Retinoic acid-inducible gene (RIG)-I-like receptors (RLRs) and Nucleotide-binding and oligomerization domain (NOD)-like receptors (NLRs) that can be assigned to the two main groups: transmembrane proteins (TLRs and CLRs) and cytoplasmic proteins (RLRs and NLRs). Recognized ligands can be derived from a huge variety of different sources, e.g. bacteria, viruses, fungi, nucleic acid and self-patterns associated with tissue damage or cell stress. Upon recognition, PRRs induce signaling cascades that lead to an inflammatory response leading to immune stimulation,

elimination of pathogens and infected cells and therefore to host defense against microbial insults [24,28]. In the following sections, this thesis will focus on ligands, signaling pathways and functions of the transmembrane receptors TLRs and CLRs.

1.1.2.1.1 TLRs

TLRs belong to the type I transmembrane proteins and their family members share a similar domain assembly. They consist of an N-terminal ectodomain including leucine-rich repeats, a single transmembrane domain and a cytosolic Toll/interleukin-1 (IL-1) receptor (TIR) domain. TLRs are highly conserved and were the first protein family to be defined as PRRs [29–31]. To date, 12 functional TLRs are known in mice (TLR1-9/11-13), while humans encode 10 TLRs (TLR1-10) [30,32]. TLRs are synthesized in the endoplasmic reticulum (ER) and subsequently transferred either to the plasma or to endosomal membranes. Their cellular localization is determined by the nature of recognized ligands. While plasma membrane located TLRs (TLR1/2/4-6) detect microbial cell surface components, ligands of endosome located TLRs (TLR3/7-9/13) are derived from nucleic acids (Figure 1.2) [29,31,33].

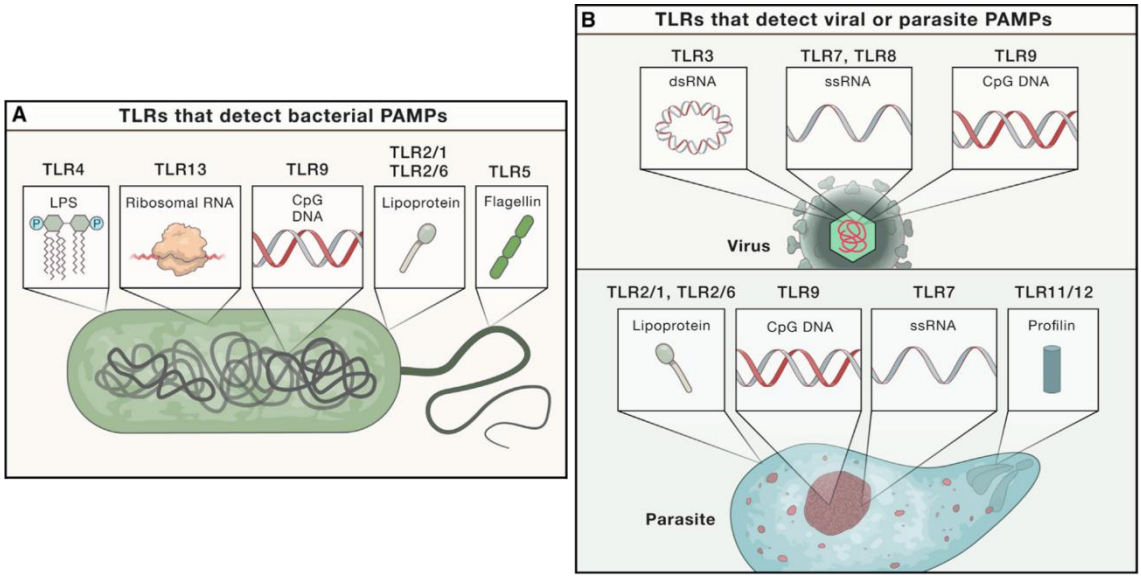

Figure 1.2: PAMPs detected by TLRs. PAMPs that are derived from (A) bacteria, (B) viruses or parasites are shown together with the murine TLRs that are responsible for their detection. Figure adapted from Fitzgerald and Kagan (2020) [29]. LPS – lipopolysaccharide, RNA – ribonucleic acid, CpG DNA – CpG-containing deoxyribonucleic acid, dsRNA – double-stranded RNA, ssRNA – single-stranded RNA.

PAMP recognition by TLRs occurs via its interaction with a TLR ectodomain dimer, where the ectodomains can be derived from the same TLRs (homodimer, e.g. TLR3-5/7-9) or different TLRs (heterodimer, TLR1/2/6) [29]. This dimerization is not only important for ligand binding but it is also necessary for signaling induction. The signaling process that is induced by TLR-ligand interaction requires the dimerization of the cytosolic TIR domains [29,33]. These dimers are recognized by distinct TIR-containing adaptors by TIR domain interactions between the TLRs and the adaptor. This leads to the formation of a multi protein complex, known as supramolecular organizing center (SMOC). Due to the containing core proteins, SMOCs and therefore the TLR signaling itself can be distinguished in two different groups (Figure 1.3): (I) myeloid differentiation primary response gene 88 (MyD88)-dependent signaling (SMOC: myddosome; used by all TLRs except TLR3) and (II) TIR-containing adaptor inducing interferon-β (TRIF)-dependent signaling (SMOC: triffosome; used by TLR3/4) [29,34,35].

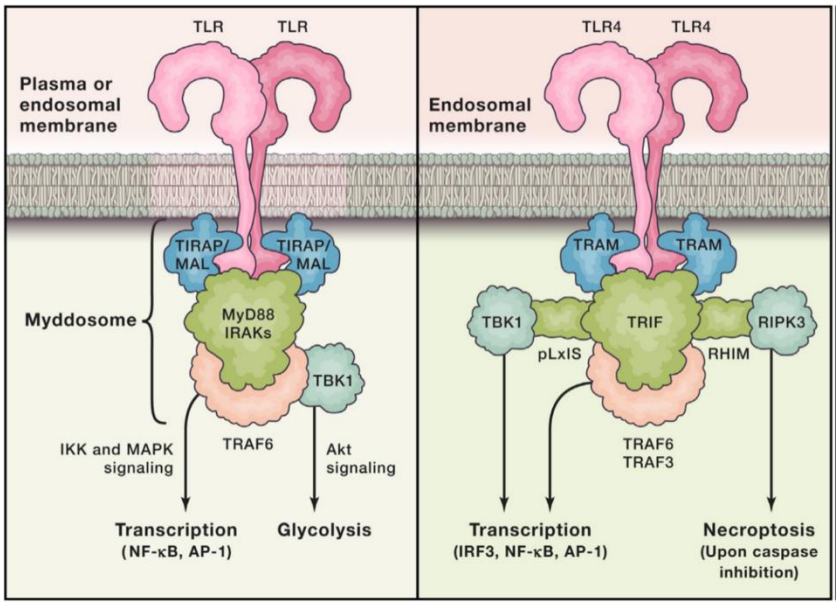

Figure 1.3: Adaptor molecules mediating the TLR signaling. TLR signaling is characterized by the composition of a multi protein complex, known as SMOC. Except of TLR3, all TLRs utilize the mydodosome upon ligand binding and receptor dimerization. This complex consists of TIRAP/MAL, TRAF6 and the core protein MyD88. Further association with TBK1 to the activation transcription factors and glycolysis. On endosomal membranes, TLR3 or TLR4 utilize the triffosome, which is built by TRAM, TRAF3/6, the core protein TRIF, TBK1 (bound to the pLxIS motif of TRIF) and RIPK3 (bound to the RHIM domain of TRIF). Subsequently induced signaling leads to transcription factor activation or necroptosis induction. Figure is taken from Fitzgerald and Kagan (2020) [29]. IKK – IκB kinase, MAPK – mitogen-activated protein kinase, RHIM – RIP homotypic interaction motif, RIPK3 – receptor-interacting serine/threonine-protein kinase 3, TBK1 – IKK-related kinase.

Tight contacts between SMOC components further lead to additional downstream events that culminate in transcription factor activation (nuclear factor 'kappa-light-chain-enhancer' of activated B cells (NFκB), activator protein-1 (AP-1) and/or interferon regulatory factor 3 (IRF3)) or the induction of glycolysis, necroptosis or other cellular responses [29,31,32,35].
In relation to DC maturation (described in detail in section 1.1.2.3), TLR activation leads to the surface upregulation of co-stimulatory molecules, like CD80 and CD86, the upregulation of peptide-MHC complexes and induces the migration towards the dLNs, which finally conveys their T cell priming capacity. Therefore, TLR signaling has the ability to drive inflammation and link innate to adaptive immunity [29,34,35].

1.1.2.1.2 CLRs

C-type lectins (CTLs) represent a structurally diverse protein family whose members are characterized by bearing at least one c-type lectin-like domain (CTLD). CTLDs were originally known for their ability to bind carbohydrates in a calcium ion (Ca^{2+})-dependent manner through conserved residues within these domains [36,37]. However, recent studies have elucidated that CTLDs can also lack the structural motifs required for Ca^{2+}-dependent carbohydrate recognition, and thereby detect a wider range of ligands in addition to carbohydrates including proteins, lipids and inorganic molecules. CTLs have been reported to detect ligands derived from self (endogenous) or non-self (exogenous) origins, while the binding capacity of a distinct CTL is not restricted to a certain ligand or even a certain class of ligands. Instead, distinct CTLs can recognize several ligands derived from both classes of ligands, which underlines their important role in many physiological functions [37–39].
CTLs can be divided into 17 subgroups, while CLRs represent members of group II (asialoglycoprotein and DC receptors), group V (NK cell receptors) and group VI (multi-CTLD endocytic receptors) [37,38]. This grouping of CLRs includes information about their structural organization. Group II CTLs are represented by type II transmembrane CLRs that consist of a short cytoplasmic tail, a transmembrane domain, an extracellular stalk region, which is important for oligomerization and a single CTLD harboring Ca^{2+} and carbohydrate binding sites. Members of group V CTLs share a similar domain composition, but in contrast, the CTLD lacks the typical Ca^{2+} and carbohydrate binding motifs. Group VI CTLs include type I transmembrane proteins that consist of a short cytoplasmic domain, a transmembrane region and an extracellular domain comprised of several domains including eight or ten CTLDs [37,38]. In addition, CLRs can be further subdivided by their cytoplasmic signaling motifs. According to this, myeloid CLRs can be

distinguished into four different groups: hemi-immunoreceptor tyrosine-based activation motif (hemITAM)-containing CLRs, ITAM-coupled CLRs, immunoreceptor tyrosine-based inhibition motif (ITIM)-containing CLRs and ITAM-ITIM-independent CLRs (Figure 1.4A) [38,40,41].

Upon ligand binding, CLRs induce intracellular signaling cascades that finally lead to multiple distinct immune responses. Signaling cascades that are induced by CLR-ligand binding can be divided into three main mechanisms: (I) caspase recruitment domain-containing protein 9 (Card9)-/spleen tyrosine kinase (Syk)-dependent signaling, (II) Raf-1-dependent/Syk-independent signaling and (III) inhibitory signaling cascades that are induced by ITIM motifs [40].

In most cases, ligand binding by CLRs will trigger Card9-/Syk-dependent signaling (Figure 1.4B). A single ITAM motif can be sufficient to directly mediate intracellular signaling upon CLR activation. This ITAM motif, either found in the cytoplasmic tail of hemITAM-coupled CLRs or within ITAM-bearing adaptor molecules like Fc receptor γ-chain (FcRγ) or DNAX activating protein of 12 kDa (DAP12) (ITAM-coupled CLRs), is phosphorylated, which subsequently leads to the recruitment and activation of Syk. Next, activated Syk recruits Card9, B-cell lymphoma/leukemia 10 (BCL-10) and mucosa-associated lymphoid tissue 1 (MALT1) forming an active protein complex (CBM complex), which finally results in the activation of transcription factors like NFκB [38,40,42].

Especially ITAM/ITIM-independent CLRs, but also some hemITAM-coupled CLRs can utilize Raf-1-dependent/Syk-independent signaling (Figure 1.4B). Ligand binding by these CLRs induces intracellular signaling by recruiting the GTPase Ras protein. Subsequently, serine/threonine-protein kinase Raf-1 is activated, which finally phosphorylates and therefore activates NFκB [40,42].

Lastly, inhibitory CLRs utilize their ITIM motif to induce intracellular signaling. Their inhibitory role is mediated by the abrogation of activation pathways through tyrosine and inositol phosphatases, like SHIP, SHP-1 and SHP-2, which finally leads to the suppression of distinct immune cell responses [38,40].

In addition to NFκB activation, CLR signaling can also trigger the production of reactive oxygen species (ROS) activating the NLR family pyrin domain containing 3 (NLRP3) inflammasome and the activation of p38, extracellular signal-regulated kinase (ERK), c-Jun N-terminal kinase (JNK) and nuclear factor of activated T cell (NFAT) pathways, which all together act on the subsequent transcription of several genes [38].

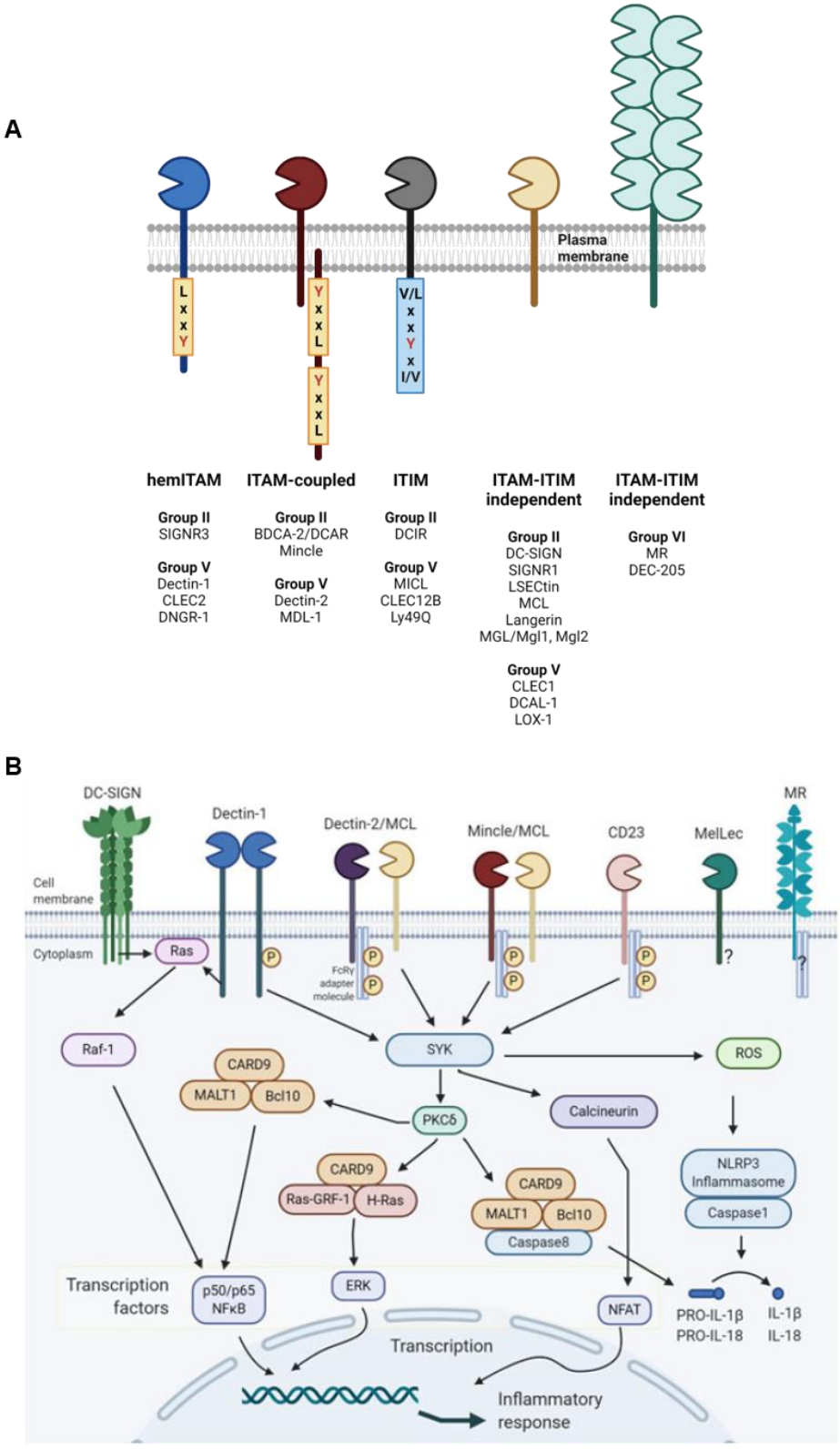

Figure 1.4: Signaling families of myeloid CLRs and their signaling cascades. (A) Subdivision of CLRs based on their cytoplasmic signaling motifs and CTL subgroups. Figure adapted from Sancho and Reis e Sousa (2012) [38]. (B) Overview about the signaling cascades introduced by CLRs in dependence of their cytoplasmic signaling motifs. CLR signaling cascades can be divided into (I) Card9 Syk-dependent signaling, (II) Raf-1 Syk-independent signaling and (III) inhibitory signaling cascades. Figure taken from Höft *et al.* (2020) [40].

Beyond the canonical signaling pathways that are induced by CLR activation, CLR signaling can be much more flexible and is modulated by physical influences, affinity, avidity, nature, density and architecture of the ligands. As stated above, a distinct CLR is often able to bind several ligands derived from different origins. Iborra *et al*. and Del Fresno *et al.* summarized factors that can impact on the CLR signaling outcome. In addition to the amino acid (AA) sequence of the CLR motif, the receptor (subcellular) location and the nature of ligands, CLR multimerization can affect the signaling outcome. The multimerization of CLRs includes the formation of homo- and hetero-complexes that lead to their cooperation in ligand binding response. Receptors involved in hetero-complexes can benefit from distinct characteristics and combine ligand avidity, endocytosis capacity and/or signal transduction capabilities [39,41].
As expected, the induced response upon ligand binding by CLRs can be as diverse as the signal flexibility. Despite inducing tolerance and mediating homeostasis, CLRs can stimulate innate and adaptive immunity. Among these, they can influence processes, like phagocytosis, cross-presentation, inflammasome activation and release of inflammatory mediators, thereby leading to antimicrobial responses [39,41,42].

SIGNR3

The murine CLR specific intercellular adhesion molecular-3 grabbing non-integrin homolog-related gene 3 (SIGNR3, CD209d) represents a member of the murine DC-specific intercellular adhesion molecule-3 grabbing non-integrin (DC-SIGN) family [43,44]. It belongs to the group II hemITAM-coupled CLRs (Figure 1.4A), characterized by a single carboxyl terminal carbohydrate recognition domain (CRD) [43,45]. In addition to the hemITAM motif, SIGNR3 harbors dileucine, tyrosine and tri-acidic cluster motifs in its cytoplasmic tail. While the hemITAM motif is important for signaling introduction upon activation, the other motifs were described to be necessary for the internalization of the CLR [46].
SIGNR3 still belongs to the less studied CLRs. However, it was reported to be expressed by myeloid mononuclear cells. The highest expression of SIGNR3 was detected within skin lysates, while Nagaoka *et al.* could identify SIGNR3^{+} skin cells as DCs and Mphs in the dermis. In addition, they showed that SIGNR3 was also expressed by DCs, Mphs and monocytes within various tissues, like spleen, LNs, lung and blood [47].
SIGNR3 represents the closest homolog of the human DC-SIGN (hDC-SIGN), especially in terms of the spectrum of bound ligands. Similar to hDC-SIGN, SIGNR3 was described to bind high mannose and fucose-terminated glycans. In addition, it was further reported to bind to N-acetylgalactosamine residues and fungal mannan structures and contributes to the recognition of intestinal microbiota and mycobacteria (*Mycobacterium (M.)*

tuberculosis), all representing exogenous ligands [44,45,48–50]. To date, there is only one study reporting endogenous ligands of SIGNR3. Phongsisay *et al.* showed weak interactions of SIGNR3 with brain-derived glycolipids by enzyme-linked immunosorbent assay (ELISA)-based binding studies, but the biological relevance was not further analyzed so far [51].

Upon ligand binding, SIGNR3 was mainly reported to initiate intracellular signaling via its hemITAM motif with subsequent utilization of Syk and Card9. This triggers downstream both the NFκB and the Raf-1 pathway and induces immune cell activation, consisting of inflammatory cytokine production and subsequent protection against pathogens [44,52]. In summary, SIGNR3 is described as a CLR with an important regulatory role, mediating both host defense against invading pathogens and immune homeostasis [44,45,49,53].

MCL

The macrophage (-restricted) C-type lectin (MCL; also known as Clecsf8, Clec4d, Dectin-3, Clec-6) is conserved between the human and mouse genome. It is a less studied member of the dendritic cell-association C-type lectin-2 (Dectin-2) family of CLRs [40,54,55]. MCL belongs to the group II ITAM/ITIM-independent CLRs (Figure 1.4A) and consists of a single extracellular CTLD, a stalk region, which is necessary for the association with other CLRs, and a transmembrane domain, followed by a short cytoplasmic tail [40,56]. Despite its naming [55], MCL is expressed on several myeloid cell types, including Mphs, DCs, neutrophils (Nphs), monocytes, and other leukocytes and B cell subsets [40,57,58].

The CTLD of MCL lacks conserved AAs normally found in the CTLDs of other members of the Dectin-2 family and associated with carbohydrate recognition, but instead harboring a surface hydrophobic domain. Therefore it was found to fail in the detection of unconjugated sugars, but in contrast allows the recognition of glycolipids and other ligands, like mycobacterial cord factor (trehalose-6,6'-dimycolate, TDM) [40,57,59,60]. To date, MCL is not only known for its ability to recognize mycobacteria, but also detects other pathogens like *Cryptococcus* (*C.) neoformans* and *Candida (C.) albicans* by binding of cell wall structures like α-mannan or glucuronoxylomannan and therefore exhibits an important role in anti-fungal immunity [40,61]. As stated for other CLRs, MCL was also reported to recognize endogenous ligands, especially derived from damaged host cells, such as the alarmin spliceosome-associated protein 130 (SAP130). However, the ability of MCL to bind to endogenous ligands is often speculated due to the ligand specificity of the CLR macrophage inducible C-type lectin (Mincle; also known as Clec4e, Clecsf9) and their capacity to form heterodimers or due to the simultaneous *knockdown*

of MCL and Mincle [62,63]. To date, endogenous ligands that are specific for MCL are not reported.

Upon activation, MCL induces intracellular signaling through the kinase Syk, but due to the lack of an intracellular signaling motif within the cytoplasmic tail, it is not able to induce signaling by its own. However, MCL was reported as an endocytic receptor, which mediates phagocytosis, respiratory burst and inflammatory cytokine production [57,59,64]. MCL is mainly known to act in a heteromeric complex together with Mincle and the ITAM-containing adaptor molecule FcRγ. Sho Yamasaki described in 2013 that the activating signal through the Syk-Card9 axis is delivered by FcRγ [65]. Additionally, Graham *et al.* could show that MCL is not able to associate with FcRγ (or other known adaptors like DAP10 or DAP12) on its own, but instead using “a novel adaptor” to fully mediate its receptor functions [57]. Therefore, heterodimerization of MCL with an adaptor and/or other CLR is essential for signaling introduction upon ligand binding to MCL.

In summary, the CLR MCL has been reported as an endocytic receptor that plays an important role in host defense by inducing phagocytosis, respiratory burst and pro-inflammatory cytokine production and possibly contributes to homeostasis by the recognition of damaged host cells [59,63].

1.1.2.2 Endocytic mechanisms – the ways of antigen uptake and processing by DCs

Endocytosis describes the process to take up extracellular material and plasma membrane into the cell interior [66,67]. For many immune and non-immune cells, endocytic mechanisms are essential for processes, such as cell development, nutrient supply, intercellular communication and cellular homeostasis [67].

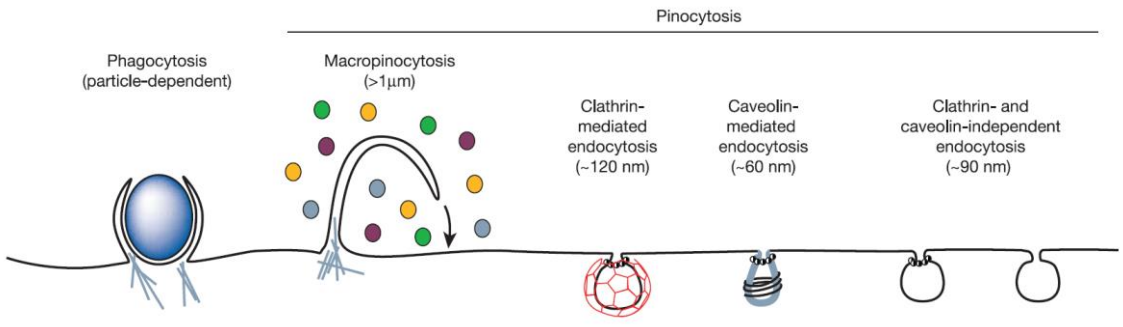

Figure 1.5: Overview about endocytic mechanisms. Endocytic pathways are divided into two main categories: phagocytosis and pinocytosis. The latter is further subdivided into macropinocytosis, CME, caveolae/caveolin-mediated and CIE. Depicted numbers indicate the approx. size of resulting endosomes. Figure taken from Conner *et al.* (2003) [67].

Endocytic pathways can be grouped into two categories: phagocytosis and pinocytosis. The phagocytosis, known as “cell eating”, represents the uptake of large particles, while pinocytosis, known as “cell drinking”, includes the uptake of fluid and soluble particles. Furthermore, pinocytosis can be divided into four subgroups: macropinocytosis, clathrin-mediated endocytosis (CME), caveolae-mediated endocytosis and clathrin-/caveolae-independent endocytosis (CIE) (Figure 1.5) [66,67].
In their function as tissue sentinels, DCs constantly capture antigens from the surrounding tissue by distinct endocytic mechanisms, namely phagocytosis, macropinocytosis and receptor-mediated endocytosis [22].

Phagocytosis

Phagocytosis is an active and highly regulated process exhibited by specialized cells, such as DCs, Mphs, monocytes or Nphs that mediates the ability to clear large particles, like bacteria, yeast or remnants of dead cells [67–69]. This type of endocytic process is mediated by specific cell surface receptors, such as Fc receptors, complement receptors or phosphatidylserine receptors [67,68].
The phagocytosis is initiated by surface receptor interactions with their ligands, which lead to receptor clustering and subsequent receptor activation. Rho-family GTPases, like cell division cycle 42 (Cdc42) and Rac, but also Src-family and Syk tyrosine kinases play an important role in most phagocytic signaling cascades [67,68,70]. The activation of GTPases and kinases induces actin assembly and remodeling to form plasma membrane extensions. Due to progressive participation of additional receptors, these membrane protrusions “zipper up” around the particle and finally fuse at their distal ends to form so-called phagosomes (Figure 1.5) [67–69]. Since the phagosome formation directly follows the particle surface, lots of different sizes of phagosomes from 0.5 µm to tens of µm are possible [68,69].
Dependent on the ligand and involved receptors, different signaling pathways can be induced during phagocytosis. Distinguishing between self- and nonself-ligands decides whether the uptake of a distinct particle also induces an inflammatory response or not [67,68]. Finally, the phagosomes undergo extensive maturation followed by the degradation of the particle for its presentation on MHC molecules to induce tolerance or immunity [68,69].

Macropinocytosis

Macropinocytosis plays important roles in nutrient acquisition, directed cell migration, immune surveillance and virus or cancer pathologies [67,71]. Macropinocytosis is characterized as receptor-independent bulk ingestion of extracellular fluids that is

defined as an actin-driven process [72–74]. This process occurs in two different forms: induced and constitutive macropinocytosis. Induced macropinocytosis is performed by several cell types, including immune and non-immune cells (e.g. DCs, Mphs, B and T cells, epithelial and endothelial cells, fibroblasts etc.) and is stimulated by growth factors, chemokines or TLR engagement. In contrast, constitutive macropinocytosis is a process mainly restricted to primary innate immune cells, like DCs and Mphs, where it mediates antigen capture and immune surveillance and confers them the ability to act as peripheral sentinels [74–76].

Constitutive and induced macropinocytosis share mechanistic features, despite their different “activation”. Macropinocytosis starts with the formation of so-called membrane ruffles that represent actin-dependent extensions of the plasma membrane, which are triggered by the involvement of Rho-family GTPases, like Rac and Cdc42 [67,71,74]. As shown in Figure 1.5, these protrusions do not extend along a distinct ligand, instead they build up a cup-like structure. Subsequently, the distal end of the protrusion fuses with the plasma membrane, forming large, phase-bright endocytic vesicles, so-called macropinosomes. They can differ strongly in size, reaching from 0.2 µm up to 5 µm in diameter thereby sampling a large volume of extracellular fluid [67,71,74,77]. Classically, the dependence on actin rearrangements and the absence of any specific marker or ligand were used to define the process of macropinocytosis. Indeed, its suppression by amiloride and its derivates can be further used for characterization [66,71,74,75].

Finally, macropinosomes undergo maturation, which includes the fusion with lysosomes, antigen degradation and presentation on MHC molecules to naïve T cells [74,78].

CME

The CME is crucial for several processes, such as intercellular communication during tissue development, nutrient uptake, cell signaling or cellular homeostasis and therefore is not only found in immune cells, but instead it is exhibited by all mammalian cells [67,79,80]. CME was referred to as “receptor-mediated endocytosis”, because of the huge variety of transmembrane receptors and their ligands that can be internalized during CME. But since also other endocytic pathways are mediated by receptor engagement, CME represents the more specific nomenclature [67,81]. CME is a highly regulated process, which course can be categorized into 5 distinct steps: (I) initiation/nucleation, (II) cargo selection/loading, (III) clathrin coat assembly/membrane bending, (IV) vesicle scission and (V) disassembly of the coat [79,80,82].

The formation of so-called “clathrin-coated pits” (CCPs) constitutes the starting point of CME. To this end, several endocytic adaptor proteins are recruited to the plasma membrane, which form the endocytic coat [80,82]. One of the most important proteins at

this point is the adaptor protein 2 (AP2), which can act as a bridge between the different components of the endocytic machinery. Together with cargo-specific, accessory adaptor proteins, AP2 mediates the cargo selection during the next step [67,80,82]. Additionally, it binds to clathrin and triggers the clathrin assembly necessary during CME. So-called clathrin triskelia are recruited to the site of cargo accumulation and assembled therefore mediating membrane bending and the formation of a coated vesicle (Figure 1.5). The vesicle scission is mediated by the large GTPase dynamin that surrounds the vesicle neck and separates the clathrin-coated vesicle (CCV) from the plasma membrane [80–82]. The last step of CME is represented by the disassembly of the clathrin coat, which subsequently releases the uncoated vesicle. These vesicles are 60 – 200 nm in diameter and therefore relatively small compared to phagosomes and macropinosomes [80,82]. Finally, they fuse with their destination intracellular compartment [81,82].

Endosomal network and antigen processing

DCs constantly capture external material and thereby sample the surrounding environment [22,66]. Once external material is internalized, it will be processed and subsequently presented on the DC surface by MHC molecules, an essential prerequisite for the induction of an adaptive immune response or for mediating tolerance to self-proteins [66,83,84].

In general, antigenic peptides can be presented either on MHC class I (MHCI) or MHCII molecules. Traditionally, intracellular antigens are thought to be presented by MHCI to naïve $CD8^+$ T cells, while extracellular antigens are bound to MHCII and presented to $CD4^+$ T cells (Figure 1.6) [84,85].

The way of antigen uptake can specify the intracellular destination compartment and therefore has a huge influence on antigen presentation [83,86]. For an efficient presentation, antigens have to be processed into antigenic peptides. These are generated by two distinct proteolytic systems within the cell: (I) the cytosolic proteasome that degrades cytosolic proteins for their subsequent binding to MHCI or (II) the lysosomal proteolysis that takes place in late endosomes/lysosomes and generates peptides that are subsequently bound by MHCII [84].

Intracellularly derived or endogenous antigens, for instance of viral or tumor origin (altered self) but also self-proteins, are degraded by the cytosolic 26S proteasome and subsequently translocated to the ER, where the generated 8 - 10 AAs peptides are bound by MHCI molecules and subsequently presented on the cell surface (Figure 1.6) [78,84–86]. Additionally, upon uptake, phagosomes, endosomes and macropinosomes that contain mainly exogenous antigens, but also those of endogenous sources are

directed to the late endosomal/lysosomal system [74,78,84,86]. Late endosomes and lysosomes represent typical proteolytic compartments. To fulfill this task, they concentrate proteolytic enzymes and disulfide reductases within their lumen. A low pH of 4 to 4.5 within lysosomes, additionally favors the activation of proteolytic enzymes, like cathepsins, that subsequently leads to the degradation of antigens generating antigenic peptides that are, in contrast to MHCI larger than 10 AAs in length [83–85]. MHCII molecules are additionally directed to the late endosomes to form peptide-MHCII complexes, which are finally transported to the surface of DCs [83].

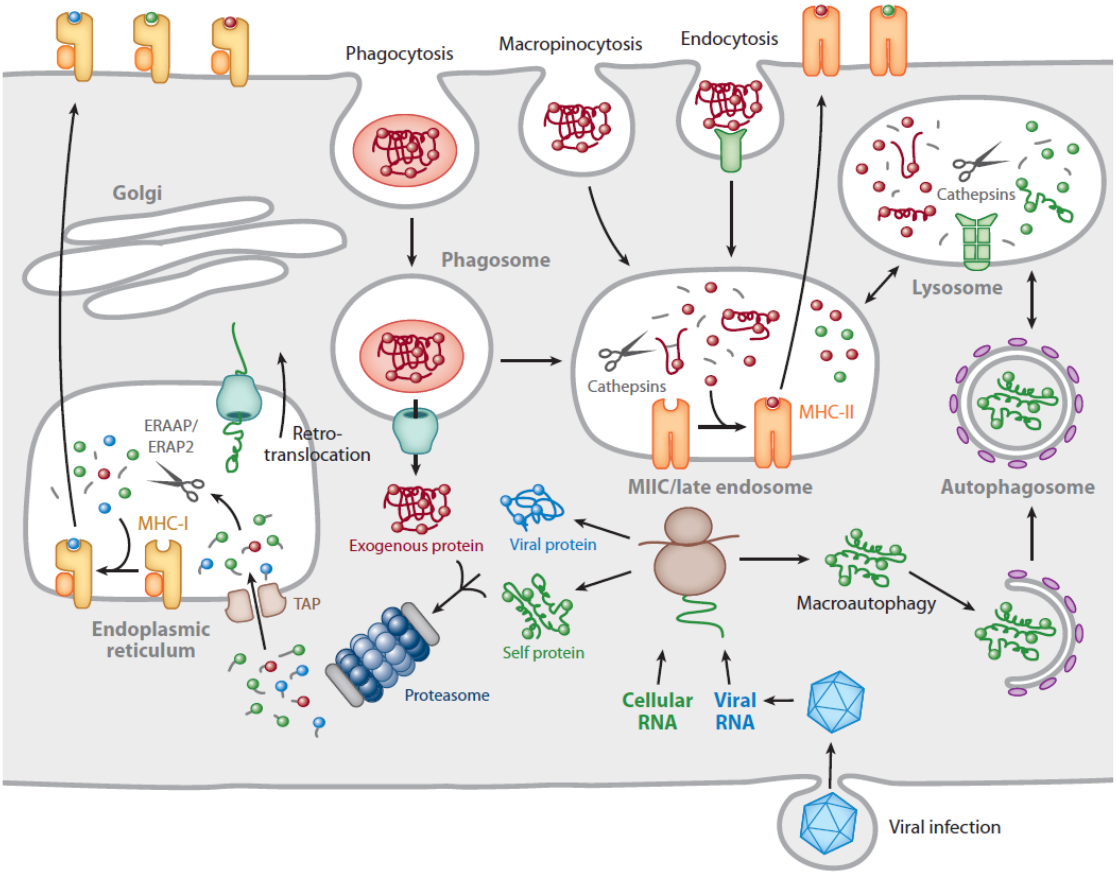

Figure 1.6: Antigen processing and presentation on MHC molecules. Overview about the basic pathways and exceptions concerning the trafficking, processing and presentation of antigens. In general, exogenous proteins are taken up by endocytic pathways (phagocytosis, macropinocytosis, endocytosis) processed by lysosomal proteolysis within late endosomes/lysosomes for their subsequent presentation on MHCII. Cytosolic proteins are processed by the cytosolic proteasome, subsequently translocated into the ER and finally presented on MHCI. Additionally, exogenous proteins can be directed to the cytosolic proteasome for their subsequent presentation on MHCI, a mechanism called cross-presentation. Figure taken from Blum *et al.* (2013) [84].

In addition to the traditional way of antigen processing and presentation, exogenous antigens that were taken up by endocytic mechanisms can also be processed to MHCI-binding peptides by the proteasome, a mechanism that is called cross-presentation [78,84,86]. In general, cross-presentation can occur in all APCs, but it is mainly performed by DCs [87]. The decision whether extracellular antigens are presented on MHCII or by cross-presentation on MHCI can be influenced by many factors. On the one hand, it can be a time-dependent process that occur in a sequential manner [78,84,88,89] or on the other hand, the decision for their presentation on MHCI or MHCII molecules can be influenced on the molecular level by involved endocytic receptors, the antigen uptake mechanism itself or by the compartment localization of antigens following their uptake [74,78,84,86].

Despite the fact that the basic steps of antigen processing and presentation are similar in different APCs, DCs differ in their antigen processing capacity compared to other APCs, especially in case of antigen uptake mechanisms, the lifetime of peptide-MHC complexes on the cell surface and their antigen processing compartments [83]. While Mphs harbor more acidic phagosomal compartments and have therefore an increased proteolytic capacity (50-times more active than DCs), DCs exhibit increased antigen presentation and therefore T cell priming capacity. This is mediated by less proteolytic compartments that maintain the antigen integrity for a prolonged time which in turn favors the antigen presentation via MHCI and MHCII [83,84].

In summary, antigen processing to MHCI- and MHCII-binding peptides is a critical step to induce an adaptive T cell response and therefore mediating host defense or tolerance [84]. The mechanisms underlying DC maturation and T cell priming are described in the following.

1.1.2.3 DC maturation and T cell priming

The activation of DCs is characterized by several processes that lead to their maturation and therefore shift their functional behavior from peripheral sentinels towards potent inducers of an adaptive immune response or tolerance [6].

DC functions are strongly dependent on their maturation status [22]. Hubo *et al.* describes imDCs as specialists for antigen uptake and processing mediating immune surveillance. In contrast, mature DCs (matDCs) strongly reduce their antigen uptake and processing capacity and instead increase their antigen presenting behavior and co-stimulatory and T cell priming capacity [22]. In line with the reduced antigen uptake capacity, maturing DCs start migrating from the peripheral tissue to dLNs, which is mediated by the expression of chemokine receptors like CC motif chemokine receptor 7

(CCR7) that guides DCs along the chemokine gradients of CC motif chemokine ligand 19 (CCL19) and CCL21 [22,90]. Finally, matDCs can be distinguished from imDCs by the upregulation of MHC molecules, their increased expression of CCR7 and co-stimulatory molecules (e.g. CD40, CD80 and CD86) and the enhanced secretion of distinct pools of cytokines [22,90,91].

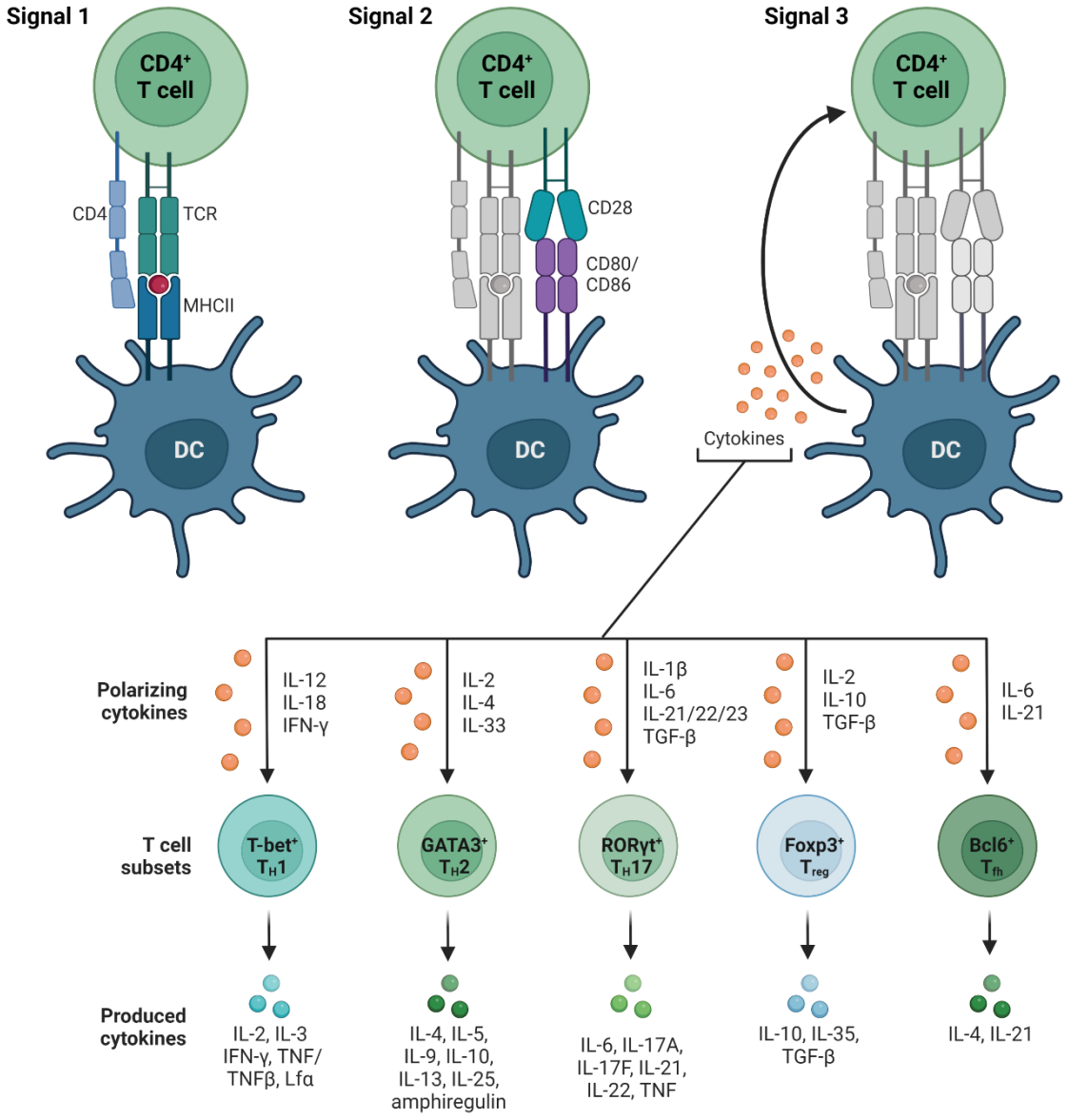

Figure 1.7: CD4⁺ T cell priming by matDCs. Three distinct signals are required for full activation and polarization of naïve CD4⁺ T cells into distinct T_H cell subsets, regulatory T (T_{reg}) cells and follicular T_H (T_{fh}) cells. Signal 1 – recognition of peptide-MHCII complexes by a specific TCR. Signal 2 – interaction of co-stimulatory molecules on DCs with their counterparts on T cells. Signal 3 – cytokine release by DCs that differentiate activated T cells. Polarizing DC cytokines and subsequently released T cell cytokines are summarized based on [85,92–94]. Figure created with Biorender.com.

Upon DC maturation and their migration to the dLNs, matDCs are able to prime naïve T cells. In general, the activation of antigen-specific T cells is dependent on three distinct signals (Figure 1.7) [92]:

1. The presentation of antigens on MHCI or MHCII molecules by APCs on the cell surface, which mediates T cell recognition of the related antigen through the T cell receptor (TCR).
2. The interaction of co-stimulatory molecules on APCs (e.g. CD80 and CD86) with CD28 on T cells is required for the activation and expansion of T cells.
3. APCs release cytokines, which influences the differentiation of activated antigen-specific T cells into distinct effector T cell subsets (T_{eff} cells).

T cells naturally occur in two main subsets: $CD4^+$ T helper (T_H) and $CD8^+$ cytotoxic T (T_c) cells. In the following, T cell activation and differentiation by DCs will be explained on $CD4^+$ T_H cells, but is also relevant, at least in part, for $CD8^+$ T_c cells [95].
Figure 1.7 demonstrates the necessary steps for a successful activation and differentiation of $CD4^+$ T cells by matured DCs. The priming of naïve T cells by DCs marks the essential step linking the innate to the adaptive immune system.
Signal one, the recognition of peptides bound to MHC molecules by a specific TCR, is essential but not sufficient for the activation and expansion of a distinct T cell pool. The TCR is not able to directly recognize intact antigens, therefore the antigen processing and presentation by DCs, or in general APCs, is a prerequisite for T cell activation. MHCII-bound antigenic peptides specifically activate $CD4^+$ T cells but not $CD8^+$ T cells mediated by the expression of the co-receptor CD4 that binds to the invariant β2 chain of MHCII. Under participation of nonantigen-specific adhesion molecules, matDCs and naïve $CD4^+$ T cells form an immunologic synapse around the MHCII/TCR complex, initiating T cell activation [85,92]. Signal two, the interaction of co-stimulatory molecules on the surface of DCs with their counterparts on the T cell surface, is necessary for the expansion of a distinct T cell population but also has influence on the functional differentiation [22,85,92]. Classically, the interaction of co-stimulatory molecules CD80 and CD86 on the DC surface with CD28 on the T cell surface mediates an activating co-stimulation signal, which leads to an immunogenic function of the generated T cell pool. In contrast, there are co-stimulatory molecules (e.g. programmed cell death-ligand 1/2 (PD-L1/2) or inducible T-cell co-stimulator ligand (ICOSL)) that do not only activate but also have inhibitory functions that lead to a tolerogenic function of the generated T cell pool (Figure 1.8) [22,85].

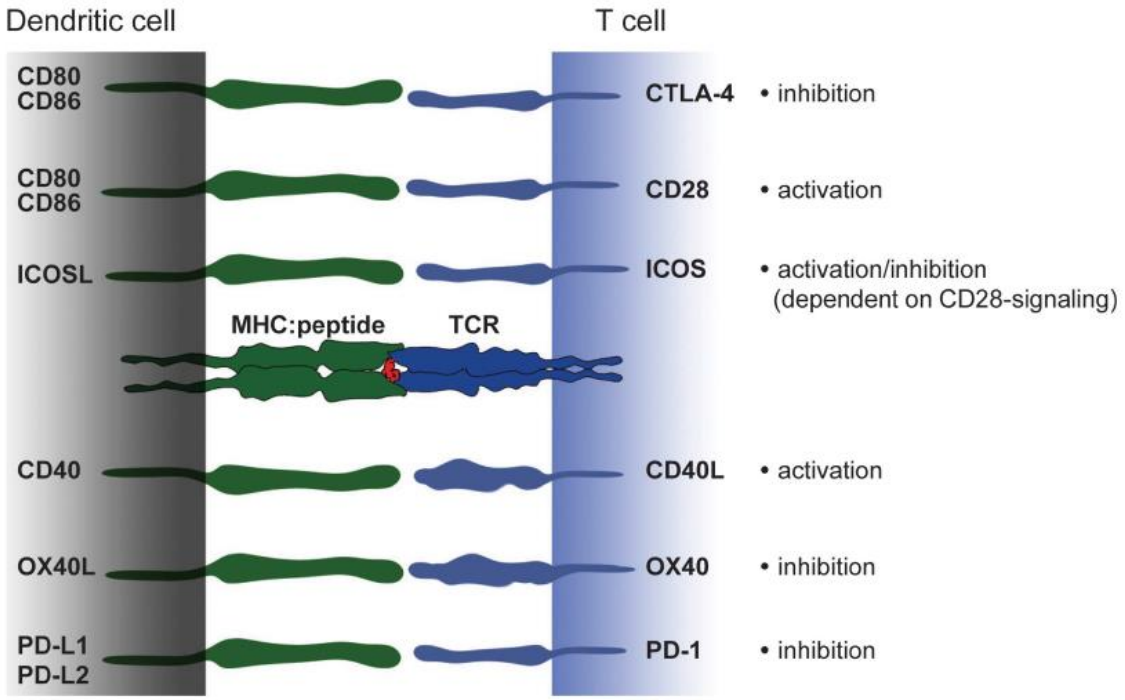

Figure 1.8: Co-stimulatory molecules on DCs and their ligands on T cells. The activation of T cells by DCs can be modulated by the engagement of different co-stimulatory molecules on the surface of DCs and their binding partners on the surface of T cells that have either tolerogenic (inhibitory) or immunogenic (activating) functions. Figure taken from Hubo *et al.* (2013) [22].

Finally, the third signal is mediated by the secretion of cytokines by DCs, whose composition determines the differentiation of activated antigen-specific T cells into functionally distinct effector T cell subsets, by activating the expression of distinct transcription factors driving T_H cell polarization (Figure 1.7) [85,92].

$CD4^+$ T_H cells are classically distinguished into five main subsets: T_H1, T_H2, T_H17, regulatory T (T_{reg}) and follicular T_H (T_{fh}) cells. Some studies described additional subsets, like T_H9 or T_H22 cells, but since it is still under debate whether these are unique subsets or a result of T cell subset plasticity, they will not be discussed in more detail within this thesis [94,96]. T-box expressed in T cells-positive (T-bet^+) T_H1 cells are known to play important roles in the defense against intracellular pathogens by the activation of cell-mediated immune responses but also contribute to autoimmunity. They are mainly triggered by the DC-derived cytokine IL-12 but also by IL-18 and interferon-γ (IFN-γ) and finally are characterized by the release of cytokines like IL-2, IL-3, IFN-γ, TNF/TNF-β and lymphotoxin α [92–94,97]. In contrast, GATA-binding protein 3-positive ($GATA3^+$) T_H2 cells, known for mediating the immune responses against extracellular pathogens by activating humoral and cell-mediated immune responses and contribute to allergy and asthma, are polarized by IL-2, IL-4 and IL-33 and subsequently release T_H2 cytokines

IL-4, IL-5, IL-9 and IL-13 but also IL-10, IL-25 and amphiregulin [93,94,97]. Mucosal barriers are maintained by RAR-Related Orphan Nuclear Receptor Variant 2-positive (RORγt$^+$) T_H17 cells and they contribute to pathogen clearance at mucosal surfaces, but also play roles in autoimmune and inflammatory disorders. T_H17 cells are induced by DC cytokines IL-1β, IL-6, IL-21/22/23 and transforming growth factor β (TGF-β) and finally produce cytokines like IL-6, IL-17A/F, IL-21/22 and TNF [85,92,93,97]. Forkhead box protein P3-positive (FoxP3$^+$) T_{reg} cells play key roles in maintaining immune tolerance/regulation and suppressing or downregulating distinct immune responses by inhibiting induction and proliferation of T_{eff} cells. They are polarized by DC-derived cytokines IL-2, IL-10 and TGF-β and in turn produce IL-10, IL-35 and TGF-β [94,96,97]. Finally, B-cell lymphoma 6-positive (Bcl6$^+$) T_{fh} cells are essential for the formation of germinal centers in the LNs and therefore for the antibody production and affinity maturation of B cells leading to humoral immunity. They are polarized by the cytokines IL-6 and IL-21 and subsequently are characterized by the secretion of IL-4 and IL-21 [85,93,96].

The decision for the activation of a distinct T_H subset can be made at different points during DC activation/maturation and T cell priming. The nature of stimulus and the environment in which they are sensed directs DC maturation and therefore T cell polarization since distinct subsets are involved in distinct defense or tolerance mechanisms [90,94]. Among other factors, distinct cDC subsets were reported to be responsible for the priming of distinct T cell subsets. Kumar *et al.* and others summarized that cDC1s, LT-derived CD8α$^+$ as well as NLT-derived CD103$^+$ cDC1s, predominantly lead to the MHCI-dependent activation of T_c cells and the MHCII-dependent activation of T_H1 cells. In contrast, CD11b$^+$ cDC2s primarily present via MHCII and therefore are mainly responsible for the polarization of T_H2, T_H17, T_{reg} and T_{fh} cells [21,94,98].

In summary DCs act as an important bridge between innate and adaptive immunity. They continuously sample tissues and engulf antigens from the local environment, which leads to DC activation and maturation and subsequent T cell activation and differentiation. Therefore, DCs play essential roles in inducing and directing appropriate immune responses to distinct incoming insults and thereby contributing to host defense or tolerance [2,3,21].

1.2 Mast cell (MC) biology

1.2.1 Development and heterogeneity

MCs were first discovered by Paul Ehrlich in 1879, who titled them as “Mastzellen” due to their nourished or overfed appearance [99,100]. They are defined by their expression of c-kit and the high-affinity immunglobulin E (IgE) receptor FcεRI (c-kit$^+$ FcεRI$^+$ cells) [101]. In addition to very early yolk sac-derived precursors, MCs represent BM-derived hematopoietic cells of the innate immune system that are derived from HSCs. HSCs develop in the BM to MPPs and subsequently to CMPs, which are further differentiated into granulocyte monocyte progenitors (GMPs). GMPs are the source of all granulocytes (Nphs, basophils and eosinophils), Mphs and MCs. In case of MC development, GMPs can directly differentiate into MC progenitors (MCps), which are already characterized as c-kit$^+$ FcεRI$^+$ cells. Finally, MCps are released into the blood stream and differentiate locally within peripheral tissues into mature MCs in response to the prevailing micromilieu in dependence of local growth factors, especially SCF and IL-3 (Figure 1.9) that are expressed by fibroblasts, stromal cells and endothelial cells [102,103]. Additionally, C57BL/6 mice exhibit a bifunctional basophil-MC lineage progenitor (BMCP) in their spleen, which can further differentiate into MCps that migrate to peripheral tissues through the blood stream and finally give rise to mature MCs [102–104].

MCs are found in almost all vascularized tissues, most abundant at sites of environmental interfaces, such as skin, lung and intestine, and are classically divided into distinct subsets due to their tissue localization and/or tryptic enzyme expression. In humans, MCs are distinguished based on the produced proteases into three different subtypes: MCs containing predominantly tryptase (MC_T) or chymase (MC_C) or both (MC_{TC}). In the murine system, two MC subtypes can be distinguished based on their tissue localization and protease content: connective tissue type MCs (CTMCs) and mucosal MCs (MMCs) [105,106].

MMCs are mainly found in the mucosa of the gastrointestinal (GI) tract and in the lamina propria of the respiratory tract and are characterized by the expression of two chymases mouse MC proteases- (mMCP-) 1 and 2. In contrast, CTMCs are located in the skin, peritoneum and submucosa of the GI tract and the lung, and predominantly express two chymases mMCP-4 and -5, but also two tetrameric tryptases mMCP-6 and -7. MMCs and CTMCs can further be distinguished by their T cell-dependency, size, lifespan, proteoglycan structure of MC granules (MCG) and histamine content [100,104,107,108].

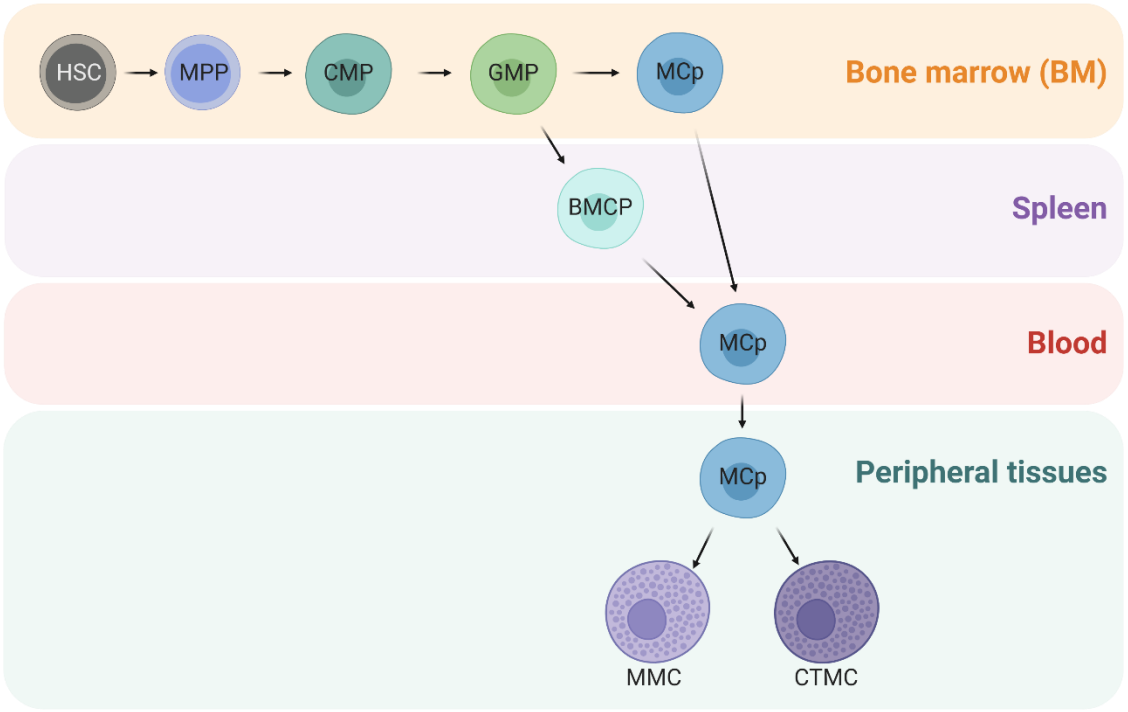

Figure 1.9: Development of murine MCs. MCs are derived from HSCs in the BM via MPPs, CMPs and GMPs. Distinct progenitor cells (MCps) migrate to the peripheral tissues, where they differentiate into mature mucosal MCs (MMCs) or connective tissue MCs (CTMCs). C57BL/6 additionally exhibit BMCPs within the spleen that can also contribute to the pool of MCps. Figure created with Biorender.com based on Dahlin *et al.* (2015) and Gurish *et al.* (2012) [102,103].

During the last years, intense research has led to a rethinking of the heterogeneity of MCs. Frossi *et al.* described the MC identity as a result of complex interactions with microenvironmental stimuli specific in a certain tissue and a distinct MC differentiation program and stated high tissue-specific differences in MC phenotypes and functions. In line, Akula *et al.* postulated an organ-specific MC heterogeneity [106,109]. For instance, Dwyer *et al.* compared CTMCs derived from different organs regarding their transcriptomes. Despite sharing a distinct MC signature distinguishing them from all other immune cells, including eosinophils and basophils, the authors found considerable differences in the tissue-specific gene expression of distinct MC subsets [110]. This dependency of the MC phenotype on the surrounding tissue is further supported by the hypothesis of Kitamura *et al*., that MMCs can differentiate into CTMCs and *vice versa* [111]. Additionally, MC heterogeneity is not only set up during their tissue-related maturation. Instead, MC are also described as “educable” in response to environmental and microenvironmental stimuli. Finally, these stimuli lead not only to an inter-tissue but also to an intra-tissue heterogeneity, influencing MC functions [106,112].

1.2.2 MCG – Biogenesis, degranulation and replenishment

MCs were discovered by Paul Ehrlich as “well fed” cells due to the high content of cytoplasmic metachromatic granules, which were firstly thought to be a result of hyper nutrition [99,105]. As most characteristic morphological feature of MCs, MCG are described as electron-dense lysosome-like secretory granules, which were initially characterized by their stainability with cationic dyes leading to their typical metachromatic staining [105]. MCs contain up to 1,000 MCG per cell, which can be 300 – 1,000 nm in size [113].

The MCG biogenesis is one of the key processes during MC maturation. However, this process is poorly characterized. To date, it is known that the biogenesis of MCG starts at the *trans*-Golgi network. Small and uniformly sized clathrin-coated vesicles bud off. Subsequently, these so-called “pro-granules” extensively fuse to generate immature granules. Immature granules undergo maturation, during which the dense core formation and mediator packaging take place, finally leading to the formation of fully functional MCG [105,114]. The dense core formation and therefore maturation of MCG is strongly dependent on the presence of proteoglycans of the serglycin family, which represent a major component of MCG. Additionally, glycosaminoglycans (GAG) are attached to the serine residues of the serglycin [105,108]. While CTMCs contain heparin as GAG attached to the core protein, MMCs utilize chondroitin sulfate [108,114]. An additional important step during MCG maturation is the packaging of mediators. MCG are filled with a huge panel of preformed mediators, like bioactive amines, lysosomal hydrolases, preformed cytokines and growth factors and MC-specific proteases [105,114,115]. The utilization of GAGs do not only play a role in dense core formation but is also very important in mediating storage of MCG content. GAGs, heparin as well as chondroitin sulfate, are highly negatively charged leading to a high anionic charge density within the proteoglycan scaffold of MCG. Subsequently, MCG content is closely packed by electrostatic interactions with GAGs, while its affinity is further increased through the low pH of MCG that is continuously decreased during MCG maturation [105,108,114].

The packaging of MCG compounds is thought to be not completely random, instead distinct compounds are packed selectively. Two models for the sorting of MCG content were proposed: “sorting-by-entry” model and “sorting-by-retention” model. The “sorting-by-entry” model hypothesizes that each MCG compound bears a sorting signal that interacts with a specific receptor, thereby leading to its packaging within MCG. The “sorting-by-retention” model suggests that multiple compounds are initially packed in the immature granules and selectively removed again during MCG maturation. Therefore, MCG itself can be reflected as heterogeneous. They differ in size and content and

contribute to the overall MC heterogeneity, depending on the tissue, species, health, age and external stimuli [105,114].

MCG are released through a process that is called degranulation, which can be induced by various external stimuli, like IgE receptor ligation, Fc receptor activation, G-protein-coupled receptor (GPCR) activation, complement components, cytokines and various peptides, requires the mobilization of Ca^{2+} and can finally lead to the release of up to 100% of the granular content. Degranulation can be categorized into two different modes of MCG release that is mainly dependent on external triggers: anaphylactic degranulation and piecemeal degranulation [105,113,114]. The anaphylactic degranulation, a process mostly characteristic for immediate hypersensitivity responses, requires multiple membrane fusion events, including MCG-MCG fusion and MCG-plasma membrane fusion, which finally leads to a rapid and massive release of MCG. Due to the increase in pH outside the cell, the affinity between MCG compounds and the proteoglycan scaffold is reduced leading to the sequential release of mediators [108,114]. In contrast, the piecemeal degranulation represents the differential release of a part of the MCG content, which is much slower compared to anaphylactic degranulation and leads to the release of small cytoplasmic vesicles. This process is mainly found during pathological processes, like allergy, urticaria or chronic inflammation and seems to play a role in intercellular communication [105,114,115].

MCG and their degranulation represent an important tool of MCs for a rapid and/or selective release of mediators. Indeed, many MC functions, both physiological and pathophysiological, are closely related to the preformed MCG compounds [105,114]. MC functions in homeostasis and disease will be discussed in detail in the following section.

Finally upon activation and degranulation, MCs exhibit several mechanisms to reconstitute their pool of MCG. They are able to recover from degranulation and undergo repeated cycles of degranulation and regranulation and mediate their MCG replenishment by the synthesis of completely new MCG (including proteoglycan scaffold and MCG mediators), by the engulfment of extracellular material or by refiling of empty MCG scaffolds. With the replenishment of their MCG, possibly with altered MCG content, MCs may be able to adapt on external stimuli, which is one more reason for MC heterogeneity and enables MCs to regulate the amount and type of released mediators and therefore favors the modulating capacity of MCs [112,114,116].

1.2.3 MC functions

In the 1950s, the role of MCs as effectors of immediate (type I) hypersensitivity reactions was discovered. Today, they are mainly known for their harmful effects during allergic reactions that are induced by crosslinking of FcεRI-IgE complexes [117–119].

MCs bind IgE due to its tight adherence to FcεRI expressed on their surface, thereby reducing levels of circulating IgE and increasing the IgE lifetime of approx. one day (within bloodstream) to weeks to months (bound to MCs) [118]. During type I hypersensitivity reactions, MCs are activated by the crosslinking of FcεRI induced by the interaction of a multivalent allergen with allergen-specific, FcεRI-bound IgE. Subsequently, this will lead to the immediate activation of intracellular signaling cascades, mediated for instance by tyrosine kinases Lyn and Syk, and finally results in distinct cellular events, such as protein phosphorylation, lipid metabolism and phosphorylation, intracellular calcium mobilization and transcription factor activation, which culminates in degranulation, production of lipid mediators and cytokines [119].

MCs are strategically located at host-environmental interfaces, such as skin and mucosa, where they represent a high amount of all immune cells (10% in the skin and 5% in the intestine) [120]. Due to their anatomical location, they are ideally positioned to additionally act as a first line of defense against external pathogens and other (micro-) environmental stimuli [112,117,119,120].

In addition to IgE-dependent activation, MCs can be stimulated in response to a wide range of endogenous and exogenous stimuli [105,112,119]. They express a huge repertoire of PRRs, such as TLRs, complement receptors, Fc receptors and purinergic receptors, to sense invading pathogens. Furthermore, MCs are able to respond to several other stimuli, such as cytokines, growth factors, toxins, neuropeptides, certain drugs and physical stimuli [112,117,119].

Once activated, MCs are known to release a broad spectrum of mediators during a multiphasic process: (I) immediate degranulation releases mediators, such as histamine, proteases and cytokines within seconds to minutes upon activation, (II) lipid mediators, like prostaglandins, are released within minutes and (III) *de novo* synthesis of soluble mediators, like cytokines, chemokines and growth factors, is initiated within hours upon activation [112,113,119]. Therefore, these multifunctional cells represent a source of a huge panel of mediators, which allow them to play important roles in lots of different physiological (e.g. angiogenesis, vascular homeostasis, innate and adaptive immune responses, venom detoxification etc.) and pathophysiological functions (e.g. diseases like allergy, asthma anaphylaxis, cardiovascular diseases etc.) [114,119,121]. Therefore, MCs are well equipped to react directly to different triggers by cytokine secretion and/or

immediate mediator release [101,118]. However, they do not only act in their function as innate immune cells, but also as essential linkers between the innate and adaptive immune response and therefore count as promotors and effectors of adaptive immunity. Different tools, such as activation and recruitment of immune cells by cytokine/chemokine release, antigen presentation to T cells and long distance effects by modulating dLNs, enable them to foster adaptive immunity and immunological memory formation [112,117].

Despite their numerous roles in host defense against pathogens and other (micro-) environmental stimuli, MCs do not have only beneficial functions, instead they also play crucial roles in a variety of disorders [107]. MC functions are tightly regulated to keep the balance between tolerance and allergy. Although underlying mechanisms are not fully understood, allergic sensitization occurs by favoring the induction of allergen-specific T_H2 cells while interrupting the induction of allergen-specific T_{reg} cells. For instance, the MC-IgE axis itself can subsequently act as a feedback loop, which potentiates the T_H2 response leading to severe allergic responses [118]. Hence, the precise control of MC functions is crucial for the termination of responses. Dysfunctional MCs or a dysregulated MC activation are responsible for several disorders, such as chronic allergic/inflammatory disorders, cancer, autoimmune diseases etc. [107,114,117,119]. Especially the MC proliferation and accumulation were reported to play a crucial role in the development of several diseases, like atopic dermatitis (AD), asthma and mastocytosis, while other MC-related diseases can be related to their dysregulated activation, such as urticaria, psoriasis and mast cell activation syndrome (MCAS) [117,122–124].

Due to their detrimental roles in several diseases, MCs became target of developing therapeutic or preventive strategies [118]. For instance, MCs were reported to be essential for successful vaccination. They are required for efficient vaccine adjuvants and therefore promote a protective immune response [112]. In line with their immunomodulatory functions, MCs are able to enhance and direct immune responses that could be the target of future research to direct or abrogate distinct immune responses.

In summary, MCs are very complex and multifunctional cells, whose function is tightly regulated in response to several pathogenic and (micro-) environmental stimuli. A dysbalance in this regulatory network can lead to abnormal MC behavior, which can culminate in MC-related and –driven diseases.

1.3 Intercellular communication between DCs and MCs

Both DCs and MCs count as first line immune sentinels since they are both located at environmental interfaces. Due to their anatomical location, for example within the skin, lung or GI tract, they reside in close proximity to each other, which increases the capacity for crosstalk responses [104,125,126]. Breedveld *et al.* summarized the capacity of granulocytes to modulate DC functions and thereby described MCs as regulators of immune responses [127].

In 2020, we summarized the ways of MCs to modulate DCs and therefore the adaptive immunity. In general, their interactions can be categorized in three different modes: (I) interaction via soluble MC mediators, (II) interaction via MCG, microvesicles (MVs) and exosomes and (III) direct DC/MC interaction [125,128].

Upon activation, MCs release a plethora of pre-formed and newly synthesized mediators (see section 1.2.3), whose influence on DC functions was studied by us and others. MC-derived mediators were described to promote DC migration, maturation and antigen-presenting capacity, thereby influencing T cell activation and differentiation. Histamine and TNF that are released upon immediate MC activation are reported to increase DC maturation, migration, antigen uptake and cross-presentation and to modulate the DC cytokine response so that it shifts the T cell priming towards T_H2 responses [104,125,127,129]. In line, several cytokines are described as modulators of DC functions. Leyva-Castillo *et al.* could demonstrate that MC-derived IL-13, which was released in an IL-33-dependent manner, modulated the subsequent T cell response. They showed that IL-12 production by neighboring skin DCs was downregulated, leading to reduced T_H1 polarization [130,131]. Additionally, other MC mediators, such as proteases, proteoglycans, CD40 ligand (CD40L), other cytokines/chemokines (granulocyte-macrophage colony-stimulating factor (GM-CSF), IL-1β, IL-6, IL-10, CCL3 etc.), prostaglandin D_2 and E_2 (PGD_2/PGE_2) or leukotriene B_4 and C_4 (LTB_4/LTC_4), can modulate DC migration, maturation and T cell priming capacity [127,129,132]. In general, Breedveld *et al.* summarized that depending on the type and strength of stimuli that activate MCs, the released pattern of mediators can vary strongly and therefore can also have different influences on DCs and other cells [127].

In addition to soluble mediators, DCs and MCs were reported to communicate via extracellular vesicles (EVs), including MVs and exosomes [133], and MCG. This communication can be bidirectional since MCs can release MCG and exosomes that are taken up by DCs and DCs can deliver MVs that in turn activate MCs [125]. EVs or exosomes represent an important tool of MCs to communicate with neighboring (immune) cells. These submicron structures are also released in a regulated manner and

contain lipids, proteins and nucleic acids and therefore are described as “multi-component communication devices”. MC-derived EVs can lead to the activation of DCs, increased antigen-presenting capacity and cytokine release (distinct cytokine patterns depending on EV content/nature of activating signal) that subsequently lead to T cell proliferation and polarization [128,129]. In addition to EVs, MCs can communicate via their characteristic MCG. We and others could demonstrate that MCs utilize MCG to communicate with other immune cells [1,134]. In addition to the findings of Kunder *et al*., who reported that MCG released by MCs in the periphery can enter the lymphatics upon activation and thereby reach the dLNs to impact on secondary lymphoid tissue, we could show in 2019 that imDCs engulfed intact MCG that were released by MC upon skin inflammation. Subsequently, DC migration, maturation and T cell priming capacity were boosted in MCG^+ DCs compared to MCG^- DCs. By this active transport of MCG to the dLNs and their DC modulating capacity, MCs exhibit an additional way to impact on the LN-borne adaptive immunity over distance [1,135,136]. In turn, DCs use MVs to communicate with MCs. Choi *et al.* demonstrated that perivascular $CD301b^+$ DCs release MVs loaded with antigens, which subsequently led to IgE/FcεRI crosslinking and therefore MC activation and degranulation [125,137].

Lastly, DCs and MCs are able to interact via direct cell-cell-contact. These physical interactions culminate in antigen or protein transfer from MCs to DCs or DCs to MCs. Several studies described DC-MC interactions as depending on the engagement of integrins and adhesion molecules [91,104,126,138]. Carrol-Portillo *et al.* reported the formation of MC-DC-synapses, which additionally depends on the MC activation and leads to the transfer of antigens from MCs to DCs. These antigens are subsequently processed by DCs and increase their T cell priming capacity [126]. Dudeck and colleagues showed additional aspects of direct DC-MC interaction. In 2011, they could demonstrate that DC maturation was increased and the released cytokine pattern was altered (towards T_H1/T_H17 responses) upon direct MC-DC crosstalk [91]. We further showed that MCs and DCs undergo long-lasting contacts during skin inflammation. In contrast, these interactions led to the protein transfer from dermal DCs to neighboring MCs that equipped MCs with functional MHCII. This cross-dressing increased T cell-driven inflammation and might warrant host defense and skin barrier integrity during the absence of DCs while migrating to the dLNs [139]. In addition, Otsuka *et al.* described the essential role of DC-MC interactions for murine contact hypersensitivity (CHS) model (see section 1.3.1), which lead to both DC and MC activation [138].

In summary, DCs and MCs exhibit a plethora of different ways to communicate with each other thereby influencing and modulating innate and adaptive immunity. Especially in several diseases, mechanisms of immune cell communication are of great interest since

they offer potential to intervene in some detrimental processes. Most people suffer from inflammatory diseases several times in life. Depending on the disease type, symptoms can reach from mild to detrimental, life-threatening ones. To date, up to one tenth of the worldwide population, for instance, suffer from at least one allergic disease, reaching from milder forms, like rhinitis, to more sever forms, like asthma or even anaphylaxis. Within the last years, allergic diseases showed rapidly increasing prevalence all over the world, which comprises sever problems for affected patients but also for the health system [140]. Therefore, effective treatments are of great importance. The development of these treatments is mostly subject to the analysis of disease-underlying mechanisms. Detailed knowledge about the causes and consequences of distinct diseases will help to develop specific therapeutic strategies. The following sections will focus on the current knowledge of allergic contact dermatitis (ACD) and allergic asthma, in which DCs and MCs play a critical role during disease development and progression.

1.3.1 Contribution of DCs and MCs to ACD

The skin is one of the largest and outermost organ of the body and serves as a barrier to the environment, which is constantly exposed to various external influences [141,142]. The skin is separated into two anatomical subunits: the epidermis and the dermis, which are separated by a basement membrane [2,8]. The immune cell network is mainly located within the dermis, which is very important for maintaining skin homeostasis and protecting against physical, chemical and microbial insults [141,143,144].

ACD is caused by contact allergens, such as small organic molecules or inorganic chemicals that are included in fragrances, dyes, cosmetics, preservatives and jewelry. About 20% of the adult human population are sensitized to common contact allergens and most of these patients also suffer from ACD. ACD can be classified as a type IV delayed-type hypersensitivity response and also counts as an important occupational skin disease, since 40% of occupational diseases are skin-related from which up to 90% are related to contact dermatitis (both irritant and allergic) [142,145–147].

ACD is characterized as a T cell-driven disease that has been intensively studied with the CHS model, the mouse model of ACD, and consists of a sensitization and elicitation phase [145]. ACD or CHS are normally induced by haptens, low-molecular-weight organic and often electrophilic compounds. Due to their low size, haptens can penetrate the skin and interact with cellular and extracellular self-proteins, which is necessary to induce the innate and subsequently the adaptive immune system [142,145]. Self-proteins become “haptenized”, which converts them into antigenic proteins. The hapten itself and “altered-self” proteins are subsequently recognized by different innate immune

receptors, such as TLRs, NLRs and CLRs, expressed on skin resident cells, most importantly epidermal Langerhans cells (LCs) and dermal DCs. Keratinocytes (KCs) play also an important role for the development of ACD. They are part of the anatomical barrier inhibiting the penetration of the hapten into the skin, as well as express several innate immune receptors and therefore also recognize haptens and haptenized proteins. Subsequently, they produce various mediators, such as TNF, IL-1β, IL-18 and PGE_2, which favors the migration and maturation of skin DCs. Additionally, KCs release alarmins, like IL-33 and adenosine triphosphate (ATP) in response to cell stress (Figure 1.10) [117,142,145].

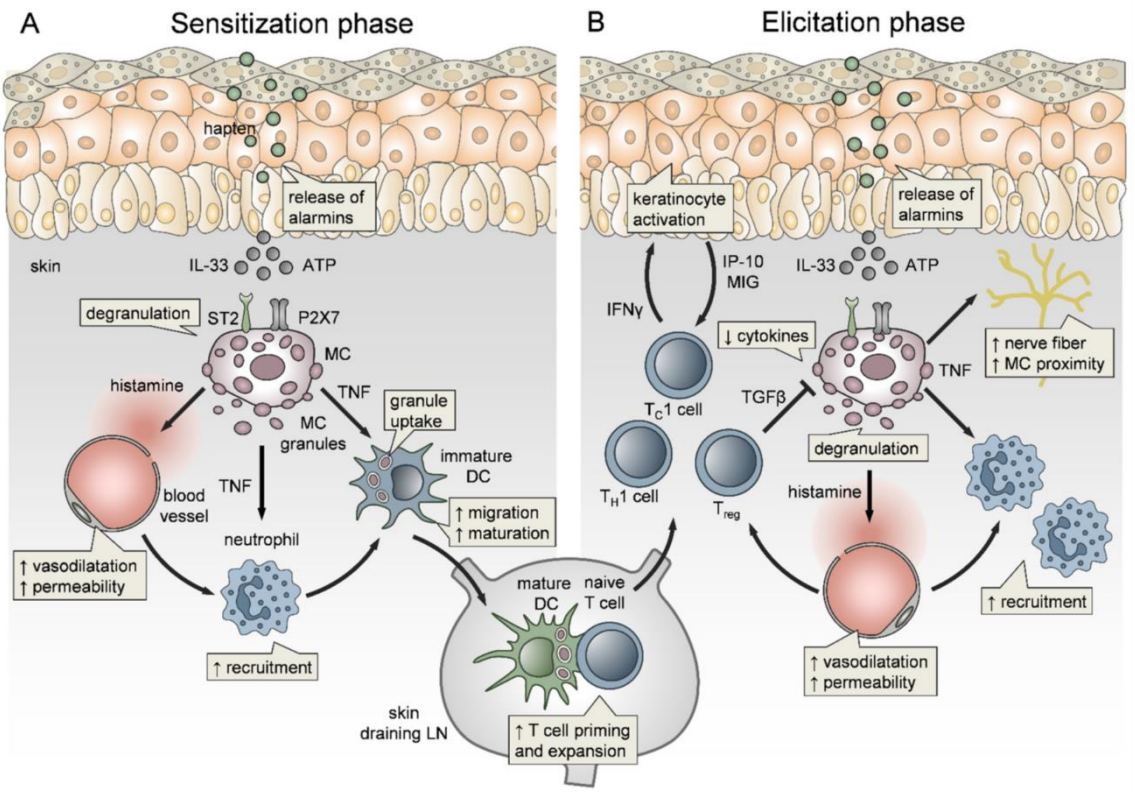

Figure 1.10: Phases of CHS. (A) During sensitization phase, haptens penetrate the skin leading to the "haptenization" of self-proteins and activation of dermal DCs. Due to released alarmins (e.g. IL-33 and ATP), MCs sense KC cell stress leading to MC activation and degranulation. They subsequently release mediators, like histamine and TNF, causing vasodilatation and permeability and Nph recruitment. Additionally, released TNF and MCG increase DC maturation, migration and subsequent T cell priming within the dLNs. (B) During elicitation phase, T_{eff} cells (mainly T_H1/T_c1 but also T_H17/T_c17 cells) enter the skin, where they release pro-inflammatory cytokines and exert their cytotoxic activity to remove allergen-loaded cells. Additionally, MCs contribute by causing again vascular responses and Nph recruitment and acting on nerves. Treg but also T_H2 cells act finally as regulators of CHS responses. Figure taken from [117].

Upon activation, DCs migrate to the dLNs where they present peptides derived from the haptenized self-proteins to $CD4^+$ and $CD8^+$ naïve T cells leading to their activation, proliferation and differentiation to hapten-specific T_{eff} cells. Main T_{eff} populations during ACD or CHS are composed of $CD4^+$ T_H1 and T_H17 cells and $CD8^+$ T_c1 and T_c17 cells that enter the blood circulation upon their activation and differentiation. In contrast, T_H2 cells act as negative regulators during ACD or CHS. During the elicitation phase, repeated contact with the same hapten leads to the recruitment of T_{eff} cells into the skin, where they release pro-inflammatory cytokines and exert their cytotoxic activity to remove allergen-loaded cells [145,148,149]. Therefore, they evoke the clinical ACD symptoms like itchy, red and flaky rashes, in part with blisters and oozing [147,150]. Additionally, different immune cell subsets, like Nphs and monocytes, enter the skin during the sensitization and elicitation phase of ACD [117,145,148].

Despite the fact that DC activation and migration to dLNs is one of the essential steps during ACD, MCs play also a very important role for the course of ACD [142,145]. Due to their location in close proximity to other (non-) immune cells, they can dramatically impact on the course of ACD. Our working group could show that MCs sense cell stress and tissue damage through the concomitant recognition of alarmins by ST2 (IL-33) and P2X7 (ATP) receptors [151]. Additionally, MCs can be activated by released IL-1β, IL-18 and produced ROS. The subsequent MC activation leads to the rapid release of histamine, which causes blood vessel vasodilatation and increased vessel permeability leading to edema formation. Additionally, TNF and other mediators, like chemokines, favor the priming and recruitment of Nphs to the inflamed ear skin [117,147]. Last, MCs characteristically degranulate in response to their activation and the released MCG, together with TNF, increases the DC maturation and migration thereby promoting the T cell priming within the dLN [1,152]. DCs and MCs extensively interact during 1-fluoro-2,4-dinitrobenzene (DNFB)-induced CHS, which culminates in the transfer of functional MHCII from DCs to MCs. This equips MCs with the capacity to ensure host defense and skin barrier integrity at the site of inflammation while DCs migrate to the dLN [139]. Additionally, Otsuka *et al.* described the necessity of DC-MC interactions during ACD/CHS development showing a reduced CHS response as a consequence of an impaired MC-DC communication [138].

Finally, immune responses during ACD are terminated by T_{reg} cells, regulatory B (B_{reg}) cells, natural killer T (NKT) cells and $CD8^+$ T_{eff} cells. For instance, T_{reg} cells are reported to release TGF-β that inhibits the cytokine production by MCs and also to degrade ATP into tolerogenic adenosine, which limits the immune response during ACD. In addition, $CD8^+$ T_{eff} cells, B_{reg} cells and NKT cells contribute to the limitation of the ACD response by the release of IL-10 at later time points during the elicitation phase [117,147].

In summary, ACD is a complex disease involving several immune and non-immune cells. To date, there are no specific treatments available that directly inhibit ACD responses. Instead, clinically relevant diseases can only be prevented by the avoidance of skin exposure to the respective contact allergen. The avoidance strategy assumes that responsible contact allergen is known, but even if it is known, it can take weeks to months for the complete resolution upon avoidance. Additionally, reducing the exposure to the contact allergen is often not possible (e.g. in case of dyes or baker's flour) finally can cause a chronic disease course. Anti -inflammatory agents (for example topical or systemic steroids), ultraviolet irradiation or systemic immunosuppressants can be used during severe diseases to initially control skin inflammation, but they can also cause severe complications [147]. Treatments that can directly inhibit ACD responses would have the advantage of being able to intervene earlier and therefore reduce the possibility of severe disease courses and chronification of skin inflammation.

1.3.2 Contribution of DCs and MCs to allergic asthma

Allergic asthma is a well-known and common chronic disease that belongs to the family of IgE-mediated type I hypersensitivities, the so-called atopic diseases, and affects approximately 8 - 10% of children and adults, in total more than 300 million people worldwide [153]. Typical symptoms include bronchial hyperreactivity (BHR), increased mucus production, wheezing, dyspnea, airway wall remodeling and airway narrowing, which can lead to variable airflow limitations [117,153].

Classically, asthma can be categorized into two main disease endotypes based on the involved immune effector cell response: (I) type 2/allergic asthma and (II) non-type 2/non-allergic asthma. Allergic asthma represents the most common type of asthma, which is characterized by T_H2 cell-mediated inflammation, the presence of specific serum IgE antibodies and/or a positive skin-prick test to proteins of common inhaled allergens like house dust mite (HDM), animal dander or plant pollen. In contrast, the non-allergic asthma is defined by the absence of T_H2 cells and IgE antibodies in the serum, instead it can be further divided by the involvement of type 2 innate lymphoid cells (ILC2s) and eosinophilia or the association with T_H1 and/or T_H17 cell-mediated inflammatory responses and neutrophilia [153]. The following section will henceforth focus on the mechanisms underlying allergic asthma since this is the most common form of asthma [153,154].

Allergic asthma is mostly initiated through allergic sensitization during childhood and often the consequence of a stepwise progress of atopic disorders in children with an early onset of atopic disease, a process that is called "atopic march" [153,155]. As

described for the skin, the lung represents a host-environmental interface that is constantly exposed to incoming allergens, pollutants and other pathogenic components. Among others, its barrier function is mediated by a close and tightly regulated network composed of several immune cells, like DCs, MCs, basophils, eosinophils, B cells, T cells and ILCs, and non-immune cell types, like epithelial cells (EpCs), goblet cells and fibroblasts [153,156].

Regardless of the asthma endotype, the activation of DCs by recognizing allergens is crucial for activating T cells and other innate immune cells [153]. Under steady state conditions, the lung DC fraction is mainly represented by cDCs and a small fraction of pDCs [153,156]. cDCs are found in the lung as $CD103^+$ cDC1s and $CD11b^+$ cDC2s that differ in their localization and function during the course of asthma. Both cDC subsets are described for distinct functions during asthma and play important roles as regulators of the immune responses. $CD11b^+$ cDC2s are important to induce allergic sensitization and the initiation of an effective T_H2-mediated adaptive immune response [153,157,158]. In some reports, $CD103^+$ cDC1s are also described for their role in inducing a T_H2-mediated immune response [159], but they are mainly reported for their function as immune regulators and inducers of tolerance to inhaled allergens [156,160,161]. In line, both cDC subsets exhibit different antigen presenting capacities. While $CD11b^+$ cDC2s are reported to present antigens via MHCII to $CD4^+$ T cells, $CD103^+$ cDC1s are responsible for cross-presentation via MHCI to $CD8^+$ T cells [162–164].

Several murine asthma models were developed to mimic human asthma in order to analyze the underlying mechanisms. Starting with ovalbumin (OVA)-induced mouse models, research turned nowadays to more physiologically relevant asthma models mediated, for instance, by the HDM *Dermatophagoides (D.) pteronyssinus* that is a common trigger of asthma worldwide [154]. The current understanding of the mechanisms of asthma initiation and progression is outlined in Figure 1.11.

cDCs play an important role during allergen sensitization since they capture inhaled allergens. The allergen itself does not necessarily lead to the induction of an immune response. The environment in which the antigen was captured determines whether mechanisms leading to immune responses or tolerance are activated. Additional “danger signals”, like microbial products or pro-inflammatory cytokines, guide it to inflammatory immune responses [153,156,162].

cDCs are well equipped with PRRs that can sense incoming stimuli. HDM, for instance, can activate cDCs via the CLRs Dectin-1 and Dectin-2 [153,165,166]. Further, cDCs cells can also be indirectly activated by EpCs since EpCs also express a wide range of PRRs and sense invading allergens. Additionally, many allergens, including HDM, exhibit protease activity leading to decreased barrier functions and the activation of

protease-activated receptors thereby additionally acting on DCs and EpCs [153,156]. The stimulation of airway EpCs by allergens leads to the release of cytokines and chemokines, like IL-1, IL-25, IL33, GM-CSF and thymic stromal lymphopoietin (TSLP) and the release of alarmins, like ATP and uric acid. These EpC-derived factors additionally stimulate cDC activation and favor a T_H2-driven allergic response [167–169]. Additionally, EpC-derived factors can act on other immune cells, like T_H2 cells, ILC2s and other innate lymphocytes (e.g. basophils, eosinophils etc.) and therefore importantly contribute to the course of allergic asthma [153,155].

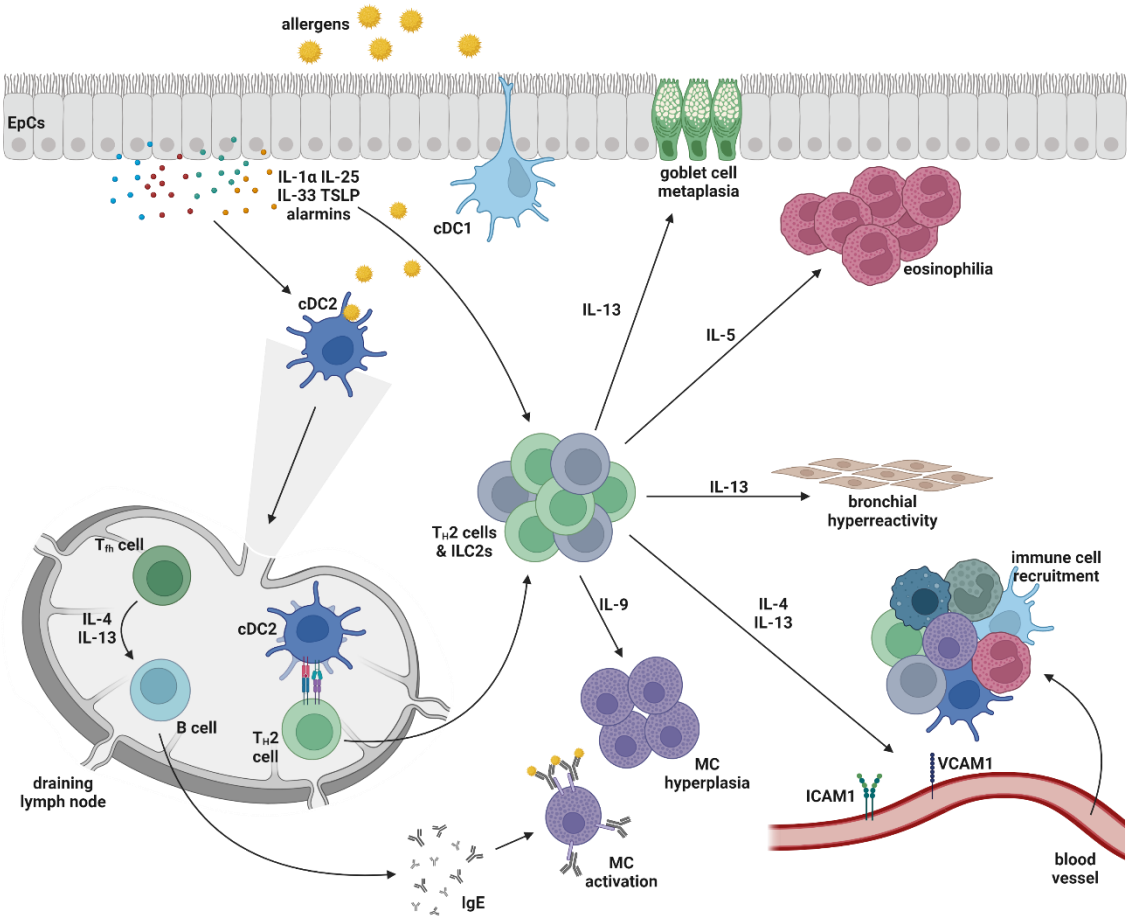

Figure 1.11: Allergic asthma. Allergens are sensed by EpCs and DCs. EpCs subsequently release cytokines, chemokines and alarmins. DCs, especially $CD11b^+$ cDC2s, take up allergens, become activated and migrate to the dLNs, where they prime T cells leading to the polarization of T_{fh} cells and T_H2 cells. T_{fh} cells release T_H2 cytokines IL-4 and IL-13, which are responsible for the class switching of B cells that subsequently produce allergen-specific IgE antibodies.T_H2 cells migrate to the lung where they release several T_H2 cytokines. During the course of allergic asthma, several immune cell subtypes are recruited and contribute to the ongoing disease characterized by increased IgE levels, MC hyperplasia, BHR, goblet cell metaplasia (incl. increased mucus production) and eosinophilia. Figure created with BioRender.com based on references described in the text.

Once activated by allergens, cDCs process the antigen, start to mature and migrate to the lung-draining mediastinal LNs. Activated EpCs mainly favor the maturation of $CD11b^+$ cDC2s, which indeed are found in higher frequencies compared to $CD103^+$ cDC1s within the $antigen^+$ DC compartment inside the dLN [153,162]. Antigens are presented to $CD4^+$ T cells, which mainly results in T_H2 cell differentiation. One part of the T helper cells will develop to T_{fh} cells that locally produce IL-4 and/or IL-13 and trigger B cells to promote the production of IgE antibodies by class switching. In contrast, effector T_H2 cells migrate back to the lung, the site of inflammation, where they produce T_H2 cytokines, like IL-4, IL-5, IL-9 and IL-13, upon allergen challenge [156,168,169]. T_H2 cytokines are not only produced by T_H2 cells. Instead, lots of other cell types are involved in the course of asthma. Basophils for instance supply help for cDCs within the LNs to support T_H2 responses. In contrast, within the lung, they can also act as effector cells and produce T_H2 cytokines by themselves. Additionally, type 2 ILCs (ILC2s) and MCs can produce T_H2 cell-associated cytokines and therefore play an important role during ongoing asthma [153,155].

IL-4 plays a central role during ongoing asthma. It is responsible for IgE and also IgG_1 synthesis by B cells. In addition, it induces the expression of adhesion molecules on endothelial cells and therefore aids the immune cell recruitment to the site of inflammation [155,168,169]. IL-13 shares many functions with IL-4 since they are both recognized by the IL-4 receptor α chain (IL-4Rα). Additionally, IL-13 is responsible for the increased mucus production by acting on goblet cells and leading to their metaplasia thereby causing BHR during asthma. Furthermore, it can act on $CD11b^+$ cDC2s to favor the recruitment of memory T_H2 cells and stimulate bronchial EpCs to release the MC growth factor SCF causing increased MC numbers within the epithelium [155,156,170,171]. Airway eosinophilia, a main characteristic of allergic asthma, is mainly caused by the cytokine IL-5. This cytokine is responsible for the development of eosinophils and their mobilization from the BM and therefore promotes tissue eosinophilia by driving activation, proliferation and survival of eosinophils in peripheral tissues [153,168,169]. Finally, IL-9 can be produced for instance by T_H2 cells, ILC2s and/or T_H9 cells. It can act as MC growth factor causing MC infiltration, growth and survival (together with IL-4 and IL-13) therefore leading to MC hyperplasia. IL-9 can therefore affect the BHR, goblet cell metaplasia and airway remodeling either directly or indirectly through the functions of MCs [153,155,172].

MC hyperplasia is also an important characteristic of allergic asthma. Upon IgE-FcεRI crosslinking, MC and basophils release bioactive mediators, like histamine, neutral proteases, lipid mediators, but also T_H2 cytokines. This amplifies the pro-inflammatory T_H2-mediated immune response but also causes vascular permeability and increased

cellular recruitment to the lung tissue. The amplification of the T_H2-mediated immune response leads, among other consequences, to the potentiated release of additional T_H2 cytokines and therefore immune cell recruitment. Finally, it drives a self-perpetuating cycle of T_H2-driven inflammation, leading to a chronic course of asthma and other atopic diseases, like AD. Additionally, MCs increase the mucus production by goblet cells by the release of mediators, like prostaglandins, leukotrienes, IL-4 and IL-13 and due to their localization within the airway smooth muscles, they also contribute to BHR [122,124,168,169,173].

In summary, allergic asthma is a chronic disease that is characterized by a highly complex network composed of lots of different immune and non-immune cells and a huge repertoire of different mediators. Based on the current understanding, many type 2-focused treatments (e.g. blocking antibodies against IL5 (Mepolizumab) or IL-4Rα (Dupilumab)) were developed that are now successfully in use. Unfortunately, not all patients respond to common, available treatments, which is most likely a result of different pathophysiological mechanisms caused by additionally or alternatively involved cell types and/or mediators (e.g. T_H17 cells, T_H1 cells, Nphs, IL-8, IL-17 etc.) [153,155,168,169]. Especially, the unresponsiveness of many patients to common (type 2-focused) treatments reflects the urgent need for extensive research to understand the underlying mechanisms more deeply and subsequently to develop improved treatment strategies that will help patients with all forms of asthma.

1.4 Aim of the study

DCs and MCs are both reported to be immune sentinels within environmental interfaces acting as a first line of defense against incoming insults. While DCs are best described for their ability to link innate and adaptive immunity by their T cell priming capacity, MCs are known as key effector cells of type I allergic reactions and host defenders against pathogens. As we recently summarized, there is increasing evidence that also MCs can act as linker between innate and adaptive immunity, most likely via the communication with DCs [125]. However, the underlying mechanisms are poorly understood. We recently showed that dermal DCs engulf intact MCG exocytosed by MCs upon skin inflammation. Consequently, MCG-bearing DCs exhibit an enhanced migratory behavior and maturation and a boosted T cell priming capacity compared to MCG-negative DCs. Thereby, we emphasized an individual feature of peripheral MCs to impact on the adaptive immunity borne within the lymphoid tissue by altering DC functions [1].
Based on this study, the main objectives of this thesis were:

1) Determining the molecular mechanisms underlying the MCG uptake by DCs.
2) Exploring the consequences of the MCG uptake on DC functions and for subsequent immune responses?

Several *in vitro*, *ex vivo* and *in vivo* methods were established and used to address these aims. First, a method to mimic the MCG uptake by DCs *in vitro* should be established to analyze the impact of the DC maturation status, endocytic mechanisms, distinct DC surface receptors and their signaling pathways on the MCG uptake mechanism. Second, by use of *in vitro* DC-T cell co-culture experiments and appropriate *in vivo* inflammation models the consequences of the MCG uptake on the DC functionality and subsequent immune responses should be analyzed.
Finally, shedding light on underlying mechanisms and consequences of the MCG uptake by DCs may help to develop future therapeutic strategies to either reduce exaggerated immune responses or purposely boost the adaptive immunity.

2 Materials

2.1 Mouse lines

All mice were bred and housed under pathogen-controlled conditions at the central animal facility (“Zentrale Tierhaltung”, ZTH) of the Otto-von-Guericke University Magdeburg (OvGU Magdeburg). All used mouse lines are summarized in Table 2.1 and were on a C57BL/6J genetic background. In all experiments, the mice were used at the age of 8 – 16 weeks. Littermates or age- and sex-matched C57BL/6JRj (wildtype, wt) mice were used as controls as depicted for each experiment. All procedures were approved by the Landesverwaltungsamt Sachsen-Anhalt (42502-2-1416UniMD and 42502-2-1633UniMD) and were performed in accordance with the institutional guidelines on animal welfare.

Prior to use, all mice (except of wt mice) were routinely analyzed for their genotype by deoxyribonucleic acid (DNA) isolation from ear skin biopsies and subsequent polymerase chain reaction (PCR) with gene-specific primers (see section 3.2.1 and Table 2.3).

Table 2.1: Inbred mouse strains used in this study.

Mouse line	International Nomenclature	Mutations	Supplier	Ref.
C57BL/6JRj	-	-	Janvier Labs Cat# JAX 000664	-
Card9	-	Conventional *knockout* (exon deletion)	Collaboration Partner (Prof. Dr. Bernd Lepenies)	[174]
CD11c-Cre x Syk-FL	B6.Cg-Tg(Itgax-cre)1-1Reiz/J [C57BL/6J] x B6.129-Gt(ROSA)26Sor$^{tm1(cre/ERT2)Tyj}$/J [C57BL/6J] x B6.129P2-Sykb$^{tm1.2Tara}$/J [C57BL/6J]	Transgenes (CD11c-Cre & R26-CreERT2), loxP insertion (Syk-FL)	In-house breeding	-

Table 2.1 (continue): Inbred mouse strains used in this study.

Mouse line	International Nomenclature	Mutations	Supplier	Ref.
CD11c-GFP	B6.FVB-1700016L21Rik$^{Tg(Itgax-DTR/EGFP)57Lan}$/J	Transgene	Janvier Labs Cat# JAX 004509	[175]
LysM-GFP	B6.129(Cg)-Lyz2$^{tm1.1Graf}$/Mmmh	Transgene	Mutant Mouse Resource & Research Centers (MMRRC) Cat# 012039-MU	[176]
Mcpt5-Cre x R-DTA	B6.129P2-Gt(ROSA)26Sor$^{tm1(DTA)Lky}$/J x B6-Tg(Cma1-cre)#Roer	Transgenes	In-house breeding	[177 – 179]
MCL	C57BL/6-Clec4d$^{tm1.1Cfg}$/Mmucd	Conventional *knockout* (exon deletion)	Collaboration Partner (Prof. Dr. Bernd Lepenies), MMRRC Cat# 031935-UCD	[180]
MCL x SIGNR3	C57BL/6-Clec4d$^{tm1.1Cfg}$/Mmucd x C57BL/6-Cd209d$^{tm1.1Cfg}$/Mmucd	Conventional *knockouts* (exon deletions)	In-house breeding	-
MyD88-FL x CD11c-Cre	B6.129P2(SJL)-Myd88^{tm1Defr}/J x B6.Cg-Tg(Itgax-cre)1-1Reiz/J [C57BL/6J]	loxP insertion (MyD88-Fl), Transgene (CD11c-Cre)	In-house breeding	[181]
OTII	C57BL/6-Tg(TcraTcrb)425Cbn/J, OT-II	Transgene	Janvier Labs Cat# JAX 004194	[182]
SIGNR3	C57BL/6-Cd209d$^{tm1.1Cfg}$/Mmucd [C57BL/6J]	Conventional *knockout* (exon deletion)	Collaboration Partner (Prof. Dr. Bernd Lepenies), MMRRC Cat# 031934-UCD	[44]
TRIF	C57BL/6J-Ticam1$^{Lps2/J}$	Loss-of-function point mutation	Collaboration Partner (Prof. Dr. Andreas Müller)	[183]

Cre-lox system

In 1987, the so-called Cre/*lox* or Cre/*loxP* system was developed and used for the first time [184]. Today, it is widely utilized to generate mouse models harboring cell-specific gene (in-) activation [185,186]. Due to genetic and pathophysiological similarities between mice and humans, it is a suitable tool for studying human diseases and for analyzing the impact of certain genes in a spatial and temporal manner [187].

The abbreviation “Cre” stands for Cre recombinase, a 38 kDa tyrosine site-specific DNA recombinase produced in bacteriophage P1. This recombinase is characterized by its recognition of a specific 34 base pair (bp) DNA sequence, the so-called *loxP* (**l**ocus **o**f **x**-over, P1) sites. As depicted in Figure 2.1A, the Cre recombinase firstly creates a DNA loop by bringing together the *loxP* sites. Subsequently, the looped DNA sequence is inverted or excised dependent on the orientation of the *loxP* sites and therefore leading to gene (in-) activation [186,187].

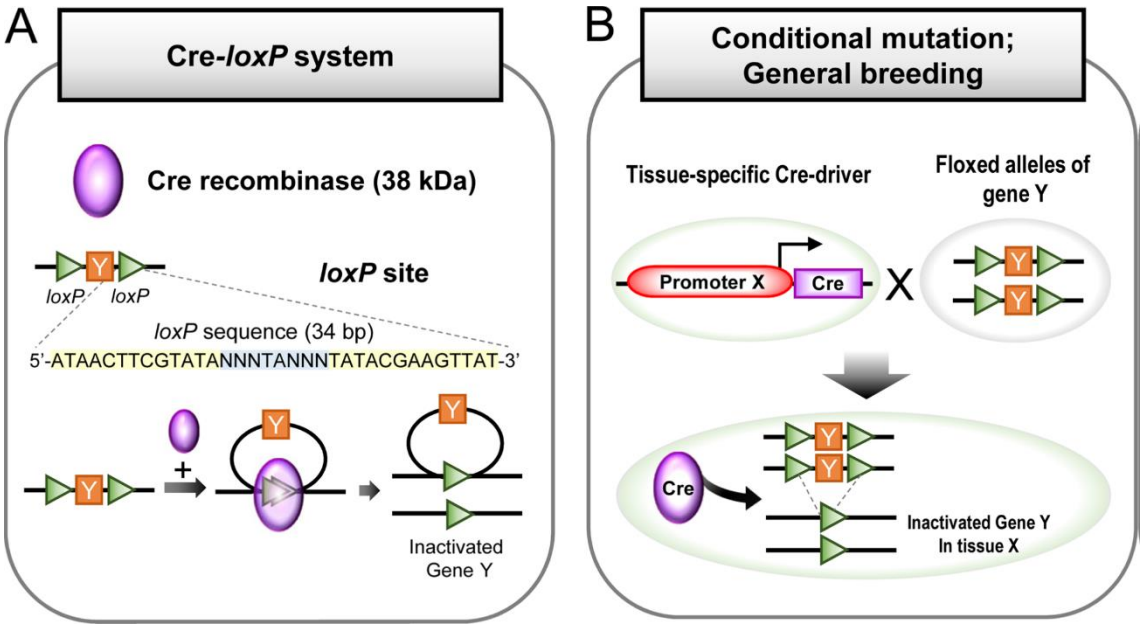

Figure 2.1: The Cre/*loxP* system. (A) Schematic representation figure of the Cre/*loxP* system. The Cre recombinase recognizes *loxP* sites, brings them together and thereby creates a DNA loop. Depending on the orientation of the *loxP* sites, the looped sequence is inverted or excised, leading to gene (in-) activation. (B) Crossing a mouse strain that expresses the Cre recombinase, under the control of a specific promotor, with a mouse strain expressing a *loxP* flanked GOI leads to mice with cell- or tissue-specific gene (in-) activation. Figure taken from Kim *et al.* (2018) [187].

Upon discovery and first applications in yeast and cultured mammalian cells, this system is used today for generating transgenic mice [184,186,188]. For this, a Cre-driver strain is set up, in which the Cre recombinase is expressed by a cell- or tissue-specific promotor. There are different ways of inserting the Cre transgene into the mouse genome

that are described, for instance in Song *et al.* [186] but will not be further described in detail within this thesis. Additionally, a mouse strain is generated containing a “floxed” (*loxP* flanked) DNA sequence of interest. Figure 2.1B shows the general breeding strategy for generating a so-called conditional *knockout* mouse line. Crossing a line containing Cre under a specific promoter with a line containing floxed alleles of a certain gene, will generate offspring that exhibit a certain gene (in-) activation specifically in distinct cells or tissues [186,187].

Kim *et al.* summarizes a list of commonly used tissue-specific promoters used for the generation of Cre lines [187]. As depicted in Table 2.1, two different Cre mouse lines for specific gene inactivation in distinct cell populations were used in this thesis. The CD11c-Cre mouse line [189] was used for the inactivation of *Myd88* and *Syk* specifically in DCs, while the Mcpt5-Cre line [178] was used to specifically target Mcpt5-expressing cells, like CTMCs.

2.2 Chemicals and reagents

Table 2.2: Chemicals and reagents.

Reagent	Source	Cat#
100 bp DNA ladder	Invitrogen	15628050
1-fluoro-2,4-dinotrobenzene (DNFB)	Sigma-Aldrich	D1526-25ML
2-propanol (Isopropanol)	Carl Roth	CP41.2
5-(N,N-dimethyl)amiloride hydrochloride (DMA)	Sigma-Aldrich	A4562
Accutase Cell Detachment Solution	Capricorn Scientific	ACC-1B
Acetic acid, 100%	Carl Roth	6755.1
Acetone	Fisher Scientific/J.T.Baker	8002
Avidin, Egg white	Invitrogen	A2667
Bovine serum albumin (BSA)	GERBU Biotechnik GmbH	15030500
Brefeldin A Solution (1000X)	BioLegend	420601
$CaCl_2x2H_2O$	AppliChem GmbH	131232 1210
Calcium ionophore A23187	Sigma-Aldrich	C7522-5MG
CountBright™ Absolute Counting Beads	Thermo Fisher Scientific	C36950
Dibutyl-phthalate	Sigma-Aldrich	524980-25ML
Dimethyl dicarbonate (DMDC)	Merck Millipore	8187580100
Dimethyl sulfoxide (DMSO)	Sigma-Aldrich	D5879-100ml
DNase I, grade II, from bovine pancreas	Roche/Sigma-Aldrich	10104159001

Table 2.2 (continue): Chemicals and reagents.

Reagent	Source	Cat#
ELISA Stop solution	Thermo Fisher Scientific	SS03
Eosin	Carl Roth	3137.2
Epredia™ Shandon™ Harris Hematoxylin	Epredia	6765003
Ethanol, 99 % denatured with MEK, IPA and Bitrex® (min. 99.8 %)	Th. Geyer	2212.9010
Ethanol, absolute	Th. Geyer/CHEMSOLUTE®	2246.1000
Ethidiumbromid solution, 1% (10 mg/ml)	Carl Roth	2218.1
Ethylenediamine tetraacetic acid disodium salt dihydrate (EDTA)	Carl Roth	8043.2
Fetal bovine serum (FBS) SUPERIOR	PAN Biotech	S0615
Fluorescein-5(6)-isothiocyanate (FITC)	Sigma-Aldrich	F3651-100MG
Formaldehyde, 30%, free of methanol	Carl Roth	4235.1
Gibco™ 2-mercaptoethanol (β-mercaptoethanol)	Thermo Fisher Scientific	21985023
GlutaMAX™ Supplement	Thermo Fisher Scientific	35050038
HCl	Carl Roth	6331.1
HEPES	Carl Roth	HN78.1
House Dust Mite (HDM) extract (*Dermatophagoides pteronyssinus*)	Citeq biologics	02.01.85
Hyaluronidase	Sigma-Aldrich	H3506
Isofluran CP	cp pharma	G83F20A
Isotonic sodium chloride solution (0.9% NaCl)	Fresenius Kabi	06605514
KCl	Carl Roth	6781.3
Ketamin, 100 mg/ml	cp pharma	19D234
KH_2PO_4	Th. Geyer/ CHEMSOLUTE®	16480250
$KHCO_3$	Carl Roth	p748.1
Liberase™ TL	Roche/Sigma-Aldrich	5401020001
Liberase™ TM	Roche/Sigma-Aldrich	5401119001
Lipofectamine™ RNAiMAX Transfection Reagent	Invitrogen	13778150
Lipopolysaccharide (LPS, *S. enterica* serotype Minnesota)	Sigma-Aldrich	L2137
Methanol	Carl Roth	8388.1
$MgCl_2x6H_2O$	AppliChem GmbH	131396 1210
Molecular Probes™ Ionomycin, Calciumsalt	Thermo Fisher Scientific	I24222
$Na_2HPO_4x2H_2O$	Th. Geyer/ CHEMSOLUTE®	8622

Table 2.2 (continue): Chemicals and reagents.

Reagent	Source	Cat#
NaCl	Th. Geyer/ CHEMSOLUTE®	13671000
Nail polish	varying manufacturers	-
NH_4Cl	Carl Roth	p726.1
Nuclease-free water	Qiagen	129114
Olive oil	Sigma-Aldrich	O1514-100ML
Ovalbumin peptide OVA323-339	InvivoGen	vac-isq
Paraffin (Surgipath Paraplast)	Leica Biosystems	39602012
Paraformaldehyde solution, 4% in PBS	Santa Cruz Biotechnology	sc-281692
Paraformaldehyde, 4% buffered (ROTI® Histofix, 4%)	Carl Roth	P087.1
Penicillin/Streptomycin	PAN Biotech	P06-07050
Phorbol 12-myristate 13-acetate (PMA)	Sigma-Aldrich	P1585-1MG
ProTaqs® Clear	quartett	400301105
ProTaqs® PARAmount	quartett	BP-167H
Proteinase K	Carl Roth	7528.5
Rompun, 2%, 20 mg/ml	BAYER	KP0EB50
RPMI1640 Medium	PAN Biotech	P04-18500
RPMI1640 w.o. phenol red	Biochrom/Merck Milliore	F1275
SDS	AppliChem GmbH	A2572,0250
Sodium pyruvate	PAN Biotech	P04-43100
Tissue-Tek® O.C.T. Compound	Sakura	12351753
TRIS	Carl Roth	4855.2
Triton® X-100	Carl Roth	3051.4
Trypan Blue Solution	Sigma-Aldrich	T8154-100ml
UltraPure™ DNase/RNase-Free Distilled Water	Thermo Fisher Scientific	10977015

AppliChem GmbH (Darmstadt, Germany), BAYER (Leverkusen, Germany), BioLegend (San Diego; USA), Capricorn Scientific (Ebsdorfergrund, Germany), Carl Roth (Karlsruhe, Germany), Citeq biologics (Groningen, The Netherlands), cp pharma (Burgdorf, Germany), Epredia (Portsmouth, UK), Fisher Scientific/J.T.Baker (Schwerte, Germany), Fresenius Kabi (Bad Homburg, Germany), GERBU Biotechnik GmbH (Heidelberg, Germany), Invitrogen (Carlsbad, USA), InvivoGen (Toulouse, France), Leica Biosystems (Wetzlar, Germany), Merck Millipore (Darmstadt, Germany), PAN Biotech (Aidenbach, Germany), Santa Cruz Biotechnology (Heidelberg, Germany), Qiagen (Hilden, Germany), quartett (Berlin, Germany), Sakura (Umkirch, Germany), Sigma-Aldrich (Taufkirchen, Germany), Thermo Fisher Scientific (Waltham, USA), Th. Geyer/ CHEMSOLUTE® (Renningen, Germany), Vector Laboratories (Burlingame, USA)

2.3 Oligonucleotides and recombinant proteins

2.3.1 Primers used for genotyping PCR

All primer sequences are depicted from the 5' end to the 3'. Primer pairs for each target were premixed and diluted to a concentration of 10 µM. In Table 2.3, indicated concentrations show the final concentration of primers within PCR reactions. The 200 bp control (ctrl) served as PCR control during PCRs for *CD11c-Cre* (400 nM 200 bp ctrl) or *CreERT2_3* (200 nM 200 bp ctrl). The *IL-2* primers were used as PCR control during PCRs for general Cre (200 nM IL-2), green fluorescent protein *(GFP*, 400 nM IL-2) or *R-DTA* wt (200 nM IL-2).

Table 2.3: Summary of primers that were used for genotyping PCRs and ordered at Thermo Fisher Scientific.

Target	Forward Primer	Reverse Primer 1	Reverse Primer 2
200 bp ctrl (200/400 nM)	CAA ATG TTG CTT GTC TGG TG	GTC AGT CGA GTG CAC AGT TT	
***Card9* (200 nM)**	CCA TAG AGG ACT ATA GCT GCC TAC AG	GGG TGG GAT TAG ATA AAT GCC TGC TC	TGG TTG ACC CAG TGG ACA GAC ATT TC
***CD11c-Cre* (200 nM)**	ACT TGG CAG CTG TCT CCA AG	GCG AAC ATC TTC AGG TTC TG	-
***CreERT2_3* (200 nM)**	AAAATTTGCCTGCAT TACCG	ATGTTTAGCTGGCCC AAATG	
***general Cre* (400 nM)**	GGA AAT GGT TTC CCG CAG AAC CTG A	GAT GAG TTG CTT CAA AAA TCC CTT CCA	
***GFP* (200 nM)**	TCC TTG AAG AAG ATG GTG CG	AAG TTC ATC TGC ACC ACC G	
***IL-2* (200/400 nM)**	CTA GGC CAC AGA ATT GAA AGA TCT	GTA GGT GGA AAT TCT AGC ATC ATC C	
***MCL* (200 nM)**	GTA TAA TGT ATG CTA TAC GAA GTT ATC TCG AG	CTG AAA AAA CTT ATT GCT CAT AAT TTA CAC AGT AT	GGA GGC TTT GGG AGC ACA TG
***Mcpt5-Cre* (200 nM)**	ACA GTG GTA TTC CCG GGG AGT GT	GTC AGT GCG TTC AAA GGC CA	TGA GAA GGG CTA TGA GTC CCA
***MyD88-FL* (200 nM)**	GTT GTG TGT GTC CGA CCG T	GTC AGA AAC AAC CAC CAC CAT GC	CCA CCC TTG ATG ACC CCC TA

Table 2.3 (continue): Summary of primers that were used for genotyping PCRs.

Target	Forward Primer	Reverse Primer 1	Reverse Primer 2
***R-DTA* mut (200 nM)**	CGA CCT GCA GGT CCT CG	CTC GAG TTT GTC CAA TTA TGT CAC	
***R-DTA* wt (200 nM)**	CCA AAG TCG CTC TGA GTT GTT ATC	GAG CGG GAG AAA TGG ATA TG	
***SIGNR3* (200 nM)**	TCC CCC TTC TGC CCT TTT GG	CCA ATT CCC AGC TTC CAC GG	GTT TGG GGG AAA TCC AGC TG
***Syk-FL* (200 nM)**	GCC CGT TCT GTG CCT ACT GG	TAG CTA ACC AAA CCC ACG GC	

Thermo Fisher Scientific (Waltham, USA)

2.3.2 Small interfering ribonucleic acids (siRNAs)

Table 2.4: siRNAs.

siRNA	Source	Cat#
Silencer® Select Negative Control siRNA #1	Thermo Fisher Scientific	4390843
Silencer® Select siRNA murine MCL, Sense-Sequence: 5'-CCUUGUCACUUUGAGGUGAtt-3' (siRNA ID s70000)	Thermo Fisher Scientific	4390771
Silencer® Select siRNA murine SIGNR3, Sense-Sequence: 5'-CUACUUUUCUGGAUCUGUAtt-3' (siRNA ID s100792)	Thermo Fisher Scientific	4390771

Thermo Fisher Scientific (Waltham, USA)

2.3.3 CLR-hFc fusion proteins

The CLR-hFc fusion protein library (fusion of carbohydrate recognition domains of CLR with human IgG1-Fc fragment) was generated as described in Mayer et al. [190] and was kindly provided by Prof. Dr. Bernd Lepenies (University of Veterinary Medicine Hannover, Institute for Immunology).

Fusion proteins were generated and used for the following CLRs: human L-SIGN (hL-SIGNR, or hDC-SIGNR), hDC-SIGN, murine CLEC12A (mCLEC12A, or mMICL), mLangerin, mDCAR, mMincle, mMGL-1, mSIGNR1, mSIGNR3, mSIGNR5, mDectin-1, mDectin-2, mDCL-1 (or mCLEC13A), mMDL-1 (or CLEC5A), mCLEC9A, mCLEC12B, mCLEC2 and mMCL. As control served the human IgG1-Fc fragment alone without fused CLR recognition domains (hFc control).

2.4 Buffers and Solutions

The distilled water that was used for the preparation of buffers was generated using a Milli-Q® water purification system.

Table 2.5: Buffers and solutions.

Buffer/Solution	Final Concentration	Component	Instructions
1x PBS	2.68 mM	KCl	in distilled water (pH 7.4 – 7.5)
	1.47 mM	KH_2PO_4	
	8.1 mM	$Na_2HPO_4x2H_2O$	
	136.9 mM	NaCl	
1x MACS buffer	2 mM	EDTA	in 1x PBS
	0.5% w/v	BSA	
1x Erythrocyte-lysis-buffer	155 mM	NH_4Cl	in distilled water
	10 mM	$KHCO_3$	
	0.13 mM	EDTA	
Ear digestion medium	198 U/ml	DNase I	in serum-free RPMI1640
	31.25 µg/ml	Liberase™ TM	
	250 µg/ml	Hyaluronidase	
Lung digestion medium	10% v/v	FBS	in RPMI1640
	2 mM	GlutaMAX™ Supplement	
	100 U/ml	Penicillin	
	100 µg/ml	Streptomycin	
	50 µM	β-mercaptoethanol	
Lectin-binding buffer	50 mM	HEPES	in distilled water (pH 7.2, sterile)
	5 mM	$MgCl_2x6H_2O$	
	5 mM	$CaCl_2x2H_2O$	
Ketanest	10 mg/ml	Ketamin	in 0.9% NaCl (sterile)
	1 mg/ml	Rompun	
Tissue lysis buffer	100 mM	TRIS (stock 1 M pH 8.5)	in distilled water
	5 mM	Na_2EDTA (stock 0.5 M pH 8.0)	
	0.2% w/v	SDS (stock 10% w/v pH 7.2)	
	200 mM	NaCl	

Table 2.5 (continue): Buffers and solutions.

Buffer/Solution	Final Concentration	Component	Instructions
1x TAE (TRIS-acetate-EDTA buffer)	40 mM	TRIS	in distilled water
	1 mM	Na_2EDTA (stock 0.5 M pH 8.0)	
	20 mM	Acetic acid	
0.5% FA	1.6% v/v	Formaldehyde, 30%	in 1x PBS

2.5 Cell culture media and cytokines

Table 2.6: Culture media.

Medium	Concentration	Component	Instructions
Culture medium	10% v/v	FBS	in RPMI1640 (sterile)
	100 U/ml	Penicillin	
	100 µg/ml	Streptomycin	
	1 mM	Sodium pyruvate	
	50 µM	β-mercaptoethanol	
Culture medium without phenol red	10% v/v	FBS	in RPMI1640 w.o. phenol red (sterile)
	100 U/ml	Penicillin	
	100 µg/ml	Streptomycin	
	1 mM	Sodium pyruvate	
	50 µM	β-mercaptoethanol	

2.5.1 Cytokines for *in vitro* differentiation of murine DCs and MCs

Table 2.7: Cytokines used for *in vitro* differentiation of murine DCs and MCs.

Cytokine	Source	Cat#
Recombinant murine IL-3	PeproTech	213-13
Recombinant murine IL-4	PeproTech	214-14
Recombinant murine GM-CSF	PeproTech	315-03
Recombinant murine SCF	PeproTech	250-03

PeproTech (Hamburg, Germany)

2.6 Antibodies and dyes

2.6.1 Antibodies

Table 2.8: Antibodies used for *in vitro* re-stimulation of T cells.

Antibody (Clone)	Source	RRID
Armenian Hamster monoclonal anti-mouse CD3ε (145-2C11)	BioLegend	AB_11150783
Syrian Hamster monoclonal anti-mouse CD28 (37.51)	BioLegend	AB_11150408

BioLegend (San Diego, USA)

Table 2.9: Antibodies used for flow cytometry or fluorescence-activated cell sorting (FACS).

Antibody (Clone)	Dilution	Source	RRID
Armenian Hamster monoclonal anti-mouse CD3ε (145-2C11)	1:100	BioLegend	AB_312685
Syrian Hamster monoclonal anti-mouse CD3ε (500A2)	1:200	eBioscience	AB_842786
Rat monoclonal anti-mouse CD4 (GK1.5)	1:160	eBioscience	AB_11150050
Rat monoclonal anti-mouse CD4 (GK1.5)	1:200	eBioscience	AB_469320
Rat monoclonal anti-mouse CD4 (RM4-5)	1:300	BioLegend	AB_493374
Rat monoclonal anti-mouse CD8a (53-6.7)	1:200	BioLegend	AB_2563057
Rat monoclonal anti-mouse/human CD11b (M1/70)	1:200	BioLegend	AB_893233
Armenian Hamster monoclonal anti-mouse CD11c (N418)	1:100	BioLegend	AB_493568
Armenian Hamster monoclonal anti-mouse CD11c (N418)	1:40	BioLegend	AB_830649
Armenian Hamster monoclonal anti-mouse CD11c (N418)	1:40	BioLegend	AB_10900261
Rat monoclonal anti-mouse CD25 (PC61)	1:160	BioLegend	AB_2562611
Rat monoclonal anti-mouse CD44 (IM7)	1:80	BioLegend	AB_312959
Rat monoclonal anti-mouse CD45 (30-F11)	1:67	BioLegend	AB_2562612
Rat monoclonal anti-mouse CD45R (RA3-6B2)	1:300	BioLegend	AB_312991
Rat monoclonal anti-mouse CD45R (RA3-6B2)	1:100	BD Biosciences	AB_396793
Rat monoclonal anti-mouse CD62L (MEL-14)	1:200	BioLegend	AB_2285839
Rat monoclonal anti-mouse CD86 (GL-1)	1:20	BioLegend	AB_439783

Table 2.9 (continue): Antibodies used for flow cytometry or FACS.

Antibody (Clone)	Dilution	Source	RRID
Armenian Hamster monoclonal anti-mouse CD103 (2E7)	1:20	eBioscience	AB_ 465798
Armenian Hamster monoclonal anti-mouse CD103 (2E7)	1:200	BioLegend	AB_535949
Rat monoclonal anti-mouse CD169 (3D6.112)	1:40	BioLegend	AB_10915697
Rat monoclonal anti-mouse CD185/CXCR5 (L138D7)	1:300	BioLegend	AB_2562209
Rat monoclonal anti-mouse CD197/CCR7 (4B12)	1:17	BioLegend	AB_389358
Rat monoclonal anti-mouse CD279/PD-1 (29F.1A12)	1:300	BioLegend	AB_1877232
Rat monoclonal anti-mouse F4/80 (BM8)	1:40	eBioscience	AB_2735036
Goat polyclonal anti-human Fc	1:200	Jackson Immuno Research	AB_2337690
Rat monoclonal anti-mouse FoxP3 (FJK-16a)	1:100	eBioscience	AB_465243
Rat monoclonal anti-mouse IL-4 (11B11)	1:100	BioLegend	AB_10898116
Rat monoclonal anti-mouse IL-4 (11B11)	1:200	BioLegend	AB_315318
Rat monoclonal anti mouse IL-13 (eBio13A)	1:200	eBioscience	AB_2016708
Rat monoclonal anti-mouse Ly-6G (1A8)	1:100	BioLegend	AB_2561340
Rat monoclonal anti-mouse MHCII (M5/114.15.2)	1:200	eBioscience	AB_1272204
Rat monoclonal anti-mouse MHC II (M5/114.15.2)	1:100	BioLegend	AB_313323
Mouse monoclonal anti-mouse Syk (5F5)	1:100	BioLegend	AB_2565305
Rat monoclonal anti-mouse TNF-a (MP6-XT22)	1:200	BioLegend	AB_315429

BD Biosciences (Heidelberg, Germany), BioLegend (San Diego, USA), eBioscience/Thermo Fisher Scientific (Waltham, USA), Jackson Immuno Research (West Grove, USA)

Table 2.10: Antibodies used for multi-epitope ligand cartography (MELC).

Antibody (Clone)	Dilution	Source	RRID
Rat monoclonal anti-mouse CD3 (17A2)	1:80	BioLegend	AB_389301
Rat monoclonal anti-mouse CD8a (53-6.7)	1:40	BioLegend	AB_389304
Rat monoclonal anti-mouse CD11b (M1/70)	1:80	eBioscience	AB_469901
Armenian Hamster monoclonal anti-mouse CD11c (N418)	1:120	BioLegend	AB_389306

Table 2.10 (continue): Antibodies used for MELC.

Antibody (Clone)	Dilution	Source	RRID
Rat monoclonal anti-mouse CD31 (390)	1:40	BioLegend	AB_493408
Rat monoclonal anti-mouse CD45 (30-F11)	1:960	BioLegend	AB_493531
Rat monoclonal anti-mouse CD45R (RA3-6B2)	1:240	BioLegend	AB_389308
Rat monoclonal anti-mouse LYVE1 (ALY7)	1:120	eBioscience	AB_10597449
Rat monoclonal anti-mouse MHCII (2G9)	1:480	BD Biosciences	AB_394958

BioLegend (San Diego, USA), eBioscience/Thermo Fisher Scientific (Waltham, USA), BD Biosciences (Heidelberg, Germany)

2.6.2 Avidins

Table 2.11: Avidin conjugates.

Avidins	Source	Cat#
Avidin, TexasRed (TR) conjugate	Invitrogen	A820
Avidin, Alexa Fluor™ 488 (AF488) conjugate	Invitrogen	A21370

Invitrogen (Carlsbad, USA)

Additionally, unlabeled avidin was fluorescently labeled using Alexa Fluor™ 647 Protein Labeling Kit according to the manufacturers' instructions. The final concentration of Alexa Fluor™ 647 (AF647)-labeled avidin could not be determined with the spectrophotometer. Therefore, prior to use, several dilutions were tested for optimal staining in immunofluorescence and immune histochemistry.

2.6.3 Dyes for microscopy and flow cytometry

Table 2.12: Dyes used for microscopy and flow cytometry.

Dyes	Source	Cat#
Bisbenzimid H 33342 (Hoechst33342)	Sigma-Aldrich	B2261-25MG
CellTrace™ CFSE Cell Proliferation Kit, for Flow Cytometry	Thermo Fisher Scientific	C34554

Sigma-Aldrich (Taufkirchen, Germany), Thermo Fisher Scientific (Waltham, USA)

2.7 Commercial assays

Table 2.13: Commercial assays.

Commercial assays	Source	Cat#
Alexa Fluor™ 647 Protein Labeling Kit	Invitrogen	A20173
CD117 MicroBeads, mouse	Miltenyi Biotec	130-091-224
DreamTaq Green DNA Polymerase	Thermo Fisher Scientific	EP0714
eBioscience™ Intracellular Fixation & Permeabilization Buffer Set	Thermo Fisher Scientific	88-8824-00
FoxP3 Staining Buffer Set	Miltenyi Biotec	130-093-142
IgE Mouse Uncoated ELISA Kit with Plates	Thermo Fisher Scientific	88-50460-22
LEGENDplex™ Mouse Mix and Match Panels	BioLegend	customized
Maxima First Strand cDNA Synthesis Kit for RT-qPCR	Thermo Fisher Scientific	K1642
Pan T Cell Isolation Kit II, mouse	Miltenyi Biotec	130-095-130
Takyon Low ROX Probe 2X MasterMix dTTP blue	Eurogentec	UF-LPMT-B0701
TaqMan™ Gene Expression Assay murine *Card9* (Mm01327594_m1)	Thermo Fisher Scientific	4331182
TaqMan™ Gene Expression Assay murine *CLEC12B* (Mm01183406_m1)	Thermo Fisher Scientific	4448892
TaqMan™ Gene Expression Assay murine *DCAR2* (Mm00651312_m1)	Thermo Fisher Scientific	4448892
TaqMan™ Gene Expression Assay murine *Dectin-1* (Mm01183349_m1)	Thermo Fisher Scientific	4448892
TaqMan™ Gene Expression Assay murine *MCL* (Mm00501738_m1)	Thermo Fisher Scientific	4331182
TaqMan™ Gene Expression Assay murine *Mincle* (Mm01183703_m1)	Thermo Fisher Scientific	4448892
TaqMan™ Gene Expression Assay murine *SIGNR3* (Mm00459972_m1)	Thermo Fisher Scientific	4331182
TaqMan™ Gene Expression Assay murine *Syk* (Mm01333032_m1)	Thermo Fisher Scientific	4331182
TaqMan™ Gene Expression Assay murine *Tbp* (Mm01277042_m1)	Thermo Fisher Scientific	4448490
Quick-RNA MicroPrep Kit	Zymo Research	R1051

BioLegend (San Diego, USA), Eurogentec (Seraing, Belgium), Invitrogen (Carlsbad, USA), Miltenyi Biotec (Bergisch Gladbach, Germany), Thermo Fisher Scientific (Waltham, USA), Zymo Research (Freiburg, Germany).

2.8 Consumables

Table 2.14 provides a list of specific consumables that were used within this thesis. Standard consumables, including reaction tubes, cell cultures flasks, petri dishes, cannulas, syringes and pipette tips, were used from varying manufacturers and therefore will not be listed separately.

Table 2.14: Specific consumables.

Product	Source	Cat#
Coverslips, thickness 1, 22 x 22 mm	Carl Roth	H874.2
Menzel-Gläser SUPERFROST® PLUS	G. Menzel B.V. & Co. KG	J1800AMNZ
MicroAmp® Fast 96-Well reaction plate (0.1 mL)	Thermo Fisher Scientific	4346907
MicroAmp® Optical Adhesive Film	Thermo Fisher Scientific	4311971

Carl Roth (Karlsruhe, Germany), G. Menzel B.V. & Co. KG (Braunschweig, Germany), Thermo Fisher Scientific (Waltham, USA)

2.9 Special equipment and devices

Table 2.15: Special equipment and devices.

Device	Source
Amnis® FlowSight® Imaging Flow Cytometer	Luminex
BD FACSAria™ III Cell Sorter	BD Bioscience
BD LSRFortessa™ Flow Cytometer	BD Bioscience
Cell Counter Luna II	Logos Biosystems
CMOS camera Hamamatsu Orca Flash 4.0 v2	Hamamatsu Photonics K.K.
DNA/RNA UV-Cleaner Box UVT-B-AR	Biosan
Heraeus Multifuge 3SR+ Centrifuge	Thermo Fisher Scientific
Herolab Transilluminator with a Herolab E.A.S.Y B-455-F camera	Herolab GmbH
CO_2 Incubator HERA cell 240	Thermo Fisher Scientific
Leica inverted confocal microscope system SP8	Leica Microsystem
Leica inverted wide-field fluorescence microscope DMI6000	Leica Microsystem
Megafuge ST4R Plus	Thermo Fisher Scientific
Microcentrifuge 5415 R/Microcentrifuge 5424 R	Eppendorf AG
Milli-Q® water purification system	Merck Millipore
MS/LC columns	Miltenyi Biotec

Table 2.15 (continue): Special equipment and devices.

Device	Source
NanoDrop 2000 Spectrophotometer	Thermo Fisher Scientific
Neubauer hemacytometer	Glaswarenfabrik Karl Hecht GmbH & CO KG
OctoMACS™/QuadroMACS™ Separator	Miltenyi Biotec
QuantStudio 3 Real-Time-PCR-System	Thermo Fisher Scientific
Precision thickness gage	Mitutoyo Deutschland GmbH
Thermocycler T3000	Biometra GmbH
ThermoMixer F1.5	Eppendorf AG
UV5Nano UV/VIS-Excellence spectrophotometer	Mettler-Toledo GmbH

BD Biosciences (Heidelberg, Germany), Biometra GmbH (Göttingen, Germany), Biosan (Riga, Latvia), Eppendorf AG (Hamburg, Germany), Hamamatsu Photonics K.K. (Hamamatsu City, Japan), Herolab GmbH (Wiesloch, Germany), Glaswarenfabrik Karl Hecht GmbH & CO KG (Sondheim vor der Röhn, Germany), Leica Microsystems (Wetzlar, Germany), Logos Biosystems (Villeneuve d'Ascq, France), Luminex ('s-Hertogenbosch, The Netherlands), Merck Millipore (Darmstadt, Germany), Mettler-Toledo GmbH (Gießen, Germany), Miltenyi Biotec (Bergisch Gladbach, Germany), Mitutoyo Deutschland GmbH (Neuss, Germany), Thermo Fisher Scientific (Waltham, USA)

2.10 Software and algorithms

Table 2.16: Software and algorithms.

Device	Source
Amnis® IDEAS Application (for Windows) Version 6.2	Luminex
CellProfiler software	[191]
Cytobank analysis software	Beckman Coulter Life Sciences
FlowJo™ Software (for Windows) Version 10	BD Biosciences
GraphPad Prism (for Windows) Version 9.0.0	Dotmatics Limited
ImageJ/Fiji	Open source [192]
LAS X Software	Leica Biosystems
LEGENDplex Software (for Windows) Version 8.0	BioLegend
QuantStudio™ Design and Analysis Software (for Windows) Version 1.5	Thermo Fisher Scientific

BD Biosciences (Heidelberg, Germany), Beckman Coulter Life Sciences (Krefeld, Germany), BioLegend (San Diego, USA), Dotmatics Limited (Windhill, UK), Leica Biosystems (Wetzlar, Germany), Luminex ('s-Hertogenbosch, The Netherlands), Thermo Fisher Scientific (Waltham, USA)

3 Methods

3.1 Cell-biological methods

3.1.1 Generation of bone marrow-derived dendritic cells (BMDCs)

In general, BMDCs were obtained as previously published by Prof. Dr. Anne Dudeck and her colleagues [91].

Mice derived from indicated mouse lines were sacrificed by cervical dislocation under isoflurane anesthesia. The hint limbs were disinfected with 70% ethanol. The skin, muscles and paws were cut off and femur and tibia removed by dislocating the hip joints. Under sterile conditions, femur and tibia were separated and the condyles were cut off with scissors and forceps. The bones of one leg were placed in a sterile 0.5 ml microcentrifuge tube with a hole in the bottom, which was subsequently placed in a 1.5 ml microcentrifuge tube containing 100 µl sterile 1x PBS and centrifuged at 16,000 g for 15 seconds. The BM cells of both legs were resuspended in 1 ml sterile 1x PBS and filtered through a cell strainer (100 µm pore diameter) to remove bone fragments and cell aggregates. To eliminate erythrocytes, the cell suspensions were precipitated at 365 g and 4°C for 5 min and subsequently resuspended in 1 ml 1x erythrocyte-lysis-buffer (Table 2.5) per mouse and incubated for 1 min at room temperature (RT). The lysis reaction was stopped by administration of 9 ml sterile 1x PBS and subsequent centrifugation at 365 g and 4°C for 5 min. Finally, the BM cells of one mouse were resuspended in 20 ml culture medium (Table 2.6) with 10 ng/ml recombinant murine GM-CSF and transferred to a 75 cm² cell culture flask. The cells were incubated at 37°C and 5% CO_2 under humid atmosphere. Non-adherent cells were removed after 24 h and replaced by fresh culture medium. After 96 h, culture medium was replaced and the concentration of GM-CSF reduced to 5 ng/ml. Additional 10 ng/ml recombinant murine IL-4 for either 3 or 10 days was used for differentiation into matDCs. Adherent imDCs and non-adherent matDCs were used earliest after 7 days of culture. The cell counts were determined using a Neubauer hemacytometer.

3.1.2 Generation of peritoneal cultured mast cells (PCMCs)

In general, PCMCs, as a model of mature CTMCs, were obtained as previously published by Prof. Dr. Anne Dudeck and her colleagues [91].

Wt mice were sacrificed under isoflurane anesthesia by increasing the isoflurane concentration to a lethal dose, until they showed no pedal reflexes anymore. A cervical dislocation should be avoided due to possible bleeding into the peritoneal cavity. Subsequently, the abdomen was disinfected with 70% ethanol in distilled water and the skin was removed without penetrating the abdominal wall. The peritoneal cavity was rinsed with 5 ml ice-cold, sterile 1x PBS through the abdominal wall by using a 5 ml-syringe with a 19G cannula. The cell suspension was subsequently transferred into 50 ml reaction tubes. For most experiments, cells of 15 – 20 mice were pooled and centrifuged at 365 g and 4°C for 5 min. Peritoneal cells of two mice were resuspended in 5 ml culture medium with 10 ng/ml IL-3 and 30 ng/ml SCF and transferred in 25 cm^2 cell culture flasks. The cells were incubated at 37°C and 5% CO_2 under humid atmosphere. To enhance the purity of PCMCs, non-adherent cells were removed after 48 h and replaced by fresh culture medium. After one week of culture, adherent macrophages were removed to further enhance the purity of PCMCs. PCMCs were used after 10 – 14 days of culture. If necessary, the purity was further enhanced by MACS® separation using the CD117 MicroBeads as described in section 3.4.1. The cell counts were determined using a Neubauer hemacytometer.

3.1.3 Generation of bone marrow-derived mast cells (BMMCs)

To generate BMMCs, BM cells, derived from wt mice, were isolated as previously described for the generation of BMDCs (see section 3.1.1). Erythrocyte lysis was performed and the remaining bone marrow cells were resuspended in 20 ml culture medium with 10 ng/ml recombinant murine IL-3 per mouse and transferred to a 75 cm^2 cell culture flask. The culture medium and culture flasks were replaced by fresh flasks and fresh medium twice a week. BMMCs were used after 4 weeks of culture. The cell counts were determined using a Neubauer hemacytometer.

3.1.4 Culturing MC/9

The MC cell line MC/9 was purchased from ATCC® (CRL-8306™) and cultured in culture medium with 10 ng/ml recombinant murine IL-3. Cells were grown at a density between 5×10^5 and 2×10^6 cells/ml. Culture medium was replaced by fresh medium twice a week. The cell counts were determined using a Neubauer hemacytometer.

3.1.5 Pharmacologic inhibition of macropinocytosis

The influence of macropinocytosis in MCG uptake was analyzed by means of pharmacologic inhibition. First, wt DCs were generated and seeded into 12-well plates (1×10^5 cells per well in 2 ml culture medium). 24 h later, the cells were washed with serum-free RPMI1640 and subsequently pre-incubated with 100 µM 5-(N,N-dimethyl)amiloride hydrochloride (DMA) in serum-free RPMI1640 at 37°C for 30 min. DCs that were treated with the respective amount of methanol served as a solvent control. Subsequently, *in vitro* isolated, AF488-labeled and PCMC-derived MCG (see section 3.1.6) were added for 2 h at 37°C. Finally, DCs were harvested and prepared for flow cytometry (see section 3.4.2.1).

3.1.6 Isolating and staining of MCG *in vitro*

MCG were isolated and stained *in vitro* as previously published [1]. PCMCs, BMMCs or MC/9 at a density of 1.6×10^6 cells/ml were stimulated with 500 ng/ml calcium ionophore A23187 and 0.3 µg/ml fluorochrome-labeled avidin (AF488-, TR- or AF647 (1:1000)-labeled avidin) in serum-free RPMI1640 at 37°C for 1 h. After removal of MCs by centrifugation (365 g, 5 min), MCG were pelleted (16,000 g, 10 min) and resuspended in sterile 1x PBS. 1×10^4 DCs were treated with MCG derived from 5×10^5 MCs.

3.1.7 T cell priming by MCG-treated DCs *in vitro*

To assess the influence of the MCG uptake by imDCs on their T cell priming capacity, imDCs, that were treated with isolated and fluorescently labeled MCG, were co-incubated with naïve T cells and their cytokine release was analyzed.
First, 1×10^6 imDCs, that were generated from LysM-GFP$^+$ mice as described above (see section 3.1.1), were seeded into 6-well plates and after one day treated with 10 µM OVA323-339 peptide for 4 h. This peptide represents the antigenic epitope of the OVA protein that binds to MHCII protein and therefore is able to induce activation of naïve antigen-specific CD4$^+$ OTII T cells [25,193]. Afterwards, the OVA peptide containing medium was replaced and DCs were treated with isolated and avidin-TR labeled MCG (see section 3.1.6) for approximately 20 h. Treated DCs were subsequently washed with sterile 1x PBS and incubated with sterile Accutase Cell Detachment Solution (1 ml per well) for 15 min at 37°C. This reaction was stopped by adding 1 ml sterile MACS buffer (Table 2.5) and cells were finally detached with a cell scraper. The cell suspensions were prepared for fluorescence-activated cell sorting (FACS) as described below (see section

3.4.2.6). LysM-GFP$^-$ CD11c$^+$ MHCII$^+$ DCs were sorted for MCG$^-$ and MCG$^+$ and plated at 1 x 10^4 cells per well in a 96-well plate. 24 h later, OTII mice were sacrificed by cervical dislocation under isoflurane inhalation and cell suspensions from spleen and peripheral LNs were obtained and prepared for FACS as described below (see section 3.4.2.6). Naïve CD4$^+$ CD62L$^+$ CD25$^-$ T cells were sorted and co-incubated with the sorted DCs for 4 d in a ratio of 1:5 (DC:T cell). Finally, the T cell cultures were re-stimulated with 2 µg/ml plate-bound anti-CD3 antibody and 4 µg/ml anti-CD28 antibody in solution for 24 h. The T cell culture supernatants were collected and analyzed for their cytokine content with LEGENDplex™ Multiplex Kits (see section 3.4.5).

3.1.8 Transfection of imDCs with specific siRNA *in vitro*

A specific gene knockdown was introduced by using ribonucleic acid (RNA) interference (RNAi) technology. To this end, imDCs were seeded into 24-well plates 24 h before treatment. After one day, the medium was replaced by 450 µl fresh culture medium with 5 ng/ml GM-CSF.

Table 3.1: Protocol for siRNA transfection of imDCs in a 24-well plate using Lipofectamine RNAiMAX Reagent.

1x transfection reaction	**50 µl**
1. Dilute Lipofectamine® RNAiMAX Reagent with serum-free RPMI1640	
RPMI1640, serum-free	23.5 µl
Lipofectamine® RNAiMAX Reagent	1.5 µl
2. Dilute siRNA with serum-free RPMI1640	
RPMI1640, serum-free	to 25 µl
siRNA (10 µM)	10 nM (SIGNR3) / 20 nM (MCL)
3. Mix diluted Lipofectamine® RNAiMAX Reagent with diluted siRNA and incubate for 5 min at RT	
4. Add mix to imDCs in 24-well plates and incubate for 72 h at 37°C	

The cells were subsequently transfected with 10 nM SIGNR3-specific siRNA (Silencer Select siRNA, Sense-Sequence: CUACUUUUCUGGAUCUGUAtt) or 20 nM MCL-specific siRNA (Silencer Select siRNA, Sense-Sequence: CCUUGUCACUUUGAGGUGAtt) using Lipofectamine RNAiMAX Reagent (Table 3.1). A nonsense control siRNA (Silencer® Select Negative Control siRNA #1) was used at same concentrations (10 nM or 20 nM respectively) as control. After 72 h, DCs were

either harvested and used for quantitative Real Time – PCR (qPCR, see sections 3.2.2 till 3.2.4) or were subsequently treated with *in vitro* isolated and AF488-labeled MCG derived from PCMCs for 24 h. Finally, DCs were harvested and prepared for flow cytometry as described below (see section 3.4.2.1).

3.2 Molecular-biological methods

3.2.1 Genotyping of mice by tissue biopsies

The genotyping of all mice (except of wt mice) was performed on small tissue samples derived from ear skin biopsies before using them for any experiments. Mice that were used for any *in vitro*, *ex vivo* or *in vivo* experiments were genotyped again after the experiment by 2 – 5 mm tail biopsies that were taken after sacrificing the mice.

For analyzing the genotype, DNA was isolated from the tissue by using Proteinase K digestions. To this end, tissue samples were incubated at least for 2 h (or overnight) in 300 µl (ear skin biopsies) or 600 µl (tail biopsies) tissue lysis buffer (Table 2.5) supplemented with 2% v/v Proteinase K at 56°C and 800 rpm in a Thermomix F1.5. Upon centrifugation at 16,000 g for 10 min, the supernatant was transferred into a new reaction tube and mixed with 300 µl or 600 µl isopropanol (volume ratio 1:1). The tubes were inverted to elicit precipitation of the DNA. The DNA was subsequently pelleted by centrifuging at 16,000 g for 10 min. The supernatant was discarded and the pellet washed with 400 µl (ear skin biopsies) or 800 µl (tail biopsies) 70% ethanol in nuclease-free water. After the last centrifugation at 16,000 g for 5 min and discarding the supernatant, the pellet was dried at RT (for approx. 2 h) and subsequently dissolved in 50 µl (ear skin biopsies) or 100 µl (tail biopsies) nuclease-free water (Qiagen) overnight at RT and 800 rpm. The dissolved DNA was stored at 4°C.

The isolated DNA was subsequently used to determine the genotype by PCR using DreamTaq Green DNA Polymerase. For each reaction, 2 µl of genomic DNA were used. As controls served reactions of wt mouse DNA (wt control) or nuclease-free water (Qiagen, negative control). The composition of PCR reactions is summarized in Table 3.2.

Depending on the analyzed gene and therefore used primers, which are summarized in Table 2.3, the temperature profiles were slightly different. They are summarized in Table 7.1 till Table 7.3. The PCR reactions were performed using a Thermocycler T3000.

Table 3.2: Reagents for a genotyping PCR using DreamTaq Green DNA Polymerase.

1x PCR reaction	**16 µl**
10x DreamTaq Green-Buffer	1.6 µl
dNTPs (10 mM)	0.32 µl (200 µM)
Primer (10 µM)	200 – 400 nM
DreamTaq DNA-Polymerase (5 U/µl)	0.3 U
DNA	2 µl
Nuclease-free water	to 16 µl

For analyzing the PCR products, an agarose gel electrophoresis was performed. The PCR reactions were completely loaded and separated with a 2% w/v agarose gel in 1x TAE buffer (Table 2.5) at 100 – 135 V. A 100 bp DNA ladder was used to determine the DNA fragment size. The products were subsequently visualized with a Herolab Transilluminator equipped with a Herolab E.A.S.Y B-455-F camera upon incubation of the gel in 1x TAE supplemented with 1 µg/ml ethidium bromide for approx. 20 min.

3.2.2 Isolation of total RNA derived from *in vitro* and *ex vivo* samples

The “Quick-RNA Microprep Kit” (Zymo Research) was used to isolate total RNA (≥ 17 nt) from *in vitro* and *ex vivo* samples. *In vitro* samples seeded in 24-well plates were washed with DMDC (dimethyl dicarbonate) -treated 1x PBS and subsequently lysed by adding 300 µl RNA Lysis Buffer directly to the well. *Ex vivo* samples were processed directly after cell sorting (see section 3.4.2.6). The sorted cells were pelleted (365 g, 4°C, 5 min) and subsequently lysed by resuspending the cell pellet with 300 µl RNA Lysis Buffer. The cell lysates were transferred into nuclease-free 1.5 ml microcentrifuge tubes and processed according to manufacturers’ instructions. The optional deoxyribonuclease I (DNase I) digestion was performed directly on the Zymo-Spin™ column and finally the RNA was eluted with 6 – 15 µl nuclease-free water (Thermo Fisher Scientific) into nuclease-free 1.5 ml microcentrifuge tubes.

The concentration of RNA samples was determined with either UV5Nano UV/VIS-Excellence spectrophotometer or NanoDrop 2000 spectrophotometer by measuring the absorption at 260 nm. RNA purity was determined as ratio of 260/280 nm and 260/230 nm. The isolated RNA was stored at -80°C for less than 12 month.

3.2.3 *first-strand* cDNA synthesis

The isolated RNA samples (see section 3.2.2) were reversely transcribed to synthesize complementary DNA (cDNA). The reaction was performed by using “Maxima First Strand cDNA Synthesis Kit for RT-qPCR” according to the manufacturers’ instructions. Depending on the isolated amount of RNA, 100 – 200 ng total RNA were used for cDNA synthesis. Table 3.3 shows the reagents used to perform the reverse transcription.

Table 3.3: Reagents for *first-strand* cDNA synthesis using “Maxima First Strand cDNA Synthesis Kit for RT-qPCR”.

1x cDNA synthesis reaction	**20 µl**
5x Reaction Mix	4 µl
Maxima Enzyme Mix	2 µl
Template RNA	100 – 200 ng
Water, nuclease-free	to 20 µl

First, 5x Reaction Mix and Maxima Enzyme Mix were mixed separately and subsequently added to the diluted RNA. The reaction was incubated for 10 min at 25°C followed by 15 min at 50°C and terminated by heating at 85°C for 5 min. To test for contaminations with genomic DNA, a “RT-minus” control was included, in which the Maxima Enzyme Mix was replaced by nuclease-free water. Therefore, total RNA cannot be transcribed into cDNA and only the genomic DNA will serve as a template for subsequent qPCR (see section 3.2.4). The cDNA was stored at -20°C (up to one week) or -80°C (longer storage than one week).

3.2.4 Gene expression analyses by qPCR

The qPCR was performed to determine the relative amount of a certain RNA by using “TaqMan® Gene Expression Assays”. Additionally to the sequence-specific primers, these assays contain a sequence-specific, fluorochrome-coupled probe. The used fluorochromes can differ between the assays, which allows to measure the *gene of interest* (*GOI*) simultaneously in one tube with the house-keeping gene TATA box binding protein (Tbp) [194], which is later used for normalization.
The synthesized cDNA (see section 3.2.2) was diluted with nuclease-free water (Thermo Fisher Scientific) to a final concentration of 2 ng/µl. Table 3.4 shows the reagents used to perform the qPCR with simultaneous measurement of the *GOI* and *Tbp* (Duplex reaction).

Table 3.4: Reagents for duplex qPCR.

1x qPCR reaction (10 µl)	Duplex
Takyon™ MasterMix	5 µl
TaqMan® Expression Assay (*GOI*-FAM)	0.5 µl
TaqMan® Expression Assay (*Tbp*-VIC)	0.5 µl
Water, nuclease-free	1.5 µl
Template cDNA (2 ng/µl)	2.5 µl

The qPCR was run with the "QuantStudio 3 Real-Time-PCR-System" due to the following profile. The relative *GOI* gene expression was analyzed based on the c_t value using the $2^{-\Delta\Delta ct}$ method. This method subsequently displays the relative gene expression, normalized to a house-keeping gene in relation to a reference group/sample [195]. Within this thesis, all *GOIs* were normalized to the house-keeping gene *Tbp* and the first sample of a distinct data set (described in each figure legend) was set to 100% serving as reference sample.

Table 3.5: Temperature profile for duplex qPCR.

	Temperature	Time
1. Takyon™ activation	95°C	3 min
2. Denaturation	95°C	10 sec
3. Annealing / Extension	60°C	60 sec
Repeat step 2 – 3: 50x		

3.3 Animal-based methods

3.3.1 MCG staining *in vivo*

Intracellular MCG were stained *in vivo* as previously published [1]. Mice were anesthetized by intraperitoneal (i.p.) injection of 10 µl/g body weight Ketanest (Table 2.5) and 50 µl fluorochrome-labeled avidin (1:100 AF647-avidin or 20 µg/ml AF488-avidin, both diluted in isotonic 0.9% NaCl) were injected intradermally (i.d.) into the mouse ear skin using a 33G insulin syringe. As gating control, isotonic 0.9% NaCl alone was injected. All following experiments were performed 21 d after avidin-staining to minimize unspecific staining or MCG uptake effects.

3.3.2 DNFB- or FITC-induced CHS

CHS serves as a murine model for the disease ACD and was performed as previously published in 2017 [139,196]. The mice were sensitized by epicutaneous application of 100 µl 0.5% v/v DNFB in acetone/olive oil (4:1) on the shaved back skin. After 6 d, mice were challenged with 10 µl 0.2% v/v DNFB in acetone/oil (4:1), epicutaneously on each side of the ear without anesthesia. Vehicle control mice were treated with acetone/oil (4:1) alone. T cell priming was assessed by flow cytometry (see section 3.4.2.3) and cytokine analyses (see section 3.4.5) of skin-draining LNs 4 d after sensitization. The adaptive CHS response was assessed by ear swelling measurements 16 or 24 h after challenge using a precision thickness gage. Additionally, MCG uptake by skin DC subsets was analyzed by flow cytometry (see section 3.4.2.2) 16 or 24 h after challenge. Alternatively, mice were sensitized epicutaneously with fluorescein isothiocyanate (FITC, 1% w/v in acetone/dibutyl-phthalate 1:1) onto the ear (10 µl each side) or shaved back skin (100 µl). 48 h after FITC administration, mice were sacrificed and skin-draining LNs were isolated and prepared for flow cytometry (see section 3.4.2.3).

3.3.3 HDM-induced allergic airway inflammation

HDM-induced allergic airway inflammation was induced as previously described [197]. HDM extract of *Dermatophagoides pteronyssinus* (*D. pteronyssinus*) was dissolved and diluted in 1x PBS to a final concentration of 0.5 µg/µl. The mice were anesthetized with isoflurane and intranasally (i.n.) sensitized with 10 µg HDM extract. This sensitization was repeated for three consecutive days (days 0 - 2). Eight days later, mice were challenged for four days with i.n. applied 10 µg HDM extract per day under isoflurane anesthesia. Control mice received no HDM treatment. On day 14 (24 h after the last challenge), the mice were sacrificed and prepared for further analyses.

First, blood was collected and incubated for at least 30 min to allow clotting. Upon centrifugation at 300 g for 10 min at RT, serum samples were collected and frozen and stored at -80°C. For analysis, the serum samples were prediluted in Assay Buffer A and processed according to manufacturer's protocol of "IgE Mouse Uncoated ELISA Kit" for analyzing total IgE levels. In addition, upper right lobes of the lung were collected and fixed with 4% buffered formaldehyde for at least 24 h. Fixed lung tissue was further processed by Kirsten Herrmanns (Otto-von-Guericke-University Magdeburg, Institute of Pathology, head of group: Prof. Dr. Christoph Garbers). She made paraffin-embedded lung sections of 2 µm and stained them with haematoxylin and eosin (HE, see section 3.4.6). Finally, HE stainings were analyzed for peribronchial airway inflammation.

Respective sections were chosen (up to 4 per animal) and the amount of bronchiole-surrounding, inflammatory cells was analyzed. Based on the work of Kim *et al.* and Kujur *et al.*, the peribronchial cellular infiltration was calculated as a semi-quantitative scores. The distribution of scores was thereby slightly adapted compared to the literature [198,199]: 0 - 0% of the bronchiole was surrounded by cells, 1: < 10% surrounded by cells, 2: 10 - <25% surrounded by cells, 3: 25 - <50% surrounded by cells; 4: 50 - <75% surrounded by cells, 5: 75 - <100% surrounded by cells, 6: 100% surrounded by cells. The remaining lung tissue and the lung-draining mediastinal LNs were finally prepared for flow cytometry and analyzed for their cellular distribution (see sections 3.4.2.3/3.4.2.5).

3.4 Immunological methods

3.4.1 Cell separation using immunomagnetic beads

If necessary, the purity of PCMC cultures was enhanced using CD117 MicroBeads according to the manufacturer's instructions. The cells were counted using a Neubauer hemacytometer and subsequently incubated with magnetic microbeads conjugated to rat monoclonal anti-mouse CD117 antibodies according to the protocol. The magnetic separation was done with MS columns using the OctoMACS™ Separator. The flow-through contained unlabeled and therefore non-MCs while MCs were magnetically labeled therefore remaining inside the column within the magnetic field (positive selection). Finally, the columns were disconnected from the separator and cells were flushed out, counted with a Neubauer hemacytometer and seeded into new cell culture flasks with a density of 0.5×10^6 cells/ml cell culture medium for at least 24 h before further usage.

Additionally, T cells were isolated from spleens of wt mice. To this end, mice were sacrificed by cervical dislocation under isoflurane anesthesia and spleens were isolated and processed as described in section 3.4.2.4. Cell counts were determined using a Neubauer hemacytometer. 1×10^7 splenocytes were processed using "Pan T Cell Isolation Kit II" according to manufacturer's instructions. This cell separation is based on a negative selection, which means that the cell suspension was firstly incubated with a mixture of biotin conjugated monoclonal antibodies against CD11b, CD11c, CD19, CD45R, CD49d, CD105, MHCII and Ter-119 and afterwards with magnetic microbeads conjugated to monoclonal anti-biotin antibodies. As a result, T cells remained unlabeled while all other cell subsets were magnetically labeled. The magnetic separation was

done with LC columns using the QuadroMACS™ Separator. Unlabeled T cells were collected within the flow-through while other cell subsets remained inside the column within the magnetic field. Subsequently, 1 x 10^6 isolated T cells were washed with DMDC-treated 1x PBS and subsequently lysed by adding 300 µl RNA Lysis Buffer. The isolation of total RNA was performed according to section 3.2.2.

3.4.2 Flow cytometry

Used antibodies/reagents are listed in Table 2.5/2.10/2.12/2.13. Detailed information regarding preparation of samples are described in following sections. Analyzed cell populations were gated based on distinct markers (Table 3.6). If necessary, absolute cell numbers were determined using CountBright™ Absolute Counting Beads.

Table 3.6: Gating of cell populations.

Cell population	Method	Marker combination
DCs	FC (*in vitro*)	Singlets$^+$ CD11c$^+$ MHCII$^+$
skin/lung DCs	FC (*in vivo*)/ FACS	(Singlets$^+$) CD45$^+$ F4/80$^-$ CD11c$^+$ MHCII$^+$ (CD11b$^{+/-}$ CD103$^{+/-}$)
spleen DCs	FC (*in vivo*)	CD45$^+$ F4/80$^-$ Ly-6G$^-$ CD11c$^+$ MHCII$^+$
CD11b$^+$ LNr DCs	FACS	Singlets$^+$ CD45$^+$ CD11c$^+$ MHCII$^{+/-}$ CD8$^-$ CD169$^-$ CD11b$^+$
CD11b$^+$ LNr DCs	MELC	Size^{high} CD11c$^+$ MHCII$^{+/-}$ CD8$^-$ CD169$^-$ CD11b$^+$
LNm DCs	FACS	Singlets$^+$ CD45$^+$ CD11c^{low} MHCII$^+$ FITC$^+$
LNm DCs	MELC	Size^{high} CD11c$^+$ MHCII$^+$ FITC$^+$
leukocytes	FC (*in vivo*)	CD45$^+$
(CD3$^+$) T cells	FC (*in vivo*)	CD45$^+$ CD3$^+$
CD4$^+$ T cells	FC (*in vivo*)	<u>LN upon DNFB treatment:</u> CD45$^+$ CD3$^+$ CD4$^+$ <u>Lung/LN upon HDM treatment:</u> CD45$^+$ CD4$^+$
CD8$^+$ T cells	FC (*in vivo*)	CD45$^+$ CD3$^+$ CD8$^+$
T_{act} cells	FC (*in vivo*)	CD45$^+$ CD3$^+$ CD4$^+$ (or CD8$^+$) CD44$^+$
T_{eff} cells	FC (*in vivo*)	CD45$^+$ CD3$^+$ CD4$^+$ (or CD8$^+$) CD44$^+$ CD25$^+$
T_{reg} cells	FC (*in vivo*)	CD45$^+$ CD3$^+$ CD4$^+$ FoxP3$^+$
CD45$^+$ non-T cells	FC (*in vivo*)	lymphocyte$^-$ CD45$^+$
CD45$^-$ cells	FC (*in vivo*)	CD45$^-$
T_{fh} cells	FC (*in vivo*)	CD45$^+$ CD4$^+$ PD-1$^+$ CXCR5$^+$
B cells	FC (*in vivo*)	CD45$^+$ CD45R$^+$

Table 3.6 (continue): Gating of cell populations.

Cell population	Method	Marker combination
Mphs	FC (*in vivo*)	$CD45^+$ $F4/80^+$ $Ly\text{-}6G^-$
Nphs	FC (*in vivo*)	$CD45^+$ $F4/80^-$ $Ly\text{-}6G^+$

FC – flow cytometry, FACS – fluorescence-activated cell sorting, MELC – multi-epitope ligand cartography. Doublets were solely excluded for *in vitro* experiments or FACS

The cells were either sorted using BD FACS Aria™ III Cell Sorter or analyzed using BD LSRFortessa™ flow cytometer or Amnis® FlowSight® Imaging Flow Cytometer. Filter settings were used as summarized in Table 3.7 for detection of the respective fluorochromes.

Table 3.7: Excitation laser and emission filters used within distinct flow cytometers.

Excitation laser (wavelength)	Filter settings [nm]	Detected fluorochromes
BD LSRFortessa™ Flow Cytometer		
Violet (405 nm)	560/40, 535LP	Brilliant Violet 570 (BV570™)
	525/50, 505LP	BV510™
	450/50	Pacific Blue, eFluor™ 450, BV421™
Blue (488 nm)	780/60, 750LP	PE-Cy7
	695/40, 685LP	PerCP-Cy5.5, PerCP-eFluor™ 710
	670/30, 635LP	PE-Cy5
	610/20, 600LP	PE-TexasRed
	575/26, 550LP	PE
	530/30, 505LP	FITC, AF488
	488/10	SSC
Red (640 nm)	780/60, 750LP	APC-Cy7, APC-eFluor™ 780
	670/30	APC, AF647
BD FACSAria™ III Cell Sorter		
Violett (405 nm)	610/20, 600LP	BV570™
	510/50, 502LP	BV510™
	450/50	eFluor™ 450
Blue (488 nm)	695/40, 655LP	PerCP-Cy5.5, PerCP-eFluor™ 710
	530/30, 502LP	FITC, GFP
	488/10	SSC
Yellow-Green (561 nm)	780/60, 735LP	PE-Cy7
	582/15, 570LP	PE
Red (640 nm)	780/60, 735LP	APC-Cy7, APC-eFluor™ 780
	660/20	APC, AF647

Table 3.7 (continue): Excitation laser and emission filters used within distinct flow cytometers.

Excitation laser (wavelength)	Filter settings [nm]	Detected fluorochromes
Amnis® FlowSight® Imaging Flow Cytometer		
Violett (405 nm)	577/35	BV570
	457/45	Pacific Blue
Blue (488 nm)	702/86	PerCP-Cy5.5
	532/55	AF488
Yellow-Green (561 nm)	772/55	PE-Cy7
	577/35	PE
Red (640 nm)	772/55	APC-Cy7
	702/86	AF647

The flow cytometers were equipped with additional lasers and filters, which were not used within this thesis and therefore are not depicted here.

3.4.2.1 Preparation of samples derived from *in vitro* cultures

Treated DCs from *in vitro cultures*, that were to be analyzed by flow cytometry, were washed with 1x PBS, first. Adherent cells were then incubated with Accutase Cell Detachment Solution (400 µl per well of a 12-well plate, 200 µl per well of a 24-well plate) for 15 min at 37°C. The reaction was stopped by adding 1 ml MACS buffer to each well and the cells were finally detached by rinsing of the bottom of the cell culture plate. The cell suspensions were transferred into 5 ml Polystyrene Round-Bottom Tubes (flow cytometry tubes, FC tubes) or 1.5 ml microcentrifuge tubes and centrifuged at 365 g and 4°C for 5 min. The supernatants were discarded. Extracellular antibody staining took place for 15 min on ice in the dark in MACS buffer. The staining procedure was stopped and cells were fixed by adding 1 ml 1x PBS, containing 0.5% v/v formaldehyde (0.5% FA, Table 2.5) and subsequently centrifuged at 365 g for 5 min. Samples were finally resuspended in 0.5% FA and measured with BD LSRFortessa™ Flow Cytometer or Amnis® FlowSight® Imaging Flow Cytometer.

3.4.2.2 Preparation of ear skin samples

For analysis of cells in the ear skin, mice were sacrificed by cervical dislocation under isoflurane inhalation and the ear pinnae was cut off with a scissor and torn apart into two ventral sheets. Subsequently, they were and cut into small pieces by using forceps and scalpels. The ear skin was digested in 1 ml ear digestion medium (Table 2.5) at 37°C

and 1400 rpm for 1 h. The reaction was stopped by placing the reaction tubes on ice. Afterwards, the solution was filtered through a cell strainer (pore size 70 or 100 µm) into an FC tube and washed with 2 ml 1x PBS. The cells were subsequently centrifuged at 365 g and 4°C for 5 min. Extracellular antibody staining took place for 15 min on ice in the dark in MACS buffer. The staining procedure was stopped and cells were fixed by adding 1 ml 0.5% FA and subsequent centrifugation at 365 g for 5 min. Samples were finally resuspended in 0.5% FA and measured with BD LSRFortessa™ Flow Cytometer.

3.4.2.3 Preparation of samples derived from dLNs

Within this thesis skin- and lung-draining LNs were analyzed. Auricular ear skin-draining LNs, inguinal back skin-draining LNs or mediastinal lung-draining LNs were used. For analysis of cells within these LNs, mice were sacrificed by cervical dislocation under isoflurane anesthesia (inguinal LNs) or under isoflurane anesthesia by increasing the isoflurane concentration to a lethal dose without cervical dislocation (auricular or mediastinal LNs). The LNs were isolated and transferred into cold 1x PBS and stored on ice till further usage. Subsequently, the LNs were squeezed in-between glass slides, flushed through a cell strainer (pore size 40 or 100 µm) and washed with MACS buffer. Extracellular antibody staining took place in FC tubes for 15 min on ice in the dark in MACS buffer. The staining procedure was stopped and cells fixed by adding 1 ml 0.5% FA and subsequent centrifugation at 365 g for 5 min. Cells were finally resuspended in 0.5% FA. Alternatively, cells derived from mediastinal LNs upon HDM-induced airway inflammation were re-stimulated in lung digestion medium (Table 2.5), supplemented with 1 µM ionomycin, 20 nM phorbol 12-myristate 13-acetate (PMA) and 5 µM Brefeldin A for 6 h at 37°C. Intracellular antibody staining, following the extracellular staining, was subsequently performed using “eBioscience™ Intracellular Fixation & Permeabilization Buffer Set”. Samples were finally measured with BD LSRFortessa™ Flow Cytometer.

3.4.2.4 Preparation of samples derived from spleens

Untreated mice were sacrificed by cervical dislocation under isoflurane anesthesia. Spleens were carefully isolated and subsequently squeezed through a cell strainer (pore size 40 or 100 µm) placed in a petri dish containing 1x PBS. The resulting cell suspensions were collected in a 50 ml reaction tube. To eliminate erythrocytes, the cell suspensions were precipitated at 365 g and 4°C for 5 min and subsequently resuspended with 3 ml 1x erythrocyte-lysis-buffer per mouse and incubated for 1 min at RT. The lysis reaction was stopped by administration of 9 ml sterile 1x PBS and

subsequent centrifugation at 365 g and 4°C for 5 min. The supernatants were discarded and the cells were either used for FACS (see section 3.4.2.6) or cell separation based on antibody-coupled magnetic beads (see section 3.4.1). Additionally, extracellular antibody staining took place in FC tubes for 15 min on ice in the dark in MACS buffer followed by intracellular antibody staining using “FoxP3 Staining Buffer Set”. Samples were finally measured with a BD LSRFortessa™ Flow Cytometer.

3.4.2.5 Preparation of lung samples

Upon HDM-induced allergic asthma, cellular composition within the lung tissue was analyzed by flow cytometry. To this end, mice were sacrificed under isoflurane anesthesia by increasing the isoflurane concentration to a lethal dose and lung tissue was prepared and collected. Upon tissue weight determination, the tissue samples were cut into 8 – 10 pieces and digested in 3 ml lung digestion medium, supplemented with 0.5 mg/ml Liberase™ TL for 40 min in a 37°C water bath. Every 5 min, the samples were mixed by vortexing. Finally, digested lung tissue was squeezed through a cell strainer (pore size 70 or 100 µm), washed with lung digestion medium and the total cell count was determined using the Cell Counter Luna II. For each antibody staining panel, 1.5×10^7 cells were used. Extracellular antibody staining took place in FC tubes for 15 min on ice in the dark in MACS buffer. The staining procedure was stopped and cells were fixed by adding 1 ml 0.5% FA and subsequent centrifugation at 365 g for 5 min. Cells were finally resuspended in 0.5% FA. Alternatively, cells were re-stimulated in lung digestion medium, supplemented with 1 µM ionomycin, 20 nM PMA and 5 µM Brefeldin A for 6 h at 37°C. Intracellular antibody staining, following the extracellular staining, was subsequently performed using “eBioscience™ Intracellular Fixation & Permeabilization Buffer Set”. Samples were finally measured with a BD LSRFortessa™ Flow Cytometer.

3.4.2.6 Fluorescence-activated cell sorting (FACS)

Samples derived from *in vitro* cultures, skin, LN and spleens were prepared as described above. Single cell suspensions were used for extracellular antibody staining that took place for 15 min on ice in the dark in MACS buffer. Subsequently, the cells were not fixed, instead washed with sterile 1x PBS and filtered directly before the measurement through a cell strainer (pore size 40 or 100 µm). The BD FACSAria™ III Cell Sorter was set up with sterile 1x PBS and an 85 µm nozzle and cooled to 4°C. Samples were finally sorted into cooled FC tubes for distinct cell populations.

3.4.2.7 Flow cytometry-based CLR binding studies

For analysis of the ability of different CLRs to bind MCG, I used a tool that was published by the group of Prof. Dr. Bernd Lepenies (University of Veterinary Medicine Hannover, Institute for Immunology) in 2018 [190].
Prof. Lepenies kindly provided the purified CLR-hFc fusion proteins. Isolated and fluorescently labeled MCG of 375,000 MCs (see section 3.1.6) were incubated with 200 ng fusion protein (listed in section 2.3.3) diluted in 100 µl lectin-binding buffer (Table 2.5) at 4°C for 1 h in the dark. The samples were centrifuged at 16,000 g and 4°C for 10 min and washed once with 200 µl lectin-binding buffer. Next, pellets were resuspended in 50 µl anti-hFc antibody (1:200 in 1x PBS) and incubated for 30 min at 4°C in the dark. Afterwards, samples were washed twice with 200 µl lectin-binding buffer and finally measured with an Amnis® FlowSight® Imaging Flow Cytometer.

3.4.3 Confocal microscopy

For analyzing the MCG uptake by imDCs by confocal microscopy, imDCs were seeded in culture medium without phenol red (Table 2.6) on sterile cover slips and treated with *in vitro* isolated and TR-labeled MCG derived from PCMCs, BMMCs and MC/9 as indicated above (see section 3.1.6). 24 h later, DCs were washed twice with serum-free RPMI1640 without phenol red. If indicated, nuclei were subsequently stained with Hoechst33342 (1:1000 in serum-free RPMI1640 without phenol red) for 15 min at 37°C. If necessary, cell membranes were stained with a fluorescently labeled antibody against murine CD11c (clone N418, AF488-labeled, 1:200), diluted in MACS buffer, for 15 min at 4°C. Finally, the cells were fixed with ice-cold methanol or 0.5% FA and cover slips were sealed with nail polish.
The analyses were done using an inverted Confocal Microscope System Leica SP8 that was controlled by LAS X software and equipped with a Plan Apo 63x/1.4 oil objective. If, necessary, sequential unidirectional scanning at 400 Hz or bidirectional scanning at 600 Hz was performed to avoid bleed-through of fluorescence emission using the distinct settings as indicated in the respective figure legend (sequences were altered between lines or lines and frames). As depicted in the respective figure legends, images of the individual channels were pseudo-colored by using LAS X or ImageJ software.

3.4.4 Multi-epitope ligand cartography (MELC)

Intracellular MCG were stained *in vivo* with AF647-labeled avidin (see section 3.3.1). Three weeks later, mice were sensitized with FITC onto the ear as described above (see section 3.3.2). The mice were sacrificed 48 h after FITC application and the ear skin-draining LNs were isolated and directly frozen in Tissue-Tek® O.C.T. Compound. Lars Philipsen and Guido Höbbel (Otto-von-Guericke University, Institute for Molecular and Clinical Immunology) prepared 10 µm cryo-sections that were adhered to silan-coated cover slides. They were subsequently fixed with 2% v/v paraformaldehyde, permeabilized with 0.2% v/v Triton X-100 and blocked with 1% w/v BSA in 1x PBS.
The analysis of tissue samples using an inverted wide-field fluorescence microscope (Leica DMI6000, 20x air lens NA 0.70) was performed as previously described [200]. Briefly, an automated cyclic process is initiated with the following steps: (I) the incubation of the first fluorescently labeled anti-body followed by a series of washing steps, (II) the acquisition of the fluorescence signals with a corresponding phase-contrast image by a cooled scientific CMOS camera (Hamamatsu Orca Flash 4.0 v2), (III) the deletion of the specific signal by bleaching the fluorescent dye, (IV) followed by recording of post-bleaching fluorescence signals. Afterwards, the next cycle of incubation, imaging and bleaching followed.
The subsequent image processing was performed by Lars Philipsen. The series of fluorescence images were aligned pixel-wise using the corresponding phase-contrast images (alignment accuracy of 0.1 pixels). Illumination artifacts of the images were corrected using flat-field correction and post-bleaching images were subtracted from the following fluorescence images. Finally, section artifacts were excluded as invalid by a manual mask-setting process. The segmentation of valid areas into cells was done with the CellProfiler software [191] using the propidium iodide (PI) signals as seed points and the signals of the marker CD45, CD3ε, CD45R and CD169 as membrane staining. Lymphatic vessels (threshold of the LYVE1 signal) and the MC granules (segmentation of the APC channel of the first step) were defined as region of interests (ROIs). The fluorescence intensities and distance to the ROIs were calculated for all detected cells. The resulting matrix of intensities and distances was exported into an FCS file and uploaded to the Cytobank analysis software for multi-parametric analysis.

3.4.5 Cytokine analysis using LEGENDplex™ Multiplex Kits

For the analysis of secreted cytokines of re-stimulated T cells, culture supernatants were analyzed with LEGENDplex™ assays. These bead-based immunoassays use the same

principle as sandwich immunoassays. Beads, which can be differentiated by size and fluorescence intensities, are conjugated with specific antibodies and serve as capture beads for particular analytes. Biotinylated detection antibodies are used to form “capture bead-analyte-detection antibody sandwiches”, which are further bound by streptavidin-phycoerythrin (SA-PE). PE fluorescent signal intensities can be used to calculate cytokine concentrations based on a standard curve [201].
For the cytokine analyses in this thesis, undiluted cell culture supernatants of re-stimulated T cells were used and processed according the manufacturers’ instructions. Finally, the samples were analyzed with BD LSRFortessa™ Flow Cytometer.

3.4.6 HE staining

HE stainings were performed by Kirsten Herrmanns (Otto-von-Guericke-University Magdeburg, Institute of Pathology, head of group: Prof. Dr. Christoph Garbers). The general procedure will be shortly summarized in this section. Fixed and paraffin-embedded lung tissue was cut into sections of 2 µm. Sections were subsequently deparaffinized using ProTaqs® Clear three times of 10 min and hydrated by washing twice with 100% ethanol, twice with 96% ethanol, once with 70% ethanol (each for 5 min). Afterwards, sections were rinsed with tab water. The nuclear staining was performed with haematoxylin for 5 min, rinsed with tab water and shortly differentiated with 70% ethanol supplemented with 0.7% HCl. The sections were rinsed with tab water again. Afterwards, they were incubated with eosin solution for 3 min and rinsed with tab water again. Sections were dehydrated by washing once with 70% ethanol, twice with 96% ethanol and twice with 100% ethanol (each for 5 min). Afterwards, lung sections were incubated with ProTaqs® Clear for three times of 5 min and mounted using ProTaqs® PARAmount. Finally, HE stainings were analyzed for peribronchial airway inflammation as described above in section 3.3.3.

3.5 Data analysis and statistics

Statistical analyses were performed using the GraphPad Prism 9 software. The data are shown as floating bars showing the minimum and maximum with line at mean. Each data set was tested for Gaussian distribution with Shapiro-Wilk normality test. Outliers within data sets were identified by using Grubbs’ (Gaussian distribution) or ROUT method (no Gaussian distribution). Statistical analyses were performed with Student’s t-test or one-way ANOVA (Gaussian distribution) or the respective non-parametric tests (no Gaussian

distribution: Wilcoxon test, Mann-Whitney test, Friedman test and Kruskal-Wallis test). Statistical significance was reached with a p value smaller than 0.05. Significance levels are indicated in each figure. If not indicated otherwise, results, shown as floating bars, were summarized from two to four independent experiments. Due to weekly renewed calibrations of equipment, it was required to calculate a fold change for some data sets in order to be able to compare the independent experiments with each other. To this end, fold change was calculated by setting the mean of a distinct data set (indicated in each figure legend) to one and calculating each data point in relation to it.

4 Results

4.1 Establishment of a protocol to mimic MCG uptake by DCs *in vitro*

In 2019, we reported that dermal DCs engulf MCG exocytosed by MCs upon skin inflammation, which subsequently leads to increased functionality of these cells [1]. Consequently, the MCG uptake by dermal DCs seems to be a feature of peripheral MCs to impact on adaptive immunity by modifying DC functions, but the underlying mechanisms and consequences remain not fully understood. To address this issue, a method to mimic the MCG uptake by DCs *in vitro* was established, in order to determine the mechanism of MCG uptake.

4.1.1 Isolating and staining of MCG *in vitro*

Firstly, a protocol for the isolation and staining of MCG *in vitro* was established. Based on the findings of Choi *et al*., Joulia *et al*. and Gaudenzio *et al*., PCMCs were seeded in serum-free RPMI1640 medium and were subsequently stimulated with the calcium ionophore A23187 in the presence of AF488-labeled avidin for 1 h [202–204]. After stimulation, MCs were removed by centrifugation (365 g for 5 min). Due to the low centrifugal acceleration, only cells were pelleted while the MCG remained in the supernatant. Subsequently, a second centrifugation step (16,000 g for 10 min) was used to concentrate MCG in 1x PBS. Finally, the isolated MCG were analyzed by confocal microscopy and imaging flow cytometry.

Isolated AF488-labeled MCG were detected by confocal microscopy (Figure 4.1A). As expected from the literature [105,114], MCG differed in size and AF488-fluorescence intensity. Nevertheless, approx. 86% of the isolated small particles could be stained with avidin and can therefore be referred to as MCG as additionally shown by imaging flow cytometry (Figure 4.1B). Therefore, this *in vitro* method can be used to collect *in vitro* isolated and fluorescently labeled MCG for further experiments.

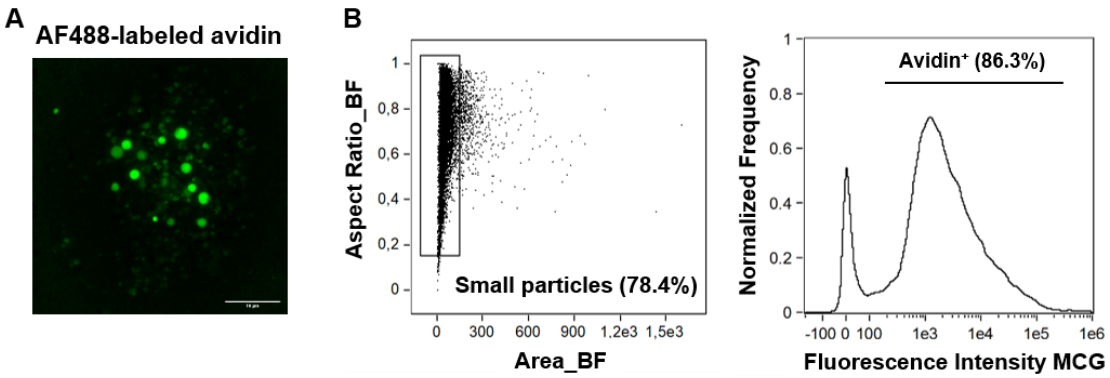

Figure 4.1: MCG staining *in vitro*. MCG derived from PCMCs were isolated and stained with fluorescently labeled avidin *in vitro*. Isolated and fluorescently labeled MCG were analyzed by (A) confocal microscopy (scale bar 10 µm) and (B) imaging flow cytometry. (A) Bidirectional scanning at 600 Hz was performed at excitation 488 nm, emission 497 nm – 570 nm. Voxel size was adjusted to 45 nm x 45 nm x 299 nm (dx, dy, dz). Channel was pseudo-colored using LAS X software. (B) Small particles were gated based on size (Area_Brightfield (BF)) and Aspect Ratio (Ratio of event height and width based on BF) of events to exclude contamination with remaining cells (left) and avidin binding was analyzed as fluorescence intensity that were plotted against frequency that was normalized by default bin counts.

4.1.2 Treatment of DCs with isolated MCG *in vitro*

BM cells of CD11c-GFP reporter mice [175] were isolated and differentiated into imDCs (see section 3.1.1). Due to the GFP (green fluorescent protein) that is coupled to the integrin CD11c expressed by DCs in these reporter mice, DCs could be easily identified with confocal microscopy without additional staining (Figure 4.2, green). MCG were isolated from PCMCs and stained with TR-coupled avidin (Figure 4.2, red). imDCs were cocultured with TR-labeled MCG for 24 h. The experimental procedure was standardized by using MCG of 5 x 10^4 MCs for the treatment of 1 x 10^4 DCs. Finally, the analysis was performed by confocal microscopy.

Figure 4.2 shows that TR^+ MCG (red) could be detected inside the GFP^+ DCs (green), while in untreated DCs no TR signal was detected. Additionally, DCs took up different amounts of MCG. While there were cells that didn't take up MCG (Figure 4.2; white arrow head), there were cells that took up only few (Figure 4.2; blue arrow head) and some that engulfed lots of MCG (Figure 4.2; yellow arrow head).

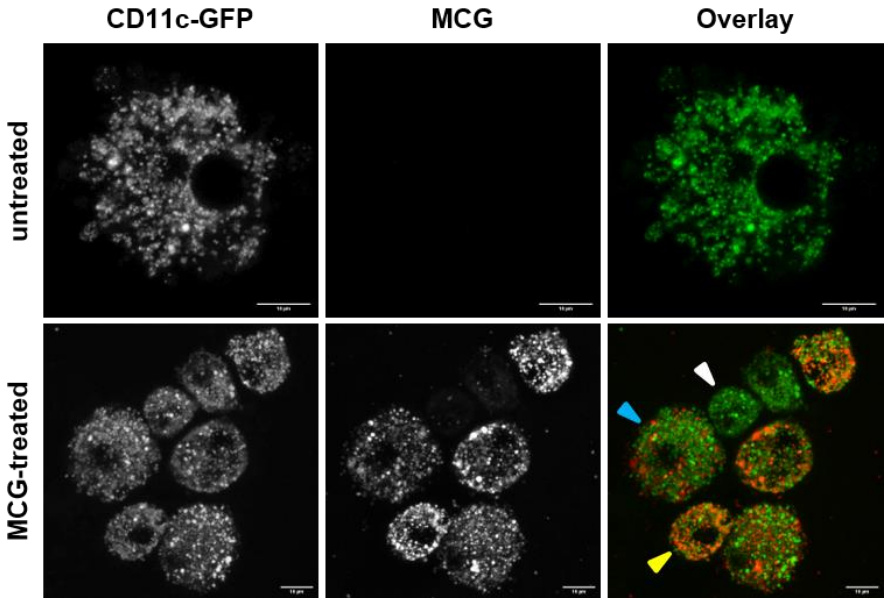

Figure 4.2: Confocal microscopy of MCG uptake by imDCs *in vitro*. imDCs derived from CD11c-GFP reporter mice were treated *in vitro* with isolated and fluorescently labeled MCG and subsequently analyzed by confocal microscopy. To avoid bleed-through of fluorescence emission, sequential bidirectional scanning at 600 Hz was performed: sequence 1: excitation 488 nm, emission 498 nm – 548 nm, sequence 2: excitation 561 nm, emission 604 nm – 654 nm (sequences were altered between frames and lines). Voxel size was adjusted to 50/82 nm x 50/82 nm x 299 nm (dx, dy, dz). First row shows untreated DCs and second row shows DCs cocultured with TR-labeled MCG (scale bars 10 µm). Single channels show either signals derived from GFP coupled to CD11c (left column) or TR-labeled MCG (middle column). Channels were pseudo-colored using ImageJ software to generate overlay (right column, CD11c-GFP – green, TR-labeled MCG – red). Arrowheads indicate DCs that engulfed no (white), few (blue) or many MCG (yellow).

In addition to confocal microscopy, *in vitro* MCG-treated DCs were analyzed by flow cytometry. The DCs were treated as described for the confocal microscopy and subsequently harvested and prepared for flow cytometric analysis using fluorochrome-labeled antibodies against CD11c, MHCII, CCR7 (CD197), CD80 and CD86 as described in section 3.4.2.1.

Figure 4.3 shows an exemplary gating strategy. Upon debris and doublet exclusion, DCs were gated as $CD11c^+$ $MHCII^+$ cells (upper right plot) and subsequently analyzed for their MCG uptake (lower plots in Figure 4.3). MCG were stained with AF488-labeled avidin before using them for the treatment of imDCs. Upon MCG uptake, MCG^+ DCs can therefore be easily identified as $AF488^+$ events. Upon MCG treatment, a clear increase in the AF488 intensity of the DCs was detected compared to untreated DCs indicating the uptake of MCG by DCs (lower right plot in Figure 4.3). Differences in the fluorescence

intensity of each MCG$^+$ DC also confirm the variations of MCG uptake previously seen with confocal microscopy.

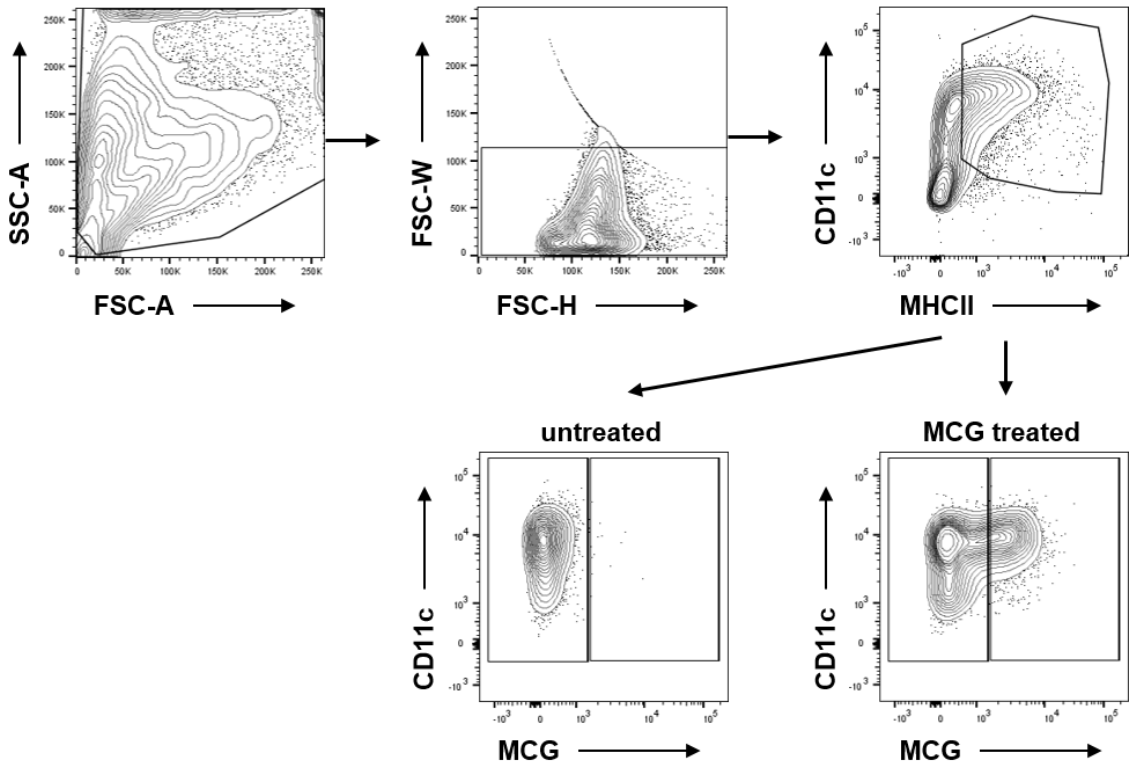

Figure 4.3: Exemplary gating strategy upon flow cytometric analysis of MCG uptake by imDCs *in vitro*. imDCs that were treated with isolated and fluorescently labeled MCG were prepared for flow cytometry 24 h after treatment. First, cell debris were excluded with subsequent doublet exclusion. Single cells were further gated for DCs, identified as CD11c$^+$ MHCII$^+$ cells. To set the gate for MCG$^+$ DCs, a fluorescence minus one (FMO) control was used for subsequent analysis of the fraction of MCG$^+$ DCs.

In previous studies, we showed that MCG uptake by imDCs upon skin inflammation *in vivo* led to an increased migration and maturation of the DCs compared to MCG$^-$ DCs [1]. DC activation leads to increased expression of the chemokine receptor CCR7, which is responsible for the migration to the dLNs, and to the upregulation of co-stimulatory molecules CD80 and CD86, which are necessary for appropriate T cell priming [22,92]. Therefore, the expression of CCR7, CD80 and CD86 by DCs upon MCG uptake was analyzed by flow cytometry.

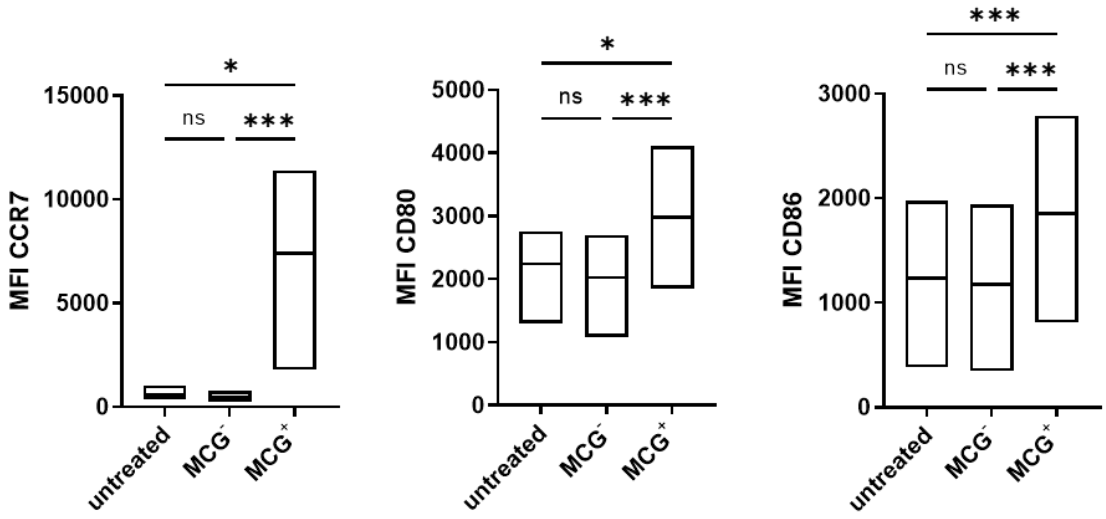

Figure 4.4: Upregulation of DC maturation markers upon MCG uptake. imDCs were treated with isolated and fluorescently labeled MCG *in vitro* for 24 h and subsequently analyzed by flow cytometry. Data are shown as floating bars showing the minimum and maximum with line at mean (see section 3.5). Untreated or MCG-treated (MCG^- or MCG^+) were analyzed for their surface marker expression of CCR7, CD80 and CD86. Expression levels are shown as median fluorescence intensity (MFI, N = 7-9). *** $p < 0.001$, ** $p < 0.01$, * $p < 0.05$, # $p \leq 0.10$, ns $p > 0.10$.

Figure 4.4 shows the median fluorescence intensity (MFI) of the analyzed maturation markers and compares their expression on untreated DCs with their expression on DCs that did not take up MCG upon MCG treatment (MCG^-) and those that took up MCG (MCG^+). The MFI of CCR7 was comparably expressed on untreated DCs and MCG^- DCs. In contrast, the expression of CCR7 was strongly increased upon MCG uptake (Figure 4.4 left), indicating an increased migration capacity of the DCs. In the same line, the co-stimulatory molecules showed no difference in their expression on untreated DCs and MCG^- DCs, but were significantly increased upon MCG uptake (Figure 4.4 middle/right). Collectively, the MCG uptake by DCs *in vitro* also led to an increased migration and maturation profile of DCs, as was already shown *in vivo* [1].

In summary, a method to mimic *in vivo* MCG uptake by DCs was successfully established using *in vitro* studies. Using different immunological methods, this tool can be subsequently used to characterize molecular mechanisms and consequences of MCG uptake by DCs. Based on these findings, all further *in vitro* experiments followed the scheme below (exceptions are indicated for the respective experiment):

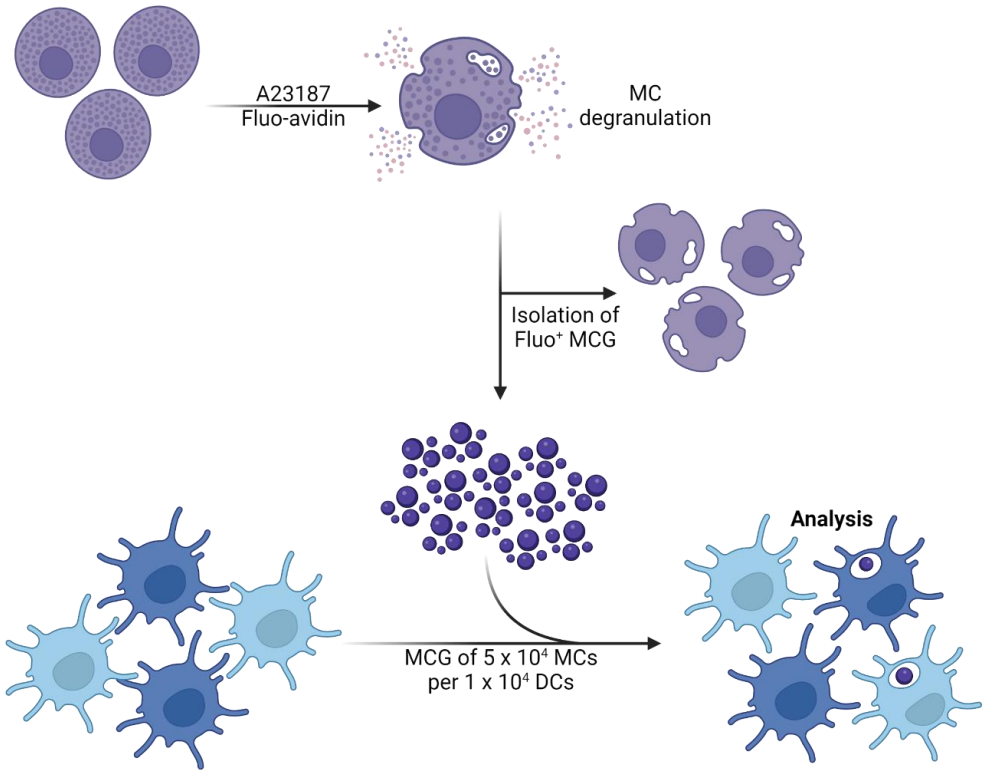

Figure 4.5: Scheme for treatment of DCs with MCG *in vitro*. DCs will be generated from BM cells. To isolate MCG, *in vitro* MC cultures will be stimulated with calcium ionophore A23187 in the presence of fluorescently labeled avidin. Upon sequential centrifugation, MCG will be resuspended in sterile 1x PBS and used for treatment of DCs *in vitro*. MCG of 5 x 10^4 MCs will be used for the treatment of 1 x 10^4 DCs.

In short, MCG will be isolated from *in vitro* cultures by the activation of MCs with the calcium ionophor A23187 and stained by adding fluorochrome-labeled avidin. MCs and MCG will be separated by slow centrifugation. Subsequently, MCG will be concentrated and resuspended in sterile 1x PBS and used for cocultures with DCs *in vitro*.

4.2 Analysis of the influence of the maturation status of DCs on MCG uptake

The uptake of antigens and other particles from the surrounding environment is mostly restricted to imDCs, because the activity of the endocytic pathways is reduced during maturation [22].

Using the established MCG uptake protocol *in vitro*, I determined whether DCs with different maturation status have varying MCG uptake capacity. These *in vitro* studies were done together with Martha Höroldt, as part of her bachelor thesis that was done in

our working group under my supervision [205]. Subsequently, I used these raw data for reanalysis.

BM cells were isolated and differentiated into imDCs or matDCs in the presence of GM-CSF with or without additional IL-4 for either 3 or 10 days (see section 3.1.1). Subsequently, they were treated with isolated fluorescently labeled PCMC-derived MCG and the MCG uptake capacity was analyzed by flow cytometry 24 h after treatment.

DCs were gated as $CD11c^+$ $MHCII^+$ cells out of the single cells as described above in Figure 4.3. Firstly, successful maturation of the DCs was verified by using flow cytometric analysis of the cell surface markers CD11c, MHCII, CCR7 and CD86 (data not shown here) [205].

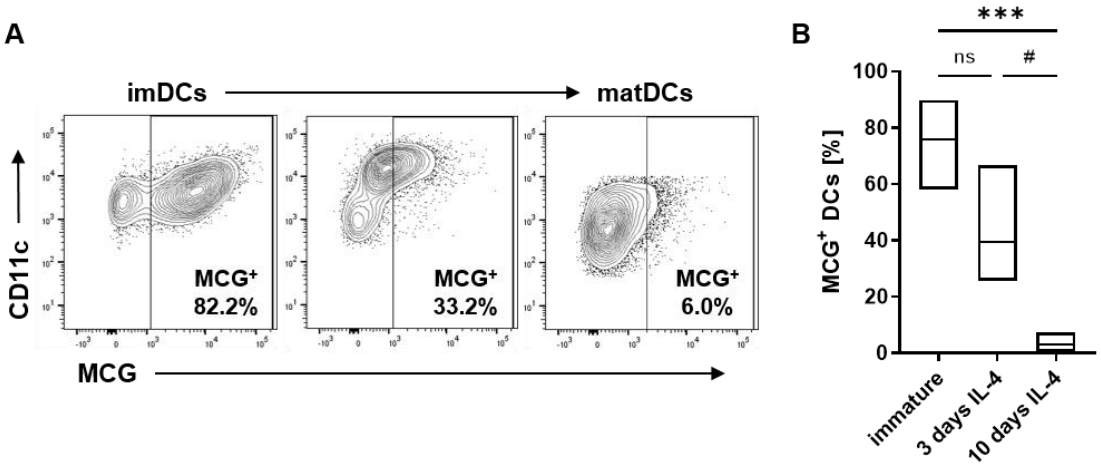

Figure 4.6: MCG uptake is restricted to imDCs *in vitro*. imDCs and matDCs were treated with isolated and fluorescently labeled MCG and analyzed by flow cytometry. (A) Representative contour plots show MCG uptake by imDCs, partially matured DCs (3 days IL-4) and fully matured DCs (10 days IL-4). (B) Floating bars quantify MCG^+ DC fractions of total DCs in different maturation states (N = 7). *** $p < 0.001$, ** $p < 0.01$, * $p < 0.05$, # $p \leq 0.10$, ns $p > 0.10$.

Figure 4.6A shows representative contour plots of MCG uptake by imDCs (only GM-CSF), partially matured DCs (3 days IL-4) and fully matured DCs (10 days IL-4). Figure 4.6B summarizes the results showing the respective fraction of MCG^+ DCs out of the total DC population. Decreasing MCG uptake capacity was shown with increasing maturation. imDCs showed the highest MCG uptake with approximately 60 - 90% MCG^+ DCs. Partially matured DCs exhibited approx. 25 - 65% MCG^+ DCs, while among the fully matured DCs less than 8% were MCG^+.

Based on the *in vitro* findings, the MCG uptake capacity of imDCs was also analyzed *ex vivo*. DCs with different maturation status were isolated from murine skin or skin-draining LNs (Table 3.6). DCs of untreated skin derived from wt mice (sorted as $CD45^+$ $F4/80^-$

CD11c$^+$ MHCII$^+$ out of single cells) could be referred to as imDCs. The FITC-induced CHS harbors the advantage that antigen$^+$ DCs (or other cells) can be easily detected by the intrinsic fluorescence of FITC [1,206]. Therefore, DCs that migrated from the skin upon FITC-induced CHS (see section 3.3.2) were isolated from the skin-draining LNs (LNm DCs, sorted as CD45$^+$ CD11c^{low} MHCII$^+$ FITC$^+$ out of single cells) and reflected matDCs. For this issue, we used MC-depleted Mcpt5-Cre$^+$ R-DTA$^+$ mice to exclude the possibility of MCG uptake already *in vivo*. CD11b$^+$ LNr, sinusoid DCs (CD11b$^+$ LNr DCs, sorted as CD45$^+$ CD11c$^+$ MHCII$^{+/-}$ CD8$^-$ CD169$^-$ CD11b$^+$ out of single cells) [19] were additionally sorted from untreated wt and FITC-treated Mcpt5-Cre$^+$ R-DTA$^+$ mice. The sorted DC populations were subsequently treated *ex vivo* with isolated and fluorescently labeled PCMC-derived MCG. MCG uptake capacity was analyzed 24 h after treatment by flow cytometry.

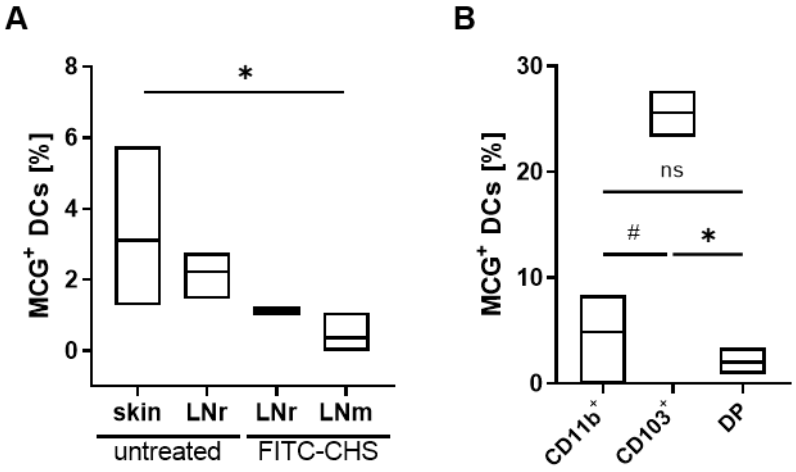

Figure 4.7: MCG uptake is restricted to imDCs *ex vivo*. Sorted imDCs and CD11b$^+$ LNr DCs (LNr) of untreated wt mice and CD11b$^+$ LNr and FITC$^+$ LNm DCs (LNm) from skin-draining LNs of MC-depleted Mcpt5-Cre$^+$ R-DTA$^+$ mice upon FITC-induced CHS (FITC-CHS) were treated *ex vivo* with isolated and fluorescently labeled MCG and analyzed by flow cytometry. (A) MCG uptake capacity was analyzed as frequency of MCG$^+$ DCs of respective DC population. Due to clarity of figure, only significant results of statistical analyses were shown. CD11b$^+$ LNr and LNm DCs could only be analyzed in one independent experiment (N = 3-6, each measured in technical duplicates or triplicates). (B) Among immature skin DCs MCG uptake by distinct DC subsets was analyzed by flow cytometry and shown as MCG$^+$ DC fraction of total DC subset. DC subsets could only be analyzed in one independent experiment (N = 3, each measured in technical triplicates). *** $p < 0.001$, ** $p < 0.01$, * $p < 0.05$, # $p \leq 0.10$, ns $p > 0.10$.

Interestingly, imDCs showed the highest *ex vivo* MCG uptake with approx. 3% MCG$^+$ DCs. Indeed, matDCs almost completely lost their MCG uptake capacity and exhibited a significantly decreased percentage of MCG$^+$ DCs (Figure 4.7A). CD11b$^+$ LNr DCs took

up MCG to an intermediate percentage, while CD11b$^+$ LNr DCs of treated mice showed a significantly reduced uptake capacity compared to those of untreated mice.

Additionally, imDCs from untreated wt mouse skin were divided into cDC1 and cDC2 subsets based on their surface expression of CD11b and CD103 [2,143,207] and analyzed for their MCG uptake capacity. Interestingly, all skin DC subsets were able to take up MCG, while CD103$^+$ DCs showed the highest MCG uptake capacity compared to CD11b$^+$ DCs and DP DCs (Figure 4.7B).

For further characterization of the MCG uptake by CD11b$^+$ LNr and LNm DCs *in vivo*, MELC analyses were performed. Therefore, MCG were stained *in vivo* with fluorescently labeled avidin and CHS was induced by epicutaneous application of FITC on the ear skin. After 48 h, the ear skin-draining auricular LNs were isolated and prepared for analysis by MELC.

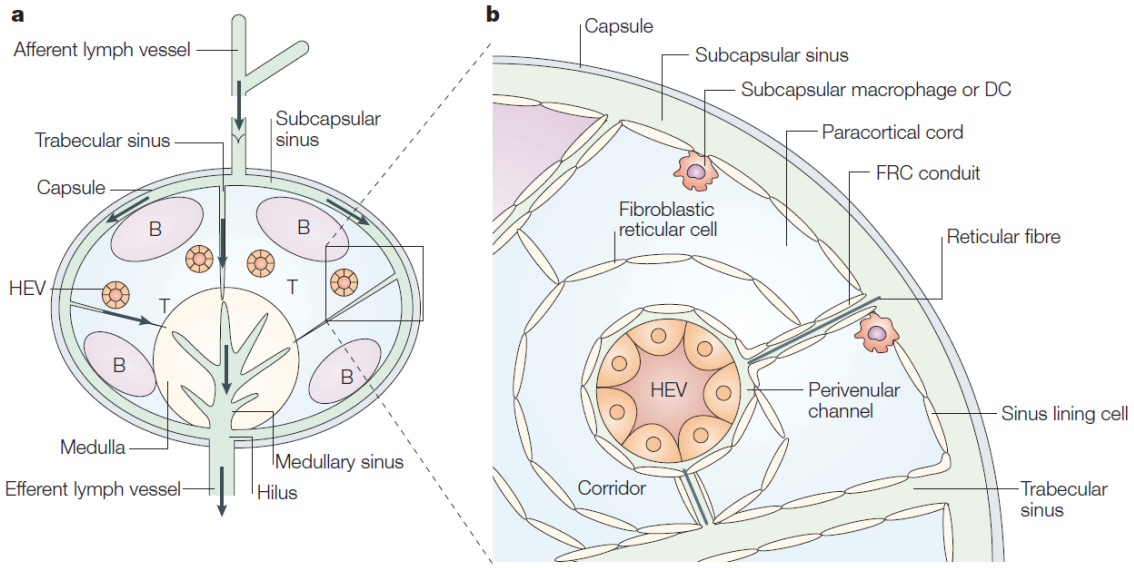

Figure 4.8: Schematic overview of the main structural components of a LN. (A) Scheme shows structural components of LNs including routes of lymph flow (indicated by arrows) through lymph vessels and sinuses. (B) Zoom-in of the schematic capsule region of a LN. Figure taken from Andrian *et al.* (2003) [208]. B – B cell zone, FRC – fibroblastic reticular cell, HEV – high endothelial venule, T – T cell zone.

Figure 4.8 shows a schematic overview of the architecture of LNs, including important structural components like lymph vessels, sinuses and T and B cell zones. The MELC procedure allows for the staining of sections with multiple, different fluorescently labeled antibodies, by cycles of staining, acquisition, bleaching and recording post-bleaching (see section 3.4.4 and [200]). The staining for T cell (CD3ε, red) and B cell zones

(CD45R, green), vascular (CD31, white) and lymphatic endothelial cells (LYVE1, blue) was used for spatial orientation (see example in Figure 4.9A).

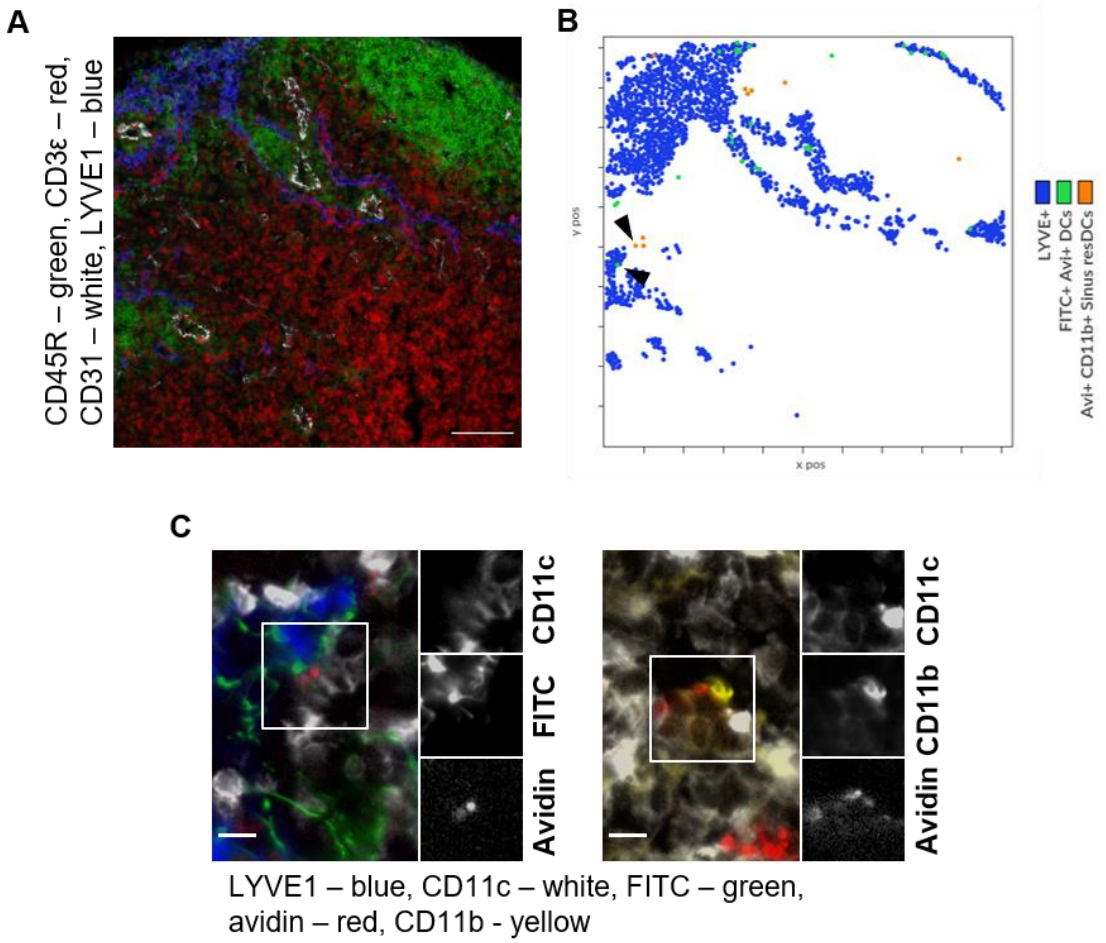

Figure 4.9: Localization of MCG⁺ DCs within skin-draining LNs. Intracellular MCG of wt mice were stained by i.d. injection of AF647-labeled avidin. 48 h after FITC-induced CHS ear skin-draining, auricular LNs were analyzed by MELC. (A) Fluorescently labeled antibodies were used to stain LN sections for B cell (CD45R, green) and T cell zones (CD3ε, red), vascular endothelial (CD31, white) and LECs (LYVE1, blue) (scale bar 100 µm). (B-C) Schematic overview (B) and representative images (C) show the number and localization (B) of MCG⁺ LNm (C left; LYVE1 – blue, CD11c – white, FITC – green, AF647-avidin – red; scale bar 10 µm) and MCG⁺ LNr DCs (C right; LYVE1 – blue, CD11c – white, CD11b – yellow, AF647-avidin – red; scale bar 10 µm).

Lymphatic endothelial cells (LECs) were stained with fluorescently labeled antibodies against the hyaluronan receptor LYVE1 and are color-coded in blue. LYVE1-expressing LECs are reported to be part of the lymphatic vessels and the LN sinus [209]. Therefore, the subcapsular and trabecular sinus of the ear skin-draining LNs were successfully visualized (Figure 4.8 and Figure 4.9A). As also represented in Figure 4.8, the B cell zones (CD45R, green) were detected in the capsule and subcapsular sinus (Figure

4.9A). They were further surrounded by the T cell zones (red) that were stained with fluorescently labeled antibodies against CD3ε (Figure 4.8 and Figure 4.9A).

Since CD11b$^+$ LNr DCs are located in close proximity to the lymphatic sinus and to minimize effects that are due to the analyzed location (LN capsule vs. center), slices that showed only LN center regions were excluded from the analyses and only those that contained LN capsule areas as well were included. As detailed in section 3.4.4, a matrix of intensities and distances was calculated and exported into FCS files that were finally analyzed with the online cytometry analysis platform “cytobank.org”.

Upon FITC application, LNm DCs represented the fraction of DCs that migrated from the skin to the dLN upon antigen (FITC) uptake. Therefore, LNm DCs were identified as FITC$^+$ DCs and further distinguished between MCG$^-$ and MCG$^+$ LNm DCs by their avidin-AF647 fluorescence intensity (Figure 4.9C left). In contrast, CD11b$^+$ LNr DCs were gated as FITC^{low} CD11b$^+$ sinusoid DCs as described above, because they were not able to directly take up antigens (FITC) applied onto the skin due to their localization within the dLNs (Figure 4.9C right). Using the Cytobank analysis software, the number and localization of MCG$^+$ LNm DCs and MCG$^+$ CD11b$^+$ LNr DCs were analyzed (Figure 4.9B/Figure 4.10).

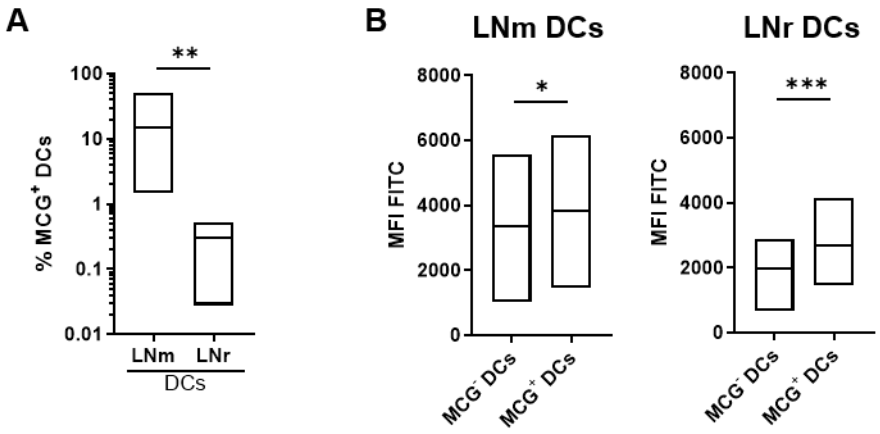

Figure 4.10: MCG are preferentially taken up by imDC in the skin and shuttled to the draining LN. (A/B) Intracellular MCG of wt mice were stained by i.d. injection of AF647-labeled avidin. 48 h after FITC-induced CHS, ear skin-draining, auricular LNs were analyzed by MELC. (A) MCG$^+$ LNm and MCG$^+$ LNr DC fractions of all LNm or CD11b$^+$ LNr DCs respectively was analyzed using Cytobank analysis software (N = 8/9). (B) MCG$^-$ and MCG$^+$ LNm and LNr DCs were analyzed for their uptake of FITC per cell as MFI (N = 9). *** $p < 0.001$, ** $p < 0.01$, * $p < 0.05$, # $p \leq 0.10$, ns $p > 0.10$.

Indeed, both MCG$^+$ FITC$^+$ skin DCs, which actively migrated to the dLN, and MCG$^+$ FITC^{low} CD11b$^+$ LNr DCs, which took up MCG that were drained from the skin to

the dLN, were detected within the LN. As shown in Figure 4.10A, a higher amount of LNm DCs that took up MCG was detected compared to MCG^+ $CD11b^+$ LNr DCs. While approx. 10% of LNm DCs were detected as MCG^+ DCs, only approx. 0.3% were identified as MCG^+ $CD11b^+$ LNr DCs. Additionally, the fluorescence intensity of FITC that has to be drained or shuttled from the skin to the skin-draining LNs was analyzed (Figure 4.10B). The direct comparison showed a significantly increased MFI in MCG^+ DCs compared to MCG^- DCs, as well as for LNm and for LNr DCs. As expected, LNm DCs in general showed a higher FITC fluorescence intensity compared to LNr DCs.
In summary, these data showed that MCG uptake (*in vitro* and *ex vivo*) is inversely correlated to the maturation status of DCs and is mainly restricted to imDCs. The *in vitro* studies have been confirmed in *ex vivo* and *in vivo* studies, where this phenomenon is valid not only for the skin but also for DCs located in the dLN.

4.3 Analysis of the role of macropinocytosis in MCG uptake by imDCs

imDCs exhibit distinct endocytic pathways that are necessary for the antigen uptake from the extracellular space. In 2018, Silke Balk did her master thesis in our working group under my supervision [210]. Using *in vitro* pharmacologic inhibition, one aim of her thesis was to define the endocytic mechanism that may play a role during MCG uptake by imDCs. Upon macropinocytosis inhibition, she showed that the macropinocytosis was involved in MCG uptake by imDCs as demonstrated by a reduced fraction of MCG^+ DCs and a reduced MCG fluorescence intensity. In contrast, a participation of dynamin-dependent endocytic pathways could not be completely excluded.
Within my thesis and in addition to Silke Balk's data, the MCG uptake by DCs that were treated with DMA, a macropinocytosis inhibitor, was analyzed by imaging flow cytometry. Compared to conventional flow cytometry, this method has the advantage of additional, imaging based information about intracellular localization and distribution of a distinct antibody or other dye [211].
In vitro differentiated imDCs were pre-incubated with 100 µM for 30 min in serum-free RPMI1640 medium and subsequently treated with *in vitro* isolated and AF488-labeled PCMC-derived MCG for 2 h and finally analyzed by imaging flow cytometry.

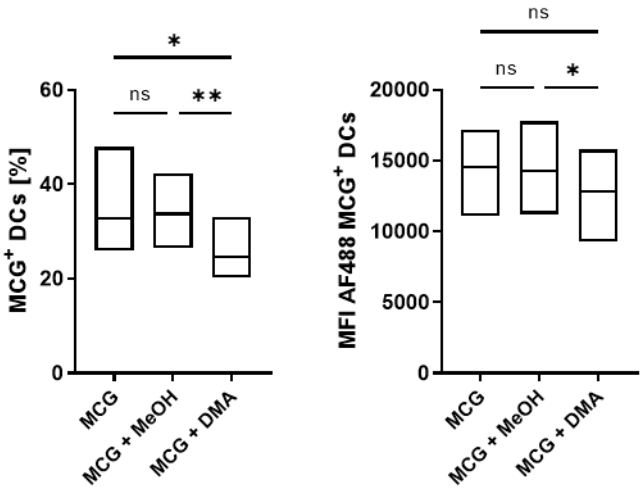

Figure 4.11: Macropinocytosis inhibition leads to reduced MCG uptake by imDCs *in vitro*. imDCs were pre-treated *in vitro* with 100 µM DMA or methanol alone for 30 min with additional treatment with isolated and Af488-labeled MCG for another 2 h. MCG uptake was analyzed as MCG^+ DC fraction of total DCs (left) or as AF488 MFI of MCG^+ DC fraction by imaging flow cytometry (N = 8). *** $p < 0.001$, ** $p < 0.01$, * $p < 0.05$, # $p \leq 0.10$, ns $p > 0.10$.

As depicted in Figure 4.11, the reduced MCG uptake by imDCs upon macropinocytosis inhibition was confirmed by imaging flow cytometry, shown as a reduced fraction of MCG^+ DCs and reduced MCG fluorescence intensity, indicating a reduced amount of engulfed MCG. Cells were stained with fluorescently labeled antibodies against CD11c (magenta) and MHCII (blue), and $CD11c^+$ $MHCII^+$ DCs were analyzed for their MCG content (green). Indeed, exemplary microscopic images showed a reduced number of MCG per cell in DMA-treated DCs compared to the solvent control (Figure 4.12A), which confirmed the reduced MCG fluorescence intensity. Additionally, the Amnis® IDEAS analysis software was used for calculating the spot (MCG) count over the whole DC population. In line, the spot count analysis showed a significantly increased spot count upon MCG treatment compared to untreated DCs (Figure 4.12B left) and a significantly reduced spot count upon DMA treatment compared to the solvent control (Figure 4.12B right).

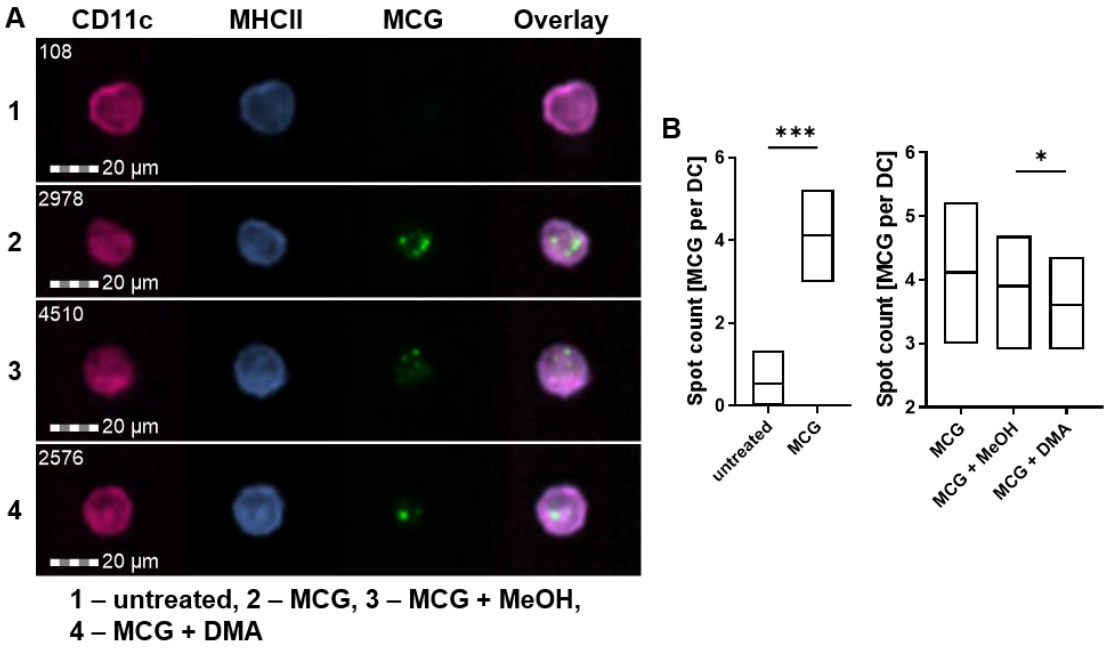

Figure 4.12: Macropinocytosis inhibition leads to reduced MCG uptake by imDCs *in vitro*. (A-C) imDCs were pre-treated with 100 µM DMA or methanol alone for 30 min and MCG uptake was analyzed by imaging flow cytometry 2 h after additional treatment with isolated and fluorescently labeled MCG. (A) Representative images show DCs that were stained with fluorescently labeled antibodies again CD11c (magenta) and MHCII (blue) upon engulfment of AF488-labeled MCG (green). (B) IDEAS software was used to calculate MCG spot count based on AF488 fluorescence (N = 8). *** $p < 0.001$, ** $p < 0.01$, * $p < 0.05$, # $p \leq 0.10$, ns $p > 0.10$.

In summary, the MCG uptake by imDCs was confirmed to involve macropinocytosis since its inhibition led to a reduced fraction of MCG^+ DCs and a reduced number of spots (MCG) per DC.

4.4 Analysis of the capacity of imDCs to take up MCG of different origin

In the past, BMMCs and different MC cell lines were widely used to study MC functions and their impact on DC maturation and functionality *in vitro* [109,125,212]. Therefore, the capacity of imDCs to take up MCG from PCMCs, BMMCs and the cell line MC/9 was compared. PCMCs, BMMCs and MC/9 were stimulated with the calcium ionophore A23187 in the presence of fluorochrome-labeled avidin and MCG were. MCG isolated from all cell types could be stained to an equal amount with fluorochrome-conjugated avidin (Figure 4.13). The MCG of the cell line MC/9 showed the lowest staining efficiency, but still with an amount of avidin labeled particles of above 75%. These results

demonstrated that PCMCs, BMMCs and the cell line MC/9 share the connective tissue type with heparin-based MCG.

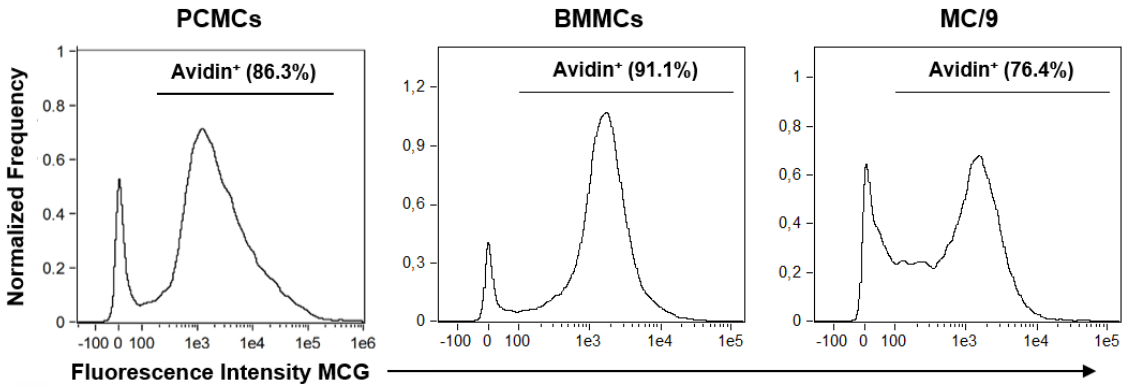

Figure 4.13: Avidin staining of MCG of different origin. PCMCs, BMMCs and MC/9 were stimulated and fluorescently labeled MCG were isolated. MCG of different origin were analyzed by imaging flow cytometry. Small particles were gated based on size (Area_Brightfield (BF)) and Aspect Ratio (Ratio of event height and width) of events to exclude contamination with remaining cells (left) and Avidin binding of small particles (as described in Figure 4.1) was analyzed as fluorescence intensity that were plotted against frequency that was normalized by default bin counts.

imDCs were subsequently cultured *in vitro* with isolated and TR (confocal microscopy)- or AF488 (flow cytometry)-labeled MCG for 24 h, and subsequently analyzed by confocal microscopy or flow cytometry.

For confocal microscopy, DCs were grown and treated on sterile cover slips and finally stained with 4',6-Diamidino-2-phenylindo (DAPI, blue) as a nuclear staining and with fluorescently labeled antibodies against CD11c (green) for a membrane staining. For flow cytometry, the cells were harvested and stained with fluorescently labeled antibodies against CD11c and MHCII.

PCMC-derived MCG were efficiently taken up by imDCs as shown by confocal microscopy (Figure 4.14A) and by the quantification upon flow cytometry with a mean frequency of approx. 55% MCG^+ DCs of all $CD11c^+$ $MHCII^+$ DCs (Figure 4.14B). In contrast, the uptake of BMMC-derived MCG was strongly reduced to approx. 4% MCG^+ DCs and almost completely absent for MC/9-derived MCG with approx. 1% MCG^+ DCs (Figure 4.14B). In line, no TR signal could be detected within DCs that were treated either with BMMC- or MC/9-derived MCG and analyzed by confocal microscopy (Figure 4.14A).

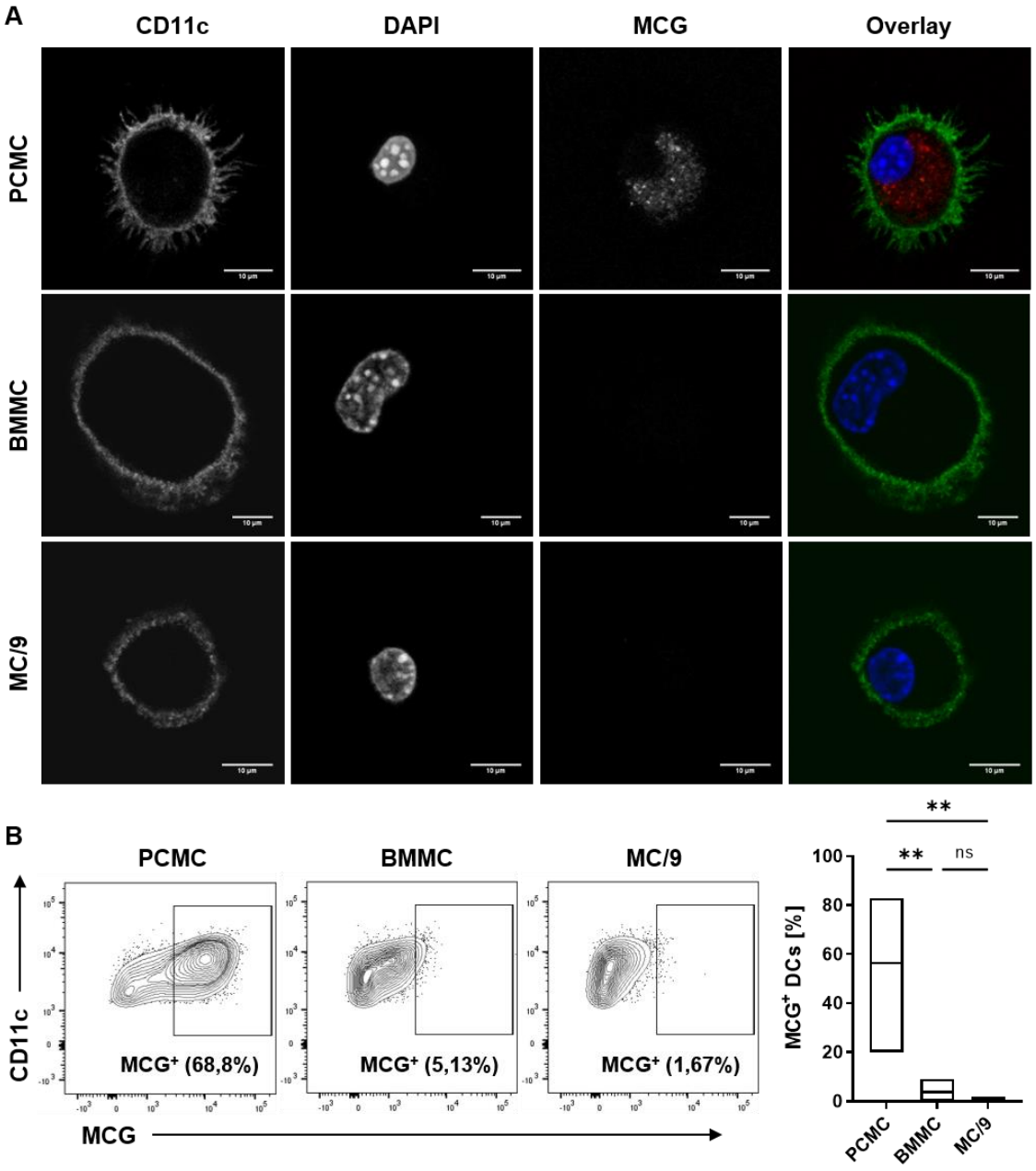

Figure 4.14: Structure-dependent sensing precedes MCG uptake by imDCs. imDCs were treated with *in vitro* isolated and fluorescently labeled MCG of different origin and analyzed by confocal microscopy (A) or flow cytometry (B). (A) To avoid bleed-through of fluorescence emission, sequential unidirectional scanning at 400 Hz was performed: sequence 1: excitation 405 nm, emission 435 nm – 475 nm, sequence 2: excitation 488 nm, emission 505 nm – 550 nm, sequence 3: excitation 561 nm, emission 600 nm – 650 nm (sequences were altered between lines). Voxel size was adjusted to 97 nm x 97 nm x 1000 nm (dx, dy, dz). Respective images show single channels of fluorescently labeled antibody against CD11c, nuclear staining with DAPI or TR-labeled MCG. Channels were pseudo-colored with ImageJ software to create overlay. (B) Uptake of PCMC-, BMMC- and MC/9-derived MCG by imDCs was analyzed as fractions of MCG^+ DCs of the total DC population (N = 6). *** $p < 0.001$, ** $p < 0.01$, * $p < 0.05$, # $p \leq 0.10$, ns $p > 0.10$.

In summary, these findings indicate that PCMC-derived MCG and those derived from BMMCs and the cell line MC/9 differ in their capacity to be taken up by imDCs. These data show that despite equal avidin staining and, hence, CTMC type, only PCMC-derived MCH are engulfed by imDCs. Thus, the uptake of MCG seems to be not driven by unspecific “cell drinking” but rather includes the sensing of a (PCMC-) specific MCG structural component.

4.5 Analysis of the role of different signaling pathways in MCG uptake by imDCs

Despite known as “non-selective cell-drinking”, macropinocytosis can also be induced by growth factors, chemokines or TLRs [75]. Due to the exclusive engulfment of PCMC-derived MCG by imDCs, the involvement of induced macropinocytosis, which leads to the MCG uptake, could be hypothesized. Therefore, the role of different signaling pathways in the induction of macropinocytosis and therefore in the MCG uptake by imDCs was investigated.

4.5.1 *In vitro* analysis of different signaling pathways involved in MCG uptake by imDCs

Firstly, the role of different signaling pathways was analyzed *in vitro*. BM cells from different conventional or conditional *knockout* mouse lines were isolated and differentiated into imDCs. Subsequently, they were treated with isolated and fluorescently labeled PCMC-derived MCG and the MCG uptake capacity was analyzed by flow cytometry 24 h after treatment.

The role of the TLR signaling in inducing macropinocytosis-mediated MCG uptake by imDCs was investigated. As described above, TLR signaling requires TIR domain containing adaptor proteins, which divide the signaling pathways into two different types: MyD88-dependent and TRIF-dependent pathway (see section 1.1.2.1 and [29]). The MyD88-FL x CD11c-Cre mouse line, which specifically lack MyD88 in DCs from Cre^+ mice, was used to analyze the role of MyD88-dependent TLRs in MCG uptake. By analyzing the uptake capacity of imDCs *in vitro*, no difference was detected in the presence (Cre^-) or absence (Cre^+) of MyD88 (Figure 4.15A).

Furthermore, the impact of TRIF-dependent TLRs and used conventional *TRIF*$^{-/-}$ mice and wt mice to generate imDCs was analyzed. Interestingly, MCG uptake capacity of imDCs *in vitro* was comparable in *TRIF*$^{-/-}$ cells compared to wt cells (Figure 4.15A).

Altogether, the participation of MyD88- and TRIF-dependent TLRs in MCG sensing and uptake by imDCs was excluded.

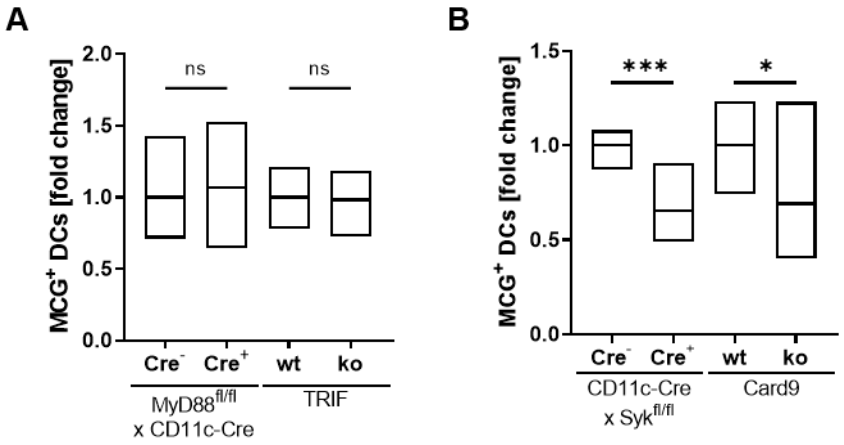

Figure 4.15: Syk-/Card9-dependent signaling contributes to *in vitro* MCG uptake by imDCs. imDCs were generated *in vitro* by using BM cells of the respective mouse line and were subsequently incubated with *in vitro* isolated and fluorescently labeled PCMC-derived MCG for 24 h to analyze the impact of TLR (A, N = 6-9) and Syk-/Card9-dependent signaling (B, N = 6-9) on MCG uptake. MCG uptake capacity was analyzed as a fraction of MCG^+ DCs of all DCs and fold change was calculated by setting the mean of MCG^+ wt or Cre^- DCs to 1. *** $p < 0.001$, ** $p < 0.01$, * $p < 0.05$, # $p \leq 0.10$, ns $p > 0.10$.

CLRs are particularly important for the function of DCs as monitors of environmental imbalances and are well-known for their Syk-/Card9-dependent signaling [40,213]. In addition to the TLRs, Syk- or Card9-dependent signaling were analyzed for their role in MCG uptake by inducing macropinocytosis.

Therefore, imDCs of conventional *Card9*$^{-/-}$ mice and corresponding wt mice were generated, treated with fluorescently labeled MCG and analyzed for their MCG uptake capacity *in vitro,* as described before. To analyze the impact of Syk on MCG uptake by imDCs, the CD11c-Cre mouse line was crossed to the Syk-FL mouse line to generate a conditional DC-specific Syk *knockout*. The Syk *knockout* within DCs was verified by flow cytometry (Appendix Figure 7.1). Apart from a slight decrease of the fraction of Syk^+ Mphs in Cre^+ compared to Cre^- mice (as expected from the data sheet of the CD11c-Cre mouse line: B6.Cg-Tg(Itgax-cre)1-1Reiz/J [C57BL/6J], RRID: IMSR_JAX:008068), Syk expression was strongly reduced in DCs derived from Cre^+ mice compared to Cre^- mice, which is line with a previously published DC-specific conditional Syk *knockout* mouse line [214]. By analyzing the MCG uptake capacity of imDCs *in vitro*, a significant reduction on average by 35% of MCG^+ DCs in the absence (Cre^+) of Syk compared to the wt (Cre^-) situation was detected (Figure 4.15B). Interestingly, the percentage of

MCG$^+$ DCs was also significantly reduced on average by 30% in the absence of Card9 compared to the wt situation (Figure 4.15B).
In summary, an impaired Syk- or Card9-dependent signaling was shown to reduce MCG uptake by imDCs *in vitro*, which indicates the involvement of CLR engagement in MCG uptake, while an involvement of TLRs could be excluded.

4.5.2 *In vivo* analysis of the impact of Syk-/Card9-dependent signaling on MCG uptake by imDCs

In addition to the *in vitro* situation, MCG uptake by DCs and its impact on skin inflammation was analyzed in the presence or absence of Card9 and Syk *in vivo* by means of a DNFB-induced CHS response.
Intracellular MCG were stained *in vivo* with fluorescently labeled avidin as described in section 3.3.1 and [1]. To induce CHS, mice were sensitized and challenged with DNFB in acetone/olive oil or with vehicle alone. Finally, the adaptive ear swelling was determined as a readout for the inflammatory response and the MCG uptake by dermal DCs analyzed by flow cytometry 16 and 24 h after challenge.
First of all, the ear swelling response and MCG uptake in the presence or absence of Syk were analyzed 24 h after DNFB challenge. Both, DNFB-treated Cre$^-$ and Cre$^+$ mice showed a significant increase of the ear swelling 24 h after DNFB challenge compared to vehicle control mice, indicating the successful induction of an inflammatory response. In contrast, the ear swelling response was not altered between mice with Syk competent and Syk deficient DCs (Figure 4.16A left). Additionally, the MCG uptake capacity was analyzed as the number of MCG$^+$ DC per 10^3 DCs. DCs were gated as CD45$^+$ F4/80$^-$ CD11c$^+$ MHCII$^+$ cells out of single cells and further distinguished by their MCG fluorescence. In contrast to the *in vitro* data, no difference in MCG$^+$ DCs within the ear skin was detected 24 h after challenge between Cre$^-$ and Cre$^+$- mice (Figure 4.16A right). Additionally, *Card9*$^{-/-}$ mice were used to analyze the impact of defective Card9-mediated signaling on the adaptive ear swelling response and MCG uptake by dermal DCs. Both, DNFB-treated wt and *Card9*$^{-/-}$ mice showed a significant increase of ear swelling 24 h after DNFB challenge compared to the vehicle control mice. Interestingly, the ear swelling response was significantly reduced 24 h after hapten challenge in *Card9*$^{-/-}$ mice compared to wt controls (Figure 4.16B left). However, no alteration of the number of MCG$^+$ DC was found between wt and *Card9*$^{-/-}$ mice within the ear skin 24 h after DNFB challenge (Figure 4.16B right).

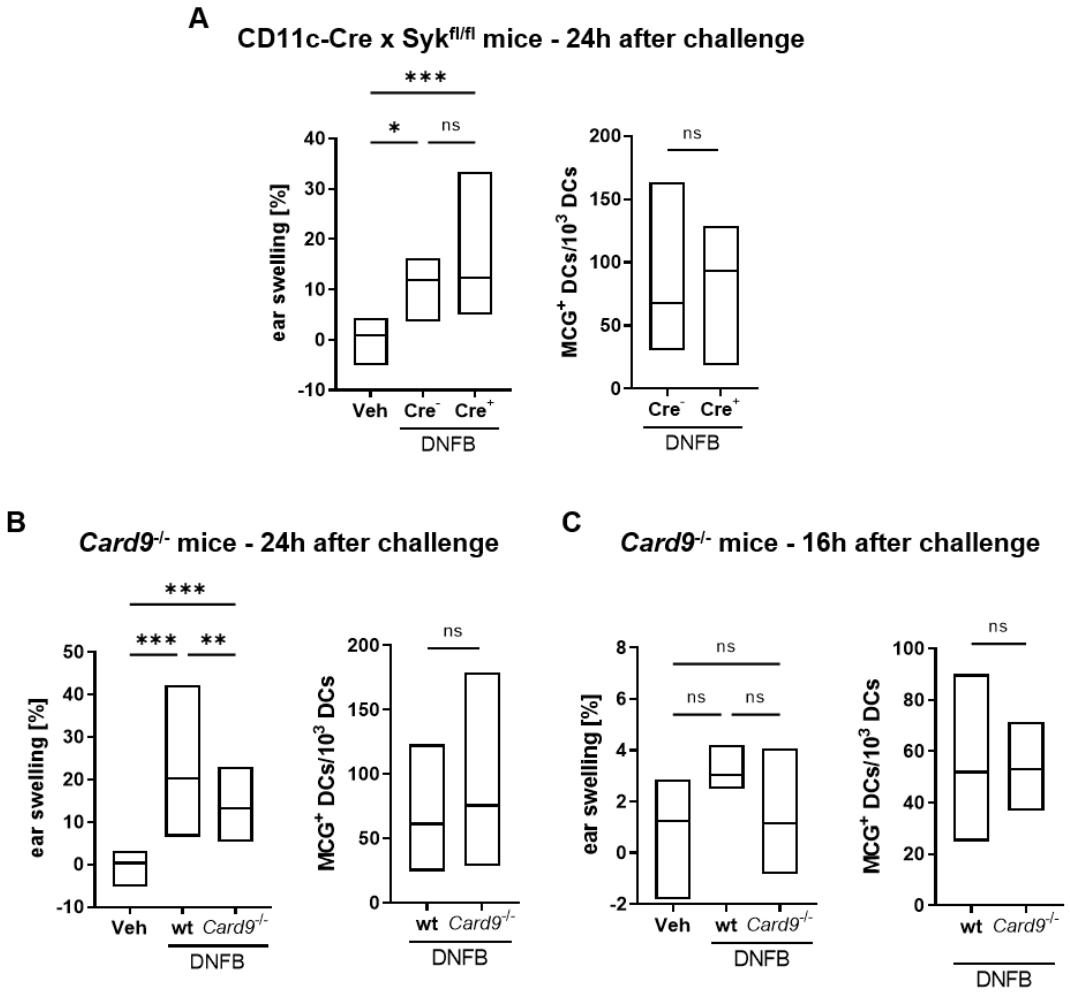

Figure 4.16: The DNFB-induced inflammatory response is influenced by Card9-dependent signaling. CD11c-Cre x Syk$^{fl/fl}$ or wt and *Card9*$^{-/-}$ mice were sensitized and challenged with DNFB in acetone/olive oil (4:1). Wt or Cre^{-} mice treated with acetone/olive oil (4:1) alone served as a control (vehicle). Inflammatory response was analyzed as ear swelling (A left, N = 9-11, B left, N = 15-19, C left, N = 3-5). Cell count of MCG^{+} DCs was analyzed from digested ear skin by flow cytometry (A right, N =10/11, B right, N = 15, C right, N = 5) 16 or 24 h after challenge and calculated as MCG^{+} DCs per 10^3 DCs. In contrast to the time point of 24 h after challenge, data of 16 h after CHS challenge derived from only one independent experiment. *** $p < 0.001$, ** $p < 0.01$, * $p < 0.05$, # $p \leq 0.10$, ns $p > 0.10$.

Due to these unexpected results, alterations of the MCG uptake kinetic were speculated. MCG^{+} DCs were previously shown to exhibit an increased migratory behavior compared to MCG^{-} DCs [1]. Therefore, I questioned, whether differences cannot be detected anymore at 24 h after challenge because a part of the MCG^{+} DCs left already the skin and migrated to dLNs. That is why the ear swelling response and MCG uptake by DCs was also analyzed 16 h after challenge (Figure 4.16C). Since additional CD11c-Cre x Syk-FL mice were not available this analysis was only performed with *Card9*$^{-/-}$ mice. The

tendency of the reduced ear swelling in *Card9*$^{-/-}$ mice compared to the wt controls was already observable 16 h after challenge but showed no significant difference yet (Figure 4.16C left). DNFB treated wt mice showed a slight increase in the ear swelling compared to vehicle controls, while the ear swelling of *Card9*$^{-/-}$ mice was reduced compared to DNFB treated wt mice and showed approximately the same level as the vehicle treated wt mice. The number of MCG^{+} DCs in the ear skin was still not altered between wt and *Card9*$^{-/-}$ mice 16 h after challenge (Figure 4.16C right).

In summary, the involvement of TLR signaling in MCG uptake by DCs was excluded, while Syk-/Card9-dependent signaling seemed to play an important role *in vitro*. *In vivo* Card9 played essential significant role in inducing a robust inflammatory response upon DNFB challenge, while Syk was dispensable in DCs for the inflammatory response. In contrast, MCG uptake was not altered in the skin neither upon Syk nor upon Card9 deficiency.

4.6 *In vitro* analysis of the impact of MCG uptake by imDCs on T cell priming and differentiation

In previous studies, our working group proved that MCG^{+} DCs induce enhanced T cell proliferation compared to MCG^{-} DCs [1]. In this thesis, the effects of MCG uptake on T cell polarization towards certain T_H cell subsets was questioned together with the help of Dr. Konstantinos Katsoulis-Dimitriou. imDCs were treated *in vitro* with OVA peptide and fluorescently labeled MCG and sorted for MCG^{-} and MCG^{+} DCs. MCG^{-}/MCG^{+} DCs were subsequently co-incubated with naïve CD4^{+} OTII T cells for 4 d in a ratio of 1:5 (DC:T cell). Successful activation of T cells was indicated by strong T cell proliferation (data not shown). Finally, T cells were re-stimulated with anti-CD3 and anti-CD28 antibody for 24 h. The T cell culture supernatants were subsequently collected and analyzed for their cytokine content with LEGENDplex™ Multiplex Kits. In total, 16 cytokines (IL-1β, IL-2, IL-4, IL-5, IL-6, IL-9, IL-10, IL-12p70, IL-13, IL-17A, IL-22, IL-23, IL-27,GM-CSF, IFN-γ, TNF) were analyzed. Figure 4.17 shows the supernatant levels of the cytokines that could be detected in concentrations above the detection limit of the assays. The production of the T_H1 cytokine TNF (Figure 4.17A) and IL-2 (Figure 4.17C) by T cells after MCG uptake by imDCs compared to MCG^{-} DCs was slightly but not significantly reduced. MCG uptake by imDCs did not influence the release of T_H1 cytokine IFN-γ by CD4^{+} T cells in this experimental setting (Figure 4.17A). In contrast, T cell production of T_H2 cytokines IL-4, IL-5, IL-9 and IL-13 was strongly increased upon co-incubation with MCG^{+} DCs compared to MCG^{-} DCs (Figure 4.17B). In line, IL-10 was only detectable

after incubation with MCG$^+$ DCs (Figure 4.17D). Additionally, also T_H17 cytokines, like IL-6, IL-17A and IL-22 could be detected at higher levels in supernatants of T cells that had contact to MCG$^+$ DCs compared to MCG$^-$ DCs (Figure 4.17E).

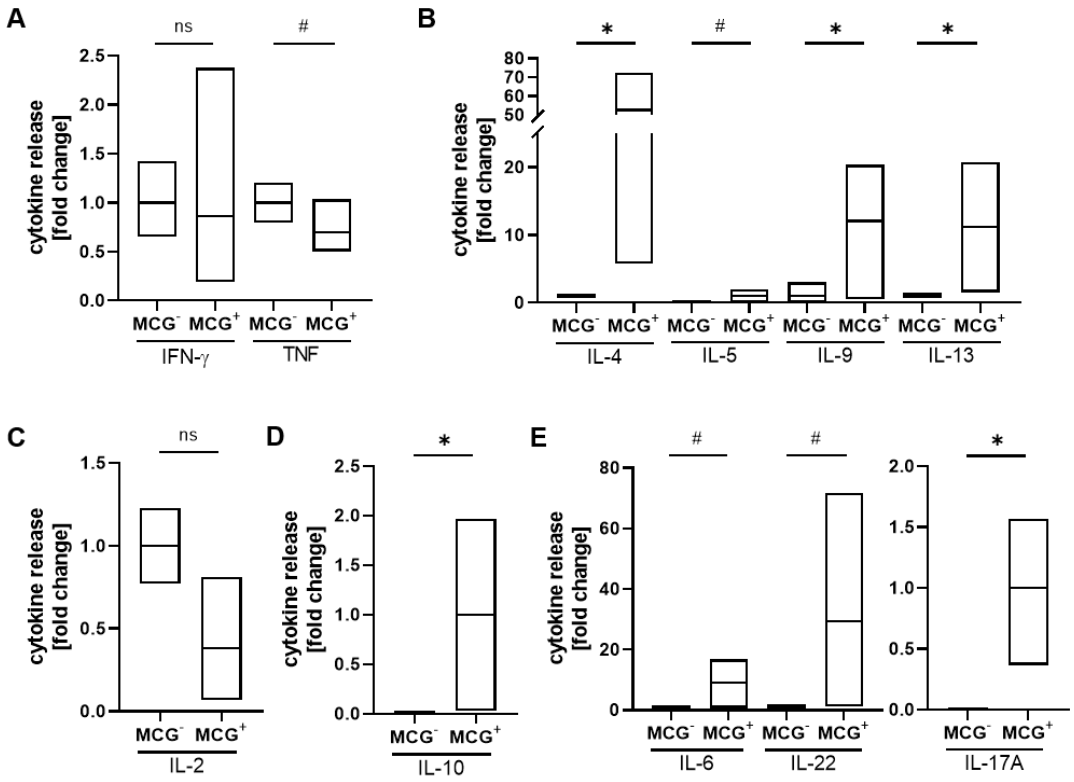

Figure 4.17: MCG uptake by imDCs skews subsequent T cell differentiation *in vitro* towards T_H2 and T_H17 response. MCG$^-$ and MCG$^+$ DCs loaded with OVA peptide were co-incubated with naïve CD4$^+$ OTII T cells *in vitro*. After 4 d of co-culture T cells were re-stimulated with anti-CD3/anti-CD28 antibodies and supernatants were analyzed for cytokine content 24 h later (N = 5). (A) T_H1 cytokines, (B) T_H2 cytokines, (C) IL-2, (D) IL-10 and (E) T_H17 cytokines were measured and the fold change was calculated setting the mean of cytokine concentration upon co-incubation with MCG$^-$ (A-C, E right) or with MCG$^+$ DCs (D, E left) to 1. *** $p < 0.001$, ** $p < 0.01$, * $p < 0.05$, # $p \leq 0.10$, ns $p > 0.10$.

Collectively, MCG uptake by imDCs led to a reprogramming of the T cells and shifted their differentiation to a T_H2- and T_H17-dominated response.

4.7 Analysis of the impact of impaired Card9-dependent signaling on T cell priming by dermal DCs

Next, the influence of a defective Card9-dependent signaling in DCs on the T cell priming was analyzed. The *Card9*$^{-/-}$ mouse line that is used in this thesis represents a

conventional *knockout* mouse line, meaning that the Card9 expression is disrupted in all cells of the mouse [174]. Therefore, the expression of Card9 was checked first by qPCR in wt imDCs and wt T cells. imDCs were differentiated from wt BM cells *in vitro* and T cells were isolated from spleens of untreated wt mice using a “Pan T Cell Isolation Kit II”, followed by isolation of total RNA, cDNA synthesis and qPCR. As shown in Figure 7.2 in the appendix, Card9 was significantly higher expressed in imDCs compared to naïve T cells. This is in line with recent knowledge that described that T cells do not express Card9 and instead use Card11 (also known as CARMA1) for signaling [174,215]. Therefore, an intrinsic effect of the Card9 deficiency on T cell priming and differentiation can be excluded for the following experiments.

Wt and *Card9*$^{-/-}$ mice were sensitized on the shaved back skin and LN cells were isolated from back skin-draining, inguinal LNs 4 days later.

The cell numbers within the inguinal LNs were analyzed by flow cytometry. CD45$^+$ leukocyte and T cell (both, CD4$^+$ and CD8$^+$ T cells) numbers were significantly increased in wt mice upon DNFB sensitization compared to the vehicle control (Figure 4.18A). In contrast, CD45$^+$ leucocyte numbers were significantly reduced in *Card9*$^{-/-}$ compared to wt mice upon DNFB treatment. Among this, especially T cell numbers, CD4$^+$ as well as CD8$^+$ T cells, were significantly reduced in the dLNs of *Card9*$^{-/-}$ mice compared to the wt controls. Additionally, activated T cells (T_{act} cells, gated as CD45$^+$ CD3$^+$ CD4$^+$/CD8$^+$ CD44$^+$), T_{eff} (gated as CD45$^+$ CD3$^+$ CD4$^+$/CD8$^+$ CD44$^+$ CD25$^+$) and T_{reg} cells (gated as CD45$^+$ CD3$^+$ CD4$^+$ FoxP3$^+$) were analyzed. *Card9*$^{-/-}$ mice showed a defect in generating CD4$^+$ T_{act} cells and T_{reg} cells after DNFB sensitization, while CD4$^+$ T_{eff} cells and CD8$^+$ T_{act} and T_{eff} cells were not affected (Figure 4.18B/C).

Additionally, CD4$^+$ T cells from the dLNs were separated by FACS and subsequently re-stimulated *ex vivo* with anti-CD3 and anti-CD28 antibodies. The T cell supernatants were analyzed for their cytokine release using the LEGENDplex™ Multiplex Kits (Figure 4.18D). The release of IL-2, IL-4 and IL-17A was strongly decreased, while the T_H1 cytokines INF-γ and TNF were slightly decreased in supernatants of T cells derived from *Card9*$^{-/-}$ mice, compared to those of wt T cells. IL-22 showed no difference between T cells derived from wt and *Card9*$^{-/-}$ mice. All additionally analyzed cytokines (IL-1β, IL-5, IL-6, IL-9, IL-10, IL-12p70, IL-13, IL-23, IL-27, GM-CSF) could not be detected in this experimental setting.

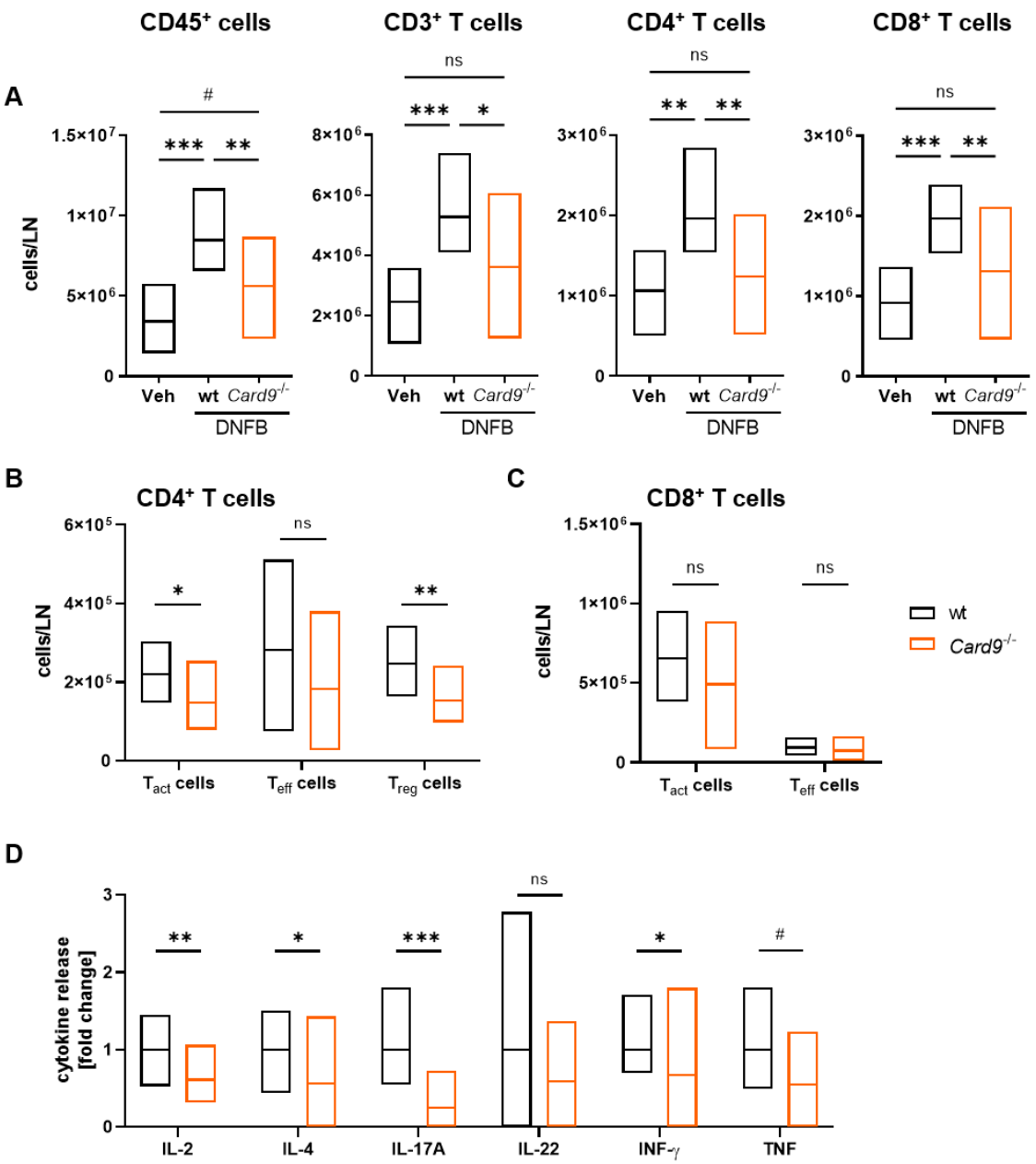

Figure 4.18: MCG uptake by imDCs skews subsequent T cell differentiation *in vivo* towards T_H2 and T_H17 response. Wt and *Card9*$^{-/-}$ mice were sensitized with 0.5% DNFB in acetone/olive oil (4:1) on the shaved back skin and T cell priming was analyzed 4 d later (N = 9). (A) Total cell counts of CD45$^+$ cells (left), CD3$^+$ T cells (middle left), CD4$^+$ T cells (middle right) and CD8$^+$ T cells (right) in back skin-draining inguinal LNs were analyzed by flow cytometry. (B/C) CD4$^+$ (B) and CD8$^+$ T cells (C) were further distinguished for total cell counts of T_{act}, T_{eff} and T_{reg} cells. (D) Sorted CD4$^+$ T cell from dLNs were additionally re-stimulated with anti-CD3/anti-CD28 antibodies and supernatants were analyzed for cytokine content 24 h later. The fold change was calculated by setting the mean of the cytokine release by cells derived from wt mice to 1. *** $p < 0.001$, ** $p < 0.01$, * $p < 0.05$, # $p \leq 0.10$, ns $p > 0.10$.

In summary, *Card9*$^{-/-}$ mice showed a defect in T cell priming and differentiation upon DNFB sensitization. Beside the reduced T cell numbers in skin-draining LNs in *Card9*$^{-/-}$

mice, the cytokine analyses indicate that Card9 deficiency led to modulated T cell differentiation with the reduction of T_H2 and T_H17 cytokines.

4.8 Analysis of CLR engagement in MCG uptake by imDCs

4.8.1 CLR binding studies to MCG

CLRs are known to activate innate Card9-dependent signaling pathways that induce or even modulate adaptive immune responses [216]. This part of my thesis was focused on the characterization of the CLR binding to MCG. To this end, a tool that was published by the group of Prof. Bernd Lepenies (University of Veterinary Medicine Hannover, Institute for Immunology) was used. CLR-hFc fusion proteins contain the carbohydrate recognition domain of the respective CLR that is fused to a human IgG1-Fc fragment [190,217]. As control, the human IgG1-Fc fragment (hFc control) was used. After purification, these fusion proteins were used to analyze the binding capacity of different CLRs to putative ligands, like MCG.

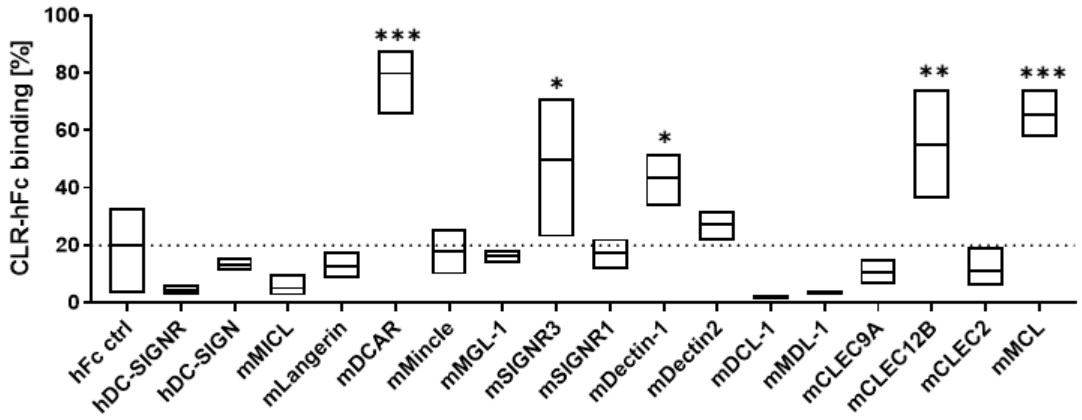

Figure 4.19: PCMC-derived MCG are ligands of CLR fusion proteins. Using CLR fusion proteins, CLR binding to PCMC-derived MCG was analyzed as fraction of bound CLR-hFc fusion proteins of the total MCG population. Binding to the hFc control (ctrl) indicated unspecific binding and was used as control for each statistical analysis (N = 3-8). Only results of statistical analyses with a p value smaller than 0.05 were depicted. *** $p < 0.001$, ** $p < 0.01$, * $p < 0.05$, # $p \leq 0.10$.

First, *in vitro* isolated and AF488-labeled PCMC-derived MCG were analyzed for their CLR binding capacity. Five CLR fusion proteins, mDCAR-hFc, mSIGNR3-hFc, mDectin-1-hFc, mCLEC12B-hFc and mMCL-hFc, were shown to exhibit an increased binding to PCMC-derived MCG compared to the hFc control (Figure 4.19).

In section 4.4, solely PCMC-derived MCG were shown to be taken up by imDCs while BMMC-derived were not. Therefore, the CLR candidate that might be responsible for specific uptake of MCG would be expected to show an increased binding to PCMC-derived MCG compared to BMMC-derived MCG.

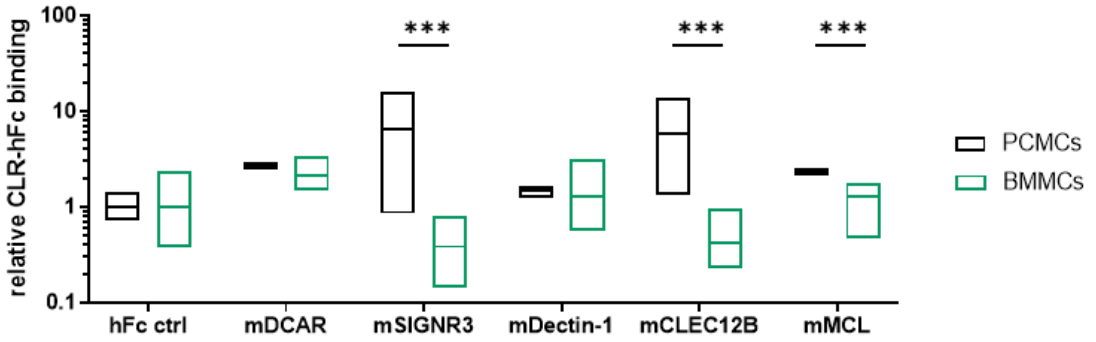

Figure 4.20: PCMC-derived MCG are specifically bound by SIGNR3, CLEC12B and MCL fusion proteins. Using CLR fusion proteins, CLR binding to PCMC-derived MCG and BMMC-derived MCG was analyzed (N = 5-11). The fold change was calculated setting the mean of each hFc control (hFc ctrl) to 1 and binding of PCMC-derived MCG (black) or BMMC-derived MCG (green) was depicted in relation to the control. Only results of statistical analyses with a p value smaller than 0.05 were depicted. *** $p < 0.001$, ** $p < 0.01$, * $p < 0.05$, # $p \leq 0.10$.

The fold change of binding was calculated setting the mean of each hFc control, meaning a relative CLR-hFc binding around or below 1 indicated no specific binding of the CLR fusion proteins to the respective MCG. By analyzing the binding capacity of PCMC-derived MCG-binding CLR-hFc fusion proteins to BMMC-derived MCG, mDCAR-hFc and mDectin-1-hFc were excluded as specific binding partners, because they showed a high binding to PCMC-derived MCG as well as to BMMC-derived MCG (Figure 4.20). In contrast, mSIGNR3-hFc, mCLEC12B-hFc and mMCL-hFc showed no binding to BMMC-derived and therefore remained as specific candidates that could be involved in PCMC-derived MCG uptake by imDCs.

4.8.2 Analysis of the expression of CLRs on DCs *in vitro* and *ex vivo*

Next, the expression of SIGNR3, CLEC12B and MCL in the context of DC maturation was studied by measuring their mRNA content in imDCs and matDCs *in vitro*. Total mRNA was isolated from *in vitro* cultured DCs and gene expression was subsequently analyzed by qPCR. The relative gene expression of CLRs was normalized to the house keeping gene Tbp [194].

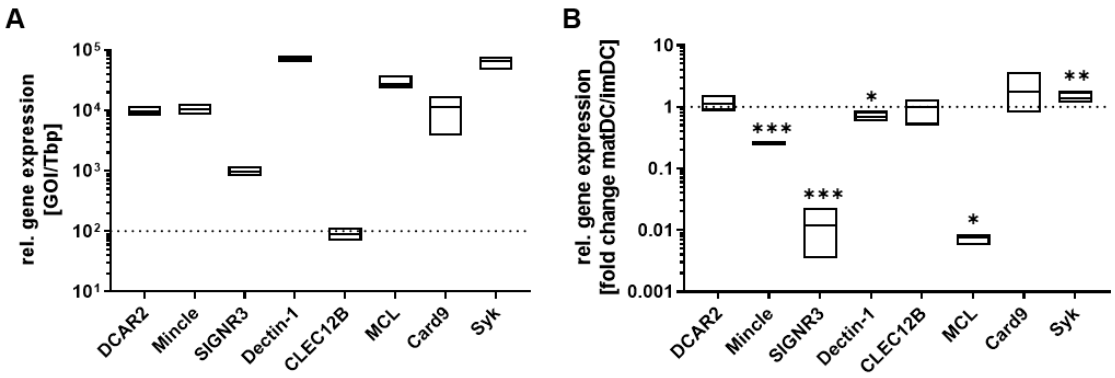

Figure 4.21: qPCR analysis of CLR expression *in vitro*. Total RNA of imDCs and matDCs *in vitro* was isolated and analyzed by qPCR for CLR expression (N = 6). (A) Relative gene expression was calculated using the $2^{-\Delta\Delta ct}$ method, normalized to the house keeping gene Tbp and set to 100% for the first sample of the lowest expressed CLR (CLEC12B). (B) Fold change was calculated by dividing the relative gene expression of matDCs by the relative gene expression of imDCs. A fold change below 1 indicates maturation-induced downregulation while fold change above 1 indicates upregulation. Indicated significance levels indicate results of statistical analyses between relative gene expression of imDCs and mat DCs. Only results of statistical analyses with a p value smaller than 0.05 were depicted. *** $p < 0.001$, ** $p < 0.01$, * $p < 0.05$, # $p \leq 0.10$.

Figure 4.21A shows the relative gene expression of distinct CLRs and their signaling molecules by imDCs. CLEC12B was detectable with a relatively high c_t value of 34.6, meaning that is was relatively low expressed by imDCs. In contrast, MCL showed a very high expression by imDCs (300 times higher than CLEC12B) and SIGNR3 an intermediate expression (10 times higher than CLEC12B). Other CLRs, like dendritic cell activating receptor 2 (DCAR2), Mincle and Dectin-1 were expressed in a comparable amount to MCL. Additionally, the signaling molecules Card9 and Syk were also highly expressed by imDCs *in vitro* (Figure 4.21A) indicating the important role of CLRs and their signaling cascades in DC biology.

Given the restriction of the MCG uptake capacity to imDCs CLRs, which are responsible for MCG uptake, should be downregulated after DC maturation. That is why, the expression of different CLRs in imDCs and matDCs was compared and the ratio according to the following equation was calculated:

$$Fold\ change\ matDCs/imDCs = \frac{relative\ gene\ expression\ of\ CLR\ by\ matDCs}{relative\ gene\ expression\ of\ CLR\ by\ imDCs}$$

Following this equation, a maturation-induced downregulation of a distinct CLR results in a ratio below one. In contrast, a maturation-induced upregulation of a distinct CLR will result in a ratio above one.

Especially, MCL and SIGNR3 showed a strongly reduced expression in matDCs compared to imDCs (Figure 4.21B). In contrast, CLEC12B was equally expressed in imDCs and matDCs, which eliminated CLEC12B as a candidate responsible for maturation status-dependent uptake of PCMC-derived MCG. Furthermore, the CLRs Mincle and Dectin-1 were slightly decreased upon DC maturation, while DCAR2 and Card9 were equally expressed in imDCs and matDCs and Syk showed an increased expression in matDCs compared to imDCs (Figure 4.21B).

Additionally, the mRNA expression of the remaining candidates for specific binding to PCMC-derived MCG, MCL and SIGNR3, and the signaling molecules was also analyzed *ex vivo*. Similar to Figure 4.7, DCs with different maturation status (immature skin DCs, LNr DCs and LNm DCs) of wt or MC-depleted Mcpt5-Cre$^+$ R-DTA$^+$ (to exclude the possibility of MCG uptake *in vivo*) mice were sorted and analyzed for the mRNA content of their respective GOIs.

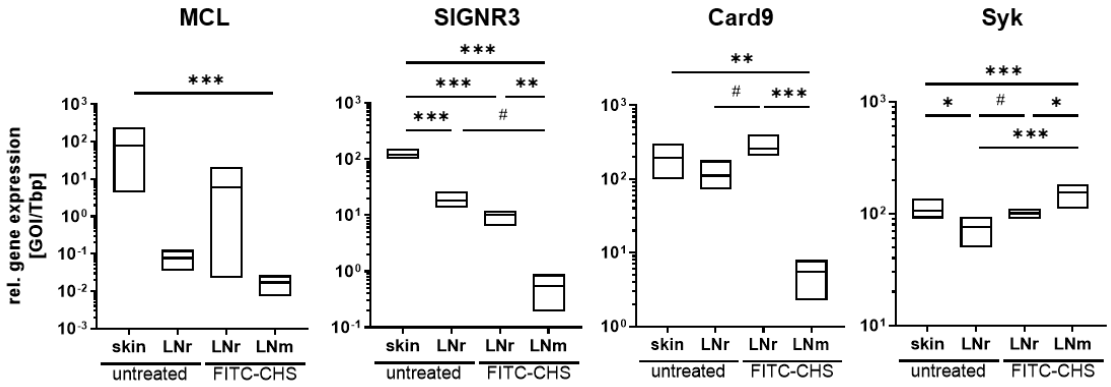

Figure 4.22: qPCR analysis of CLR expression and their signaling molecules *ex vivo*. Immature skin DCs and CD11b$^+$ LNr DCs of untreated wt mice and CD11b$^+$ LNr and LNm DCs from skin-draining LNs of MC-depleted Mcpt5-Cre$^+$ R-DTA$^+$ mice upon FITC-induced CHS were sorted and gene expression of MCL, SIGNR3, Card9 and Syk was analyzed *ex vivo* by qPCR. Relative expression of GOIs was calculated using the $2^{-\Delta\Delta ct}$ method and normalized to the house keeping gene Tbp and set to 100% for the first sample of immature skin DCs of each data set (N = 5-6). Due to clarity of figure, only results of statistical analyses with a p value smaller than or equal to 0.10 were depicted. *** $p < 0.001$, ** $p < 0.01$, * $p < 0.05$, # $p \leq 0.10$.

In line with the *in vitro* data, I could show that the expression of MCL and SIGNR3 was significantly reduced by matDCs (LNm) to 0.02% (MCL) and 0.5% (SIGNR3) of the initial gene expression of imDCs (skin). CD11b$^+$ LNr DCs, before and after FITC-induced CHS, expressed an intermediate level of MCL and SIGNR3. Card9 was comparably expressed by imDCs (skin) and CD11b$^+$ LNr DCs, but strongly reduced by matDCs (LNm) to approx. 2.8% of the initial gene expression of imDCs (skin). In contrast, FITC application

led to an increase in the gene expression of Syk by imDCs (skin) compared to matDCs (LNm) and by CD11b$^+$ LNr DCs before and after FITC-induced CHS. The expression of Syk was increased to approx. 145% of the initial gene expression of imDCs (Figure 4.22). In summary, the CLRs MCL and SIGNR3 exhibited a specific binding capacity to PCMC-derived MCG while they did not bind to BMMC-derived MCG. Additionally, they were highly expressed by imDCs and both were downregulated upon DC maturation *in vitro* and *ex vivo*, which is correlative to the MCG uptake capacity. Therefore, MCL and SIGNR3 remained as candidates that might be responsible for MCG sensing and uptake by imDCs.

4.8.3 Analysis of the impact of an MCL and/or SIGNR3 *knockdown*/*knockout* on MCG uptake by imDCs

In order to analyze the role of MCL and SIGNR3 in MCG uptake by imDCs, I was able to use conventional *knockout* mouse lines that were kindly provided by Prof. Bernd Lepenies (University of Veterinary Medicine Hannover, Institute for Immunology).

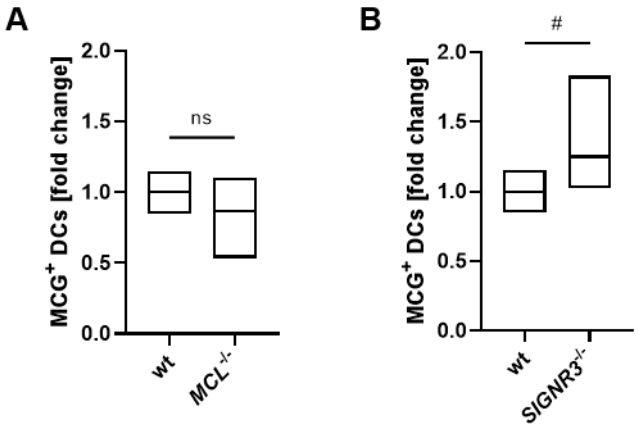

Figure 4.23: MCG uptake is not inhibited by CLR single *knockouts*. imDCs were generated *in vitro* by using BM cells of the respective mouse line and were subsequently incubated with *in vitro* isolated and fluorescently labeled PCMC-derived MCG for 24 h to analyze the impact of MCL (A, N = 7) or SIGNR3 deficiency (B, N = 5) on MCG uptake. MCG uptake capacity was analyzed as fraction of MCG$^+$ DCs and fold change was calculated setting the mean of MCG$^+$ wt DCs to 1. *** $p < 0.001$, ** $p < 0.01$, * $p < 0.05$, # $p \leq 0.10$, ns $p > 0.10$.

imDCs of conventional *MCL*$^{-/-}$ or *SIGNR3*$^{-/-}$ mice and corresponding wt mice were generated and analyzed for their MCG uptake capacity *in vitro* by flow cytometry. Neither *MCL*$^{-/-}$ (Figure 4.23A) nor *SIGNR3*$^{-/-}$ (Figure 4.23B) DCs showed a defect in MCG uptake compared to the wt controls. Interestingly, *SIGNR3*$^{-/-}$ DCs showed a slight tendency to

exhibit increased MCG uptake capacity compared to wt DCs (Figure 4.23B). However, MCL or SIGNR3 alone did not seem to be responsible for MCG uptake by imDCs.

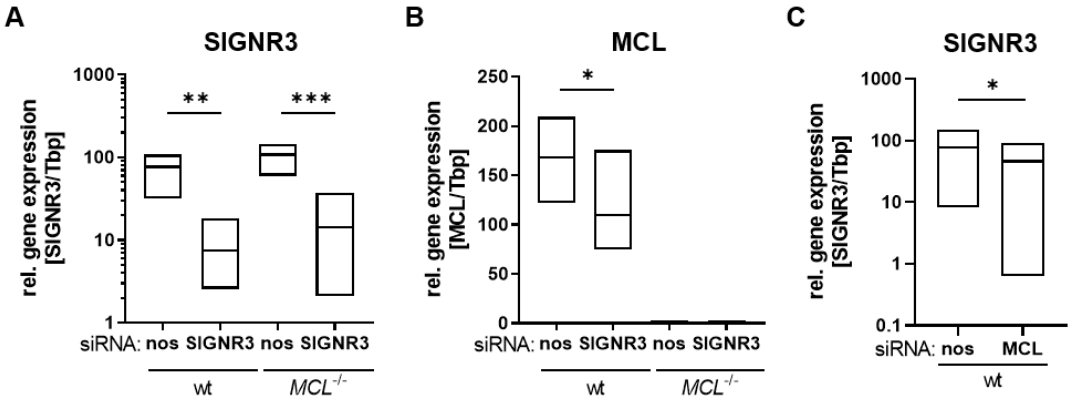

Figure 4.24: Generation of CLR double *knockdown* DCs by targeted gene silencing in CLR single *knockout* DCs. imDCs were generated *in vitro* by using BM cells of the respective mouse line and were subsequently transfected with nos or CLR-specific siRNAs. Total RNA of transfected imDCs *in vitro* was isolated and relative CLR expression by DCs of SIGNR3 (A, N = 6; C, N = 7) or MCL (B, N = 6) *in vitro* was calculated using the $2^{-\Delta\Delta ct}$ method, normalized to the house keeping gene Tbp and set to 100% for the first sample of nos-transfected wt DCs of each data set. *** $p < 0.001$, ** $p < 0.01$, * $p < 0.05$, # $p \leq 0.10$, ns $p > 0.10$.

CLRs are known for their ability to form heterodimers and act in concert with each other to mediate ligand binding and signaling transduction [41]. Therefore, the question whether MCL and SIGNR3 could act together in MCG uptake by imDCs was addressed. imDCs of *MCL*$^{-/-}$ and wt mice were generated and transfected with SIGNR3-specific siRNA to additionally knockdown the expression of SIGNR3 (see section 3.1.8). A nonsense (nos) siRNA that cannot specifically bind to mRNA served as a control. First, SIGNR3 expression was successfully reduced upon siRNA transfection in wt as well as in *MCL*$^{-/-}$ DCs. On average, the gene expression was reduced by approx. 87 – 90% (Figure 4.24A). Interestingly, MCL mRNA was also slightly reduced in wt DCs upon transfection with SIGNR3-specific siRNAs by approx. 35% on average, despite missing relevant sequence homologies between the SIGNR3-specific siRNA and MCL mRNA (see appendix Figure 7.3). As expected, no MCL expression in *MCL*$^{-/-}$ DCs was detected (Figure 4.24B). The simultaneously decreased expression of MCL upon treatment with SIGNR3-specific siRNA could be a hint for compensatory mechanisms and therefore for interactions between SIGNR3 and MCL. Therefore, the expression of SIGNR3 by imDCs upon transfection with an MCL-specific siRNA was additionally analyzed. Indeed, the MCL expression was also slightly decreased by approx. 40% (Figure 4.24C) despite missing relevant sequence homologies between the MCL-specific siRNA and SIGNR3

mRNA (see appendix Figure 7.4) underlining the hypothesis of mutual interactions between SIGNR3 and MCL.

Subsequently, their MCG uptake capacity was compared between wt cells (nos-transfected wt), single *knockout* cells (SIGNR3-transfected wt, nos-transfected *MCL*$^{-/-}$) and double *knockout* cells (SIGNR3-transfected *MCL*$^{-/-}$).

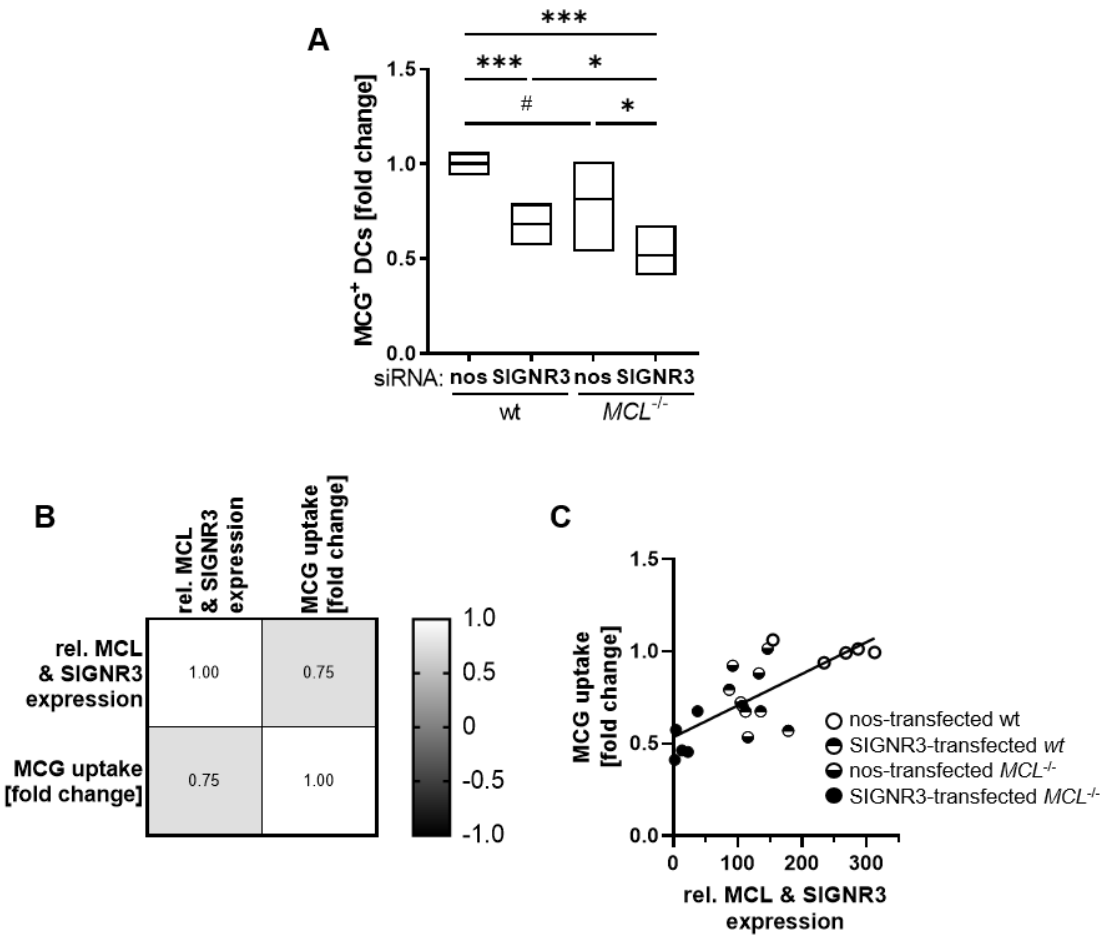

Figure 4.25: MCG uptake is reduced in siRNA-induced MCL/SIGNR3 double *knockout/knockdown* DCs. imDCs were generated *in vitro* by using BM cells of the respective mouse line and were subsequently transfected with nos or SIGNR3-specific siRNAs. Transfected imDCs were subsequently incubated with *in vitro* isolated and fluorescently labeled PCMC-derived MCG for 24 h to analyze the impact of MCL and SIGNR3 deficiency on MCG uptake. (A) MCG uptake capacity was analyzed as fraction of MCG^{+} DCs by flow cytometry (N = 5). (B/C) The combined relative MCL-SIGNR3 gene expression was correlated to the MCG uptake by using Pearson correlation analysis (B, N = 20) or linear regression (C, N = 20). *** $p < 0.001$, ** $p < 0.01$, * $p < 0.05$, # $p \leq 0.10$, ns $p > 0.10$.

Importantly, no significant difference between the MCG uptake by wt or *MCL*$^{-/-}$ cells was detected in this experimental setting as well, but a slight tendency to be decreased in

MCL$^{-/-}$ mice was observable. In contrast, *SIGNR3*$^{-/-}$ DCs showed significantly reduced MCG uptake capacity compared to wt DCs. The MCG uptake by *SIGNR3*$^{-/-}$ DCs was reduced by approx. 30% compared to the wt DCs. This effect was further increased in double *knockout* DCs, which led to a decreased MCG uptake by approx. 50% compared to wt DCs (Figure 4.25A).

Finally, the relative gene expression of MCL and SIGNR3 was combined and analyzed for its correlation to MCG uptake by imDCs. Interestingly, a highly significant, positive correlation between MCL/SIGNR3 expression and MCG uptake capacity was found, meaning that reduced gene expression led to decreased MCG uptake by imDCs (Figure 4.25B/C).

To further confirm this finding, also by *in vivo* experiments, I crossed the mouse lines *MCL*$^{-/-}$ (C57BL/6-Clec4d$^{tm1.1Cfg}$/Mmucd) and *SIGNR3*$^{-/-}$ (C57BL/6-Cd209d$^{tm1.1Cfg}$/Mmucd) to generate a conventional *knockout* mouse line that lack both CLRs MCL and SIGNR3. imDCs of conventional *MCL*$^{-/-}$ *SIGNR3*$^{-/-}$ mice and corresponding wt mice were generated and analyzed for their MCG uptake capacity *in vitro by* flow cytometry in one initial experiment. Due to breeding restrictions because of a potentially compromised phenotype of this mouse line, the number of mice that could be used within this thesis was limited. Therefore, it was not possible to repeat this experiment so far.

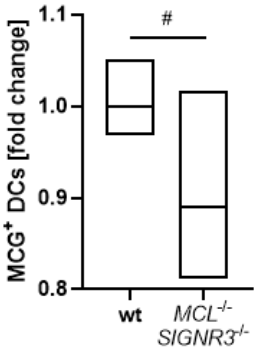

Figure 4.26: MCG uptake is reduced in *MCL*$^{-/-}$ *SIGNR3*$^{-/-}$ DCs. imDCs were generated *in vitro* by using BM cells of wt and *MCL*$^{-/-}$ *SIGNR3*$^{-/-}$ mice and were subsequently incubated with *in vitro* isolated and fluorescently labeled PCMC-derived MCG for 24 h to analyze the impact of a MCL and SIGNR3 deficiency on MCG uptake (N = 4). MCG uptake capacity was analyzed as fraction of MCG$^+$ DCs and the fold change was calculated setting the mean of MCG$^+$ wt DCs to 1. *** $p < 0.001$, ** $p < 0.01$, * $p < 0.05$, # $p \leq 0.10$, ns $p > 0.10$.

Figure 4.26 shows the MCG uptake capacity of wt and *MCL*$^{-/-}$ *SIGNR3*$^{-/-}$ imDCs. Indeed, imDCs derived from conventional double *knockout* mice also showed a reduced MCG uptake capacity compared to the wt controls (Figure 4.26), but just past the significance

level with a p value of 6%. To encourage this effect, this experiment should be repeated to increase the number of mice. Nevertheless, this result underlined the important effects of a MCL SIGNR3 double *knockout* on the MCG uptake capacity of imDCs.
In summary, binding studies with CLR-hFc fusion proteins revealed that mSIGNR3-hFc, mCLEC12B-hFc and mMCL-hFc, specifically bind to PCMC-derived MCG. While all of these CLRs were expressed by imDCs, only MCL and SIGNR3 were significantly downregulated upon DC maturation, which fits to the maturation status related MCG uptake. Therefore, MCL and SIGNR3 were figured out as candidates that might be involved in MCG uptake by imDCs. While conventional MCL and SIGNR3 single *knockouts* did not inhibit the MCG uptake capacity of imDCs *in vitro*, an MCL/SIGNR3 double *knockdown* was shown to significantly impair the MCG uptake by imDCs, which is supported by imDCs of the newly generated MCL/SIGNR3 double *knockout* mice.

4.9 Analysis of the impact of MCG uptake by imDCs on the acute allergic airway inflammation

By using *in vitro* and *in vivo* studies, the MCG uptake by imDCs was shown to influence T cell activation and differentiation towards T_H2 and T_H17 mediated responses.
DNFB-induced CHS is known to induce a mixed T helper cell response that includes $CD4^+$ T_H1 and T_H17 cells and $CD8^+$ T_c1 and T_c17 cells [142,149]. Therefore, the impact of defective Card9-dependent signaling (analyzed in *Card9*$^{-/-}$ mice) or disrupted MCG uptake (analyzed in *MCL*$^{-/-}$ *SIGNR3*$^{-/-}$ mice) on acute allergic asthma, characterized by a T_H2-driven inflammation [153] was analyzed to validate the previous findings.

4.9.1 Influence of defective Card9-dependent signaling on allergic airway inflammation

Card9$^{-/-}$ and corresponding wt mice were sensitized with 10 µg HDM extract in 20 µl 1x PBS i.n. for three consecutive days. Mice were challenged one week later with 10 µg HDM extract in 20 µl 1x PBS i.n. for another four days. 24 h later, lung tissue was finally analyzed by histology and lung tissue and mediastinal LNs were isolated and cell numbers and fluorescence intensities were analyzed by flow cytometry. The gating strategies for each cell population are summarized in Table 3.6, Figure 7.5 and Figure 7.6. Serum samples were additionally analyzed for their total IgE concentration.

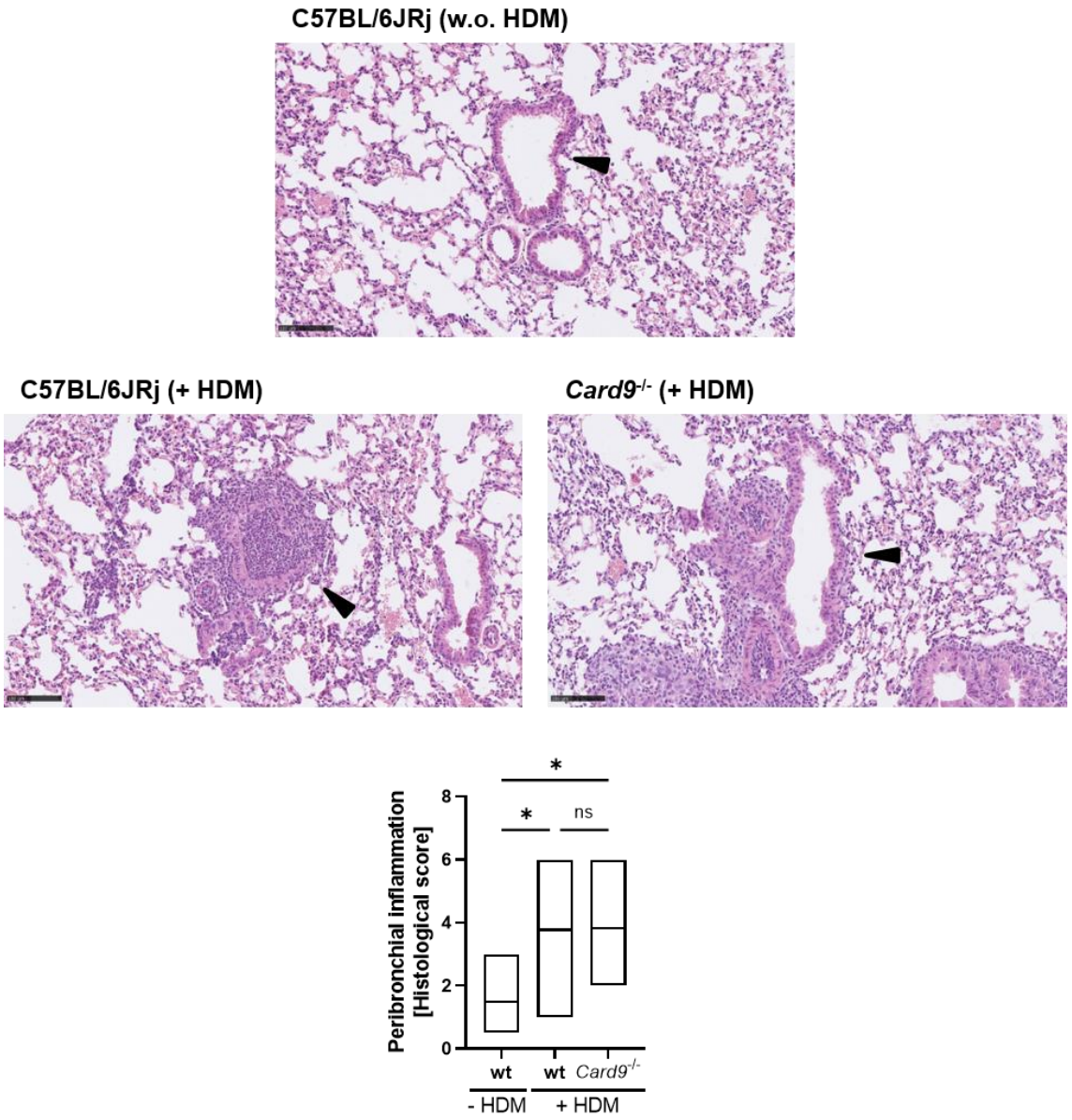

Figure 4.27: Peribronchial inflammation of wt and *Card9*$^{-/-}$ mice upon allergic airway inflammation. Allergic airway inflammation was introduced by HDM extract. Paraffin-embedded lung tissues were cut and subsequently stained with HE. Representative sections show bronchioles (arrow heads) that were analyzed for their peribronchial inflammation by a semi-quantitative histological score (N = 5/10). *** $p < 0.001$, ** $p < 0.01$, * $p < 0.05$, # $p \leq 0.10$, ns $p > 0.10$.

In collaboration with the institute of pathology (Otto-von-Guericke-University Magdeburg, head of group: Prof. Dr. Christoph Garbers) the upper right lobes of the lung tissue were fixed with 4% buffered formaldehyde, embedded in paraffine and HE staining was performed at sections. Figure 4.27 shows representative HE staining of *Card9*$^{-/-}$ and their corresponding wt mice. The upper image shows the lung tissue of a wt mouse that was not treated with HDM extract. The depicted bronchiole, often in close proximity to blood

vessels, was surrounded by non-inflamed lung tissue characterized by a loose distribution of cells (Figure 4.27). The lower left image represents lung tissue of an HDM-treated wt mouse. The bronchiole was densely filled and approx. 80% of the brochiole were surrounded by infiltrated, indicating high peribronchial inflammation upon the induction of allergic airway inflammation. In line, the right image shows lung tissue of an HDM-treated *Card9*$^{-/-}$ mouse. The bronchiole was also surrounded by infiltrating cells but only to an extent of approx. 30%. The amount of surrounding inflammatory cells was translated into a semi-quantitative histological score based on published reports [198,199]. As described in detail in section 3.3.3, scores were chosen as following: 0 - 0% of the bronchiole was surrounded by cells, 1: < 10% surrounded by cells, 2: 10 - <25% surrounded by cells, 3: 25 - <50% surrounded by cells; 4: 50 - <75% surrounded by cells, 5: 75 - <100% surrounded by cells, 6: 100% surrounded by cells. Figure 4.27 additionally shows the peribronchial inflammation depicted as a semi-quantitative histological score. The peribronchial inflammation was significantly increased upon HDM treatment in wt as well as *Card9*$^{-/-}$ mice compared to wt controls that were not treated with HDM. In contrast, HDM-treated wt and *Card9*$^{-/-}$ mice showed no differences in peribronchial inflammation during allergic airway inflammation (Figure 4.27).

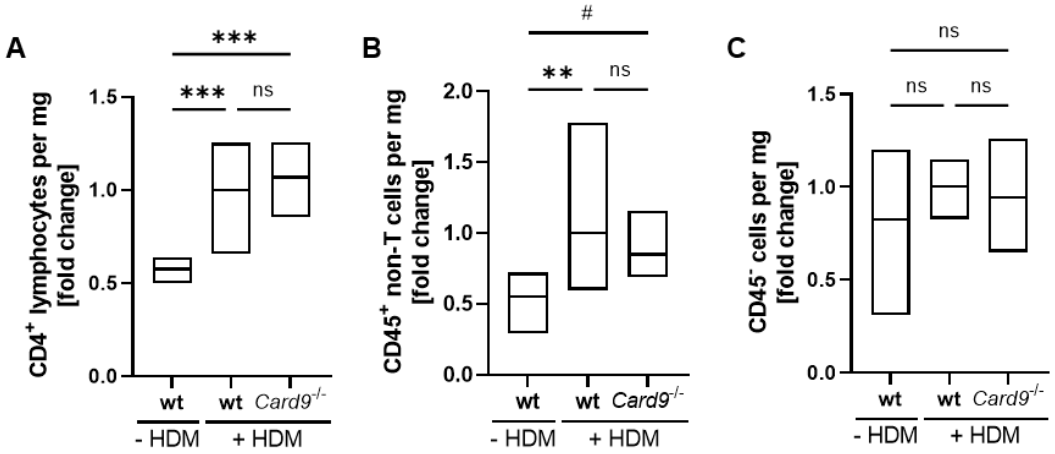

Figure 4.28: Flow cytometric analysis of lung tissue of wt and *Card9*$^{-/-}$ mice upon allergic airway inflammation. Allergic airway inflammation was introduced by HDM extract in wt and *Card9*$^{-/-}$ mice and lung tissue was finally analyzed flow cytometry. Wt mice that did not receive HDM treatment served as control. Total cell counts were determined and normalized to the tissue weight for (A) $CD4^+$ T cells, (B) $CD45^+$ non-T cells and (C) $CD45^-$ cells (N = 5-12). Fold change was calculated setting the mean of HDM-treated wt cells to 1. *** $p < 0.001$, ** $p < 0.01$, * $p < 0.05$, # $p \leq 0.10$, ns $p > 0.10$.

$CD4^+$ T cells play an important role during the course of allergic airway inflammation. Therefore, the overall numbers of $CD4^+$ T cells within the lung tissue of *Card9*$^{-/-}$ and the corresponding wt mice were analyzed. For minimizing artifacts, which were caused by different amount of lung tissue that were collected, cell numbers within the lung tissue were normalized to the tissue weight in all following experiments. $CD4^+$ T cells were significantly increased upon HDM treatment in wt as well as *Card9*$^{-/-}$ mice but showed no difference in the case of Card9 deficiency (Figure 4.28A). Additionally, the numbers of $CD45^+$ non-T cells and $CD45^-$ cells, which include EpCs, endothelial cells, fibroblasts and smooth muscle cells, were analyzed within the lung [218]. Importantly, both HDM-treated wt and *Card9*$^{-/-}$ mice showed increased infiltration of $CD45^+$ non-T cells into the lung compared to non-HDM control mice, but with no significant difference between each other (Figure 4.28B). In contrast, numbers of $CD45^-$ cells were not altered upon HDM treatment and between wt and *Card9*$^{-/-}$ mice (Figure 4.28C).

T_H2 cytokines and their producing cells play a very important role during ongoing asthma [155]. Therefore, the cells producing the T_H2 cytokines IL-4 and IL-13 and the pro-inflammatory cytokine TNF, which is responsible for the inflammation in general were analyzed.

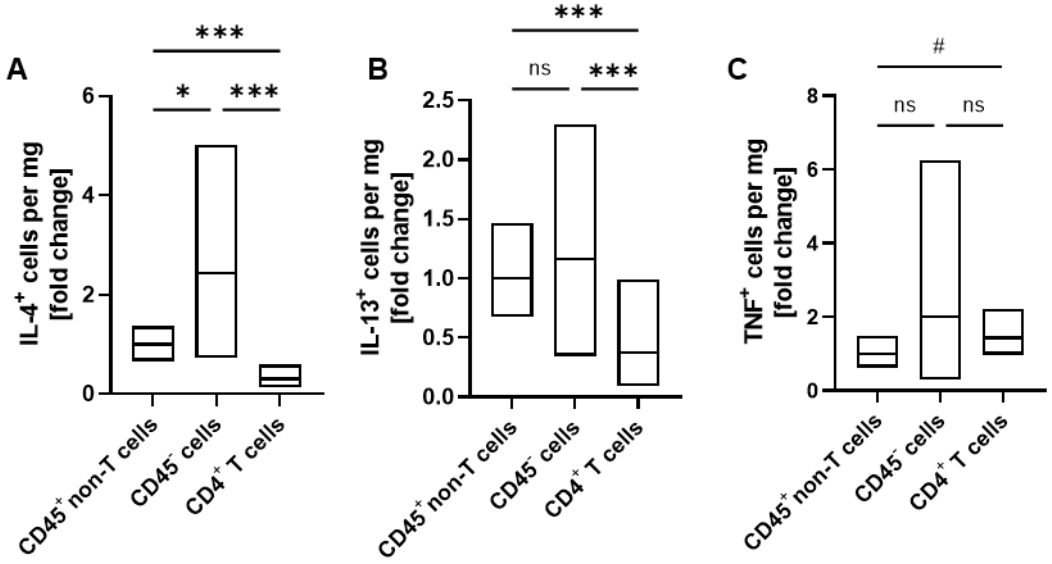

Figure 4.29: Number of cytokine-producing cells within the lung tissue of wt mice upon allergic airway inflammation (introduced in wt/*Card9*$^{-/-}$ mice). Allergic airway inflammation was introduced by HDM extract in wt and *Card9*$^{-/-}$ mice and lung tissue was analyzed by flow cytometry. Total cell counts were determined and normalized to the tissue weight for (A) IL-4-, (B) IL-13- and (C) TNF-producing wt $CD45^+$ non-T cells, $CD45^-$ cells and $CD4^+$ T cells (N = 12). Fold change was calculated setting the mean of cytokine$^+$ $CD45^+$ non-T cells to 1. *** $p < 0.001$, ** $p < 0.01$, * $p < 0.05$, # $p \leq 0.10$, ns $p > 0.10$.

Figure 4.29 and Figure 4.30 show the comparison of the numbers and fluorescence intensities of cytokine-producing cells within the different cell compartments of HDM-treated wt mice.

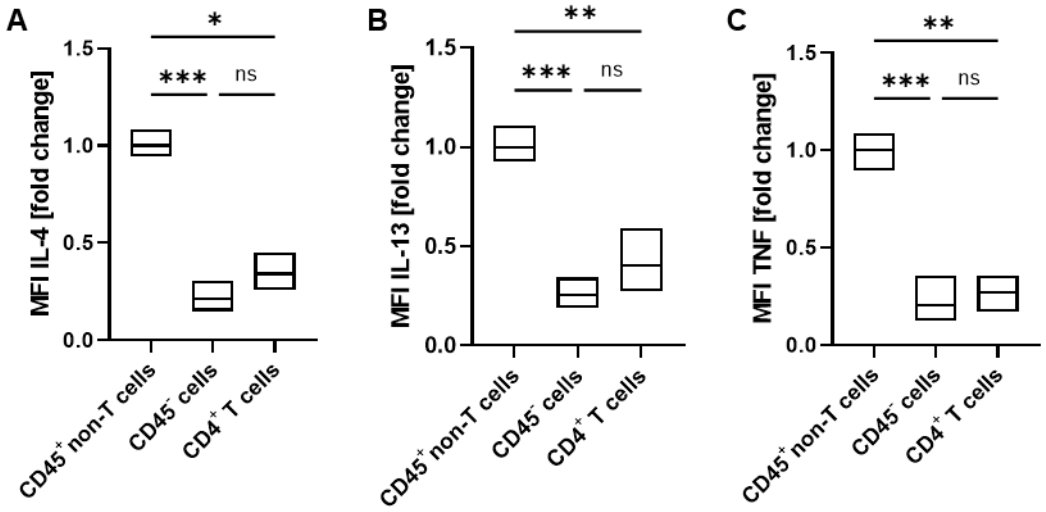

Figure 4.30: Fluorescence intensity of cytokine-producing cells within the lung tissue of wt mice upon allergic airway inflammation (introduced in wt/*Card9*$^{-/-}$ mice). Allergic airway inflammation was introduced by HDM extract in wt and *Card9*$^{-/-}$ mice and lung tissue was analyzed by flow cytometry. Cytokine production per cell was analyzed as MFI of (A) IL-4, (B) IL-13 and (C) TNF per wt CD45$^+$ non-T cell, CD45$^-$ cell and CD4$^+$ T cell (N = 12). Fold change was calculated setting the mean of cytokine$^+$ CD45$^+$ non-T cells to 1. *** $p < 0.001$, ** $p < 0.01$, * $p < 0.05$, # $p \leq 0.10$, ns $p > 0.10$.

Interestingly, IL-4$^+$ cells of HDM-treated wt mice were mainly found in the compartment of CD45$^-$ cells. The subsets of CD45$^+$ non-T cells and CD4$^+$ T cells exhibited significantly less IL-4-producing cells, while CD4$^+$ T cells showed even less compared to CD45$^+$ non-T cells (Figure 4.29A). IL-13$^+$ cells were found in comparable numbers within the CD45$^+$ non-T cells and CD45$^-$ cells. The CD4$^+$ T cell compartment exhibited significantly less IL-13-producing cells (Figure 4.29B). In contrast, the numbers of TNF$^+$ cells were not significantly altered between the different compartments, but showed a slight tendency to be mainly present within the CD45$^-$ and CD4$^+$ T cell compartment (Figure 4.29C).

The amount of all analyzed cytokines per cell was significantly higher for CD45$^+$ non-T cells compared to CD45$^-$ cells and CD4$^+$ T cells. In contrast, the MFI of the analyzed cytokines showed no significant difference between CD45$^-$ cells and CD4$^+$ T cells (Figure 4.30A-C).

Especially in case of CD45$^-$ cells, it was obvious that lots of cytokine$^+$ CD45$^-$ cells produced lower levels of cytokines per cell. In line, fewer CD45$^+$ non-T cells expressed

higher amounts of cytokines per cell. To judge on the overall cytokine production, the cell numbers and fluorescence intensities of the respective cytokines within distinct cell compartments were combined based on the following equation:

$$overall\ cytokine\ production = cytokine\ producing\ cells\ [fold\ change] * MFI\ cytokine\ [fold\ change]$$

Figure 4.31 shows the overall cytokine production by $CD4^+$ T cells, $CD45^+$ non-T cells and $CD45^-$ cells within the lung tissue of wt mice.

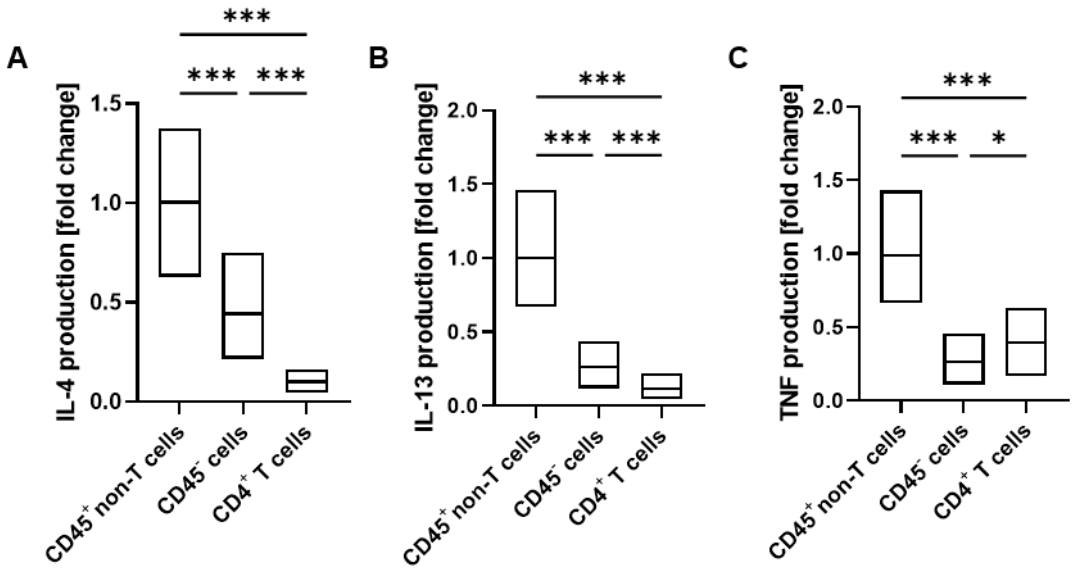

Figure 4.31: Overall cytokine production within the lung tissue of wt mice upon allergic airway inflammation (introduced in wt/*Card9*$^{-/-}$ mice). Allergic airway inflammation was introduced by HDM extract in wt and *Card9*$^{-/-}$ mice and lung tissue was analyzed by flow cytometry. The overall cytokine production of (A) IL-4, (B) IL-13 and (C) TNF by wt $CD45^+$ non-T cells, $CD45^-$ cells and $CD4^+$ T cells was calculated based on the numbers of cytokine-producing cells and their respective MFI (N = 11/12). Fold change was calculated setting the mean of overall cytokine production of $CD45^+$ non-T cells to 1. *** $p < 0.001$, ** $p < 0.01$, * $p < 0.05$, # $p \leq 0.10$, ns $p > 0.10$.

The calculated overall cytokine production showed that $CD45^+$ non-T cells represented the main producers of IL-4, IL-13 and TNF. $CD4^+$ T cells and $CD45^-$ cells contributed significantly less to cytokine production. In case of the T_H2 cytokines IL-4 and IL-13 the $CD45^-$ cell compartment showed an intermediate production of cytokines (appr. 44% (IL-4) or 25% (IL-13) of the amount of $CD45^+$ non-T cells), while $CD4^+$ T cells contribute to an even lower amount of approx. 10% of the amount of $CD45^+$ non-T cells (Figure 4.31).

In contrast, TNF was produced by CD4$^+$ T cells to an amount of approx. 40% of the amount of CD45$^+$ non-T cells and even significantly less by CD45- cells (approx. 26% of the amount of CD45$^+$ non-T cells, Figure 4.31C).
In addition, cytokine production by cells derived from wt and *Card9*$^{-/-}$ mice was compared. Figure 4.32 shows the calculated overall cytokine production based on the numbers of cytokine$^+$ cells (Appendix Figure 7.7) and the amount of cytokines produced per cell (Appendix Figure 7.8).

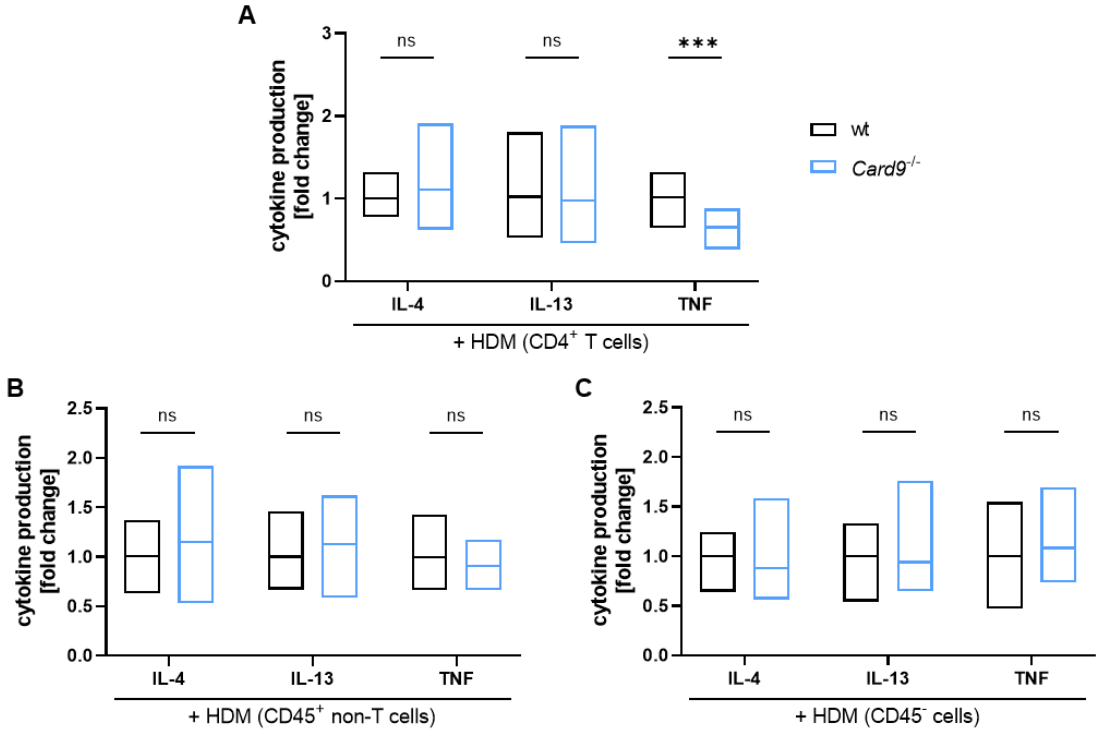

Figure 4.32: Analysis of the overall cytokine production within lung tissues of wt and *Card9*$^{-/-}$ mice upon allergic airway inflammation. Allergic airway inflammation was introduced by HDM extract in wt and *Card9*$^{-/-}$ mice and lung tissue was finally isolated and analyzed by flow cytometry. The overall cytokine production of IL-4, IL-13 and TNF by (A) CD4$^+$ T cells, (B) CD45$^+$ non-T cells and (C) CD45$^-$ cells was calculated based on the numbers of cytokine-producing cells and their respective MFI (N = 9-12). Fold change was calculated setting the mean of overall cytokine production by wt cells of each data set to 1. *** $p < 0.001$, ** $p < 0.01$, * $p < 0.05$, # $p \leq 0.10$, ns $p > 0.10$.

The T_H2 cytokines IL-4 and IL-13 were equally produced by all analyzed cellular subsets between wt and *Card9*$^{-/-}$ mice (Figure 4.32A/B). In contrast, the production of TNF by CD4$^+$ T cells was significantly reduced by approx. 35% within the lung tissue of *Card9*$^{-/-}$ compared to wt mice, while CD45$^+$ non-T cells and CD45$^-$ cells still contributed equally to the production of TNF (Figure 4.32C).

As described above, allergic airway inflammation can also be characterized by increased blood IgE levels. Therefore, serum samples were collected upon induction of the airway inflammation and analyzed for the total IgE content.

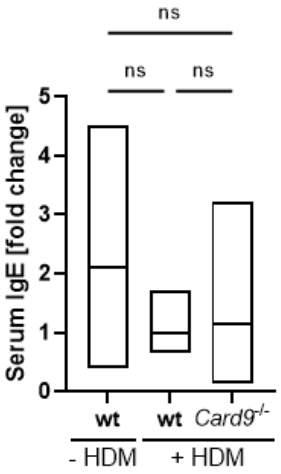

Figure 4.33: Analysis of total IgE serum levels upon allergic airway inflammation in wt and *Card9*$^{-/-}$ mice. Allergic airway inflammation was introduced by HDM extract in wt and *Card9*$^{-/-}$ mice and serum was analyzed for total IgE content (N = 5/11). Fold change was calculated setting the mean of HDM-treated wt cells to 1. *** $p < 0.001$, ** $p < 0.01$, * $p < 0.05$, # $p \leq 0.10$, ns $p > 0.10$.

The results of IgE analysis are depicted in Figure 4.33 and show no differences in IgE concentrations neither between mice that did not receive HDM extract and those that were treated with HDM extract nor between HDM-treated wt and *Card9*$^{-/-}$ mice.

In addition to the lung tissue and serum samples, the lung-draining mediastinal LNs were analyzed by flow cytometry. As described for the lung, the numbers of $CD4^+$ T cells, $CD45^+$ non-T cells and $CD45^-$ cells were analyzed within the LN upon HDM challenge in *Card9*$^{-/-}$ and the corresponding wt mice. $CD4^+$ T cells, $CD45^+$ non-T cells and $CD45^-$ cells within the mediastinal LNs of wt mice were slightly but not significantly increased upon HDM treatment compared to wt mice that were not treated with HDM extract. In contrast, the cell numbers of these compartments were not altered between HDM-treated wt and *Card9*$^{-/-}$ mice (Figure 4.34A-C). Within LNs, I additionally analyzed numbers of T_{fh} cells and B cells. In line with the other cell subsets, T_{fh} and B cells within LNs were increased on average upon HDM treatment in wt and *Card9*$^{-/-}$ mice but were not statistically significant. Differences of T_{fh} and B cell numbers between wt and *Card9*$^{-/-}$ mice were not detected (Figure 4.34D/E).

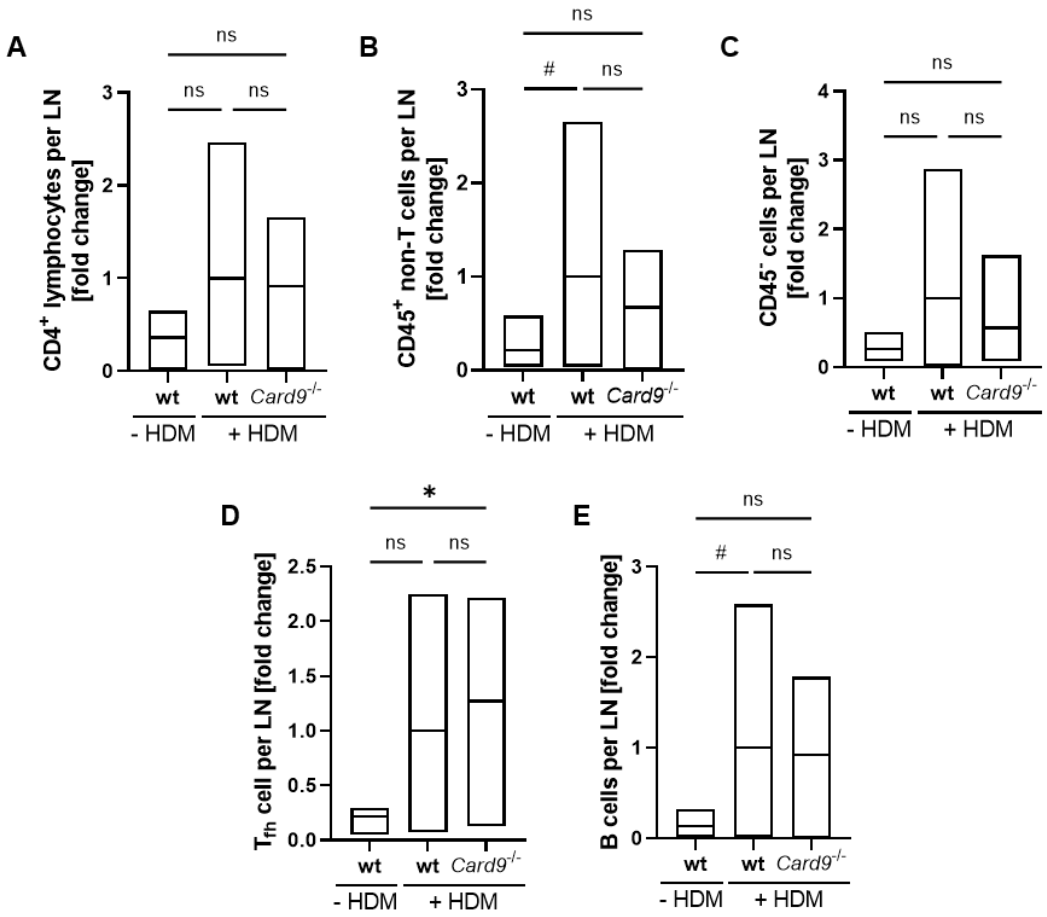

Figure 4.34: Flow cytometric analysis of mediastinal LNs of wt and *Card9*$^{-/-}$ mice upon allergic airway inflammation. Allergic airway inflammation was introduced by HDM extract in wt and *Card9*$^{-/-}$ mice and mediastinal LNs were analyzed by flow cytometry. Total cell counts per LN were analyzed for (A) CD4$^+$ T cells, (B) CD45$^+$ non-T cells, (C) CD45$^-$ cells, (D) T_{fh} cells and (E) B cells (N = 5-11). Fold change was calculated setting the mean of HDM-treated wt cells of each data set to 1. *** $p < 0.001$, ** $p < 0.01$, * $p < 0.05$, # $p \leq 0.10$, ns $p > 0.10$.

Additionally, the overall cytokine production by LN cells of HDM-treated wt mice was studied. Figure 4.35 shows the overall cytokine production calculated based on the cell numbers (Appendix Figure 7.9) and the cytokine MFI (Appendix Figure 7.10).

The T_H2 cytokines IL-4 and IL-13 were mainly produced by CD45$^+$ non-T cells. CD4$^+$ T cell contributed less but still to an extent of approx. 40% to the IL-4 and IL-13 production. In contrast, TNF was produced by CD45$^+$ non-T cells and CD4$^+$ T cells to a comparable extent. CD45$^-$ cells contributed significantly less to the production of all analyzed cytokines (Figure 4.35).

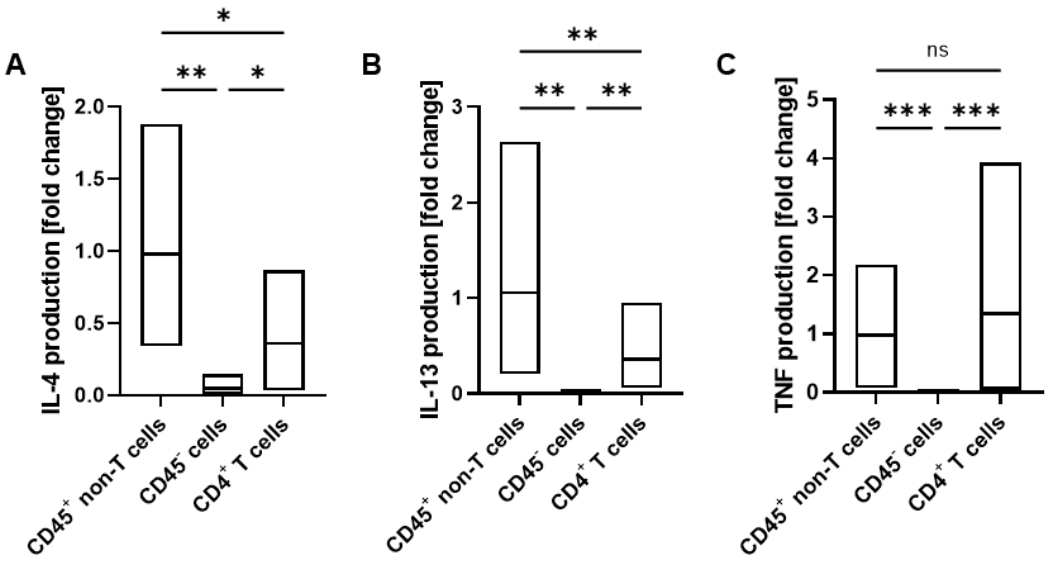

Figure 4.35: Overall cytokine production within the mediastinal LNs of wt mice upon allergic airway inflammation (introduced in wt/*Card9*$^{-/-}$ mice). Allergic airway inflammation was introduced by HDM extract in wt and *Card9*$^{-/-}$ mice and mediastinal LNs were analyzed by flow cytometry. The overall cytokine production of (A) IL-4, (B) IL-13 and (C) TNF by wt CD45^{+} non-T cells, CD45^{-} cells and CD4^{+} T cells was calculated based on the numbers of cytokine-producing cells and their respective MFI (N = 9/10). Fold change was calculated setting the mean of overall cytokine production by CD45^{+} non-T cells to 1. *** $p < 0.001$, ** $p < 0.01$, * $p < 0.05$, # $p \leq 0.10$, ns $p > 0.10$.

The analysis of cytokine-producing CD4^{+} T cells, CD45^{+} non-T cells and CD45^{-} cells within the LNs of wt and *Card9*$^{-/-}$ mice showed no alteration of the cell numbers and the amount of cytokines. Apart from that, the amount of TNF produced by CD45^{-} cells was slightly reduced in *Card9*$^{-/-}$ compared to wt mice (Appendix Figure 7.11 and Figure 7.12). This difference in the fluorescence intensity of TNF was not sufficient to have an impact on the overall production of TNF by CD45^{-} cells that was still not altered between wt and *Card9*$^{-/-}$ mice (Figure 4.36).

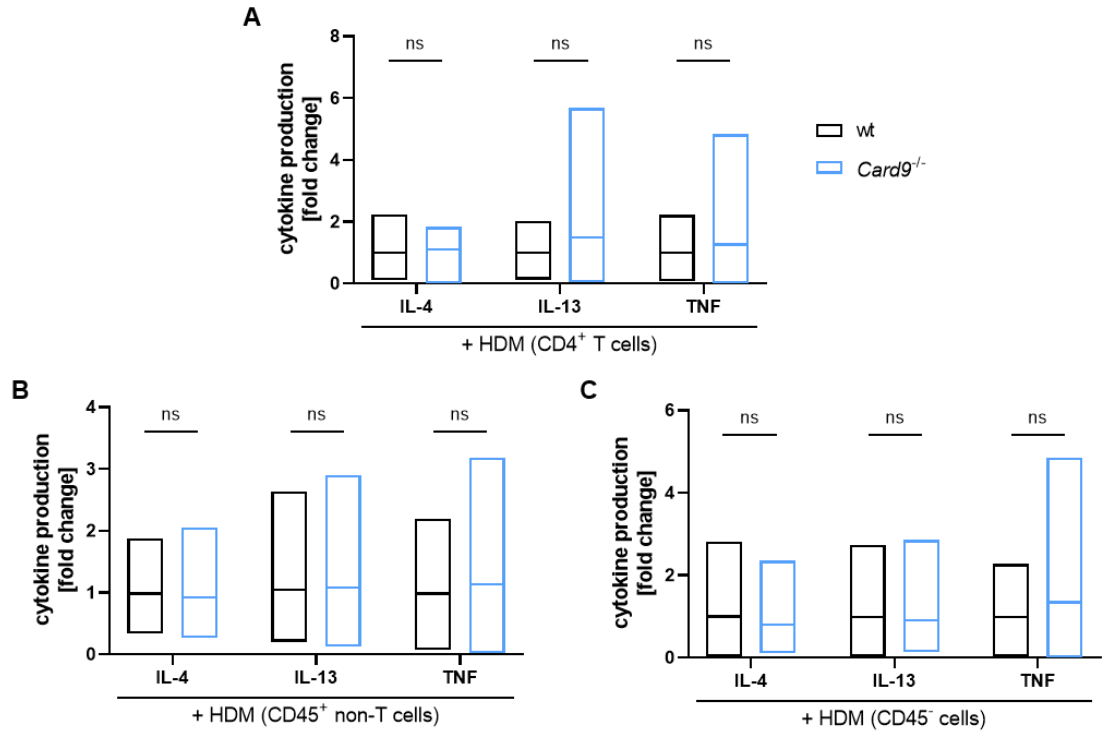

Figure 4.36: Analysis of the overall cytokine production within mediastinal LNs of wt and *Card9*$^{-/-}$ mice upon allergic airway inflammation. Allergic airway inflammation was introduced by HDM extract in wt and *Card9*$^{-/-}$ mice and mediastinal LNs were analyzed by flow cytometry. The overall cytokine production of IL-4, IL-13 and TNF by (A) CD4^{+} T cells, (B) CD45^{+} non-T cells and (C) CD45^{-} cells was calculated based on the numbers of cytokine-producing cells and their respective MFI (N = 10/11). Fold change was calculated setting the mean of overall cytokine production by wt cells of each data set to 1. *** $p < 0.001$, ** $p < 0.01$, * $p < 0.05$, # $p \leq 0.10$, ns $p > 0.10$.

4.9.2 Influence of disrupted MCG uptake on the allergic airway inflammation

Finally, the impact of disrupted MCG uptake on the development of acute allergic airway inflammation was analyzed in *MCL*$^{-/-}$ *SIGNR3*$^{-/-}$ and their corresponding wt mice. The allergic airway inflammation was introduced and subsequently analyzed as described for *Card9*$^{-/-}$ mice.

In Figure 4.37, the upper image shows a representative HE-stained section of a wt mouse that was not treated with HDM extract. The bronchioles were surrounded by loosely packed non-inflamed lung tissue. In contrast, HDM-treated wt mice (left image) showed a high amount of infiltrating cells around the bronchioles, which could be translated to a significantly increased histological score indicating increased peribronchial inflammation compared to wt mice that were not treated with HDM extract. HDM-treated *MCL*$^{-/-}$ *SIGNR3*$^{-/-}$ mice also showed cellular infiltration that was increased

compared to non-HDM controls. They additionally showed slightly but not significantly reduced peribronchial inflammation compared to HDM-treated wt mice (Figure 4.37).

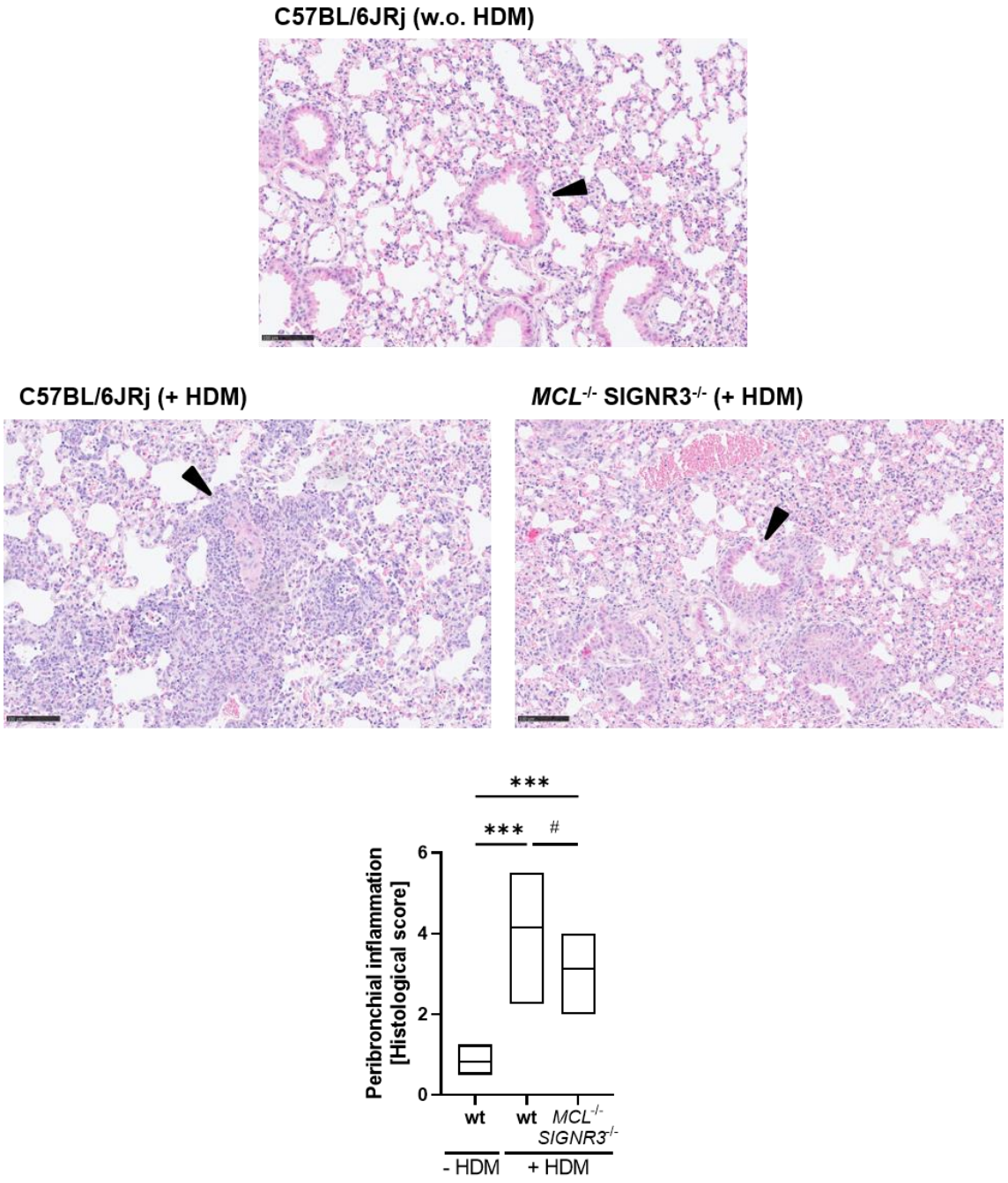

Figure 4.37: Peribronchial inflammation of wt and *MCL*$^{-/-}$ *SIGNR3*$^{-/-}$ mice upon allergic airway inflammation. Allergic airway inflammation was introduced by HDM extract. Paraffin-embedded lung tissues were cut and subsequently stained with HE. Representative sections show bronchioles (arrow heads) that were analyzed for their peribronchial inflammation by a semi-quantitative histological score (N = 5-8). *** $p < 0.001$, ** $p < 0.01$, * $p < 0.05$, # $p \leq 0.10$, ns $p > 0.10$.

By flow cytometry, the numbers of $CD4^+$ T cell, $CD45^+$ non-T cells and $CD45^-$ cells within the lung tissue were additionally analyzed as described for the *Card9*$^{-/-}$ mice (Figure 4.38). The number of $CD4^+$ T cells was significantly increased upon HDM treatment of wt mice compared to control mice, while it was decreased in HDM-treated *MCL*$^{-/-}$ *SIGNR3*$^{-/-}$ compared to treated wt mice, which, however, failed to reach statistical significance (Figure 4.38A). The numbers of $CD45^+$ non-T cells were significantly increased upon HDM treatment in wt mice compared to wt mice that were not treated with HDM extract. Importantly, the number of $CD45^+$ non-T cells within the lung tissue of *MCL*$^{-/-}$ *SIGNR3*$^{-/-}$ mice was significantly decreased compared to HDM-treated wt mice (Figure 4.38B). The analysis of $CD45^-$ cells within the lung tissue showed a decreased cell number upon HDM treatment in both wt and *MCL*$^{-/-}$ *SIGNR3*$^{-/-}$ mice compared to wt mice that were not treated with HDM extract. The cell number within lungs of *MCL*$^{-/-}$ *SIGNR3*$^{-/-}$ mice was even slightly more reduced compared to treated wt mice (Figure 4.38C).

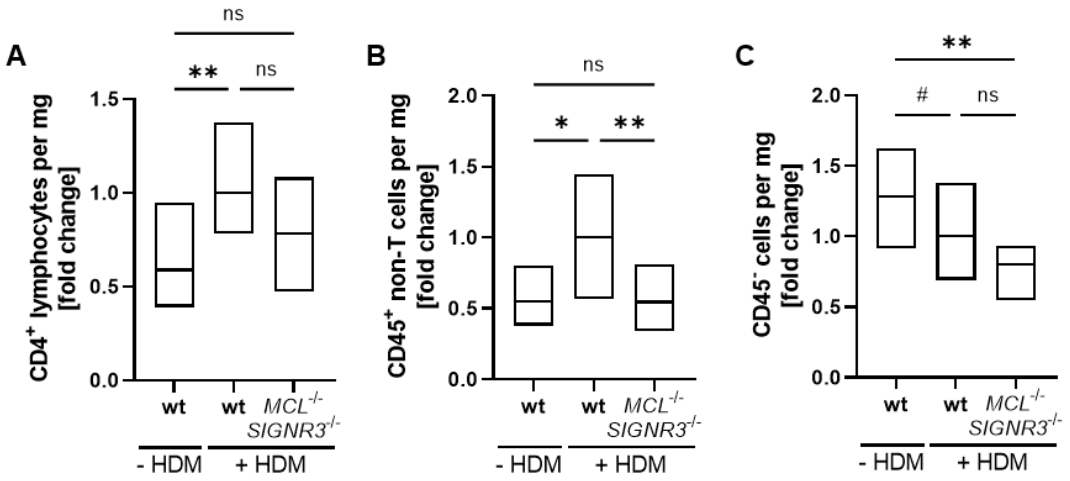

Figure 4.38: Flow cytometric analysis of lung tissue of wt and *MCL*$^{-/-}$ *SIGNR3*$^{-/-}$ mice upon allergic airway inflammation. Allergic airway inflammation was introduced by HDM extract in wt and *MCL*$^{-/-}$ *SIGNR3*$^{-/-}$ mice and lung tissue was analyzed flow cytometry. Wt mice that did not receive HDM treatment served as control. Total cell counts were determined and normalized to the tissue weight for (A) $CD4^+$ T cells, (B) $CD45^+$ non-T cells and (C) $CD45^-$ cells (N = 5-8). Fold change was calculated setting the mean of HDM-treated wt cells of each data set to 1. *** $p < 0.001$, ** $p < 0.01$, * $p < 0.05$, # $p \leq 0.10$, ns $p > 0.10$.

DCs play an important role during the course of allergic airway inflammation. Therefore, the DC numbers within the lung tissue were analyzed upon HDM treatment in wt and *MCL*$^{-/-}$ *SIGNR3*$^{-/-}$ mice. The overall DC numbers, characterized as $CD11c^+$ $MHCII^+$ cells, were not altered between HDM-treated wt and *MCL*$^{-/-}$ *SIGNR3*$^{-/-}$ mice (Figure 4.39 left).

By analyzing the numbers of cDC subsets, significantly reduced numbers were found in CD11b$^+$ cDC2s in *MCL*$^{-/-}$ *SIGNR3*$^{-/-}$ mice, but there was no alteration in the number of CD103$^+$ cDC1s compared to HDM-treated wt (Figure 4.39 middle and right).

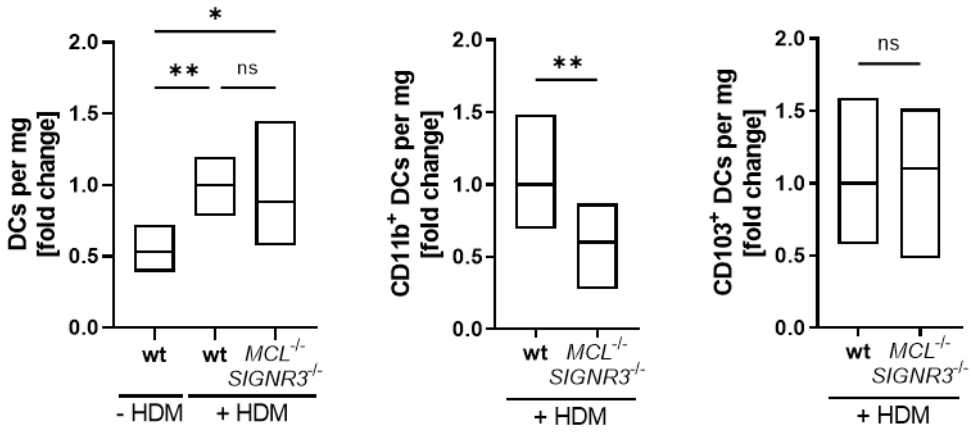

Figure 4.39: Flow cytometric analysis of wt and *MCL*$^{-/-}$ *SIGNR3*$^{-/-}$ mice for DC subsets within the lung tissue upon allergic airway inflammation. Allergic airway inflammation was introduced by HDM extract in wt and *MCL*$^{-/-}$ *SIGNR3*$^{-/-}$ mice and lung tissue was finally analyzed flow cytometry. Wt mice that did not receive HDM treatment served as control. Total cell counts were determined and normalized to the tissue weight for overall DC numbers and numbers of CD11b$^+$ cDC2s and CD103$^+$ cDC1s (N = 5-8). Fold change was calculated setting the mean of HDM-treated wt cells of each data set to 1. *** $p < 0.001$, ** $p < 0.01$, * $p < 0.05$, # $p \leq 0.10$, ns $p > 0.10$.

Subsequently, the number of cytokine-producing cells and their amount of produced cytokines within the CD4$^+$ T cell, CD45$^+$ non-T cell and CD45$^-$ cell compartment were analyzed in the lung of HDM-treated wt mice also within this experimental setting (Appendix Figure 7.13 and Figure 7.14). Figure 4.40 shows the overall cytokine production by CD4$^+$ T cells, CD45$^+$ non-T cells and CD45$^-$ cells within the lung tissue of wt mice calculated as described above.

Within this experimental setting, the main production of the T_H2 cytokines IL-4 and IL-13 by CD45$^+$ non-T cells within the lung tissue was also confirmed, while TNF was comparably produced by CD45$^+$ non-T cells and CD4$^+$ T cells (Figure 4.40A/B).

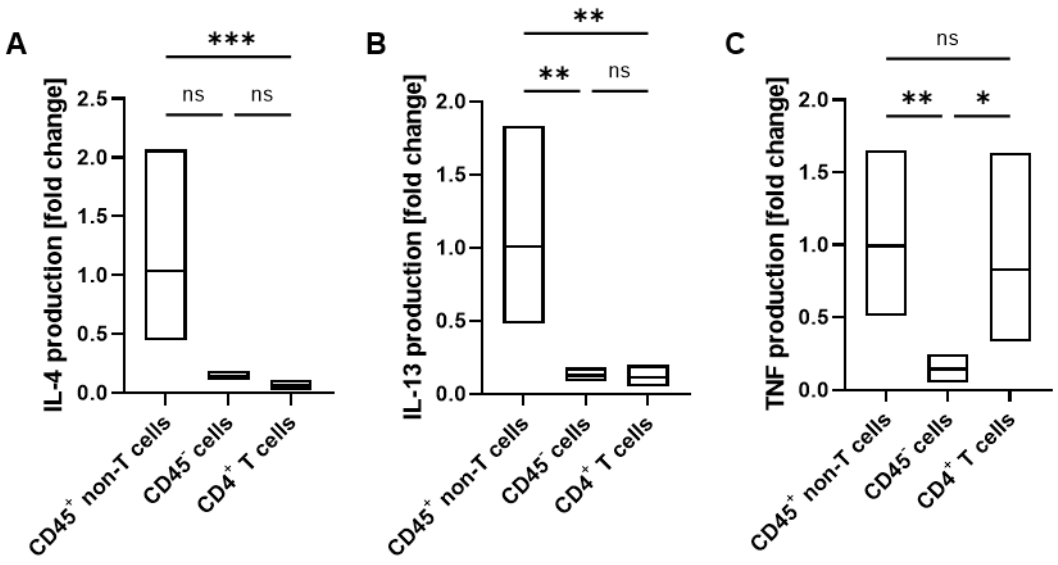

Figure 4.40: Overall cytokine production within the lung tissue of wt mice during allergic airway inflammation (introduced in wt/*MCL*$^{-/-}$ *SIGNR3*$^{-/-}$ mice). Allergic airway inflammation was introduced by HDM extract in wt and *MCL*$^{-/-}$ *SIGNR3*$^{-/-}$ mice and lung tissue was analyzed by flow cytometry. The overall cytokine production of (A) IL-4, (B) IL-13 and (C) TNF by wt CD45^{+} non-T cells, CD45^{-} cells and CD4^{+} T cells was calculated based on the numbers of cytokine-producing cells and their respective MFI (N = 7/8). Fold change was calculated setting the mean of overall cytokine production of CD45^{+} non-T cells to 1. *** $p < 0.001$, ** $p < 0.01$, * $p < 0.05$, # $p \leq 0.10$, ns $p > 0.10$.

Next, the overall cytokine production by CD4^{+} T cells, CD45^{+} non-T cells and CD45^{-} cells was compared within the lung tissue of wt and *MCL*$^{-/-}$ *SIGNR3*$^{-/-}$ mice. Figure 4.41 shows the overall cytokine production that was calculated based on the numbers of cytokine^{+} cells and the amount of cytokines produced per cell (Appendix Figure 7.15 and Figure 7.16). Within the compartment of CD4^{+} T cells, the production of T_H2 cytokines IL-4 and IL-13 were slightly but not significantly reduced within the lung tissue of *MCL*$^{-/-}$ *SIGNR3*$^{-/-}$ compared to wt mice, while the production of TNF was not altered (Figure 4.41A).
Interestingly, IL-4 production by CD45^{+} non-T cells, which is the major source of IL-4, was significantly reduced by approx. 60% within the lung tissue of HDM-treated *MCL*$^{-/-}$ *SIGNR3*$^{-/-}$ compared to wt mice. In line, the production of IL-13 trended to be also reduced but with no statistical significance. In contrast to CD4^{+} T cells, TNF production by CD45^{+} non-T cells was also slightly reduced by approx. 30% within lungs of *MCL*$^{-/-}$ *SIGNR3*$^{-/-}$ compared to wt mice (Figure 4.41B). The cytokine production of IL-4, IL-13 and TNF by CD45^{-} cells was significantly reduced by approx. 20 - 35% within the lung tissue of *MCL*$^{-/-}$ *SIGNR3*$^{-/-}$ compared to wt mice (Figure 4.41C).

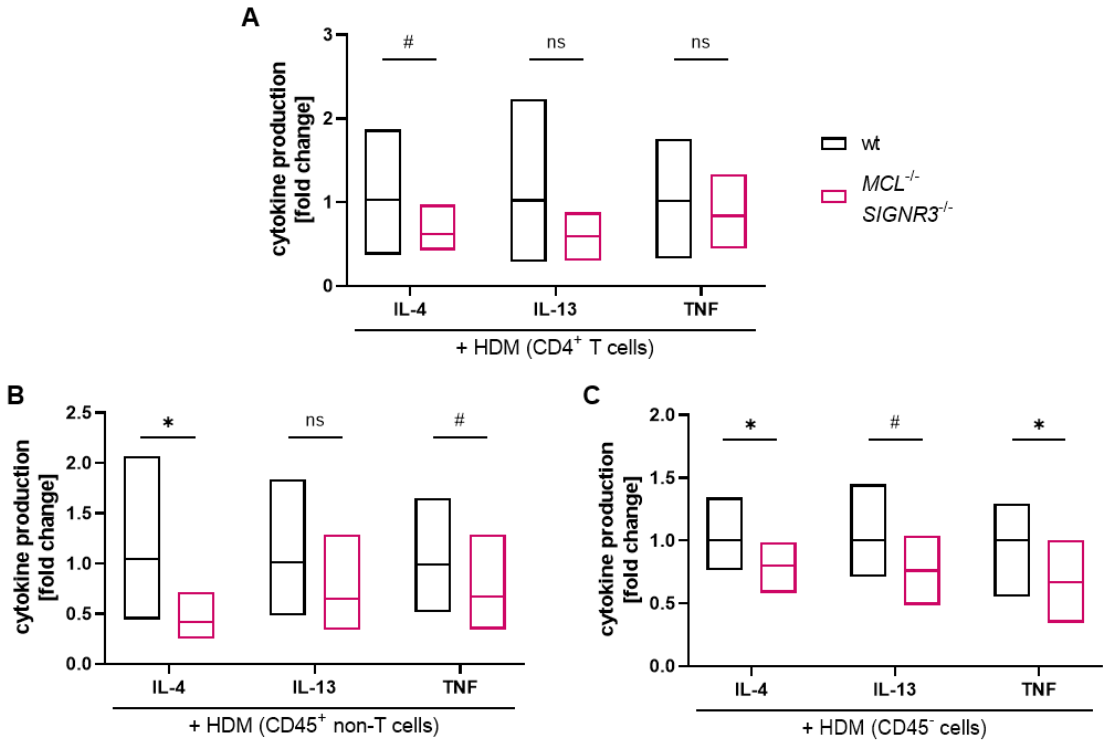

Figure 4.41: Analysis of the overall cytokines production within lung tissues of wt and *MCL*$^{-/-}$ *SIGNR3*$^{-/-}$ mice upon allergic airway inflammation. Allergic airway inflammation was introduced by HDM extract in wt and *MCL*$^{-/-}$ *SIGNR3*$^{-/-}$mice and lung tissue was analyzed by flow cytometry. The overall cytokine production of IL-4, IL-13 and TNF by (A) CD4^{+} T cells, (B) CD45^{+} non-T cells and (C) CD45^{-} cells was calculated based on the numbers of cytokine-producing cells and their respective MFI (N = 7/8). Fold change was calculated setting the mean of overall cytokine production by wt cells of each data set to 1. *** $p < 0.001$, ** $p < 0.01$, * $p < 0.05$, # $p \leq 0.10$, ns $p > 0.10$.

In addition, total IgE content was analyzed in serum samples of wt and *MCL*$^{-/-}$ *SIGNR3*$^{-/-}$ mice. HDM treatment of wt mice led to an increase of serum IgE of approx. 30% compared to wt mice that were not treated with HDM extract. The serum levels of IgE of *MCL*$^{-/-}$ *SIGNR3*$^{-/-}$ mice were in average reduced by 30% compared to HDM-treated wt mice and were detected in the same range of wt mice that did not receive HDM extract. But due to the high variance, detected differences had no statistical significance (Figure 4.42).

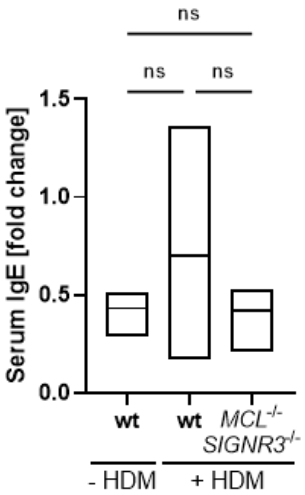

Figure 4.42: Analysis of total IgE serum levels upon allergic airway inflammation in wt and *MCL*$^{-/-}$ *SIGNR3*$^{-/-}$ mice. Allergic airway inflammation was introduced by HDM extract in wt and *MCL*$^{-/-}$ *SIGNR3*$^{-/-}$mice and serum was analyzed for total IgE content (N = 5/7). Fold change was calculated setting the mean of HDM-treated wt cells to 1. *** $p < 0.001$, ** $p < 0.01$, * $p < 0.05$, # $p \leq 0.10$, ns $p > 0.10$.

In addition to the lung tissue and serum samples, the mediastinal lung-draining LNs of *MCL*$^{-/-}$ *SIGNR3*$^{-/-}$ mice were also analyzed. The numbers of CD4^{+} T cells, CD45^{+} non-T cells and CD45^{-} cells were analyzed within the LNs upon HDM treatment of wt and *MCL*$^{-/-}$ *SIGNR3*$^{-/-}$ mice. The cell numbers within LNs of HDM-treated wt mice were increased compared to wt mice that were not treated with HDM extract. Interestingly, cell numbers of CD4^{+} T cells, CD45^{+} non-T cells as well as CD45^{-} cells within LNs of *MCL*$^{-/-}$ *SIGNR3*$^{-/-}$ mice trend to be increased compared to HDM-treated wt mice (Figure 4.43). Similar to *Card9*$^{-/-}$ mice, the numbers of T_{fh} and B cells of *MCL*$^{-/-}$ *SIGNR3*$^{-/-}$ mice were analyzed compared to wt mice. The numbers of T_{fh} cells within LNs of wt mice were slightly but not significantly increased upon HDM treatment compared to wt controls without HDM treatment. Interestingly, *MCL*$^{-/-}$ *SIGNR3*$^{-/-}$ mice exhibited slightly increased T_{fh} cell numbers compared to HDM treated wt mice and significantly increased numbers compared to the non-HDM-treated wt mice (Figure 4.43D). Same results could be observed for B cells within the mediastinal LNs. Compared to wt mice that were not treated with HDM extract, HDM treatment of wt mice led to an increase in B cell numbers that was further increased in *MCL*$^{-/-}$ *SIGNR3*$^{-/-}$ mice (Figure 4.43E).

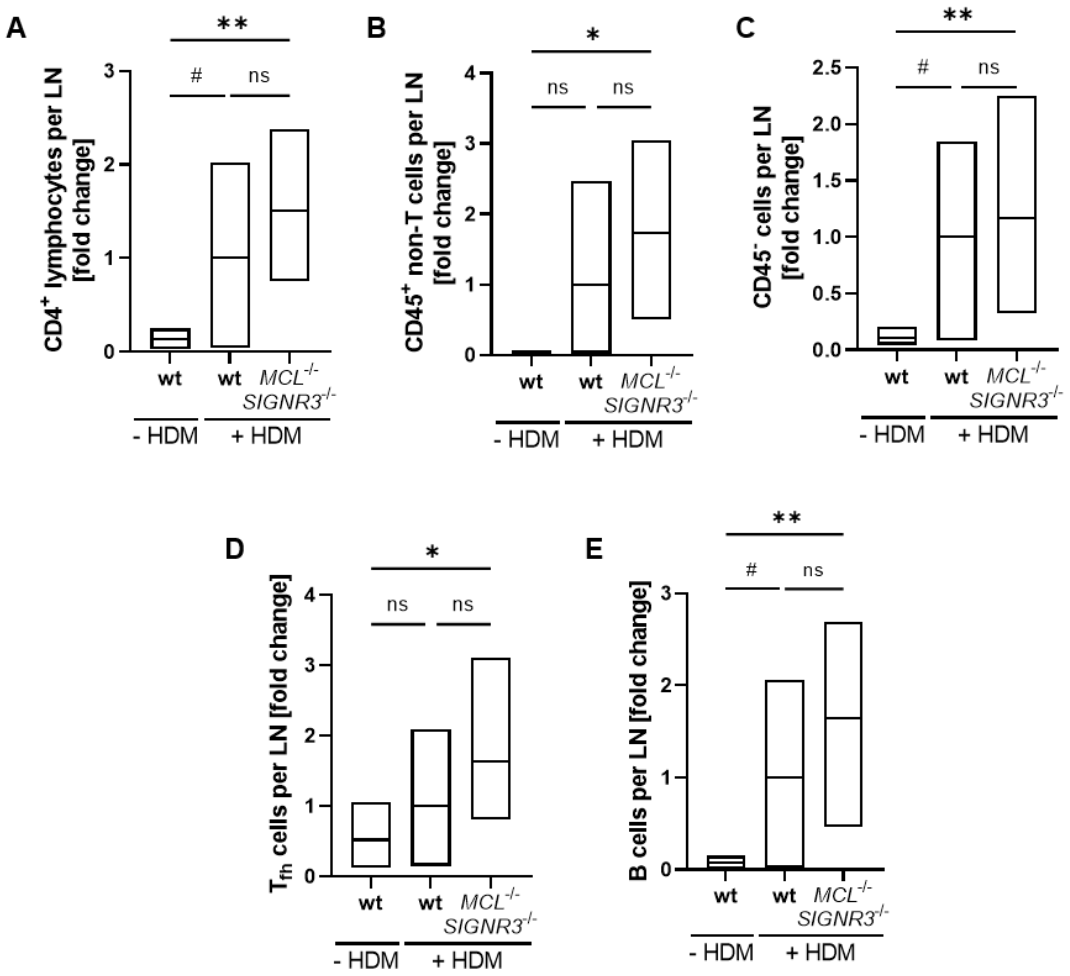

Figure 4.43: Flow cytometric analysis of mediastinal LNs of wt and *MCL*$^{-/-}$ *SIGNR3*$^{-/-}$ mice upon allergic airway inflammation. Allergic airway inflammation was introduced by HDM extract in wt and *MCL*$^{-/-}$ *SIGNR3*$^{-/-}$ mice and mediastinal LNs were analyzed by flow cytometry. Wt mice that did not receive HDM treatment served as control. Total cell counts per LN were determined for (A) CD4$^+$ T cells, (B) CD45$^+$ non-T cells, (C) CD45$^-$ cells, (D) T_{fh} cells and (E) B cells (N = 4-8). Fold change was calculated setting the mean of HDM-treated wt cells of each data set to 1. *** $p < 0.001$, ** $p < 0.01$, * $p < 0.05$, # $p \leq 0.10$, ns $p > 0.10$.

In addition, the overall cytokine production by CD4$^+$ T cells, CD45$^+$ non-T cells and CD45$^-$ cells was studied within the mediastinal LNs of HDM-treated wt mice based on their cell numbers and amount of produced cytokines (Appendix Figure 7.17 and Figure 7.18). Figure 4.44 shows the overall cytokine production of IL-4, IL-13 and TNF. As expected, CD45$^-$ cells played a significantly reduced role in the production of cytokines while CD45$^+$ non-T cells and CD4$^+$ T cells contributed equally to the production of IL-4, IL-13 and TNF within the mediastinal LNs of HDM-treated wt mice (Figure 4.44).

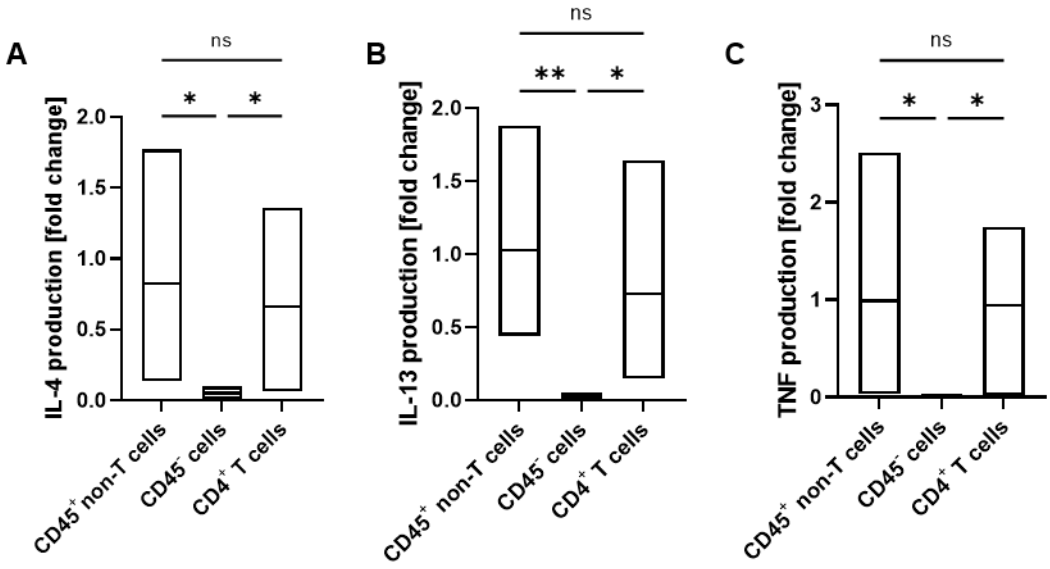

Figure 4.44: Overall cytokine production within mediastinal LNs of wt mice during allergic airway inflammation (introduced in wt/*MCL*$^{-/-}$ *SIGNR3*$^{-/-}$ mice). Allergic airway inflammation was introduced by HDM extract in wt and *MCL*$^{-/-}$ *SIGNR3*$^{-/-}$ mice and mediastinal LNs were analyzed by flow cytometry. The overall cytokine production of (A) IL-4, (B) IL-13 and (C) TNF by wt CD45^{+} non-T cells, CD45^{-} cells and CD4^{+} T cells was calculated based on the numbers of cytokine-producing cells and their respective MFI (N = 7/8). Fold change was calculated setting the mean of overall cytokine production by CD45^{+} non-T cells of each data set to 1. *** $p < 0.001$, ** $p < 0.01$, * $p < 0.05$, # $p \leq 0.10$, ns $p > 0.10$.

Finally, the cytokine production between wt and *MCL*$^{-/-}$ *SIGNR3*$^{-/-}$ mice was compared. As previously described, overall cytokine production was calculated based on the cell numbers of cytokine^{+} cell and the amount of cytokines per cell (Appendix Figure 7.19 and Figure 7.20).

Within the mediastinal LNs, the cytokine production by CD4^{+} T cells was slightly increased within LNs derived from *MCL*$^{-/-}$ *SIGNR3*$^{-/-}$ compared to wt mice. Especially TNF was increased by approx. 90% but just missed the statistical significance with a p value of 9% (Figure 4.45A).

Within the compartment of CD45^{+} non-T cells, the production of IL-4 and TNF was also slightly but not significantly increased within mediastinal LNs of *MCL*$^{-/-}$ *SIGNR3*$^{-/-}$ mice compared to wt mice. In contrast, IL-13 was not altered (Figure 4.45B). CD45^{-} cells of mediastinal LNs showed no differences in the production of IL-4, IL-13 and TNF between wt and *MCL*$^{-/-}$ *SIGNR3*$^{-/-}$ mice (Figure 4.45C).

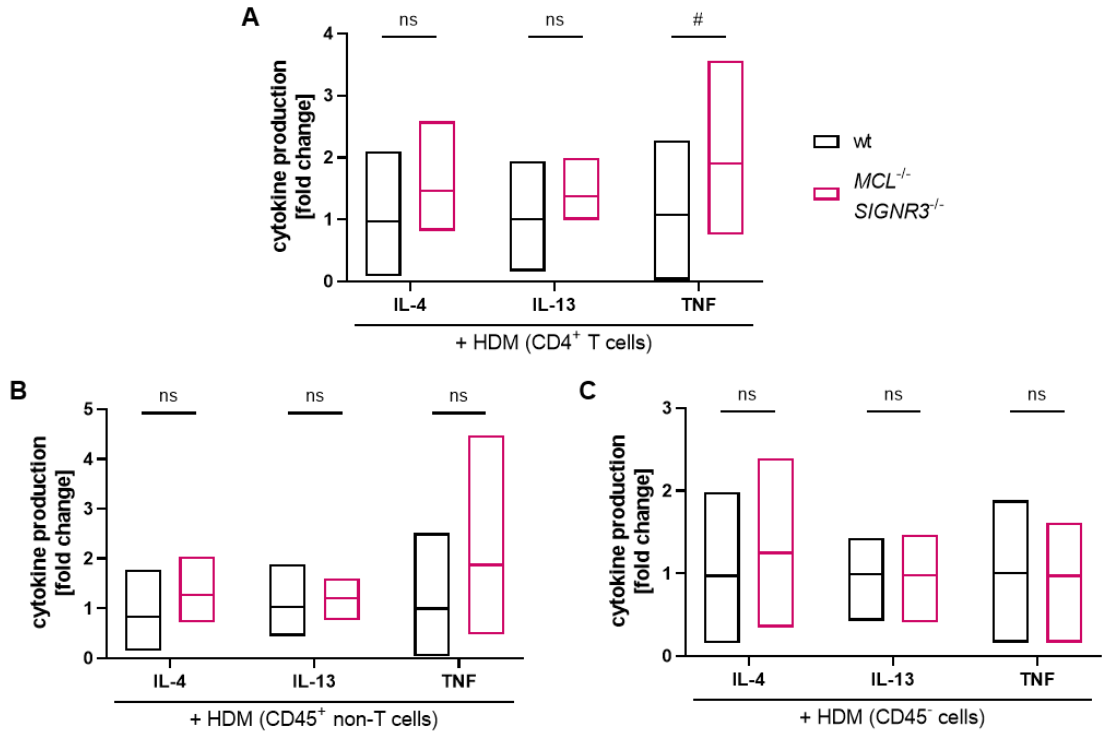

Figure 4.45: Analysis of the overall cytokines production within mediastinal LNs of wt and *MCL*$^{-/-}$ *SIGNR3*$^{-/-}$ mice upon allergic airway inflammation. Allergic airway inflammation was introduced by HDM extract in wt and *MCL*$^{-/-}$ *SIGNR3*$^{-/-}$ mice and mediastinal LNs were analyzed by flow cytometry. The overall cytokine production of IL-4, IL-13 and TNF by (A) CD4^{+} T cells, (B) CD45^{+} non-T cells and (C) CD45^{-} cells was calculated based on the numbers of cytokine-producing cells and their respective MFI (N = 8). Fold change was calculated setting the mean of overall cytokine production by wt cells of each data set to 1. *** $p < 0.001$, ** $p < 0.01$, * $p < 0.05$, # $p \leq 0.10$, ns $p > 0.10$.

In summary, the impact of defective Card9-dependent signaling (*Card9*$^{-/-}$ mice) or disrupted MCG uptake by imDCs (*MCL*$^{-/-}$ *SIGNR3*$^{-/-}$ mice) on the T_H2-driven acute allergic airway inflammation was successfully analyzed. In wt mice, CD45^{+} non-T cells were identified as main producers of IL-4, IL-13 and TNF within the lung tissue while both CD45^{+} non-T cells and CD4^{+} T cells highly contributed to the production of IL-4, IL-13 and TNF within dLNs of wt mice. In case of *Card9*$^{-/-}$ mice, defective Card9-dependent signaling did not influence the cell recruitment to the lung or the cellular composition within the mediastinal LNs and showed almost no influence on the cytokine production. In contrast, disrupted MCG uptake by imDCs (*MCL*$^{-/-}$ *SIGNR3*$^{-/-}$ mice) led to reduced peribronchial inflammation accompanied by reduced cellular infiltration in the lung while cell numbers within the lung-draining LNs were slightly increased. Most importantly, numbers of cDC2s and T_H2 cytokine-producing cells were significantly reduced within lung tissues of *MCL*$^{-/-}$ *SIGNR3*$^{-/-}$ compared to wt mice. CD45^{+} non-T cells and CD45^{-} cells

of *MCL*$^{-/-}$ *SIGNR3*$^{-/-}$ mice produced significantly fewer cytokines within the lung tissue compared to wt mice and in part slightly increased levels within the mediastinal LNs. Taken together, I could show that disrupted MCG uptake by imDCs (*MCL*$^{-/-}$ *SIGNR3*$^{-/-}$ mice) had a higher impact on the T_H2-driven acute allergic airway inflammation compared to defective Card9-dependent signaling in general (*Card9*$^{-/-}$ mice) and led to an overall reduced allergic airway inflammation compared to wt mice.

5 Discussion

MCG are the most characteristic feature of MCs. But they do not only characterize MCs in a morphological way, instead they also maintain important MC functions by the release of containing mediators [105,114]. In 2019, our group published that dermal DCs engulf MCG upon skin inflammation. MCG^+ DCs subsequently exhibited an increased migratory behavior, boosted maturation and T cell priming capacity compared to MCG^- DCs [1]. Nevertheless, the underlying mechanisms leading to MCG uptake by DCs and the consequences caused by MCG uptake remained not fully understood. Therefore, my thesis was focused on the identification of important mechanistic aspects of the MCG uptake mode by DCs and the resulting consequences by using different *in vitro*, *ex vivo* and *in vivo* methods.

5.1 Molecular mechanisms underlying MCG uptake by DCs

5.1.1 imDCs engulf MCG in a structure-dependent and macropinocytosis-mediated manner

The first aim of my thesis was to identify molecular mechanisms underlying MCG uptake by dermal DCs. To this end, an *in vitro* system was established to mimic MCG uptake *in vivo*, which was before solely established as a consequence of *in vivo* inflammation models. Even if *in vitro* systems have some limitations, they bear the opportunity to be performed in an isolated and controlled setting. With this, they can complement *in vivo* analyses in order to study molecular mechanisms and consequences [219,220].
Within this thesis, MCG derived from PCMC cultures were successfully isolated and simultaneously stained with fluorescently labeled avidin. In 2019, we published this procedure as part of the study described above and could additionally show that these isolated and fluorescently labeled MCG were functionally active demonstrated by their capacity to recruit and activate dermal DCs without any additional stimuli [1]. Additionally, MCG uptake by DCs was successfully mimicked *in vitro*, which induced DC maturation, indicated by the upregulation of MHCII and co-stimulatory molecules. This confirms the DC activation, which was shown upon uptake of MCG in response to a skin inflammation model *in vivo* [1]. Consequently, the *in vitro* method was identified as suitable to mimic MCG uptake *in vivo* and therefore to study the underlying mechanisms. Additionally, my

data underlines the fact that MCG alone are sufficient and do not necessarily need an additional stimulus to induce DC activation *in vitro* and *in vivo*.

cDCs reside in an immature state within peripheral tissue, where they act as sentinels constantly sampling the surrounding environment [6]. As summarized by Hubo *et al*. in 2013, DC functions change with their maturation status. Upon antigen uptake, imDCs become activated leading to antigen processing and presentation on MHC molecules and subsequent DC maturation. This maturation process is accompanied by the downregulation of endocytic processes and the upregulation of surface proteins that mediate their migratory, antigen presenting and T cell priming capacity [22].

In this study, imDCs were identified as most potent in engulfing MCG. In contrast, matDCs showed a strongly reduced capacity for taking up MCG. These data are supported by a study published by Diken *et al.* in 2011, who also reported a maturation status-dependent antigen uptake by reduced uptake of naked vaccine RNA *in vitro* and *in vivo* via macropinocytosis upon DC maturation [221]. In addition, another group found that cigarette smoke extract (CSE) induced DC maturation *in vitro* upon short-term treatment (18 - 24 h) shown by the upregulation of MHCII and co-stimulatory molecules, which also led to a reduced antigen uptake capacity (measured as FITC-Dextran uptake) [222]. Taken together, our results indicate that MCG serve as targets for imDCs derived from a self-source that are taken up in an antigen-like manner, similar to other targets like RNA [221] or Dextran [222]. In contrast to other self-ligands that induce tolerogenic functions of DCs (summarized in [22,223]), MCG induce DC activation and maturation, leading to an immunogenic phenotype (Figure 4.4 and [1]).

In addition to imDCs and matDCs *in vitro*, the respective counterparts were analyzed *ex vivo*. DCs of untreated skin were referred to as imDCs, while DCs that migrated from the skin upon FITC-induced CHS were isolated from the skin-draining LNs and reflected matDCs. Additionally, $CD11b^+$ LNr DCs were isolated from LNs derived from untreated or FITC treated mice. imDCs were confirmed as most potent engulfers of MCG and in addition to the *in vitro* studies, the MCG uptake by distinct skin DC subsets was also analyzed *ex vivo*. In this context, $CD103^+$ cDC1s were found to be most potent in taking up MCG, while $CD11b^+$ cDC2s and DP DCs contributed to the MCG uptake to a significantly less proportion, which is supported by *in vivo* data we gained upon LPS-induced skin inflammation. In [1], a pronounced MCG uptake was detected by $CD103^+$ cDC1s, while $CD11b^+$ cDC2s and DP DCs still took up MCG but to a lesser extent. Additionally, studies of Tomura *et al.* and Shklovskaya *et al.* showed a higher migratory behavior and tissue turnover of $CD11b^+$ ($CD103^-$) dDCs compared to their $CD103^+$ counterparts, under steady state and inflammatory conditions [206,224]. Taken together, $CD103^+$ cDC1s were shown to be most potent in MCG uptake, but due to the higher

turnover rate of CD11b$^+$ cDC2s, they might also have a great impact on the subsequently induced adaptive immune response because they will reach the dLN faster than CD103$^+$ cDC1s.

LNs harbor several subsets of LNr DCs, which are also described to play important roles for the induction of a humoral immunity, and are categorized by their expression of CD8α and CD11b. Within this thesis, a distinct subset of CD11b$^+$ sinusoid LNr DCs that was described and characterized by Gerner *et al.* in 2012 and 2015 [19,20] was studied. Gerner *et al.* showed that these DCs are crucial for the uptake of drained antigens from the conduit system of the dLNs and are subsequently required for the optimal induction of an adaptive, T cell-driven immune response. Since DCs *in vitro* and within the ear skin seem to handle MCG similar to other antigens and Kunder *et al.* demonstrated that MC-derived particles are drained to the dLNs [136], CD11b$^+$ LNr DCs were hypothesized to take up MCG, when released in the skin and drained to the dLNs. Indeed, CD11b$^+$ LNr DCs were able to engulf MCG *ex vivo* upon treatment with *in vitro* isolated and fluorescently labeled PCMC-derived MCG. Thereby, they showed an intermediate MCG uptake capacity, slightly reduced compared to imDCs but still higher compared to LNm DCs. To date, researchers only compared the maturation status of LNr DCs with tissue-derived (LNm) DCs within the LNs. It was shown that LNm DCs exhibit an increased maturational status compared to LNr DCs [225]. In contrast, no comparison between imDCs within the peripheral tissue and LNr DCs was made so far regarding their maturation status. The intermediate *ex vivo* MCG uptake capacity of CD11b$^+$ LNr DCs is comparable to the capacity of *in vitro* partially matured DCs (3 days IL-4 treatment). Therefore, this suggests an intermediate maturation status of CD11b$^+$ LNr DCs between imDCs and matDCs. This is further supported by the finding that MCG uptake capacity was even more reduced upon FITC-induced CHS, which presumably led to increased maturation not only of skin-derived DCs but also of LNr DCs. Defining the maturation status of CD11b$^+$ LNr DCs compared to imDCs and matDCs may be interesting to judge their role in the uptake and presentation of antigens drained to the LNs. Overall, the data generated *ex vivo* show the ability of CD11b$^+$ LNr DCs to take up MCG in general and support the hypothesis that MCG are not only actively shuttled to the dLNs within migratory DCs. Instead, they are also passively drained to the LNs where they might have the ability to impact on the adaptive immune responses when taken up by CD11b$^+$ LNr DCs. However, the physiologic relevance of these two parallel processes cannot be judged from this experimental setting.

Therefore, FITC-induced CHS was performed on mice, whose MCG were stained before *in vivo* with fluorescently labeled avidin and the ear skin-draining LNs were analyzed 48 h upon FITC painting by using MELC. As described for other haptens like DNFB,

FITC-conjugated proteins are taken up by dermal DCs leading to DC activation and migration to the dLNs [226,227]. In addition, soluble antigens, like FITC and FITC-conjugated antigens, can also be directly drained itself and taken up by LNr DCs locally within the dLNs [228]. Within this thesis, both MCG^+ LNm and $CD11b^+$ LNr DCs were found within the ear skin-draining LNs, while the MCG uptake by LNm DCs was higher compared to $CD11b^+$ LNr DCs. With flow cytometry, we observed approx. 25% MCG^+ DCs within the $FITC^+$ DC population [1], which is comparable when considering the different methods. Using MELC, the hypothesis was confirmed that indeed MCG are drained passively upon skin inflammation to the dLNs and additionally that $CD11b^+$ LNr DCs are able to engulf them, which is also in line with the data of Kunder *et al*. [136]. However, the active shuttling within migDCs represents the main route of MCG entry into the LNs. This was further supported by the analysis of the FITC fluorescence intensity within $MCG^{-/+}$ LNm and $CD11b^+$ LNr DCs. In line with the MCG uptake itself, the uptake of FITC was most prominent in LNm DCs and significantly reduced in LNr DCs. These data indicates that the MCG sensing and/or uptake boosted the antigen uptake capacity. MCG^+ DCs showed a higher overall antigen uptake compared to MCG^- DCs. This underlines the main route of antigen and/or MCG transport from the periphery to the dLNs within migratory DCs, while the direct drainage is possible but used to a smaller proportion. The proportion of MCG that become directly drained to the dLNs may also be dependent on the degree of MC degranulation and on edema formation within peripheral tissues, the more edema the more drainage [1]. The groups of Heath and Carbone published an additional explanation of antigen uptake by LNr DCs. They described skin- and lung-derived migDCs as transporters of antigens that subsequently transfer them to $CD8^+$ LNr DCs. The mechanisms of antigen transfer are still unclear, but they found that the antigen donation was crucial for T_c cell priming during dermal and airway viral infections [229,230]. It might be that this antigen transfer is not restricted to $CD8^+$ LNr DCs, but also occurs between migDCs and $CD11b^+$ LNr DCs and thereby transmitting “antigens” like FITC and MCG and subsequently priming $CD4^+$ T cells.

In addition to the DC maturation, the antigen uptake is influenced by different endocytic mechanisms that are exhibited by imDCs. By utilizing endocytic mechanisms, they maintain their sentinel function because of capturing self and foreign antigens [6]. The aim of shedding light on the underlying mechanisms also implemented the question about the endocytic pathway that mediates MCG uptake by imDCs.

My work within this thesis together with data from Silke Balk (Master thesis [210]) demonstrated that MCG uptake by imDCs involves macropinocytosis while an additional influence of other endocytic mechanisms could not be completely excluded. Within the literature, there are several hints supporting the participation of macropinocytosis.

Macropinocytosis was described to be diminished upon DC maturation, while CME and phagocytosis capacity were not influenced by DC maturation [221,231–233]. In addition, Martha Höroldt showed within her Bachelor thesis that macropinocytosis was more influenced by DC maturation compared to phagocytosis capacity [205]. These reports support the findings that MCG uptake involves macropinocytosis and is reduced upon DC maturation.

An increased DC maturation often goes in line with a decreased receptor expression as described for TLR expression [234], which may also provide an additional explanation for reduced macropinocytosis capacity in matDCs since macropinocytosis can also be induced by receptor engagement [235]. Therefore, the question raised whether MCG are taken up via “non-selective cell-drinking” (constitutive form) or whether this involves the induced form of macropinocytosis. To address this, the uptake capacity of imDCs for MCG derived from PCMCs, BMMCs and the MC/9 cell line was analyzed, which are widely used to study MC functions despite differences in mediator and scaffold composition [212]. The staining of PCMC-, BMMC- and MC/9-derived MCG with fluorochrome-conjugated avidin indicates their shared connective tissue type with heparin-based MCG [1,105]. The fact that solely PCMC-derived MCG were engulfed may dependent on maturation status of MCs and/or altered surface receptor and mediator composition. PCMCs reflect a fully differentiated state of CTMCs [91], while BMMCs and cell lines, like MC/9, display a more immature phenotype, which was shown by an altered expression of surface receptors or mediators like histamine and MC-specific proteases [109,212,236–238]. The mediator composition within the MCG can further vary strongly in response to the microenvironment [105,112]. Additionally, it is reported that BMMC- and MC/9-derived MCG exhibit a different composition of their GAGs compared to PCMC-derived MCG, since they bear chondroitin sulfate side chains in addition to heparin [236,237,239]. If the scaffold structure is sensed by the DCs, the altered composition of BMMC- and MC/9-derived MCG compared to PCMC-derived MCG may explain the varying capacities of imDCs to take up these MCG. This hypothesis led me conclude that the communication via MCG may be a mechanism that is restricted to fully differentiated, solely heparin-containing CTMCs. Since it cannot be completely excluded that the mediator composition contributes to the altered uptake capacity, future studies may also aim to identify the component of MCG that induces uptake via macropinocytosis. For instance, the comparison between the uptake capacity of “filled” and “empty” MCG could give a hint about the relevance of the mediator content. “Empty” MCG should solely consist of the proteoglycan scaffold, while the mediators would be completely removed. A comparable uptake capacity of “empty” MCG compared to “filled” MCG (still containing mediators) could indicate the importance of the core

structure. First experiments were already done to test this hypothesis, but the lack of an appropriate method to prove the complete emptiness of the MCG led to a delay during this experimental setup.

Intact MCG are released upon inflammation and subsequently release their mediators in a sequential manner depending on their strength of electrostatic interactions with the GAGs [105,108,114]. Therefore, hypothesizing that the scaffold structure is responsible for MCG uptake, the time point of MCG uptake *in vivo* can also alter the resulting consequences due to the composition of remaining mediators. In addition, due to the active engulfment of MCG by DCs, MCG structures may serve as template to build synthetic heparin-based polymers that exhibit adjuvant effects and carry for instance distinct mediators, peptides or mRNA for a directed DC and subsequent T cell activation. This hypothesis is supported by a study of St. John *et al.*, who built synthetic particles based on chitosan and heparin and incorporated TNF and/or IL-12, which were taken up *in vivo* by DCs and also Mphs promoting a specific antibody response [240]. However, detailed knowledge about underlying mechanisms (including signal transductions) and consequences of MCG uptake by DCs may be required to be able to use (synthetic) MCG for triggering adaptive immunity in a targeted manner.

In summary, the communication between DCs and MCs via exocytosed MCG seem to be a mechanism restricted to imDCs and fully differentiated CTMCs, which are residing in close proximity in peripheral tissues, like the skin. Additionally, the donor cell-dependent uptake of MCG led to the assumption that distinct MCG components are sensed thereby involving the induced form of macropinocytosis in the MCG uptake imDCs.

5.1.2 Role of Syk-/Card9-dependent signaling in MCG sensing and uptake

As discussed, MCG uptake may involve induced form of macropinocytosis that is known to be stimulated by different factors, e.g. innate immune receptor engagement [235].

Within this thesis, a participation of TLR signaling during MCG uptake could be excluded due to unaltered MCG uptake capacity *in vitro* of MyD88- and TRIF-deficient DCs compared to wt DCs. In contrast, a Syk or Card9 deficiency of DCs resulted in a significantly reduced MCG uptake capacity in comparison to wt DCs.

Syk is described for its multifaceted role during several biological functions. Importantly, it can mediate for instance Rho-family-mediated cytoskeletal rearrangement but also immunoreceptor-mediated pro-inflammatory responses (e.g. via the activation of NFκB) [241]. Since CLRs frequently utilize Syk for signaling introduction upon activation, it is

likely that this tyrosine kinase can connect CLR signaling (or other ITAM-based signaling pathways) to the macropinocytosis induction.

To date, nothing is known about the direct connection between any CLR activation, as the most popular example of Syk-/Card9-mediated signaling, and the induction of macropinocytosis, instead they are mainly reported to be involved in phagocytosis and receptor-mediated endocytosis [26,242,243]. Nevertheless, there are several reports that connect CLRs to known regulators of macropinocytosis [77]. For instance, Src family kinases are described for their role in the induction of macropinocytosis [244]. However, together with Syk kinases, they are also important for appropriate platelet adhesion mediated by CLEC2 [245], a CLR that belongs to the hemITAM-coupled group of CLRs. Additionally, Cdc42 should be mentioned. On the one hand it is described as critical inducer of macropinocytosis [233], and on the other hand it is utilized by the CLR MR, an ITAM/ITIM-independent CLR, to induce phagocytosis in Mphs [246]. Taken together, there are several reports that describe factors in downstream signaling of different CLRs that were already reported to be linked to the induction of macropinocytosis. Therefore, it is most likely that, as it was described for TLR signaling, also CLR engagement can lead to the macropinocytosis induction. In line with this, I could show that a defect in Syk-/Card9-dependent signaling, frequently utilized by CLRs and possibly leading to reduced induction of macropinocytosis, led to a reduced MCG uptake by imDCs.

Within this thesis, the impact of a defective Syk-/Card9-dependent signaling on MCG uptake by DCs was also analyzed *in vivo*. A Card9 deficiency led to a reduced inflammatory response upon DNFB challenge while a DC-specific Syk deficiency had no influence on the adaptive ear swelling response. Of note, no difference in the number of MCG^+ DCs was detected within the ear skin upon Card9- or DC-specific Syk deficiency compared to wt mice. While, *in vitro* studies represent a more isolated setting, *in vivo* studies include the complex interplay of all biological processes within an organism [219,220]. This might provide an explanation for the discrepancy between the reduced MCG uptake by Syk or Card9 deficient DCs *in vitro* and the cell count of MCG^+ DCs within the ear skin that was not altered between wt or CD11c-Cre^- and *Card9*$^{-/-}$ or CD11c-Cre^+ $Syk^{fl/fl}$ mice. Within a living organism, several factors might influence the inflammatory response leading to a compensation for the Syk/Card9 deficiency by bypassing the disrupted signaling pathway.

To date, little is known about the role of Syk-/Card9-dependent signaling during the course of CHS, or ACD in general. As the only report analyzing the role of Card9 during CHS, Yasukawa *et al.* reported that signaling via Syk and Card9 but not TLR signaling via MyD88 is required for T cell-driven CHS response upon hapten challenge [247]. Additionally, several groups have identified MCs as important drivers of CHS response.

By using different MC depletion models and different haptens, they showed that the inflammatory CHS response was diminished in the absence of MCs [179,248]. Given the fact that the absence of Card9 led to a decreased MCG uptake capacity of imDCs *in vitro*, it may be possible that, although the numbers of MCG^+ DC were not altered *in vivo,* a Card9-dependent sensing contributed to the development of the CHS response. It may be that a Card9 deficiency is the reason that MC degranulation inducing signals cannot be forwarded properly and transformed into an appropriate inflammatory response.

Talking about Syk- and Card9-mediated signaling, one will directly think about CLR signaling. Nevertheless, there are several reports linking also other receptors, especially ITAM-coupled receptors, to Syk [241] and Card9 [215]. In general, Card9-dependent signaling in myeloid cells was reported to be essential for the production of several cytokines and chemokines during different inflammatory conditions (summarized in [249]). Several cytokines and chemokines, like TNF, IL-1β or CXCL1, are further reported to be crucial for the recruitment of other immune cells, like Nphs, that also play a role during CHS [145]. Therefore, it might be possible that a reduced cytokine and chemokine production in response to a Card9 deficiency also led to a reduced CHS response while MCG uptake by DCs may be one of the components driving cytokine and chemokine release. Furthermore, the reduced cytokine/chemokine production in response to a Card9 deficiency, in line with a possible defect in MCG sensing, may lead to a reduced cellular infiltration causing a reduced ear swelling response. However, it may be impossible to judge whether the effect shown in Card9 deficient mice is caused by a disrupted MCG sensing and/or uptake or whether other mechanisms are involved. Therefore, it is of high importance to identify DC surface receptors that are involved in MCG uptake for judging on direct effect of MCG uptake by imDCs.

With special regard to DCs, Card9 was shown to play roles in antigen presentation and subsequent T cell priming [249]. Among these, the study of Yasukawa *et al.* showed that Card9 was required for a robust adaptive ear swelling response upon hapten challenge and an appropriate T cell priming with subsequent release of adaptive cytokines. By using adoptive transfer experiments, they further found that especially Card9-dependent signaling in DCs was required for the sensitization phase, cytokine release including IL-1 and IL-12 and subsequent T cell priming [247]. Additionally, DCs and Mphs from patients with Card9 deficiencies (caused by frameshift and nonsense mutations) were reported to release significantly reduced levels of IL-6, TNF, IL-1β and IL-23p19, which was hypothesized to be responsible for the reduced fraction of T_H17 cells within the peripheral lymphocytes [250]. Atif *et al.* further showed that Syk/Card9 signaling in DCs overlaps with the TLR5 signaling triggered by flagellin and contributed to appropriate antigen presentation and subsequent priming of flagellin-specific T cells [251]. These

results support the hypothesis that a defect in Card9-dependent signaling, especially in DCs, is responsible for a defective T cell priming and therefore a reduced adaptive ear swelling response upon DNFB challenge possibly due to a defect in MCG sensing and uptake.

Taken together, Card9 deficiency was shown to cause a reduced adaptive ear swelling response upon DNFB challenge, which may be a result of an insufficient cell recruitment to the inflamed skin, insufficient cytokine and chemokine production and T cell priming and dysregulated cell differentiation/polarization. These effects may be caused by disrupted MCG sensing by DCs, despite the fact that the MCG uptake by DCs was not altered during Card9 deficiency. As mentioned above, distinguishing between direct effects of the MCG uptake and other mechanisms that may be involved in a Card9-deficient setting is not possible. Therefore, the next part of my thesis was focused on the identification of DC surface receptors involved in MCG uptake to judge on their direct effects on immune responses.

5.1.3 Identification of CLRs MCL and SIGNR3 as MCG sensing DC surface receptors

Since, Syk and Card9 activation is best known for CLR signaling. The participation of CLRs in MCG sensing and uptake by imDCs was hypothesized. In line with current literature [252], several CLRs were found to be expressed by imDCs within this thesis. In 2014, Maglinao *et al.* published a tool to examine CLR binding to distinct targets [217]. For instance, this tool was previously used to study CLR binding to bacteria [190]. Within this thesis, these CLR binding studies identified CLRs SIGNR3, CLEC12B and MCL specifically binding to PCMC-derived MCG. The CLRs MCL and SIGNR3 remained as potential candidates involved in MCG uptake by imDCs due to their high, specific binding to PCMC-derived MCG, their high expression by imDCs and their downregulation upon DC maturation. However, the MCG uptake by imDCs *in vitro* was not inhibited in the absence of either MCL or SIGNR3 in the respective single *knockout* imDCs. Instead, only a double *knockout*, which was either introduced by RNAi techniques or by using cells derived from the herein newly generated conventional double *knockout* mice that lack both CLRs, resulted in a significantly decreased MCG uptake by imDCs.

In line with the qPCR analyses within this thesis, MCL and SIGNR3 are both reported to be expressed on several DC subsets and Mphs in the dermis, but also in other organs like spleen, thymus, lung and LNs [47,57]. Both CLRs belong to the less studied ones, but were described as receptors for ligands derived from mycobacteria [44,253], which indicates shared ligand specificity. Upon ligand binding, SIGNR3 is mainly known to induce intracellular signaling via Syk and Card9 with subsequent immune cell actication

and cytokine production [44,52], while MCL was reported as endocytic receptor mediating for instance phagocytosis and cytokine production [59,63]. Due to the following points, I hypothesize that MCL and SIGNR3 act together to mediate MCG sensing and uptake by imDCs: (I) imDCs simultaneously lacking both CLRs exhibited a significantly decreased MCG uptake compared to wt DCs, (II) MCL mRNA was simultaneously reduced upon transfection with SIGNR3-specific siRNA and *vice versa* and (III) the combined gene expression of MCL and SIGNR3 and the MCG uptake by imDCs showed a highly positive correlation.

The most striking hint for the participation of both CLRs MCL and SIGNR3 in the MCG uptake by imDCs is represented by the significantly reduced uptake by DCs that simultaneously lack both CLRs compared to wt DCs, while in contrast single conventional *knockouts* did not inhibit the MCG uptake.

Within this thesis, a conventional *knockout* of SIGNR3 did not inhibit the MCG uptake by imDCs while a siRNA-induced *knockdown* of SIGNR3 in imDCs resulted in a decreased MCG uptake capacity. For many years, differences between *knockouts* and *knockdowns* were thought to be a consequence of off-target effects or toxicity of the *knockdown* reagent. In contrast and as summarized by El-Brolosy *et al.*, genetic compensation, a mechanism that functionally compensates the loss of function of a certain gene with alterations in RNA or protein levels of other genes, may also give an explanation [254]. The discrepancy between the MCG uptake by DCs derived from conventional *knockouts* and from siRNA-induced *knockdowns* might be explained by genetic compensation. Therefore, it might be that *MCL*$^{-/-}$ and *SIGNR3*$^{-/-}$ mice did not show an inhibiting effect on the MCG uptake by imDCs since the conventional *knockout* of the gene leads to the upregulation of the other receptor (SIGNR3 or MCL respectively), while this is not the case upon short-term siRNA-induced *knockdown*. Hence, the analysis of the receptors on protein level may be needed but is challenged by the lack of appropriate, commercially available antibodies.

Both CLRs are reported for their ability to form dimers. While SIGNR3 was reported to have the ability to form homodimers [48], Yamasaki *et al.* have published the formation of a functional heterodimeric complex of MCL with Mincle-FcRγ [65]. Additionally, Kalantari *et al.* described a cooperation of CD209a (SIGNR5) and Dectin-2/Mincle during infection with *Schistosoma* (*S.*) *mansoni*) [255]. CD209a belongs to the same group of CLRs as SIGNR3 [46] while MCL, together with Dectin-2 and Mincle, is a member of the Dectin-2 family of CLRs [54]. Graham *et al.* further found out that the surface expression of MCL requires an adaptor that is expressed by myeloid cells but is not represented by the well-known adaptors FcRγ, DAP10 or DAP12 [57]. Further reports demonstrated that the expression of Mincle is necessary for the sufficient cell surface expression of MCL

[256,257], but also that the expression of MCL or MCL signaling can induce the expression of Mincle [258,259].

The simultaneous reduction of MCL and SIGNR3 mRNA upon *knockdown* with a specific siRNA against one of the receptors provides another hint of the cooperation of the CLRs MCL and SIGNR3. The results of Kalantari *et al.* underline the possibility of cooperation between members of the DC-SIGN and Dectin-2 families of CLRs supporting the hypothesis of MCL and SIGNR3 cooperation. Furthermore, the data showing that CLRs can mutually influence their (surface) expression together with the simultaneous reduction of MCL and SIGNR3 mRNA upon *knockdown* with specific siRNAs indicate the possibility that MCL and SIGNR3 mutually influence each other's expression. Finally, the hypothesis of MCL-SIGNR3 cooperation or interaction is further supported by the fact that both receptors share ligand specificities, since MCL and SIGNR3 were described to be receptors for mycobacterial components [44,57].

However, the nature of a possible cooperation or interaction of MCL and SIGNR3 is not yet understood and may be addressed in more detail in the future. Syk, which mediates downstream signaling of CLRs consists of two Src homology 2 (SH2) domains [260]. These domains are required for binding to phosphorylated tyrosine residues and therefore connect the receptor activation that led to the phosphorylation of tyrosines within ITAM motifs to further downstream signaling [261]. The activation of the kinase domain of Syk necessarily needs the binding of both SH2 domains to phosphorylate tyrosine residues [260]. Due to the structure of the tyrosine kinase Syk, it also might be possible that multimers are formed instead of dimers. Thereby, the single tyrosine residue within the hemITAM motif of a single SIGNR3 receptor might not be enough to activate Syk and subsequent downstream signaling.

In general, CLRs are described for their ability to bind ligands derived from endogenous and exogenous sources [39]. To date, little is known about endogenous ligands specific for MCL and SIGNR3. For SIGNR3, brain-derived glycolipids were found as potential self-ligands without describing its biological relevance [51], while for MCL, endogenous ligands were speculated due to the heterodimer formation with Mincle and its specificity to ligands especially derived from damaged host cells [62,63]. Within this thesis, MCG were identified as endogenous ligands of MCL and SIGNR3, thereby showing for the first time biological relevant, endogenous ligands of MCL and SIGNR3. In contrast to other speculated ligands, MCG serve as ligands, which seem not to be associated with (MC) cell stress or death.

Taken together, my data indicates that the CLRs MCL and SIGNR3 are jointly involved in the MCG uptake by imDCs *in vitro*. Further research may reveal the molecular basis

of MCL/SIGNR3 interactions and the relevance of the CLRs MCL and SIGNR3 in MCG uptake *in vivo*, for instance during DNFB-induced skin inflammation.

5.2 Consequences of MCG uptake by DCs for the immune system

Understanding the underlying mechanisms may help identify prospective targets for therapeutic approaches. However, this requires knowledge about the consequences of the MCG uptake for DCs and the induced adaptive immunity, which will be focused in the following section.

DCs can link the innate and adaptive immunity since they are the most efficient, highly professional APCs and primers of naïve T cells [6]. Therefore, an *in vitro* system was used to analyze the effect of MCG uptake by imDCs on their capacity to polarize T cells. Confirming the *in vivo* data [1], $CD4^+$ T cell activation by MCG^-/MCG^+ DCs was shown by released cytokines. Sorted MCG^+ DCs were able to prime $CD4^+$ T cells, which subsequently release slightly reduced levels of T_H1 cytokines and strongly increased levels of T_H2 and T_H17 cytokines. Validating these findings, Card9 deficiency led to decreased cell numbers within dLNs and reduced T_H2 and T_H17 cell differentiation upon DNFB-induced sensitization. This confirms the reduced T cell-driven adaptive ear swelling response upon DNFB challenge in *Card9*$^{-/-}$ compared to wt mice and strengthens the fact that an insufficient T cell activation and polarization during Card9 deficiency caused a reduced adaptive CHS response.

These data further showed that a Card9-dependent signaling during DNFB-induced CHS is important for $CD4^+$ T cell but not for $CD8^+$ T_{act} and T_{eff} cell responses, which was not reported elsewhere before. Yasukawa *et al.* proposed a model that linked Card9-dependent signaling in skin DCs to the priming of T_H17/T_c17 and T_H1/T_c1 effector cells during hapten-induced CHS. Card9-dependent signaling led to the activation of NFκB with subsequent cytokine production, which contributes to the priming of T_{eff} cells. The authors showed reduced production of IFN-γ and IL-17(A) in response to a defective Card9 signaling in DCs upon trinitrochlorobenzene (TNCB)- or trinitrophenyl (TNP)-induced CHS and additionally reduced levels of TNF, IL-12p70 and IL-6 released by *Card9*$^{-/-}$ BMDCs upon stimulation with trinitrobenzene sulfonic acid (TNBS) *in vitro*. In contrast, the cytokine production upon DNFB treatment of *Card9*$^{-/-}$ mice or BMDCs was not analyzed. They concluded that Card9 signaling in DCs contributed to cytokine production during hapten-induced CHS [247], which supports the findings of this thesis. Herein, the importance of the Card9-dependent signaling was additionally shown for the cytokine production upon DNFB-induced CHS. In addition to Yasukawa *et al.*, this thesis

showed that a defective Card9 signaling impaired the production of IL-4 in addition to IFN-γ and IL-17A upon DNFB treatment, which was not analyzed elsewhere before.
Within my analyses, the IL-17A release was shown to be reduced strongest by $CD4^+$ T cells upon defective Card9 signaling, which is supported by the study of *Pennino et al.*. They described that IL-17^+ cells are crucial for the development of ACD and found increasing numbers of infiltrating IL-17^+ T cells during the progression of the ACD reaction. Pennino *et al.* figured out that hapten-specific IL-17^+ T cells showed a more plastic phenotype instead of being pure T_H17 cells meaning that they also produced IFN-γ and/or IL-4. Finally, they showed that secreted IL-17 during ACD acts on keratinocytes and subsequently modulates innate immunity, thereby enhancing ACD severity [262].
Taken together, a tightly regulated T cell polarization in line with their released cytokines is important for hapten-induced CHS, which seems to be influenced by Card9 signaling. In line with studies mentioned above, an appropriate Card9 signaling is important for a sufficient T cell polarization and cytokine release during CHS in response to various haptens. A defect in Card9 signaling cause a reduced T cell priming with decreased levels of released cytokines. The effects shown *in vitro* upon MCG uptake and *in vivo* upon Card9 deficiency confirm each other, indicating that a defective MCG sensing by imDCs is responsible for the reduced CHS response in *Card9*$^{-/-}$ mice. A reduced DC activation due to reduced MCG sensing in *Card9*$^{-/-}$ mice may mainly cause a reduced T_H17 cell differentiation leading to a reduced adaptive immune response. Additionally, reduced levels of IL-4 released by T cells derived from *Card9*$^{-/-}$ mice may indicate either a role of Card9 signaling-induced T_H2 cells during ACD or a Card9 signaling-induced plasticity of T_H17 cells. Since CLRs MCL and SIGNR3 were identified as MCG-sensing DC surface receptors, the analysis of the effects of MCL/SIGNR3 deficiency on the CHS response may be helpful to distinguish between the direct effects of the MCG sensing and uptake and additional effects of a defective Card9 signaling and therefore will be added in the future.
MCs were shown to respond to keratinocyte cell stress upon DNFB treatment. Thereby, sensing the extracellular alarmins ATP and IL-33 led to MC degranulation [151]. Additionally, there are several ways of interactions between MCs and DCs, which can impact the adaptive immune response (reviewed in [118,125]). A. Dudeck and her previous colleagues demonstrated in 2011 that direct MC-DC contact leads to the activation of T_H1 and T_H17 responses. In contrast, the treatment of DCs with soluble mediators derived from IgE/antigen-stimulated MCs failed to activate DCs in the way that they were unable to induce T cell proliferation and polarization [91]. Leyva-Castillo *et al.* recently showed that MCs released IL-13 upon skin injury, which modulated the subsequent T cell response. Neighboring skin DCs downregulated their IL-12 production

in response to MC-derived IL-13 leading to a reduced T_H1 response. The authors further showed that T_H1 polarization of naïve $CD4^+$ T cells was inhibited by MC-derived IL-13 while the DC migration and the induction of T_H2 differentiation was not affected [130]. Furthermore, several studies describe histamine for its capacity to modulate DC functions by inhibiting IL-12 production [263,264]. Histamine is a well-known component of MCG that is rapidly (within 15 - 90 s) released upon degranulation [265]. However, within this thesis, MCG were isolated from *in vitro* cultured MCs upon stimulation and sequential centrifugation steps. Mediators stored within MCG are diffused in a sequential manner dependent on their electrostatic interactions with GAGs, while histamine is less negatively charged and therefore diffuses first from released MCG [105,114,265]. Therefore, histamine was most likely diffused already from MCG during their preparation *in vitro*, which excludes an effect of histamine on the DC activation with subsequent T cell polarization. Thereby, this indicates that additional MCG components have the ability to promote T_H2- and T_H17-mediated responses by modulation DC functions. However, the mediator diffusion from MCG continues also upon coculture with imDCs *in vitro* (or even within the peripheral tissue before taken up by imDCs). Diffused mediators may be sensed by all DCs (including MCG^- DCs) meaning that the mediators that remained within MCG till their uptake by DCs and the MCG core structure itself may be responsible for the MCG effect on DCs. Since we cannot synchronize the MCG uptake by imDCs, it is challenging to judge on the exact MCG mediator composition present during their uptake.

In line with the data of Dudeck *et al.* and Leyva-Castillo *et al.*, MCG, as an additional tool of MCs, were shown to impact on the T cell priming capacity of DCs. However, the fact that the soluble mediators described by Dudeck *et al.* failed to activate DCs indicate that the way of MC activation also influences the modes of MCG and/or mediator release, as also described by Gaudenzio *et al.* [203]. Therefore, the way of MC degranulation may also contribute to the DC modulating effect of MCG.

Since MCs are tissue-resident cells that sense peripheral cell stress, MCG seem to serve as a tool to influence T cell differentiation within the LNs remotely by modulating migratory DCs. Hence, within this thesis, an additional way of MCs to modulate the T cell priming capacity of imDCs was shown. Beside the MC communication with DCs by soluble mediators and direct physical interactions, MCG have the additional ability to promote T_H2 and T_H17 differentiation of naïve $CD4^+$ T cells.

Given the fact that the MCG uptake by imDCs and a defective Card9-dependent signaling modulated the T cell priming towards a T_H2-mediated response, the impact of a Card9 deficiency on the course of HDM-induced allergic airway inflammation, a mouse

model for human allergic asthma, which largely involves a T_H2 immune response signature [154], was analyzed. A defective Card9-dependent signaling was shown to have no effect on the cellular composition and peribronchial inflammation within the lung and the cellular composition within the lung-draining LNs upon HDM challenge. In line, IgE levels in the serum and the overall cytokine production by $CD4^+$ T cells, $CD45^+$ non-T cells and $CD45^-$ cells were not altered between wt and *Card9*$^{-/-}$ mice. Solely, a significantly reduced TNF production by $CD4^+$ T cells was detected within the lung derived from *Card9*$^{-/-}$ compared to wt mice.

The role of Card9 in allergic diseases is discussed controversially. DeVore and Hershey very recently summarized the role of the CBM complex in allergic inflammation and disease. Among these, they also discussed the impact of the Card9-dependent CBM complex on allergic inflammation and asthma. The authors described that the Card9-dependent CBM complex impact on allergic sensitization by modulating the T cell priming capacity of APCs. They pointed out that Card9-deficient patients exhibit increased biomarkers associated with allergy (e.g. eosinophilia, high IgE serum levels) but apart from this, they lack allergic diseases underlining the complex role of Card9 in such disorders [266].

The airway epithelium and DCs play important roles during the course of allergic airway inflammation. Both share expression patterns of several PRRs that are triggered by inhaled allergens [156]. For instance, they express TLRs, NLRs and CLRs that are (at least partially) dependent on Card9 [267] and therefore an influence of a Card9 deficiency could have been speculated. However, the data of this thesis on HDM-induced airway inflammation in *Card9*$^{-/-}$ mice showed almost no influence of the Card9 deficiency on the outcome of allergic airway inflammation and the production of T_H2 cytokines indicating that Card9 was dispensable in this experimental setting.

Using an OVA-based model of murine allergic airway inflammation, Li *et al.* showed that TNF/TNF receptor 2 (TNFR2) signaling influences T_H2 and T_H17 polarization. TNFR2 is mainly expressed by $CD4^+$ T cells, which were decreased upon airway inflammation. Additionally, they found that an impaired TNF/TNFR2 signaling, blocked by the i.n. application of TNFR2 antibodies, further decreased the expression of TNFR2 and subsequently led to an increased differentiation of T_H2 and T_H17 cells [268]. In line with this, it might be that the reduced TNF production by $CD4^+$ T cells derived from *Card9*$^{-/-}$ mice was a consequence of a compensatory mechanism to settle possible effects of Card9 deficiency on T_H2 polarization. Reduced levels of TNF indicate a reduced TNF/TNFR2 signaling, which may increase the differentiation of T_H2 cells leading to an equalized T_H2 cytokine production by cells of wt and *Card9*$^{-/-}$ mice. Further research may address this hypothesis and analyses of other time points during allergic airway

inflammation (for instance upon sensitization or during chronification) may give a hint about a compensated effect of a defective Card9 signaling. Additionally, the impact of T_H17 cells and their cytokines may be investigated, which were not analyzed within this thesis so far.

Since the CLRs MCL and SIGNR3 were identified as DC surface receptors mediating MCG sensing and uptake, the role of an MCL/SIGNR3 deficiency on the course of an allergic airway inflammation was also analyzed. In contrast to the data of *Card9*$^{-/-}$ mice, an MCL/SIGNR3 deficiency led to reduced cellular infiltration of the lung (shown as reduced peribronchial inflammation and reduced cell numbers) and a slight LN hyperplasia.

While almost nothing is known about the impact of (Card9-dependent) downstream signaling on the course of allergic asthma, there are indeed some reports about the role of CLRs during allergic airway inflammation. Already in 2002, Deslée *et al.* showed that the CLR MR was expressed on human moDCs that was increased in allergic patients compared to healthy controls. Additionally, they found that the MR was involved in the uptake of the main HDM allergen *D. pteronyssinus* peptidase 1 (Der p 1) mediated by CME [269]. Almost 10 years later, Royer *et al.* confirmed that MR is involved in the uptake of Der p 1 (but also of other natural airborne and food allergens) by human moDCs and demonstrated that the Der p 1/MR axis was important for T_H2 cell differentiation [270]. In addition to the CLR MR, Dectin-2 (Clec4n) was also reported to be involved in airway inflammation. Dectin-2 was shown to be responsible for an appropriate cytokine production upon stimulation with HDM *Dermatophagoides farinae* (*Df*) *in vitro*. Adoptively transferred DCs that were stimulated before with *Df* were shown to induce recipients' sensitization causing a T_H2-dominated inflammatory response upon i.n. *Df* challenge [166]. This was reduced upon transfer of Dectin-2 deficient DCs, which was also confirmed by the same and also other groups using a blocking antibody against Dectin-2 or *Clec4n*$^{-/-}$ mice during HDM-mediated airway inflammation [165,166,271,272]. Additionally, the CLR hDC-SIGN, the human homolog of SIGNR3, is involved in allergic asthma. Huang *et al.* showed that moDCs derived from asthmatic patients exhibit an increased IL-6 and decreased IL-12p70 production and an increased T_H2 cell priming capacity compared to moDCs derived from nonallergic controls. These effects were reduced by blocking anti-hDC-SIGN antibodies, indicating the role of hDC-SIGN during human allergic asthma [273]. In summary with other reports about the role of Dectin-1 (summarized in [274]) during T_H2- and T_H17-mediated allergic airway inflammation, these data underline the importance of CLRs for ongoing asthma. In addition to these studies, CLRs MCL and SIGNR3 were shown within this thesis playing important roles during HDM-induced allergic airway inflammation, which was not reported elsewhere

before. The effect may be related to their role in MCG uptake by imDCs. As shown before, the MCG uptake by imDCs promotes the induction of T_H2- and T_H17-mediated responses, which are necessary for the development of allergic asthma. Therefore, reducing the MCG uptake by a MCL/SIGNR3 deficiency may cause an overall reduced allergic airway inflammation. However, MCL and SIGNR3 may also contribute to allergic airway inflammation by direct allergen recognition as it was shown for other CLRs. To address this, another model of allergic airway inflammation, for instance the OVA-based model, which may lack additional allergenic ligands of MCL and SIGNR3, may be helpful to distinguish between effects of the direct MCG-MCL/SIGNR3 axis and potential, additional effects of the allergen itself. Since hDC-SIGN, the human homolog of SIGNR3, was also found to be involved in allergic asthma, the findings of this thesis that were collected within the murine system may also be linked to human diseases underlining the therapeutic potential of the MCG uptake by CLRs MCL and SIGNR3.

Within this thesis, the numbers of $CD45^+$ non-T cells, importantly of $CD11b^+$ cDC2s, and $CD4^+$ T cells within the lung were reduced in mice lacking CLRs MCL and SIGNR3 compared to wt mice.

With regards on distinct DC subsets during HDM-induced airway inflammation, Platinga *et al.* identified $CD11b^+$ cDC2s as most efficient in allergen uptake compared to $CD103^+$ cDC1s, which subsequently also represented the main fraction of allergen-bearing migDCs within the dLNs. By measuring the surface expression of co-stimulatory molecules, they further found that $CD11b^+$ cDC2s express TNF superfamily member 4 (TNFSF4, OX40L) known to induce a T_H2-mediated response and $CD103^+$ cDC1s express ICOSL that is reported to be responsible for tolerance induction. Finally, they reported that $CD11b^+$ cDC2s were important for the induction of a T_H2-mediated response upon HDM treatment [157]. This was confirmed by *ex vivo* T cell priming studies by Furuhashi *et al.*, who showed that T cells that were primed with $CD11b^+$ cDC2s produced higher levels of IL-4 but reduced levels of IFN-γ and IL-17A compared to T cells primed by $CD103^+$ cDC2s [158]. In addition, MCL was reported to be expressed within the Dectin-2 complex by $CD11b^+$ DCs and to a minor extend by $CD103^+$ DCs and alveolar Mphs within the lung tissue upon HDM-induced allergic inflammation [165].

In line with these studies, I showed reduced numbers of $CD11b^+$ cDC2s within the lung tissue upon HDM challenge together with an overall reduced peribronchial inflammation, which supports the important role of this DC subset during allergic airway inflammation. This effect may be a consequence of a reduced MCG uptake by DCs in MCL/SIGNR3 deficient mice. The MCL expression preferentially on cDC2s may also indicate a higher impact of the MCG uptake on cDC2s, which further supports their role during T_H2-mediated allergic airway inflammation. A reduced MCG uptake capacity of imDCs will

result in a reduced capacity to prime $CD4^+$ T cells towards T_H2- and T_H17 cells, which finally cause a reduced recruitment of $CD4^+$ T cells and other immune cell subsets to the lung, which in turn will lead to a dampened airway inflammation. Additionally, reduced numbers of cDC2 upon HDM challenge implies that also less cDC2s can migrate to the dLNs upon further allergen challenges, which may lead to increasing differences between wt and MCL/SIGNR3 deficient mice with every HDM challenge. Therefore, this may reflect an additional mechanism how allergic asthma is potentiated over time leading to chronification and maintenance of the vicious cycle of the disease.

Apart from the immune cells itself, their released cytokines play also an important role during allergic airway inflammation. Interestingly, $CD45^+$ non-T cells were identified as main producers of the cytokines IL-4, IL-13 and TNF within the lung tissue, which was significantly reduced in *MCL*$^{-/-}$ *SIGNR3*$^{-/-}$ compared to wt mice. In addition, TNF was also highly produced by $CD4^+$ T cells within the lung but was not altered in response to an MCL/SIGNR3 deficiency.

As summarized by Lambrecht and Hammad, several $CD45^+$ non-T cells subsets, including DCs, eosinophils, MCs, basophils, alveolar Mphs and ILCs, play important roles during asthma including T_H2 cytokine release [155]. Basophils were shown to be important producers of IL-4, thereby causing eosinophilia and the activation of lung ILCs further promoting lung inflammation [275]. Additionally, Halim *et al.* described ILC2s as important producers of T_H2 cytokines during the early (innate) phase of lung inflammation, while at later (adaptive) phases both ILC2s and $CD4^+$ T cells contributed to the production of T_H2 cytokines. ILC2-derived T_H2 cytokines were further shown to foster DC migration to the dLN and to be necessary for the induction of the adaptive T_H2-mediated response [276]. DCs are described as important inducers of T_H2 responses during asthma. In line, they are found to be an important source of T_H2 cytokines themselves. DCs derived from asthmatic patients showed an increased production of IL-4 and IL-13 upon stimulation with Der p 1 compared to DCs derived from healthy donors, which was in line with an increased capacity to prime T_H2 cells [277]. Additionally, MCs are reported as important source of pro-inflammatory cytokines, including IL-4, IL-13 and TNF, during airway diseases that lead, for instance, to eosinophilic inflammation, BHR, mucus production and T_H2 cell polarization (summarized in [278]). In general, they are described as important players during atopic diseases, including allergic asthma and AD [117]. Upon antigen challenge, antigen-specific IgE leads to IgE-FcεRI-crosslinking, which subsequently induces MC activation and therefore cytokine release that favors T_H2 cell and eosinophil recruitment. The release of T_H2 cytokines within the lung tissue mediates the differentiation, maturation and accumulation of MCs, increasing the number of MCs that can respond to the next antigen challenge and therefore driving the often

described self-perpetuating cycle of T_H2-driven inflammation [124,173,202]. Additionally to the cytokine release, the activation of MCs will also lead to degranulation. An increased fraction of degranulated MCs were found within the airways of asthmatic patients compared to non-asthmatic patients, while higher numbers of degranulated MCs were related to increased disease severity [279].

In line, the data of this thesis underlined the importance of the cytokine milieu for the course of allergic airway inflammations. As described above, a reduced MCG uptake capacity of imDCs may result in a reduced $CD4^+$ T cell priming capacity, which finally cause a reduced recruitment of $CD4^+$ T cells and other immune cell subsets to the lung, which in turn will lead to reduced cytokine milieu within the lung, thereby further reducing the subsequent immune cell recruitment. Therefore, this indicates that the MCG uptake by imDCs reflects a crucial step for the induction and progression of allergic airway inflammation, which is also supported by the findings that the amount of degranulated MCs was positively correlated to asthma severity. With regards on reduced cDC2 numbers and the fact that they act as source of T_H2 cytokines themselves, the reduced cytokine production by $CD45^+$ non-T cells may be related to this or to a potential feedback loop, which recruited cDC2s and their released cytokine may have on other immune cell subsets. Of course, an additional reduction of other non-T cells apart from DCs and their specific contribution to the cytokine production cannot be judged at the moment, but is likely since there are several reports about their recruitment and cytokine production, as described above. Further research may address to specify immune cell subsets and their functions that are included within the $CD45^+$ non-T cells.

Apart from immune cells, the airway epithelium play also an important role during allergic asthma [280]. Within this thesis, despite contributing less to the overall cytokine production, the production of IL-4, IL-13 and TNF by $CD45^-$ cells was even more reduced in *MCL*$^{-/-}$ *SIGNR3*$^{-/-}$ compared to wt mice.

As summarized by Hammad and Lambrecht, the airway epithelium plays an important role during allergic asthma, because it supports the recruitment of immune cells and thereby promotes the T_H2-mediated immune response by the release of DAMPs and alarmins [280]. Despite being important producers of alarmins, Allahverdian *et al.* showed that airway EpCs can release T_H2 cytokines as well. Epithelial damage, which is also a symptom of asthma, induced the rapid release of IL-13 that subsequently leads to epithelial repair [281]. In line, another study showed that human airway EpCs were able to release IL-13 in response to the treatment with TSLP, which was even increased in cells from asthmatic patients compared to healthy controls. Confirming the study of Allahverdian *et al.*, Semlali *et al.* futher showed that the TSLP-induced EpC repair was reduced by blocking IL-13 [282].

In line with these studies, $CD45^-$ cells, including airway EpCs, were shown within this thesis to contribute to the overall production of T_H2 cytokines IL-4 and IL-13 and the pro-inflammatory cytokine TNF, which was reduced in response to a MCL/SIGNR3 deficiency. This may be explained by the reduced MCG uptake by imDCs in *MCL*$^{-/-}$ *SIGNR3*$^{-/-}$ compared to wt mice that lead to an overall reduced T_H2 response with a decreased number of $CD45^+$ non-T cells that also produce less T_H2 cytokines. In line with the study of Allahverdian *et al.* [281], this reduced T_H2 response may result in less epithelial damage leading to less cytokine production by EpCs. Additionally, due to the shared expression pattern of PRRs between DCs and EpCs [153,156], it might be that released MCG can directly impact on EpCs. However, the expression of MCL and SIGNR3 by airway EpCs and the possibility of a direct effect of MCG on EpCs may be addressed in the future.

Summarizing this part of my thesis, the CLRs MCL and SIGNR3, identified as receptors binding released MCG, were shown for the first time to impact on HDM-induced allergic airway inflammation. A *knockout* of both receptors led to a less sever course of allergic airway inflammation. This may be hypothesized on the fact that a combined MCL and SIGNR3 deficiency caused significantly reduced MCG uptake by imDCs as it was shown *in vitro*. The disrupted MCG uptake might have led to a decreased capacity of DCs to induce T_H2 responses, which subsequently cause reduced immune cell recruitment ($CD4^+$ T cells, $CD11b^+$ cDC2s and other $CD45^+$ non-T cells) and peribronchial inflammation. Despite their well-known direct effect on allergic asthma, MCs can thereby indirectly affect the disease course by modulating DC functions. This effect was mostly shown by impaired functions of $CD45^+$ non-T cells and $CD45^-$ cells while $CD4^+$ T cells were reduced in numbers but did not show a markedly decreased cytokine production. Consequently, the MCG uptake by MCL and SIGNR3 expressed by imDCs may additionally contribute to the vicious cycle because of further promoting T_H2 and/or T_H17-mediated inflammation. Despite their role in MCG sensing and uptake, the CLRs MCL and SIGNR3 may also play a role in direct allergen recognition as it was shown for other CLRs.

In conclusion, I aim to summarize the results of this thesis in the following model (depicted in Figure 5.1).

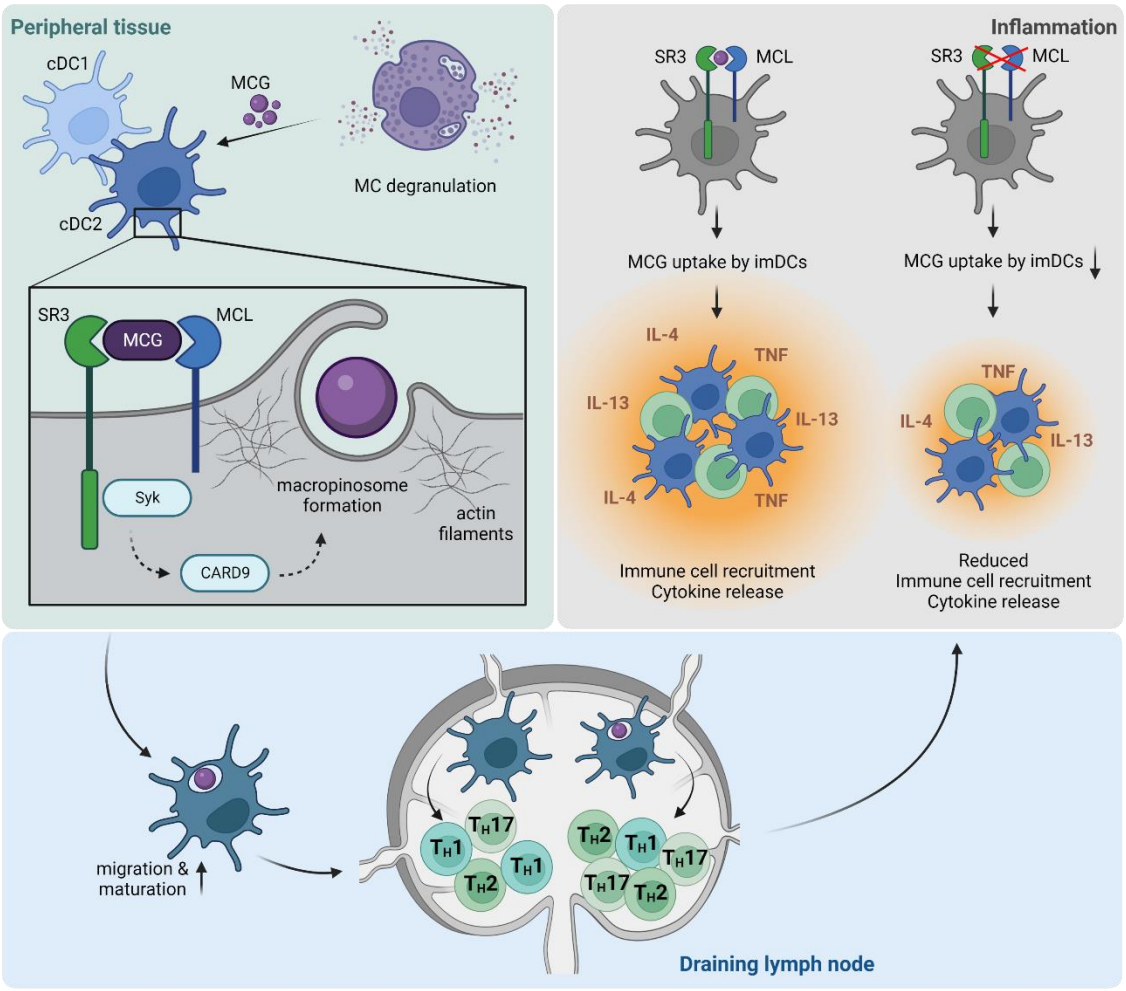

Figure 5.1: Hypothesized model for the mechanism of MCG uptake by imDCs and its consequences on inflammatory disorders. Upon MC degranulation within peripheral tissues, released MCG are taken up by neighboring imDCs in a MCL- and SIGNR3 (SR3)-induced manner that involves macropinocytosis. MCG^+ DCs show an increased maturation and migration capacity, in line with boosted T cell priming capacity compared to MCG^- DCs. In contrast to MCG^- DCs, MCG uptake will further favor the induction of T_H2- and T_H17-mediated immune responses. In terms of allergic airway inflammation, disrupting MCG uptake by imDCs by MCL/SIGNR3 deficiency will lead to reduced recruitment of cDC2s and $CD4^+$ T cells (and potentially other $CD45^+$ non-T cell subsets) with subsequently reduced cytokine production by $CD45^+$ non-T cells and $CD45^-$ cells. Figure created with BioRender.com.

Within peripheral tissues (like skin or lung), MCs and DCs reside in close proximity to each other. Incoming insults (e.g. haptens or allergens) will firstly trigger the skin or airway epithelium as the first physical barrier. As a consequence, EpCs will release alarmins like ATP, IL-33 and TSLP. This cell stress is subsequently sensed by MCs, which become activated and release their MCG, which contain preformed mediators, to the surrounding tissue. Neighboring DCs engulf MCG in a MCL- and SIGNR3-induced manner that involves macropinocytosis. Afterwards, MCG^+ DCs exhibit increased

maturation and boosted migratory behavior and preferentially lead to the induction of a T_H2- and T_H17-mediated immune response compared to MCG^- DCs.

Collectively, MCG seem to serve as endogenous CLR ligands that are not associated with (MC) cell death and translate MC degranulation inducing signals in the periphery into adjuvant effects that promote and modulate the adaptive immunity borne within the LNs. The disease models used within this thesis further support the hypothesis that this mechanism might exacerbate harmful MC functions in allergic diseases, because of contributing to the vicious cycle of T_H2-driven inflammation. Thereby, disrupting the MCG uptake by imDCs may be a promising target for therapeutic strategies for patients with MC-related disorders to prevent a life-threatening disease outcome and chronification. Additionally, targeted MC degranulation or strategic administration of MCG or MCG-based artificial vesicles could be employed therapeutically to control adaptive immune responses or to serve as possible vaccine adjuvants.

6 References

1. Dudeck, J.; Froebel, J.; Kotrba, J.; Lehmann, C.H.K.; Dudziak, D.; Speier, S.; Nedospasov, S.A.; Schraven, B.; Dudeck, A. Engulfment of mast cell secretory granules on skin inflammation boosts dendritic cell migration and priming efficiency. *J. Allergy Clin. Immunol.* 2019, *143*, 1849-1864.e4, doi:10.1016/j.jaci.2018.08.052.
2. Clausen, B.E.; Stoitzner, P. Functional Specialization of Skin Dendritic Cell Subsets in Regulating T Cell Responses. *Front. Immunol.* 2015, *6*, 534, doi:10.3389/fimmu.2015.00534.
3. Hackstein, H.; Thomson, A.W. Dendritic cells: emerging pharmacological targets of immunosuppressive drugs. *Nat. Rev. Immunol.* 2004, *4*, 24–34, doi:10.1038/nri1256.
4. Steinman, R.M. Dendritic cells: understanding immunogenicity. *Eur. J. Immunol.* 2007, *37 Suppl 1*, S53-60, doi:10.1002/eji.200737400.
5. Steinman, R.M.; Cohn, Z.A. Identification of a novel cell type in peripheral lymphoid organs of mice. I. Morphology, quantitation, tissue distribution. *J. Exp. Med.* 1973, *137*, 1142–1162, doi:10.1084/jem.137.5.1142.
6. Merad, M.; Sathe, P.; Helft, J.; Miller, J.; Mortha, A. The dendritic cell lineage: ontogeny and function of dendritic cells and their subsets in the steady state and the inflamed setting. *Annu. Rev. Immunol.* 2013, *31*, 563–604, doi:10.1146/annurev-immunol-020711-074950.
7. Collin, M.; Bigley, V. Human dendritic cell subsets: an update. *Immunology* 2018, *154*, 3–20, doi:10.1111/imm.12888.
8. Malissen, B.; Tamoutounour, S.; Henri, S. The origins and functions of dendritic cells and macrophages in the skin. *Nat. Rev. Immunol.* 2014, *14*, 417–428, doi:10.1038/nri3683.
9. Amon, L.; Lehmann, C.H.K.; Baranska, A.; Schoen, J.; Heger, L.; Dudziak, D. Transcriptional control of dendritic cell development and functions. *Int. Rev. Cell Mol. Biol.* 2019, *349*, 55–151, doi:10.1016/bs.ircmb.2019.10.001.
10. Liu, K.; Nussenzweig, M.C. Origin and development of dendritic cells. *Immunol. Rev.* 2010, *234*, 45–54, doi:10.1111/j.0105-2896.2009.00879.x.
11. Fogg, D.K.; Sibon, C.; Miled, C.; Jung, S.; Aucouturier, P.; Littman, D.R.; Cumano, A.; Geissmann, F. A clonogenic bone marrow progenitor specific for macrophages and dendritic cells. *Science* 2006, *311*, 83–87, doi:10.1126/science.1117729.
12. Diao, J.; Winter, E.; Cantin, C.; Chen, W.; Xu, L.; Kelvin, D.; Phillips, J.; Cattral, M.S. In situ replication of immediate dendritic cell (DC) precursors contributes to conventional DC homeostasis in lymphoid tissue. *J. Immunol.* 2006, *176*, 7196–7206, doi:10.4049/jimmunol.176.12.7196.
13. Naik, S.H.; Metcalf, D.; van Nieuwenhuijze, A.; Wicks, I.; Wu, L.; O'Keeffe, M.; Shortman, K. Intrasplenic steady-state dendritic cell precursors that are distinct from monocytes. *Nat. Immunol.* 2006, *7*, 663–671, doi:10.1038/ni1340.
14. Guilliams, M.; Dutertre, C.-A.; Scott, C.L.; McGovern, N.; Sichien, D.; Chakarov, S.; van Gassen, S.; Chen, J.; Poidinger, M.; Prijck, S. de; et al. Unsupervised High-

Dimensional Analysis Aligns Dendritic Cells across Tissues and Species. *Immunity* 2016, *45*, 669–684, doi:10.1016/j.immuni.2016.08.015.

15. Murphy, T.L.; Grajales-Reyes, G.E.; Wu, X.; Tussiwand, R.; Briseño, C.G.; Iwata, A.; Kretzer, N.M.; Durai, V.; Murphy, K.M. Transcriptional Control of Dendritic Cell Development. *Annu. Rev. Immunol.* 2016, *34*, 93–119, doi:10.1146/annurev-immunol-032713-120204.
16. Kashem, S.W.; Haniffa, M.; Kaplan, D.H. Antigen-Presenting Cells in the Skin. *Annu. Rev. Immunol.* 2017, *35*, 469–499, doi:10.1146/annurev-immunol-051116-052215.
17. Heath, W.R.; Carbone, F.R. Dendritic cell subsets in primary and secondary T cell responses at body surfaces. *Nat. Immunol.* 2009, *10*, 1237–1244, doi:10.1038/ni.1822.
18. Gurka, S.; Hartung, E.; Becker, M.; Kroczek, R.A. Mouse Conventional Dendritic Cells Can be Universally Classified Based on the Mutually Exclusive Expression of XCR1 and SIRPα. *Front. Immunol.* 2015, *6*, 35, doi:10.3389/fimmu.2015.00035.
19. Gerner, M.Y.; Torabi-Parizi, P.; Germain, R.N. Strategically localized dendritic cells promote rapid T cell responses to lymph-borne particulate antigens. *Immunity* 2015, *42*, 172–185, doi:10.1016/j.immuni.2014.12.024.
20. Gerner, M.Y.; Kastenmuller, W.; Ifrim, I.; Kabat, J.; Germain, R.N. Histo-cytometry: a method for highly multiplex quantitative tissue imaging analysis applied to dendritic cell subset microanatomy in lymph nodes. *Immunity* 2012, *37*, 364–376, doi:10.1016/j.immuni.2012.07.011.
21. Winde, C.M. de; Munday, C.; Acton, S.E. Molecular mechanisms of dendritic cell migration in immunity and cancer. *Med. Microbiol. Immunol.* 2020, *209*, 515–529, doi:10.1007/s00430-020-00680-4.
22. Hubo, M.; Trinschek, B.; Kryczanowsky, F.; Tuettenberg, A.; Steinbrink, K.; Jonuleit, H. Costimulatory molecules on immunogenic versus tolerogenic human dendritic cells. *Front. Immunol.* 2013, *4*, 82, doi:10.3389/fimmu.2013.00082.
23. Tiberio, L.; Del Prete, A.; Schioppa, T.; Sozio, F.; Bosisio, D.; Sozzani, S. Chemokine and chemotactic signals in dendritic cell migration. *Cell. Mol. Immunol.* 2018, *15*, 346–352, doi:10.1038/s41423-018-0005-3.
24. Takeuchi, O.; Akira, S. Pattern recognition receptors and inflammation. *Cell* 2010, *140*, 805–820, doi:10.1016/j.cell.2010.01.022.
25. Murphy, K.P.; Weaver, C.; Mowat, A. *Janeway Immunologie*, 9. Auflage, 2018, ISBN 978-3-662-56003-7.
26. Li, K.; Underhill, D.M. C-Type Lectin Receptors in Phagocytosis. *Curr. Top. Microbiol. Immunol.* 2020, *429*, 1–18, doi:10.1007/82_2020_198.
27. Kawai, T.; Akira, S. Toll-like Receptors and Their Crosstalk with Other Innate Receptors in Infection and Immunity. *Immunity* 2011, *34*, 637–650, doi:10.1016/j.immuni.2011.05.006.
28. Akira, S.; Uematsu, S.; Takeuchi, O. Pathogen Recognition and Innate Immunity. *Cell* 2006, *124*, 783–801, doi:10.1016/j.cell.2006.02.015.
29. Fitzgerald, K.A.; Kagan, J.C. Toll-like Receptors and the Control of Immunity. *Cell* 2020, *180*, 1044–1066, doi:10.1016/j.cell.2020.02.041.
30. Kawasaki, T.; Kawai, T. Toll-like receptor signaling pathways. *Front. Immunol.* 2014, *5*, 461, doi:10.3389/fimmu.2014.00461.

31. Kawai, T.; Akira, S. The role of pattern-recognition receptors in innate immunity: update on Toll-like receptors. *Nat. Immunol.* 2010, *11*, 373–384, doi:10.1038/ni.1863.
32. El-Zayat, S.R.; Sibaii, H.; Mannaa, F.A. Toll-like receptors activation, signaling, and targeting: an overview. *Bull Natl Res Cent* 2019, *43*, doi:10.1186/s42269-019-0227-2.
33. Kumar, H.; Kawai, T.; Akira, S. Toll-like receptors and innate immunity. *Biochem. Biophys. Res. Commun.* 2009, *388*, 621–625, doi:10.1016/j.bbrc.2009.08.062.
34. Kawai, T.; Akira, S. TLR signaling. *Semin. Immunol.* 2007, *19*, 24–32, doi:10.1016/j.smim.2006.12.004.
35. Kawai, T.; Akira, S. Signaling to NF-kappaB by Toll-like receptors. *Trends Mol. Med.* 2007, *13*, 460–469, doi:10.1016/j.molmed.2007.09.002.
36. Weis, W.I.; Taylor, M.E.; Drickamer, K. The C-type lectin superfamily in the immune system. *Immunol Rev* 1998, *163*, 19–34, doi:10.1111/j.1600-065X.1998.tb01185.x.
37. Brown, G.D.; Willment, J.A.; Whitehead, L. C-type lectins in immunity and homeostasis. *Nat. Rev. Immunol.* 2018, *18*, 374–389, doi:10.1038/s41577-018-0004-8.
38. Sancho, D.; Reis e Sousa, C. Signaling by myeloid C-type lectin receptors in immunity and homeostasis. *Annu. Rev. Immunol.* 2012, *30*, 491–529, doi:10.1146/annurev-immunol-031210-101352.
39. Iborra, S.; Sancho, D. Signalling versatility following self and non-self sensing by myeloid C-type lectin receptors. *Immunobiology* 2015, *220*, 175–184, doi:10.1016/j.imbio.2014.09.013.
40. Höft, M.A.; Hoving, J.C.; Brown, G.D. Signaling C-Type Lectin Receptors in Antifungal Immunity. *Curr. Top. Microbiol. Immunol.* 2020, *429*, 63–101, doi:10.1007/82_2020_224.
41. Del Fresno, C.; Iborra, S.; Saz-Leal, P.; Martínez-López, M.; Sancho, D. Flexible Signaling of Myeloid C-Type Lectin Receptors in Immunity and Inflammation. *Front. Immunol.* 2018, *9*, 804, doi:10.3389/fimmu.2018.00804.
42. Hoving, J.C.; Wilson, G.J.; Brown, G.D. Signalling C-type lectin receptors, microbial recognition and immunity. *Cell. Microbiol.* 2014, *16*, 185–194, doi:10.1111/cmi.12249.
43. Park, C.G.; Takahara, K.; Umemoto, E.; Yashima, Y.; Matsubara, K.; Matsuda, Y.; Clausen, B.E.; Inaba, K.; Steinman, R.M. Five mouse homologues of the human dendritic cell C-type lectin, DC-SIGN. *Int. Immunol.* 2001, *13*, 1283–1290, doi:10.1093/intimm/13.10.1283.
44. Tanne, A.; Ma, B.; Boudou, F.; Tailleux, L.; Botella, H.; Badell, E.; Levillain, F.; Taylor, M.E.; Drickamer, K.; Nigou, J.; et al. A murine DC-SIGN homologue contributes to early host defense against Mycobacterium tuberculosis. *J. Exp. Med.* 2009, *206*, 2205–2220, doi:10.1084/jem.20090188.
45. Takahara, K.; Yashima, Y.; Omatsu, Y.; Yoshida, H.; Kimura, Y.; Kang, Y.-S.; Steinman, R.M.; Park, C.G.; Inaba, K. Functional comparison of the mouse DC-SIGN, SIGNR1, SIGNR3 and Langerin, C-type lectins. *Int. Immunol.* 2004, *16*, 819–829, doi:10.1093/intimm/dxh084.
46. Tanne, A.; Neyrolles, O. C-type lectins in immune defense against pathogens: the murine DC-SIGN homologue SIGNR3 confers early protection against

Mycobacterium tuberculosis infection. *Virulence* 2010, *1*, 285–290, doi:10.4161/viru.1.4.11967.

47. Nagaoka, K.; Takahara, K.; Minamino, K.; Takeda, T.; Yoshida, Y.; Inaba, K. Expression of C-type lectin, SIGNR3, on subsets of dendritic cells, macrophages, and monocytes. *J. Leukoc. Biol.* 2010, *88*, 913–924, doi:10.1189/jlb.0510251.
48. Powlesland, A.S.; Ward, E.M.; Sadhu, S.K.; Guo, Y.; Taylor, M.E.; Drickamer, K. Widely divergent biochemical properties of the complete set of mouse DC-SIGN-related proteins. *J. Biol. Chem.* 2006, *281*, 20440–20449, doi:10.1074/jbc.M601925200.
49. Eriksson, M.; Johannssen, T.; Smolinski, D. von; Gruber, A.D.; Seeberger, P.H.; Lepenies, B. The C-Type Lectin Receptor SIGNR3 Binds to Fungi Present in Commensal Microbiota and Influences Immune Regulation in Experimental Colitis. *Front. Immunol.* 2013, *4*, 196, doi:10.3389/fimmu.2013.00196.
50. Galustian, C.; Park, C.G.; Chai, W.; Kiso, M.; Bruening, S.A.; Kang, Y.-S.; Steinman, R.M.; Feizi, T. High and low affinity carbohydrate ligands revealed for murine SIGN-R1 by carbohydrate array and cell binding approaches, and differing specificities for SIGN-R3 and langerin. *Int. Immunol.* 2004, *16*, 853–866, doi:10.1093/intimm/dxh089.
51. Phongsisay, V.; Iizasa, E.; Hara, H.; Yamasaki, S. 3-O-sulfo-β-D-galactose moiety of endogenous sulfoglycolipids is a potential ligand for immunoglobulin-like receptor LMIR5. *Mol. Immunol.* 2015, *63*, 595–599, doi:10.1016/j.molimm.2014.07.023.
52. Malamud, M.; Cavallero, G.J.; Casabuono, A.C.; Lepenies, B.; Serradell, M.d.L.Á.; Couto, A.S. Immunostimulation by Lactobacillus kefiri S-layer proteins with distinct glycosylation patterns requires different lectin partners. *J. Biol. Chem.* 2020, *295*, 14430–14444, doi:10.1074/jbc.RA120.013934.
53. Lefèvre, L.; Lugo-Villarino, G.; Meunier, E.; Valentin, A.; Olagnier, D.; Authier, H.; Duval, C.; Dardenne, C.; Bernad, J.; Lemesre, J.L.; et al. The C-type lectin receptors dectin-1, MR, and SIGNR3 contribute both positively and negatively to the macrophage response to Leishmania infantum. *Immunity* 2013, *38*, 1038–1049, doi:10.1016/j.immuni.2013.04.010.
54. Graham, L.M.; Brown, G.D. The Dectin-2 family of C-type lectins in immunity and homeostasis. *Cytokine* 2009, *48*, 148–155, doi:10.1016/j.cyto.2009.07.010.
55. Balch, S.G.; McKnight, A.J.; Seldin, M.F.; Gordon, S. Cloning of a novel C-type lectin expressed by murine macrophages. *J. Biol. Chem.* 1998, *273*, 18656–18664, doi:10.1074/jbc.273.29.18656.
56. Wilson, G.J.; Marakalala, M.J.; Hoving, J.C.; van Laarhoven, A.; Drummond, R.A.; Kerscher, B.; Keeton, R.; van de Vosse, E.; Ottenhoff, T.H.M.; Plantinga, T.S.; et al. The C-type lectin receptor CLECSF8/CLEC4D is a key component of anti-mycobacterial immunity. *Cell Host Microbe* 2015, *17*, 252–259, doi:10.1016/j.chom.2015.01.004.
57. Graham, L.M.; Gupta, V.; Schafer, G.; Reid, D.M.; Kimberg, M.; Dennehy, K.M.; Hornsell, W.G.; Guler, R.; Campanero-Rhodes, M.A.; Palma, A.S.; et al. The C-type lectin receptor CLECSF8 (CLEC4D) is expressed by myeloid cells and triggers cellular activation through Syk kinase. *J. Biol. Chem.* 2012, *287*, 25964–25974, doi:10.1074/jbc.M112.384164.

58. Brown, G.D.; Crocker, P.R. Lectin Receptors Expressed on Myeloid Cells. *Microbiol. Spectr.* 2016, *4*, doi:10.1128/microbiolspec.MCHD-0036-2016.
59. Kerscher, B.; Willment, J.A.; Brown, G.D. The Dectin-2 family of C-type lectin-like receptors: an update. *Int. Immunol.* 2013, *25*, 271–277, doi:10.1093/intimm/dxt006.
60. Furukawa, A.; Kamishikiryo, J.; Mori, D.; Toyonaga, K.; Okabe, Y.; Toji, A.; Kanda, R.; Miyake, Y.; Ose, T.; Yamasaki, S.; et al. Structural analysis for glycolipid recognition by the C-type lectins Mincle and MCL. *Proc. Natl. Acad. Sci. U. S. A.* 2013, *110*, 17438–17443, doi:10.1073/pnas.1312649110.
61. Raymond, B.B.A.; Neyrolles, O.; Rombouts, Y. C-type Lectins in Immunity to Lung Pathogens. *Curr. Top. Microbiol. Immunol.* 2020, *429*, 19–62, doi:10.1007/82_2020_197.
62. Richardson, M.B.; Williams, S.J. MCL and Mincle: C-Type Lectin Receptors That Sense Damaged Self and Pathogen-Associated Molecular Patterns. *Front. Immunol.* 2014, *5*, 288, doi:10.3389/fimmu.2014.00288.
63. N'diaye, M.; Brauner, S.; Flytzani, S.; Kular, L.; Warnecke, A.; Adzemovic, M.Z.; Piket, E.; Min, J.-H.; Edwards, W.; Mela, F.; et al. C-type lectin receptors Mcl and Mincle control development of multiple sclerosis-like neuroinflammation. *J. Clin. Invest.* 2020, *130*, 838–852, doi:10.1172/JCI125857.
64. Arce, I.; Martínez-Muñoz, L.; Roda-Navarro, P.; Fernández-Ruiz, E. The human C-type lectin CLECSF8 is a novel monocyte/macrophage endocytic receptor. *Eur. J. Immunol.* 2004, *34*, 210–220, doi:10.1002/eji.200324230.
65. Yamasaki, S. Signaling while eating: MCL is coupled with Mincle. *Eur. J. Immunol.* 2013, *43*, 3156–3158, doi:10.1002/eji.201344131.
66. Dutta, D.; Donaldson, J.G. Search for inhibitors of endocytosis: Intended specificity and unintended consequences. *Cell. Logist.* 2012, *2*, 203–208, doi:10.4161/cl.23967.
67. Conner, S.D.; Schmid, S.L. Regulated portals of entry into the cell. *Nature* 2003, *422*, 37–44, doi:10.1038/nature01451.
68. Jaumouillé, V.; Grinstein, S. Molecular Mechanisms of Phagosome Formation. *Microbiol. Spectr.* 2016, *4*, doi:10.1128/microbiolspec.MCHD-0013-2015.
69. Levin, R.; Grinstein, S.; Canton, J. The life cycle of phagosomes: formation, maturation, and resolution. *Immunol Rev* 2016, *273*, 156–179, doi:10.1111/imr.12439.
70. Berton, G.; Mócsai, A.; Lowell, C.A. Src and Syk kinases: key regulators of phagocytic cell activation. *Trends Immunol.* 2005, *26*, 208–214, doi:10.1016/j.it.2005.02.002.
71. Canton, J. Macropinocytosis: New Insights Into Its Underappreciated Role in Innate Immune Cell Surveillance. *Front. Immunol.* 2018, *9*, 2286, doi:10.3389/fimmu.2018.02286.
72. Swanson, J.A.; Watts, C. Macropinocytosis. *Trends Cell Biol.* 1995, *5*, 424–428, doi:10.1016/s0962-8924(00)89101-1.
73. Swanson, J.A. Shaping cups into phagosomes and macropinosomes. *Nat. Rev. Mol. Cell Biol.* 2008, *9*, 639–649, doi:10.1038/nrm2447.
74. Kerr, M.C.; Teasdale, R.D. Defining macropinocytosis. *Traffic* 2009, *10*, 364–371, doi:10.1111/j.1600-0854.2009.00878.x.

75. Canton, J.; Schlam, D.; Breuer, C.; Gütschow, M.; Glogauer, M.; Grinstein, S. Calcium-sensing receptors signal constitutive macropinocytosis and facilitate the uptake of NOD2 ligands in macrophages. *Nat. Commun.* 2016, *7*, 11284, doi:10.1038/ncomms11284.
76. Lin, X.P.; Mintern, J.D.; Gleeson, P.A. Macropinocytosis in Different Cell Types: Similarities and Differences. *Membranes (Basel)* 2020, *10*, doi:10.3390/membranes10080177.
77. Lim, J.P.; Gleeson, P.A. Macropinocytosis: an endocytic pathway for internalising large gulps. *Immunol. Cell Biol.* 2011, *89*, 836–843, doi:10.1038/icb.2011.20.
78. Burgdorf, S.; Kurts, C. Endocytosis mechanisms and the cell biology of antigen presentation. *Curr. Opin. Immunol.* 2008, *20*, 89–95, doi:10.1016/j.coi.2007.12.002.
79. Mettlen, M.; Chen, P.-H.; Srinivasan, S.; Danuser, G.; Schmid, S.L. Regulation of Clathrin-Mediated Endocytosis. *Annu. Rev. Biochem.* 2018, *87*, 871–896, doi:10.1146/annurev-biochem-062917-012644.
80. Kaksonen, M.; Roux, A. Mechanisms of clathrin-mediated endocytosis. *Nat. Rev. Mol. Cell Biol.* 2018, *19*, 313–326, doi:10.1038/nrm.2017.132.
81. Doherty, G.J.; McMahon, H.T. Mechanisms of endocytosis. *Annu. Rev. Biochem.* 2009, *78*, 857–902, doi:10.1146/annurev.biochem.78.081307.110540.
82. McMahon, H.T.; Boucrot, E. Molecular mechanism and physiological functions of clathrin-mediated endocytosis. *Nat. Rev. Mol. Cell Biol.* 2011, *12*, 517–533, doi:10.1038/nrm3151.
83. Roche, P.A.; Furuta, K. The ins and outs of MHC class II-mediated antigen processing and presentation. *Nat. Rev. Immunol.* 2015, *15*, 203–216, doi:10.1038/nri3818.
84. Blum, J.S.; Wearsch, P.A.; Cresswell, P. Pathways of antigen processing. *Annu. Rev. Immunol.* 2013, *31*, 443–473, doi:10.1146/annurev-immunol-032712-095910.
85. Hall, B.M. T Cells: Soldiers and Spies--The Surveillance and Control of Effector T Cells by Regulatory T Cells. *Clin. J. Am. Soc. Nephrol.* 2015, *10*, 2050–2064, doi:10.2215/CJN.06620714.
86. Burgdorf, S.; Kautz, A.; Böhnert, V.; Knolle, P.A.; Kurts, C. Distinct pathways of antigen uptake and intracellular routing in CD4 and CD8 T cell activation. *Science* 2007, *316*, 612–616, doi:10.1126/science.1137971.
87. Joffre, O.P.; Segura, E.; Savina, A.; Amigorena, S. Cross-presentation by dendritic cells. *Nat. Rev. Immunol.* 2012, *12*, 557–569, doi:10.1038/nri3254.
88. Savina, A.; Jancic, C.; Hugues, S.; Guermonprez, P.; Vargas, P.; Moura, I.C.; Lennon-Duménil, A.-M.; Seabra, M.C.; Raposo, G.; Amigorena, S. NOX2 controls phagosomal pH to regulate antigen processing during crosspresentation by dendritic cells. *Cell* 2006, *126*, 205–218, doi:10.1016/j.cell.2006.05.035.
89. Villadangos, J.A.; Ploegh, H.L. Proteolysis in MHC class II antigen presentation: who's in charge? *Immunity* 2000, *12*, 233–239, doi:10.1016/s1074-7613(00)80176-4.
90. Worbs, T.; Hammerschmidt, S.I.; Förster, R. Dendritic cell migration in health and disease. *Nat. Rev. Immunol.* 2017, *17*, 30–48, doi:10.1038/nri.2016.116.
91. Dudeck, A.; Suender, C.A.; Kostka, S.L.; Stebut, E. von; Maurer, M. Mast cells promote Th1 and Th17 responses by modulating dendritic cell maturation and function. *Eur. J. Immunol.* 2011, *41*, 1883–1893, doi:10.1002/eji.201040994.

92. Gutcher, I.; Becher, B. APC-derived cytokines and T cell polarization in autoimmune inflammation. *J. Clin. Invest.* 2007, *117*, 1119–1127, doi:10.1172/JCI31720.
93. Guisier, F.; Barros-Filho, M.C.; Rock, L.D.; Strachan-Whaley, M.; Marshall, E.A.; Dellaire, G.; Lam, W.L. Janus or Hydra: The Many Faces of T Helper Cells in the Human Tumour Microenvironment. *Adv. Exp. Med. Biol.* 2020, *1224*, 35–51, doi:10.1007/978-3-030-35723-8_3.
94. Kumar, S.; Jeong, Y.; Ashraf, M.U.; Bae, Y.-S. Dendritic Cell-Mediated Th2 Immunity and Immune Disorders. *IJMS* 2019, *20*, doi:10.3390/ijms20092159.
95. Mittrücker, H.-W.; Visekruna, A.; Huber, M. Heterogeneity in the differentiation and function of $CD8^+$ T cells. *Arch. Immunol. Ther. Exp. (Warsz)* 2014, *62*, 449–458, doi:10.1007/s00005-014-0293-y.
96. Zhu, X.; Zhu, J. CD4 T Helper Cell Subsets and Related Human Immunological Disorders. *IJMS* 2020, *21*, doi:10.3390/ijms21218011.
97. Zhu, J.; Paul, W.E. CD4 T cells: fates, functions, and faults. *Blood* 2008, *112*, 1557–1569, doi:10.1182/blood-2008-05-078154.
98. Butcher, M.J.; Zhu, J. Recent advances in understanding the Th1/Th2 effector choice. *Fac. Rev.* 2021, *10*, 30, doi:10.12703/r/10-30.
99. Ribatti, D.; Crivellato, E. Mast cell ontogeny: an historical overview. *Immunol. Lett.* 2014, *159*, 11–14, doi:10.1016/j.imlet.2014.02.003.
100. Welle, M. Development, significance, and heterogeneity of mast cells with particular regard to the mast cell-specific proteases chymase and tryptase. *J Leukoc Biol* 1997, *61*, 233–245, doi:10.1002/jlb.61.3.233.
101. Elieh Ali Komi, D.; Grauwet, K. Role of Mast Cells in Regulation of T Cell Responses in Experimental and Clinical Settings. *Clin. Rev. Allergy Immunol.* 2018, *54*, 432–445, doi:10.1007/s12016-017-8646-z.
102. Dahlin, J.S.; Hallgren, J. Mast cell progenitors: origin, development and migration to tissues. *Mol. Immunol.* 2015, *63*, 9–17, doi:10.1016/j.molimm.2014.01.018.
103. Gurish, M.F.; Austen, K.F. Developmental origin and functional specialization of mast cell subsets. *Immunity* 2012, *37*, 25–33, doi:10.1016/j.immuni.2012.07.003.
104. Gri, G.; Frossi, B.; D'Inca, F.; Danelli, L.; Betto, E.; Mion, F.; Sibilano, R.; Pucillo, C. Mast cell: an emerging partner in immune interaction. *Front. Immunol.* 2012, *3*, 120, doi:10.3389/fimmu.2012.00120.
105. Wernersson, S.; Pejler, G. Mast cell secretory granules: armed for battle. *Nat. Rev. Immunol.* 2014, *14*, 478–494, doi:10.1038/nri3690.
106. Frossi, B.; Mion, F.; Sibilano, R.; Danelli, L.; Pucillo, C.E.M. Is it time for a new classification of mast cells? What do we know about mast cell heterogeneity? *Immunol. Rev.* 2018, *282*, 35–46, doi:10.1111/imr.12636.
107. Pejler, G.; Rönnberg, E.; Waern, I.; Wernersson, S. Mast cell proteases: multifaceted regulators of inflammatory disease. *Blood* 2010, *115*, 4981–4990, doi:10.1182/blood-2010-01-257287.
108. Mulloy, B.; Lever, R.; Page, C.P. Mast cell glycosaminoglycans. *Glycoconj. J.* 2017, *34*, 351–361, doi:10.1007/s10719-016-9749-0.
109. Akula, S.; Paivandy, A.; Fu, Z.; Thorpe, M.; Pejler, G.; Hellman, L. Quantitative In-Depth Analysis of the Mouse Mast Cell Transcriptome Reveals Organ-Specific Mast Cell Heterogeneity. *Cells* 2020, *9*, doi:10.3390/cells9010211.

110. Dwyer, D.F.; Barrett, N.A.; Austen, K.F. Expression profiling of constitutive mast cells reveals a unique identity within the immune system. *Nat. Immunol.* 2016, *17*, 878–887, doi:10.1038/ni.3445.
111. Kitamura, Y.; Kanakura, Y.; Sonoda, S.; Asai, H.; Nakano, T. Mutual Phenotypic Changes between Connective Tissue Type and Mucosal Mast Cells. *Int Arch Allergy Immunol* 1987, *82*, 244–248, doi:10.1159/000234198.
112. Abraham, S.N.; St John, A.L. Mast cell-orchestrated immunity to pathogens. *Nat. Rev. Immunol.* 2010, *10*, 440–452, doi:10.1038/nri2782.
113. Blank, U.; Madera-Salcedo, I.K.; Danelli, L.; Claver, J.; Tiwari, N.; Sánchez-Miranda, E.; Vázquez-Victorio, G.; Ramírez-Valadez, K.A.; Macias-Silva, M.; González-Espinosa, C. Vesicular trafficking and signaling for cytokine and chemokine secretion in mast cells. *Front. Immunol.* 2014, *5*, 453, doi:10.3389/fimmu.2014.00453.
114. Flores, J.A.; Balseiro-Gómez, S.; Ales, E. Emerging Roles of Granule Recycling in Mast Cell Plasticity and Homeostasis. *Crit Rev Immunol* 2016, *36*, 461–484, doi:10.1615/CritRevImmunol.2017020025.
115. Vukman, K.V.; Försönits, A.; Oszvald, Á.; Tóth, E.Á.; Buzás, E.I. Mast cell secretome: Soluble and vesicular components. *Semin. Cell Dev. Biol.* 2017, *67*, 65–73, doi:10.1016/j.semcdb.2017.02.002.
116. Balseiro-Gomez, S.; Flores, J.A.; Acosta, J.; Ramirez-Ponce, M.P.; Ales, E. Transient fusion ensures granule replenishment to maintain repeated release after IgE-mediated mast cell degranulation. *J. Cell Sci.* 2016, doi:10.1242/jcs.194340.
117. Voss, M.; Kotrba, J.; Gaffal, E.; Katsoulis-Dimitriou, K.; Dudeck, A. Mast Cells in the Skin: Defenders of Integrity or Offenders in Inflammation? *Int. J. Mol. Sci.* 2021, *22*, doi:10.3390/ijms22094589.
118. El Ansari, Y.S.; Kanagaratham, C.; Lewis, O.L.; Oettgen, H.C. IgE and mast cells: The endogenous adjuvant. *Adv. Immunol.* 2020, *148*, 93–153, doi:10.1016/bs.ai.2020.10.003.
119. da Silva, E.Z.M.; Jamur, M.C.; Oliver, C. Mast cell function: a new vision of an old cell. *J. Histochem. Cytochem.* 2014, *62*, 698–738, doi:10.1369/0022155414545334.
120. Espinosa, E.; Valitutti, S. New roles and controls of mast cells. *Curr. Opin. Immunol.* 2018, *50*, 39–47, doi:10.1016/j.coi.2017.10.012.
121. Krystel-Whittemore, M.; Dileepan, K.N.; Wood, J.G. Mast Cell: A Multi-Functional Master Cell. *Front. Immunol.* 2016, *6*, doi:10.3389/fimmu.2015.00620.
122. Liu, F.-T.; Goodarzi, H.; Chen, H.-Y. IgE, mast cells, and eosinophils in atopic dermatitis. *Clin. Rev. Allergy Immunol.* 2011, *41*, 298–310, doi:10.1007/s12016-011-8252-4.
123. Pawankar, R. Mast cells in allergic airway disease and chronic rhinosinusitis. *Chem. Immunol. Allergy* 2005, *87*, 111–129, doi:10.1159/000087639.
124. Gurram, R.K.; Zhu, J. Orchestration between ILC2s and Th2 cells in shaping type 2 immune responses. *Cell. Mol. Immunol.* 2019, *16*, 225–235, doi:10.1038/s41423-019-0210-8.
125. Katsoulis-Dimitriou, K.; Kotrba, J.; Voss, M.; Dudeck, J.; Dudeck, A. Mast Cell Functions Linking Innate Sensing to Adaptive Immunity. *Cells* 2020, *9*, doi:10.3390/cells9122538.

126. Carroll-Portillo, A.; Cannon, J.L.; te Riet, J.; Holmes, A.; Kawakami, Y.; Kawakami, T.; Cambi, A.; Lidke, D.S. Mast cells and dendritic cells form synapses that facilitate antigen transfer for T cell activation. *J. Cell Biol.* 2015, *210*, 851–864, doi:10.1083/jcb.201412074.
127. Breedveld, A.; Groot Kormelink, T.; van Egmond, M.; Jong, E.C. de. Granulocytes as modulators of dendritic cell function. *J. Leukoc. Biol.* 2017, *102*, 1003–1016, doi:10.1189/jlb.4MR0217-048RR.
128. Groot Kormelink, T.; Mol, S.; Jong, E.C. de; Wauben, M.H.M. The role of extracellular vesicles when innate meets adaptive. *Semin. Immunopathol.* 2018, *40*, 439–452, doi:10.1007/s00281-018-0681-1.
129. Carroll-Portillo, A.; Surviladze, Z.; Cambi, A.; Lidke, D.S.; Wilson, B.S. Mast cell synapses and exosomes: membrane contacts for information exchange. *Front. Immunol.* 2012, *3*, 46, doi:10.3389/fimmu.2012.00046.
130. Leyva-Castillo, J.M.; Das, M.; Artru, E.; Yoon, J.; Galand, C.; Geha, R.S. Mast cell-derived IL-13 downregulates IL-12 production by skin dendritic cells to inhibit the TH1 cell response to cutaneous antigen exposure. *J. Allergy Clin. Immunol.* 2021, *147*, 2305-2315.e3, doi:10.1016/j.jaci.2020.11.036.
131. Theoharides, T.C.; Conti, P. Mast cells to dendritic cells: Let IL-13 shut your IL-12 down. *J. Allergy Clin. Immunol.* 2021, *147*, 2073–2074, doi:10.1016/j.jaci.2021.03.032.
132. Elieh Ali Komi, D.; Wöhrl, S.; Bielory, L. Mast Cell Biology at Molecular Level: a Comprehensive Review. *Clin. Rev. Allergy Immunol.* 2020, *58*, 342–365, doi:10.1007/s12016-019-08769-2.
133. Doyle, L.M.; Wang, M.Z. Overview of Extracellular Vesicles, Their Origin, Composition, Purpose, and Methods for Exosome Isolation and Analysis. *Cells* 2019, *8*, doi:10.3390/cells8070727.
134. Baggiolini, M.; Horisberger, U.; Martin, U. Phagocytosis of mast cell granules by mononuclear phagocytes, neutrophils and eosinophils during anaphylaxis. *Int. Arch. Allergy Appl. Immunol.* 1982, *67*, 219–226, doi:10.1159/000233022.
135. Jain, R.; Tikoo, S.; Weninger, W. Mast cell granules: Modulating adaptive immune response remotely. *J. Allergy Clin. Immunol.* 2019, *143*, 1731–1733, doi:10.1016/j.jaci.2018.11.029.
136. Kunder, C.A.; St John, A.L.; Li, G.; Leong, K.W.; Berwin, B.; Staats, H.F.; Abraham, S.N. Mast cell-derived particles deliver peripheral signals to remote lymph nodes. *J. Exp. Med.* 2009, *206*, 2455–2467, doi:10.1084/jem.20090805.
137. Choi, H.W.; Suwanpradid, J.; Kim, I.H.; Staats, H.F.; Haniffa, M.; MacLeod, A.S.; Abraham, S.N. Perivascular dendritic cells elicit anaphylaxis by relaying allergens to mast cells via microvesicles. *Science* 2018, *362*, doi:10.1126/science.aao0666.
138. Otsuka, A.; Kubo, M.; Honda, T.; Egawa, G.; Nakajima, S.; Tanizaki, H.; Kim, B.; Matsuoka, S.; Watanabe, T.; Nakae, S.; et al. Requirement of interaction between mast cells and skin dendritic cells to establish contact hypersensitivity. *PLoS One* 2011, *6*, e25538, doi:10.1371/journal.pone.0025538.
139. Dudeck, J.; Medyukhina, A.; Fröbel, J.; Svensson, C.-M.; Kotrba, J.; Gerlach, M.; Gradtke, A.-C.; Schröder, B.; Speier, S.; Figge, M.T.; et al. Mast cells acquire MHCII from dendritic cells during skin inflammation. *J. Exp. Med.* 2017, *214*, 3791–3811, doi:10.1084/jem.20160783.

140. Aldakheel, F.M. Allergic Diseases: A Comprehensive Review on Risk Factors, Immunological Mechanisms, Link with COVID-19, Potential Treatments, and Role of Allergen Bioinformatics. *Int. J. Environ. Res. Public Health* 2021, *18*, doi:10.3390/ijerph182212105.
141. Kabashima, K.; Honda, T.; Ginhoux, F.; Egawa, G. The immunological anatomy of the skin. *Nat. Rev. Immunol.* 2019, *19*, 19–30, doi:10.1038/s41577-018-0084-5.
142. Kaplan, D.H.; Igyártó, B.Z.; Gaspari, A.A. Early immune events in the induction of allergic contact dermatitis. *Nat. Rev. Immunol.* 2012, *12*, 114–124, doi:10.1038/nri3150.
143. Sumpter, T.L.; Balmert, S.C.; Kaplan, D.H. Cutaneous immune responses mediated by dendritic cells and mast cells. *JCI Insight* 2019, *4*, doi:10.1172/jci.insight.123947.
144. Nguyen, A.V.; Soulika, A.M. The Dynamics of the Skin's Immune System. *Int. J. Mol. Sci.* 2019, *20*, doi:10.3390/ijms20081811.
145. Honda, T.; Egawa, G.; Grabbe, S.; Kabashima, K. Update of immune events in the murine contact hypersensitivity model: toward the understanding of allergic contact dermatitis. *J. Invest. Dermatol.* 2013, *133*, 303–315, doi:10.1038/jid.2012.284.
146. Martin, S.F. Immunological mechanisms in allergic contact dermatitis. *Curr. Opin. Allergy Clin. Immunol.* 2015, *15*, 124–130, doi:10.1097/ACI.0000000000000142.
147. Martin, S.F.; Rustemeyer, T.; Thyssen, J.P. Recent advances in understanding and managing contact dermatitis. *F1000Res.* 2018, *7*, doi:10.12688/f1000research.13499.1.
148. Martin, S.F.; Esser, P.R.; Weber, F.C.; Jakob, T.; Freudenberg, M.A.; Schmidt, M.; Goebeler, M. Mechanisms of chemical-induced innate immunity in allergic contact dermatitis. *Allergy* 2011, *66*, 1152–1163, doi:10.1111/j.1398-9995.2011.02652.x.
149. Wang, B.; Fujisawa, H.; Zhuang, L.; Freed, I.; Howell, B.G.; Shahid, S.; Shivji, G.M.; Mak, T.W.; Sauder, D.N. CD4+ Th1 and CD8+ type 1 cytotoxic T cells both play a crucial role in the full development of contact hypersensitivity. *J. Immunol.* 2000, *165*, 6783–6790, doi:10.4049/jimmunol.165.12.6783.
150. Adler, B.L.; DeLeo, V.A. Allergic Contact Dermatitis. *JAMA Dermatol.* 2021, *157*, 364, doi:10.1001/jamadermatol.2020.5639.
151. Hoppe, A.; Katsoulis-Dimitriou, K.; Edler, H.J.; Dudeck, J.; Drube, S.; Dudeck, A. Mast cells initiate the vascular response to contact allergens by sensing cell stress. *J. Allergy Clin. Immunol.* 2020, *145*, 1476-1479.e3, doi:10.1016/j.jaci.2020.01.036.
152. Dudeck, J.; Ghouse, S.M.; Lehmann, C.H.K.; Hoppe, A.; Schubert, N.; Nedospasov, S.A.; Dudziak, D.; Dudeck, A. Mast-Cell-Derived TNF Amplifies CD8(+) Dendritic Cell Functionality and CD8(+) T Cell Priming. *Cell Rep.* 2015, *13*, 399–411, doi:10.1016/j.celrep.2015.08.078.
153. Lambrecht, B.N.; Hammad, H. The immunology of asthma. *Nat. Immunol.* 2015, *16*, 45–56, doi:10.1038/ni.3049.
154. Debeuf, N.; Haspeslagh, E.; van Helden, M.; Hammad, H.; Lambrecht, B.N. Mouse Models of Asthma. *Curr. Protoc. Mouse Biol.* 2016, *6*, 169–184, doi:10.1002/cpmo.4.
155. Lambrecht, B.N.; Hammad, H.; Fahy, J.V. The Cytokines of Asthma. *Immunity* 2019, *50*, 975–991, doi:10.1016/j.immuni.2019.03.018.
156. Morianos, I.; Semitekolou, M. Dendritic Cells: Critical Regulators of Allergic Asthma. *Int. J. Mol. Sci.* 2020, *21*, doi:10.3390/ijms21217930.

157. Plantinga, M.; Guilliams, M.; Vanheerswynghels, M.; Deswarte, K.; Branco-Madeira, F.; Toussaint, W.; Vanhoutte, L.; Neyt, K.; Killeen, N.; Malissen, B.; et al. Conventional and monocyte-derived CD11b(+) dendritic cells initiate and maintain T helper 2 cell-mediated immunity to house dust mite allergen. *Immunity* 2013, *38*, 322–335, doi:10.1016/j.immuni.2012.10.016.
158. Furuhashi, K.; Suda, T.; Hasegawa, H.; Suzuki, Y.; Hashimoto, D.; Enomoto, N.; Fujisawa, T.; Nakamura, Y.; Inui, N.; Shibata, K.; et al. Mouse lung CD103+ and CD11bhigh dendritic cells preferentially induce distinct CD4+ T-cell responses. *Am. J. Respir. Cell Mol. Biol.* 2012, *46*, 165–172, doi:10.1165/rcmb.2011-0070OC.
159. Nakano, H.; Free, M.E.; Whitehead, G.S.; Maruoka, S.; Wilson, R.H.; Nakano, K.; Cook, D.N. Pulmonary CD103(+) dendritic cells prime Th2 responses to inhaled allergens. *Mucosal Immunol.* 2012, *5*, 53–65, doi:10.1038/mi.2011.47.
160. Khare, A.; Krishnamoorthy, N.; Oriss, T.B.; Fei, M.; Ray, P.; Ray, A. Cutting edge: inhaled antigen upregulates retinaldehyde dehydrogenase in lung CD103+ but not plasmacytoid dendritic cells to induce Foxp3 de novo in CD4+ T cells and promote airway tolerance. *J. Immunol.* 2013, *191*, 25–29, doi:10.4049/jimmunol.1300193.
161. Semmrich, M.; Plantinga, M.; Svensson-Frej, M.; Uronen-Hansson, H.; Gustafsson, T.; Mowat, A.M.; Yrlid, U.; Lambrecht, B.N.; Agace, W.W. Directed antigen targeting in vivo identifies a role for CD103+ dendritic cells in both tolerogenic and immunogenic T-cell responses. *Mucosal Immunol.* 2012, *5*, 150–160, doi:10.1038/mi.2011.61.
162. Desch, A.N.; Henson, P.M.; Jakubzick, C.V. Pulmonary dendritic cell development and antigen acquisition. *Immunol. Res.* 2013, *55*, 178–186, doi:10.1007/s12026-012-8359-6.
163. Desch, A.N.; Randolph, G.J.; Murphy, K.; Gautier, E.L.; Kedl, R.M.; Lahoud, M.H.; Caminschi, I.; Shortman, K.; Henson, P.M.; Jakubzick, C.V. CD103+ pulmonary dendritic cells preferentially acquire and present apoptotic cell-associated antigen. *J. Exp. Med.* 2011, *208*, 1789–1797, doi:10.1084/jem.20110538.
164. del Rio, M.-L.; Rodriguez-Barbosa, J.-I.; Kremmer, E.; Förster, R. CD103- and CD103+ bronchial lymph node dendritic cells are specialized in presenting and cross-presenting innocuous antigen to CD4+ and CD8+ T cells. *J. Immunol.* 2007, *178*, 6861–6866, doi:10.4049/jimmunol.178.11.6861.
165. Norimoto, A.; Hirose, K.; Iwata, A.; Tamachi, T.; Yokota, M.; Takahashi, K.; Saijo, S.; Iwakura, Y.; Nakajima, H. Dectin-2 promotes house dust mite-induced T helper type 2 and type 17 cell differentiation and allergic airway inflammation in mice. *Am. J. Respir. Cell Mol. Biol.* 2014, *51*, 201–209, doi:10.1165/rcmb.2013-0522OC.
166. Barrett, N.A.; Rahman, O.M.; Fernandez, J.M.; Parsons, M.W.; Xing, W.; Austen, K.F.; Kanaoka, Y. Dectin-2 mediates Th2 immunity through the generation of cysteinyl leukotrienes. *J. Exp. Med.* 2011, *208*, 593–604, doi:10.1084/jem.20100793.
167. Lambrecht, B.N.; Hammad, H. The airway epithelium in asthma. *Nat. Med.* 2012, *18*, 684–692, doi:10.1038/nm.2737.
168. Hammad, H.; Lambrecht, B.N. The basic immunology of asthma. *Cell* 2021, *184*, 1469–1485, doi:10.1016/j.cell.2021.02.016.
169. Hammad, H.; Lambrecht, B.N. The basic immunology of asthma. *Cell* 2021, *184*, 2521–2522, doi:10.1016/j.cell.2021.04.019.

170. Dougherty, R.H.; Sidhu, S.S.; Raman, K.; Solon, M.; Solberg, O.D.; Caughey, G.H.; Woodruff, P.G.; Fahy, J.V. Accumulation of intraepithelial mast cells with a unique protease phenotype in T(H)2-high asthma. *J. Allergy Clin. Immunol.* 2010, *125*, 1046-1053.e8, doi:10.1016/j.jaci.2010.03.003.
171. Halim, T.Y.F.; Hwang, Y.Y.; Scanlon, S.T.; Zaghouani, H.; Garbi, N.; Fallon, P.G.; McKenzie, A.N.J. Group 2 innate lymphoid cells license dendritic cells to potentiate memory TH2 cell responses. *Nat. Immunol.* 2016, *17*, 57–64, doi:10.1038/ni.3294.
172. Kearley, J.; Erjefalt, J.S.; Andersson, C.; Benjamin, E.; Jones, C.P.; Robichaud, A.; Pegorier, S.; Brewah, Y.; Burwell, T.J.; Bjermer, L.; et al. IL-9 governs allergen-induced mast cell numbers in the lung and chronic remodeling of the airways. *Am. J. Respir. Crit. Care Med.* 2011, *183*, 865–875, doi:10.1164/rccm.200909-1462OC.
173. Koch, S.; Sopel, N.; Finotto, S. Th9 and other IL-9-producing cells in allergic asthma. *Semin. Immunopathol.* 2017, *39*, 55–68, doi:10.1007/s00281-016-0601-1.
174. Gross, O.; Gewies, A.; Finger, K.; Schäfer, M.; Sparwasser, T.; Peschel, C.; Förster, I.; Ruland, J. Card9 controls a non-TLR signalling pathway for innate anti-fungal immunity. *Nature* 2006, *442*, 651–656, doi:10.1038/nature04926.
175. Jung, S.; Unutmaz, D.; Wong, P.; Sano, G.-I.; los Santos, K. de; Sparwasser, T.; Wu, S.; Vuthoori, S.; Ko, K.; Zavala, F.; et al. In vivo depletion of CD11c+ dendritic cells abrogates priming of CD8+ T cells by exogenous cell-associated antigens. *Immunity* 2002, *17*, 211–220, doi:10.1016/s1074-7613(02)00365-5.
176. Faust, N.; Varas, F.; Kelly, L.M.; Heck, S.; Graf, T. Insertion of enhanced green fluorescent protein into the lysozyme gene creates mice with green fluorescent granulocytes and macrophages. *Blood* 2000, *96*, 719–726.
177. Voehringer, D.; Liang, H.-E.; Locksley, R.M. Homeostasis and effector function of lymphopenia-induced "memory-like" T cells in constitutively T cell-depleted mice. *J. Immunol.* 2008, *180*, 4742–4753, doi:10.4049/jimmunol.180.7.4742.
178. Scholten, J.; Hartmann, K.; Gerbaulet, A.; Krieg, T.; Müller, W.; Testa, G.; Roers, A. Mast cell-specific Cre/loxP-mediated recombination in vivo. *Transgenic Res.* 2008, *17*, 307–315, doi:10.1007/s11248-007-9153-4.
179. Dudeck, A.; Dudeck, J.; Scholten, J.; Petzold, A.; Surianarayanan, S.; Köhler, A.; Peschke, K.; Vöhringer, D.; Waskow, C.; Krieg, T.; et al. Mast cells are key promoters of contact allergy that mediate the adjuvant effects of haptens. *Immunity* 2011, *34*, 973–984, doi:10.1016/j.immuni.2011.03.028.
180. Steichen, A.L.; Binstock, B.J.; Mishra, B.B.; Sharma, J. C-type lectin receptor Clec4d plays a protective role in resolution of Gram-negative pneumonia. *J Leukoc Biol* 2013, *94*, 393–398, doi:10.1189/jlb.1212622.
181. Hou, B.; Reizis, B.; DeFranco, A.L. Toll-like Receptors Activate Innate and Adaptive Immunity by using Dendritic Cell-Intrinsic and -Extrinsic Mechanisms. *Immunity* 2008, *29*, 272–282, doi:10.1016/j.immuni.2008.05.016.
182. Barnden, M.J.; Allison, J.; Heath, W.R.; Carbone, F.R. Defective TCR expression in transgenic mice constructed using cDNA-based alpha- and beta-chain genes under the control of heterologous regulatory elements. *Immunol. Cell Biol.* 1998, *76*, 34–40, doi:10.1046/j.1440-1711.1998.00709.x.
183. Hoebe, K.; Du, X.; Georgel, P.; Janssen, E.; Tabeta, K.; Kim, S.O.; Goode, J.; Lin, P.; Mann, N.; Mudd, S.; et al. Identification of Lps2 as a key transducer of MyD88-independent TIR signalling. *Nature* 2003, *424*, 743–748, doi:10.1038/nature01889.

184. Sauer, B. Functional expression of the cre-lox site-specific recombination system in the yeast Saccharomyces cerevisiae. *Mol. Cell. Biol.* 1987, *7*, 2087–2096, doi:10.1128/MCB.7.6.2087.
185. Sauer, B. Inducible gene targeting in mice using the Cre/lox system. *Methods* 1998, *14*, 381–392, doi:10.1006/meth.1998.0593.
186. Song, A.J.; Palmiter, R.D. Detecting and Avoiding Problems When Using the Cre-lox System. *Trends Genet.* 2018, *34*, 333–340, doi:10.1016/j.tig.2017.12.008.
187. Kim, H.; Kim, M.; Im, S.-K.; Fang, S. Mouse Cre-LoxP system: general principles to determine tissue-specific roles of target genes. *Lab. Anim. Res.* 2018, *34*, 147–159, doi:10.5625/lar.2018.34.4.147.
188. Sauer, B.; Henderson, N. Site-specific DNA recombination in mammalian cells by the Cre recombinase of bacteriophage P1. *Proc. Natl. Acad. Sci. U. S. A.* 1988, *85*, 5166–5170, doi:10.1073/pnas.85.14.5166.
189. Caton, M.L.; Smith-Raska, M.R.; Reizis, B. Notch-RBP-J signaling controls the homeostasis of CD8- dendritic cells in the spleen. *J. Exp. Med.* 2007, *204*, 1653–1664, doi:10.1084/jem.20062648.
190. Mayer, S.; Moeller, R.; Monteiro, J.T.; Ellrott, K.; Josenhans, C.; Lepenies, B. C-Type Lectin Receptor (CLR)-Fc Fusion Proteins As Tools to Screen for Novel CLR/Bacteria Interactions: An Exemplary Study on Preselected Campylobacter jejuni Isolates. *Front. Immunol.* 2018, *9*, 213, doi:10.3389/fimmu.2018.00213.
191. McQuin, C.; Goodman, A.; Chernyshev, V.; Kamentsky, L.; Cimini, B.A.; Karhohs, K.W.; Doan, M.; Ding, L.; Rafelski, S.M.; Thirstrup, D.; et al. CellProfiler 3.0: Next-generation image processing for biology. *PLoS Biol.* 2018, *16*, e2005970, doi:10.1371/journal.pbio.2005970.
192. Schneider, C.A.; Rasband, W.S.; Eliceiri, K.W. NIH Image to ImageJ: 25 years of image analysis. *Nat. Methods* 2012, *9*, 671–675, doi:10.1038/nmeth.2089.
193. InvivoGen. *OVA 323-339*: *Chicken egg albumin peptide*. Datasheet # vac-isq.
194. Jang, S.-J.; Jeon, R.-H.; Kim, H.-D.; Hwang, J.-C.; Lee, H.-J.; Bae, S.-G.; Lee, S.-L.; Rho, G.-J.; Kim, S.-J.; Lee, W.-J. TATA box binding protein and ribosomal protein 4 are suitable reference genes for normalization during quantitative polymerase chain reaction study in bovine mesenchymal stem cells. *Asian-Australas. J. Anim. Sci.* 2020, *33*, 2021–2030, doi:10.5713/ajas.20.0238.
195. Livak, K.J.; Schmittgen, T.D. Analysis of relative gene expression data using real-time quantitative PCR and the 2(-Delta Delta C(T)) Method. *Methods* 2001, *25*, 402–408, doi:10.1006/meth.2001.1262.
196. Gaspari, A.A.; Katz, S.I.; Martin, S.F. Contact Hypersensitivity. *Curr. Protoc. Immunol.* 2016, *113*, 4.2.1-4.2.7, doi:10.1002/0471142735.im0402s113.
197. Krone, A.; Fu, Y.; Schreiber, S.; Kotrba, J.; Borde, L.; Nötzold, A.; Thurm, C.; Negele, J.; Franz, T.; Stegemann-Koniszewski, S.; et al. Ionic mitigation of CD4+ T cell metabolic fitness, Th1 central nervous system autoimmunity and Th2 asthmatic airway inflammation by therapeutic zinc. *Sci. Rep.* 2022, *12*, 1943, doi:10.1038/s41598-022-04827-6.
198. Im Kim, D.; Song, M.-K.; Lee, K. Comparison of asthma phenotypes in OVA-induced mice challenged via inhaled and intranasal routes. *BMC Pulm. Med.* 2019, *19*, 241, doi:10.1186/s12890-019-1001-9.

199. Kujur, W.; Gurram, R.K.; Haleem, N.; Maurya, S.K.; Agrewala, J.N. Caerulomycin A inhibits Th2 cell activity: a possible role in the management of asthma. *Sci. Rep.* 2015, *5*, 15396, doi:10.1038/srep15396.
200. Schubert, W.; Bonnekoh, B.; Pommer, A.J.; Philipsen, L.; Böckelmann, R.; Malykh, Y.; Gollnick, H.; Friedenberger, M.; Bode, M.; Dress, A.W.M. Analyzing proteome topology and function by automated multidimensional fluorescence microscopy. *Nat Biotechnol* 2006, *24*, 1270–1278, doi:10.1038/nbt1250.
201. BioLegend. *LEGENDplex*: *Multi-Analyte Flow Assay Kit*. Datasheet # 7407.
202. Choi, H.W.; Bowen, S.E.; Miao, Y.; Chan, C.Y.; Miao, E.A.; Abrink, M.; Moeser, A.J.; Abraham, S.N. Loss of Bladder Epithelium Induced by Cytolytic Mast Cell Granules. *Immunity* 2016, *45*, 1258–1269, doi:10.1016/j.immuni.2016.11.003.
203. Gaudenzio, N.; Sibilano, R.; Marichal, T.; Starkl, P.; Reber, L.L.; Cenac, N.; McNeil, B.D.; Dong, X.; Hernandez, J.D.; Sagi-Eisenberg, R.; et al. Different activation signals induce distinct mast cell degranulation strategies. *J. Clin. Invest.* 2016, *126*, 3981–3998, doi:10.1172/JCI85538.
204. Joulia, R.; Gaudenzio, N.; Rodrigues, M.; Lopez, J.; Blanchard, N.; Valitutti, S.; Espinosa, E. Mast cells form antibody-dependent degranulatory synapse for dedicated secretion and defence. *Nat. Commun.* 2015, *6*, 6174, doi:10.1038/ncomms7174.
205. Höroldt, M. *Modulation von Dendritischen Zellen durch die Aufnahme von Mastzellgranula*: *Einfluss des Differenzierungszustandes*. Bachelorarbeit, 2018.
206. Shklovskaya, E.; Roediger, B.; Fazekas de St Groth, B. Epidermal and dermal dendritic cells display differential activation and migratory behavior while sharing the ability to stimulate CD4+ T cell proliferation in vivo. *J. Immunol.* 2008, *181*, 418–430, doi:10.4049/jimmunol.181.1.418.
207. Kaplan, D.H. Ontogeny and function of murine epidermal Langerhans cells. *Nat. Immunol.* 2017, *18*, 1068–1075, doi:10.1038/ni.3815.
208. Andrian, U.H. von; Mempel, T.R. Homing and cellular traffic in lymph nodes. *Nat. Rev. Immunol.* 2003, *3*, 867–878, doi:10.1038/nri1222.
209. Gale, N.W.; Prevo, R.; Espinosa, J.; Ferguson, D.J.; Dominguez, M.G.; Yancopoulos, G.D.; Thurston, G.; Jackson, D.G. Normal lymphatic development and function in mice deficient for the lymphatic hyaluronan receptor LYVE-1. *Mol. Cell. Biol.* 2007, *27*, 595–604, doi:10.1128/MCB.01503-06.
210. Balk, S. *Analyse der Aufnahme von Mastzellgranula in Dendritische Zellen und deren intrazelluläre Degradation*. Masterarbeit, 2019.
211. Barteneva, N.S.; Fasler-Kan, E.; Vorobjev, I.A. Imaging flow cytometry: coping with heterogeneity in biological systems. *J. Histochem. Cytochem.* 2012, *60*, 723–733, doi:10.1369/0022155412453052.
212. Akula, S.; Paivandy, A.; Fu, Z.; Thorpe, M.; Pejler, G.; Hellman, L. How Relevant Are Bone Marrow-Derived Mast Cells (BMMCs) as Models for Tissue Mast Cells? A Comparative Transcriptome Analysis of BMMCs and Peritoneal Mast Cells. *Cells* 2020, *9*, doi:10.3390/cells9092118.
213. Hoober, J.K.; Eggink, L.L.; Cote, R. Stories From the Dendritic Cell Guardhouse. *Front. Immunol.* 2019, *10*, doi:10.3389/fimmu.2019.02880.
214. Whitney, P.G.; Bär, E.; Osorio, F.; Rogers, N.C.; Schraml, B.U.; Deddouche, S.; LeibundGut-Landmann, S.; Reis e Sousa, C. Syk signaling in dendritic cells

orchestrates innate resistance to systemic fungal infection. *PLoS Pathog.* 2014, *10*, e1004276, doi:10.1371/journal.ppat.1004276.
215. Hara, H.; Ishihara, C.; Takeuchi, A.; Imanishi, T.; Xue, L.; Morris, S.W.; Inui, M.; Takai, T.; Shibuya, A.; Saijo, S.; et al. The adaptor protein CARD9 is essential for the activation of myeloid cells through ITAM-associated and Toll-like receptors. *Nat. Immunol.* 2007, *8*, 619–629, doi:10.1038/ni1466.
216. Geijtenbeek, T.B.H.; Gringhuis, S.I. C-type lectin receptors in the control of T helper cell differentiation. *Nat. Rev. Immunol.* 2016, *16*, 433–448, doi:10.1038/nri.2016.55.
217. Maglinao, M.; Eriksson, M.; Schlegel, M.K.; Zimmermann, S.; Johannssen, T.; Götze, S.; Seeberger, P.H.; Lepenies, B. A platform to screen for C-type lectin receptor-binding carbohydrates and their potential for cell-specific targeting and immune modulation. *Journal of Controlled Release* 2014, *175*, 36–42, doi:10.1016/j.jconrel.2013.12.011.
218. Virk, H.; Arthur, G.; Bradding, P. Mast cells and their activation in lung disease. *Transl. Res.* 2016, *174*, 60–76, doi:10.1016/j.trsl.2016.01.005.
219. Uttekar, P.S. Why Is In Vivo Better Than In Vitro? (accessed on 11 October 2022).
220. Dornell, J. In Vivo vs In Vitro: Definition, Pros and Cons. Available online: https://www.technologynetworks.com/drug-discovery/articles/in-vivo-vs-in-vitro-definition-pros-and-cons-350415 (accessed on 11 October 2022).
221. Diken, M.; Kreiter, S.; Selmi, A.; Britten, C.M.; Huber, C.; Türeci, Ö.; Sahin, U. Selective uptake of naked vaccine RNA by dendritic cells is driven by macropinocytosis and abrogated upon DC maturation. *Gene Ther.* 2011, *18*, 702–708, doi:10.1038/gt.2011.17.
222. Givi, M.E.; Folkerts, G.; Wagenaar, G.T.M.; Redegeld, F.A.; Mortaz, E. Cigarette smoke differentially modulates dendritic cell maturation and function in time. *Respir. Res.* 2015, *16*, 131, doi:10.1186/s12931-015-0291-6.
223. Manicassamy, S.; Pulendran, B. Dendritic cell control of tolerogenic responses. *Immunol Rev* 2011, *241*, 206–227, doi:10.1111/j.1600-065X.2011.01015.x.
224. Tomura, M.; Hata, A.; Matsuoka, S.; Shand, F.H.W.; Nakanishi, Y.; Ikebuchi, R.; Ueha, S.; Tsutsui, H.; Inaba, K.; Matsushima, K.; et al. Tracking and quantification of dendritic cell migration and antigen trafficking between the skin and lymph nodes. *Sci. Rep.* 2014, *4*, 6030, doi:10.1038/srep06030.
225. Villadangos, J.A.; Heath, W.R. Life cycle, migration and antigen presenting functions of spleen and lymph node dendritic cells: limitations of the Langerhans cells paradigm. *Semin. Immunol.* 2005, *17*, 262–272, doi:10.1016/j.smim.2005.05.015.
226. Maruyama, T.; Shiba, T.; Iizuka, H.; Matsuda, T.; Kurohane, K.; Imai, Y. Effects of phthalate esters on dendritic cell subsets and interleukin-4 production in fluorescein isothiocyanate-induced contact hypersensitivity. *Microbiol. Immunol.* 2007, *51*, 321–326, doi:10.1111/j.1348-0421.2007.tb03914.x.
227. Nara, H.; Komatsu, M.; Tekeda, Y.; Araki, A.; Akhter, N.; Asao, H. IL-21 Attenuates FITC-Induced Contact Hypersensitivity Response via Regulation of Dendritic Cell Function. *J. Invest. Dermatol.* 2018, *138*, 2174–2184, doi:10.1016/j.jid.2018.03.1508.
228. Sixt, M.; Kanazawa, N.; Selg, M.; Samson, T.; Roos, G.; Reinhardt, D.P.; Pabst, R.; Lutz, M.B.; Sorokin, L. The conduit system transports soluble antigens from the

afferent lymph to resident dendritic cells in the T cell area of the lymph node. *Immunity* 2005, *22*, 19–29, doi:10.1016/j.immuni.2004.11.013.

229. Allan, R.S.; Waithman, J.; Bedoui, S.; Jones, C.M.; Villadangos, J.A.; Zhan, Y.; Lew, A.M.; Shortman, K.; Heath, W.R.; Carbone, F.R. Migratory dendritic cells transfer antigen to a lymph node-resident dendritic cell population for efficient CTL priming. *Immunity* 2006, *25*, 153–162, doi:10.1016/j.immuni.2006.04.017.
230. Belz, G.T.; Smith, C.M.; Kleinert, L.; Reading, P.; Brooks, A.; Shortman, K.; Carbone, F.R.; Heath, W.R. Distinct migrating and nonmigrating dendritic cell populations are involved in MHC class I-restricted antigen presentation after lung infection with virus. *Proc. Natl. Acad. Sci. U. S. A.* 2004, *101*, 8670–8675, doi:10.1073/pnas.0402644101.
231. Sallusto, F.; Cella, M.; Danieli, C.; Lanzavecchia, A. Dendritic cells use macropinocytosis and the mannose receptor to concentrate macromolecules in the major histocompatibility complex class II compartment: downregulation by cytokines and bacterial products. *J. Exp. Med.* 1995, *182*, 389–400, doi:10.1084/jem.182.2.389.
232. Platt, C.D.; Ma, J.K.; Chalouni, C.; Ebersold, M.; Bou-Reslan, H.; Carano, R.A.D.; Mellman, I.; Delamarre, L. Mature dendritic cells use endocytic receptors to capture and present antigens. *Proc. Natl. Acad. Sci. U. S. A.* 2010, *107*, 4287–4292, doi:10.1073/pnas.0910609107.
233. Garrett, W.S.; Chen, L.M.; Kroschewski, R.; Ebersold, M.; Turley, S.; Trombetta, S.; Galán, J.E.; Mellman, I. Developmental control of endocytosis in dendritic cells by Cdc42. *Cell* 2000, *102*, 325–334, doi:10.1016/s0092-8674(00)00038-6.
234. Visintin, A.; Mazzoni, A.; Spitzer, J.H.; Wyllie, D.H.; Dower, S.K.; Segal, D.M. Regulation of Toll-like receptors in human monocytes and dendritic cells. *J. Immunol.* 2001, *166*, 249–255, doi:10.4049/jimmunol.166.1.249.
235. Marques, P.E.; Grinstein, S.; Freeman, S.A. SnapShot:Macropinocytosis. *Cell* 2017, *169*, 766-766.e1, doi:10.1016/j.cell.2017.04.031.
236. Galli, S.J.; Dvorak, A.M.; Marcum, J.A.; Ishizaka, T.; Nabel, G.; Der Simonian, H.; Pyne, K.; Goldin, J.M.; Rosenberg, R.D.; Cantor, H.; et al. Mast cell clones: a model for the analysis of cellular maturation. *J. Cell Biol.* 1982, *95*, 435–444, doi:10.1083/jcb.95.2.435.
237. Stevens, R.L.; Rothenberg, M.E.; Levi-Schaffer, F.; Austen, K.F. Ontogeny of in vitro-differentiated mouse mast cells. *Fed. Proc.* 1987, *46*, 1915–1919.
238. Malbec, O.; Roget, K.; Schiffer, C.; Iannascoli, B.; Dumas, A.R.; Arock, M.; Daëron, M. Peritoneal cell-derived mast cells: an in vitro model of mature serosal-type mouse mast cells. *J. Immunol.* 2007, *178*, 6465–6475, doi:10.4049/jimmunol.178.10.6465.
239. Serafin, W.E.; Katz, H.R.; Austen, K.F.; Stevens, R.L. Complexes of heparin proteoglycans, chondroitin sulfate E proteoglycans, and 3Hdiisopropyl fluorophosphate-binding proteins are exocytosed from activated mouse bone marrow-derived mast cells. *J. Biol. Chem.* 1986, *261*, 15017–15021.
240. St John, A.L.; Chan, C.Y.; Staats, H.F.; Leong, K.W.; Abraham, S.N. Synthetic mast-cell granules as adjuvants to promote and polarize immunity in lymph nodes. *Nat. Mater.* 2012, *11*, 250–257, doi:10.1038/nmat3222.

241. Mócsai, A.; Ruland, J.; Tybulewicz, V.L.J. The SYK tyrosine kinase: a crucial player in diverse biological functions. *Nat Rev Immunol* 2010, *10*, 387–402, doi:10.1038/nri2765.
242. Stahl, P.; Schlesinger, P.H.; Sigardson, E.; Rodman, J.S.; Lee, Y.C. Receptor-mediated pinocytosis of mannose glycoconjugates by macrophages: characterization and evidence for receptor recycling. *Cell* 1980, *19*, 207–215, doi:10.1016/0092-8674(80)90402-x.
243. Léger, P.; Tetard, M.; Youness, B.; Cordes, N.; Rouxel, R.N.; Flamand, M.; Lozach, P.-Y. Differential Use of the C-Type Lectins L-SIGN and DC-SIGN for Phlebovirus Endocytosis. *Traffic* 2016, *17*, 639–656, doi:10.1111/tra.12393.
244. Veithen, A.; Cupers, P.; Baudhuin, P.; Courtoy, P.J. v-Src induces constitutive macropinocytosis in rat fibroblasts. *J. Cell Sci.* 1996, *109 (Pt 8)*, 2005–2012, doi:10.1242/jcs.109.8.2005.
245. Pollitt, A.Y.; Poulter, N.S.; Gitz, E.; Navarro-Nuñez, L.; Wang, Y.-J.; Hughes, C.E.; Thomas, S.G.; Nieswandt, B.; Douglas, M.R.; Owen, D.M.; et al. Syk and Src family kinases regulate C-type lectin receptor 2 (CLEC-2)-mediated clustering of podoplanin and platelet adhesion to lymphatic endothelial cells. *J. Biol. Chem.* 2014, *289*, 35695–35710, doi:10.1074/jbc.M114.584284.
246. Zhang, J.; Zhu, J.; Bu, X.; Cushion, M.; Kinane, T.B.; Avraham, H.; Koziel, H. Cdc42 and RhoB activation are required for mannose receptor-mediated phagocytosis by human alveolar macrophages. *Mol. Biol. Cell* 2005, *16*, 824–834, doi:10.1091/mbc.e04-06-0463.
247. Yasukawa, S.; Miyazaki, Y.; Yoshii, C.; Nakaya, M.; Ozaki, N.; Toda, S.; Kuroda, E.; Ishibashi, K.; Yasuda, T.; Natsuaki, Y.; et al. An ITAM-Syk-CARD9 signalling axis triggers contact hypersensitivity by stimulating IL-1 production in dendritic cells. *Nat. Commun.* 2014, *5*, 3755, doi:10.1038/ncomms4755.
248. Norman, M.U.; Hwang, J.; Hulliger, S.; Bonder, C.S.; Yamanouchi, J.; Santamaria, P.; Kubes, P. Mast cells regulate the magnitude and the cytokine microenvironment of the contact hypersensitivity response. *Am. J. Pathol.* 2008, *172*, 1638–1649, doi:10.2353/ajpath.2008.070559.
249. Liu, X.; Jiang, B.; Hao, H.; Liu, Z. CARD9 Signaling, Inflammation, and Diseases. *Front. Immunol.* 2022, *13*, 880879, doi:10.3389/fimmu.2022.880879.
250. Wang, X.; Wang, W.; Lin, Z.; Wang, X.; Li, T.; Yu, J.; Liu, W.; Tong, Z.; Xu, Y.; Zhang, J.; et al. CARD9 mutations linked to subcutaneous phaeohyphomycosis and TH17 cell deficiencies. *J. Allergy Clin. Immunol.* 2014, *133*, 905-8.e3, doi:10.1016/j.jaci.2013.09.033.
251. Atif, S.M.; Lee, S.-J.; Li, L.-X.; Uematsu, S.; Akira, S.; Gorjestani, S.; Lin, X.; Schweighoffer, E.; Tybulewicz, V.L.J.; McSorley, S.J. Rapid CD4+ T-cell responses to bacterial flagellin require dendritic cell expression of Syk and CARD9. *Eur. J. Immunol.* 2015, *45*, 513–524, doi:10.1002/eji.201444744.
252. Mayer, S.; Raulf, M.-K.; Lepenies, B. C-type lectins: their network and roles in pathogen recognition and immunity. *Histochem. Cell Biol.* 2017, *147*, 223–237, doi:10.1007/s00418-016-1523-7.
253. Miyake, Y.; Toyonaga, K.; Mori, D.; Kakuta, S.; Hoshino, Y.; Oyamada, A.; Yamada, H.; Ono, K.-I.; Suyama, M.; Iwakura, Y.; et al. C-type lectin MCL is an FcRγ-coupled

receptor that mediates the adjuvanticity of mycobacterial cord factor. *Immunity* 2013, *38*, 1050–1062, doi:10.1016/j.immuni.2013.03.010.

254. El-Brolosy, M.A.; Stainier, D.Y.R. Genetic compensation: A phenomenon in search of mechanisms. *PLoS Genet.* 2017, *13*, e1006780, doi:10.1371/journal.pgen.1006780.
255. Kalantari, P.; Morales, Y.; Miller, E.A.; Jaramillo, L.D.; Ponichtera, H.E.; Wuethrich, M.A.; Cheong, C.; Seminario, M.C.; Russo, J.M.; Bunnell, S.C.; et al. CD209a Synergizes with Dectin-2 and Mincle to Drive Severe Th17 Cell-Mediated Schistosome Egg-Induced Immunopathology. *Cell Rep.* 2018, *22*, 1288–1300, doi:10.1016/j.celrep.2018.01.001.
256. Kerscher, B.; Wilson, G.J.; Reid, D.M.; Mori, D.; Taylor, J.A.; Besra, G.S.; Yamasaki, S.; Willment, J.A.; Brown, G.D. Mycobacterial receptor, Clec4d (CLECSF8, MCL), is coregulated with Mincle and upregulated on mouse myeloid cells following microbial challenge. *Eur. J. Immunol.* 2016, *46*, 381–389, doi:10.1002/eji.201545858.
257. Kerscher, B.; Dambuza, I.M.; Christofi, M.; Reid, D.M.; Yamasaki, S.; Willment, J.A.; Brown, G.D. Signalling through MyD88 drives surface expression of the mycobacterial receptors MCL (Clecsf8, Clec4d) and Mincle (Clec4e) following microbial stimulation. *Microbes and Infection* 2016, *18*, 505–509, doi:10.1016/j.micinf.2016.03.007.
258. Miyake, Y.; Masatsugu, O.; Yamasaki, S. C-Type Lectin Receptor MCL Facilitates Mincle Expression and Signaling through Complex Formation. *J. Immunol.* 2015, *194*, 5366–5374, doi:10.4049/jimmunol.1402429.
259. Zhao, X.-Q.; Zhu, L.-L.; Chang, Q.; Jiang, C.; You, Y.; Luo, T.; Jia, X.-M.; Lin, X. C-type lectin receptor dectin-3 mediates trehalose 6,6'-dimycolate (TDM)-induced Mincle expression through CARD9/Bcl10/MALT1-dependent nuclear factor (NF)-κB activation. *J. Biol. Chem.* 2014, *289*, 30052–30062, doi:10.1074/jbc.M114.588574.
260. Antenucci, L.; Hytönen, V.P.; Ylänne, J. Phosphorylated immunoreceptor tyrosine-based activation motifs and integrin cytoplasmic domains activate spleen tyrosine kinase via distinct mechanisms. *J. Biol. Chem.* 2018, *293*, 4591–4602, doi:10.1074/jbc.RA117.000660.
261. Waksman, G.; Kumaran, S.; Lubman, O. SH2 domains: role, structure and implications for molecular medicine. *Expert Rev. Mol. Med.* 2004, *6*, 1–18, doi:10.1017/S1462399404007331.
262. Pennino, D.; Eyerich, K.; Scarponi, C.; Carbone, T.; Eyerich, S.; Nasorri, F.; Garcovich, S.; Traidl-Hoffmann, C.; Albanesi, C.; Cavani, A. IL-17 amplifies human contact hypersensitivity by licensing hapten nonspecific Th1 cells to kill autologous keratinocytes. *J. Immunol.* 2010, *184*, 4880–4888, doi:10.4049/jimmunol.0901767.
263. Mazzoni, A.; Young, H.A.; Spitzer, J.H.; Visintin, A.; Segal, D.M. Histamine regulates cytokine production in maturing dendritic cells, resulting in altered T cell polarization. *J. Clin. Invest.* 2001, *108*, 1865–1873, doi:10.1172/JCI13930.
264. Caron, G.; Delneste, Y.; Roelandts, E.; Duez, C.; Bonnefoy, J.Y.; Pestel, J.; Jeannin, P. Histamine polarizes human dendritic cells into Th2 cell-promoting effector dendritic cells. *J. Immunol.* 2001, *167*, 3682–3686, doi:10.4049/jimmunol.167.7.3682.

265. Moon, T.C.; Befus, A.D.; Kulka, M. Mast cell mediators: their differential release and the secretory pathways involved. *Front. Immunol.* 2014, *5*, 569, doi:10.3389/fimmu.2014.00569.
266. DeVore, S.B.; Khurana Hershey, G.K. The role of the CBM complex in allergic inflammation and disease. *J. Allergy Clin. Immunol.* 2022, doi:10.1016/j.jaci.2022.06.023.
267. Kawai, T.; Akira, S. The roles of TLRs, RLRs and NLRs in pathogen recognition. *Int. Immunol.* 2009, *21*, 317–337, doi:10.1093/intimm/dxp017.
268. Li, X.-M.; Chen, X.; Gu, W.; Guo, Y.-J.; Cheng, Y.; Peng, J.; Guo, X.-J. Impaired TNF/TNFR2 signaling enhances Th2 and Th17 polarization and aggravates allergic airway inflammation. *Am. J. Physiol. Lung Cell. Mol. Physiol.* 2017, *313*, L592-L601, doi:10.1152/ajplung.00409.2016.
269. Deslée, G.; Charbonnier, A.-S.; Hammad, H.; Angyalosi, G.; Tillie-Leblond, I.; Mantovani, A.; Tonnel, A.-B.; Pestel, J. Involvement of the mannose receptor in the uptake of Der p 1, a major mite allergen, by human dendritic cells. *J. Allergy Clin. Immunol.* 2002, *110*, 763–770, doi:10.1067/mai.2002.129121.
270. Royer, P.-J.; Emara, M.; Yang, C.; Al-Ghouleh, A.; Tighe, P.; Jones, N.; Sewell, H.F.; Shakib, F.; Martinez-Pomares, L.; Ghaemmaghami, A.M. The mannose receptor mediates the uptake of diverse native allergens by dendritic cells and determines allergen-induced T cell polarization through modulation of IDO activity. *J. Immunol.* 2010, *185*, 1522–1531, doi:10.4049/jimmunol.1000774.
271. Clarke, D.L.; Davis, N.H.E.; Campion, C.L.; Foster, M.L.; Heasman, S.C.; Lewis, A.R.; Anderson, I.K.; Corkill, D.J.; Sleeman, M.A.; May, R.D.; et al. Dectin-2 sensing of house dust mite is critical for the initiation of airway inflammation. *Mucosal Immunol* 2014, *7*, 558–567, doi:10.1038/mi.2013.74.
272. Parsons, M.W.; Li, L.; Wallace, A.M.; Lee, M.J.; Katz, H.R.; Fernandez, J.M.; Saijo, S.; Iwakura, Y.; Austen, K.F.; Kanaoka, Y.; et al. Dectin-2 regulates the effector phase of house dust mite-elicited pulmonary inflammation independently from its role in sensitization. *J. Immunol.* 2014, *192*, 1361–1371, doi:10.4049/jimmunol.1301809.
273. Huang, H.-J.; Lin, Y.-L.; Liu, C.-F.; Kao, H.-F.; Wang, J.-Y. Mite allergen decreases DC-SIGN expression and modulates human dendritic cell differentiation and function in allergic asthma. *Mucosal Immunol* 2011, *4*, 519–527, doi:10.1038/mi.2011.17.
274. Hirose, K.; Ito, T.; Nakajima, H. Roles of Dectin-1 in Allergic Airway Inflammation. *Crit Rev Immunol* 2017, *37*, 15–21, doi:10.1615/CritRevImmunol.2017024718.
275. Motomura, Y.; Morita, H.; Moro, K.; Nakae, S.; Artis, D.; Endo, T.A.; Kuroki, Y.; Ohara, O.; Koyasu, S.; Kubo, M. Basophil-derived interleukin-4 controls the function of natural helper cells, a member of ILC2s, in lung inflammation. *Immunity* 2014, *40*, 758–771, doi:10.1016/j.immuni.2014.04.013.
276. Halim, T.Y.F.; Steer, C.A.; Mathä, L.; Gold, M.J.; Martinez-Gonzalez, I.; McNagny, K.M.; McKenzie, A.N.J.; Takei, F. Group 2 innate lymphoid cells are critical for the initiation of adaptive T helper 2 cell-mediated allergic lung inflammation. *Immunity* 2014, *40*, 425–435, doi:10.1016/j.immuni.2014.01.011.

277. Cernescu, L.D.; Haidar, L.; Panaitescu, C. Dendritic cell-CD4+ T cell interaction: The differential role of IL-4/IL-13 in serum IgE levels in house dust mite allergic patients. *Exp. Ther. Med.* 2021, *21*, 95, doi:10.3892/etm.2020.9527.
278. Cruse, G.; Bradding, P. Mast cells in airway diseases and interstitial lung disease. *Eur. J. Pharmacol.* 2016, *778*, 125–138, doi:10.1016/j.ejphar.2015.04.046.
279. Carroll, N.G.; Mutavdzic, S.; James, A.L. Distribution and degranulation of airway mast cells in normal and asthmatic subjects. *Eur. Respir. J.* 2002, *19*, 879–885, doi:10.1183/09031936.02.00275802.
280. Hammad, H.; Lambrecht, B.N. Barrier Epithelial Cells and the Control of Type 2 Immunity. *Immunity* 2015, *43*, 29–40, doi:10.1016/j.immuni.2015.07.007.
281. Allahverdian, S.; Harada, N.; Singhera, G.K.; Knight, D.A.; Dorscheid, D.R. Secretion of IL-13 by airway epithelial cells enhances epithelial repair via HB-EGF. *Am. J. Respir. Cell Mol. Biol.* 2008, *38*, 153–160, doi:10.1165/rcmb.2007-0173OC.
282. Semlali, A.; Jacques, E.; Koussih, L.; Gounni, A.S.; Chakir, J. Thymic stromal lymphopoietin-induced human asthmatic airway epithelial cell proliferation through an IL-13-dependent pathway. *J. Allergy Clin. Immunol.* 2010, *125*, 844–850, doi:10.1016/j.jaci.2010.01.044.
283. Naito, Y.; Ui-Tei, K. siRNA Design Software for a Target Gene-Specific RNA Interference. *Front. Genet.* 2012, *3*, 102, doi:10.3389/fgene.2012.00102.

7 Appendix

To 3.2.1 Genotyping of mice by tissue biopsies

Table 7.1: Temperature profiles for the genotyping PCR using DreamTaq Green DNA Polymerase. Program “Touch-hi” (Card9, MCL): X = 65°C/63°C/61°C/59°C; Program “Touch” (general Cre, GFP, MyD88-FL, Mcpt5-Cre, R-DTA wt, R-DTA mut, SIGNR3, Syk-FL): X = 60°C/58°C/56°C/54°C.

	Temperature	Time	Cycles
Initial denaturation	95°C	4 min	
Denaturation	95°C	30 sec	2x
Annealing	x	30 sec	
Extension	72°C	45 sec	
Denaturation	95°C	30 sec	2x
Annealing	x	30 sec	
Extension	72°C	45 sec	
Denaturation	95°C	30 sec	2x
Annealing	x	30 sec	
Extension	72°C	45 sec	
Denaturation	95°C	30 sec	34x
Annealing	x	30 sec	
Extension	72°C	45 sec	
Final Extension	72°C	10 min	
Cooling	15°C	∞	

Table 7.2: Temperature profiles for the CreERT2_3 genotyping PCR using DreamTaq Green DNA Polymerase.

	Temperature	Time	Cycles
Initial denaturation	95°C	3 min	
Denaturation	95°C	30 sec	8x, -0.5°C/cycle
Annealing	60°C	30 sec	
Extension	72°C	45 sec	
Denaturation	95°C	30 sec	25x
Annealing	56°C	30 sec	
Extension	72°C	45 sec	
Cooling	15°C	∞	

Table 7.3: Temperature profiles for the CD11c-Cre genotyping PCR using DreamTaq Green DNA Polymerase.

	Temperature	Time	Cycles
Initial denaturation	95°C	2 min	
Denaturation	95°C	30 sec	
Annealing	63°C	45 sec	30x
Extension	72°C	45 sec	
Final Extension	72°C	5 min	
Cooling	15°C	∞	

To 4.5.1 In vitro analysis of different signaling pathways involved in MCG uptake by imDCs

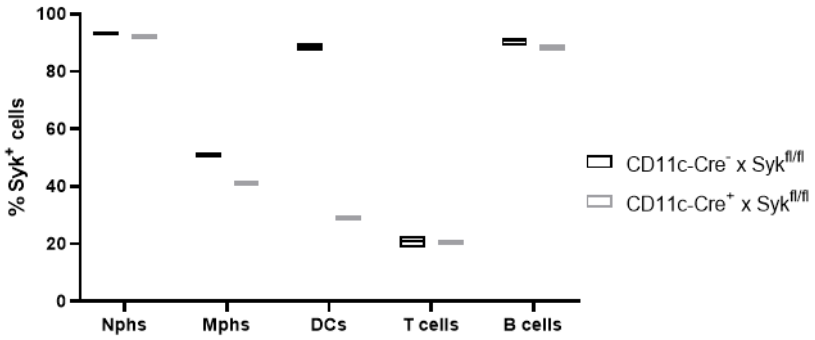

Figure 7.1: Conditional Syk *knockout* in CD11c-Cre x Syk-FL mice. Splenocytes were isolated from untreated CD11c-Cre^{-} x Syk$^{fl/fl}$ (N = 3) and CD11c-Cre^{+} x Syk$^{fl/fl}$ and analyzed by intracellular flow cytometry. Syk *knockout* was analyzed as fraction of Syk^{+} cells of the whole indicated immune cell subset.

To 4.7 Analysis of the impact of an impaired Card9-dependent signaling on T cell priming by dermal DCs

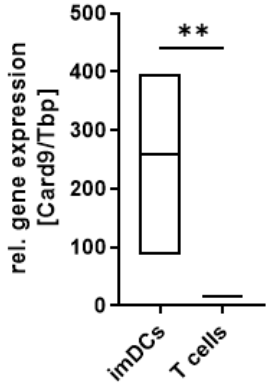

Figure 7.2: Card9 gene expression by imDCs and T cells. imDCs were generated *in vitro* by using BM cells of wt mice. T cells were isolated from wt splenocytes using “Pan T Cell Isolation Kit II”. The relative Card9 gene expression by imDCs and T cells was calculated using the $2^{-\Delta\Delta ct}$ method, normalized to the house keeping gene Tbp and set to 100% for the first sample of imDCs. *** $p < 0.001$, ** $p < 0.01$, * $p < 0.05$, # $p \leq 0.10$, ns $p > 0.10$.

To 4.8 MCG uptake by imDCs is mediated by CLRs MCL and SIGNR3

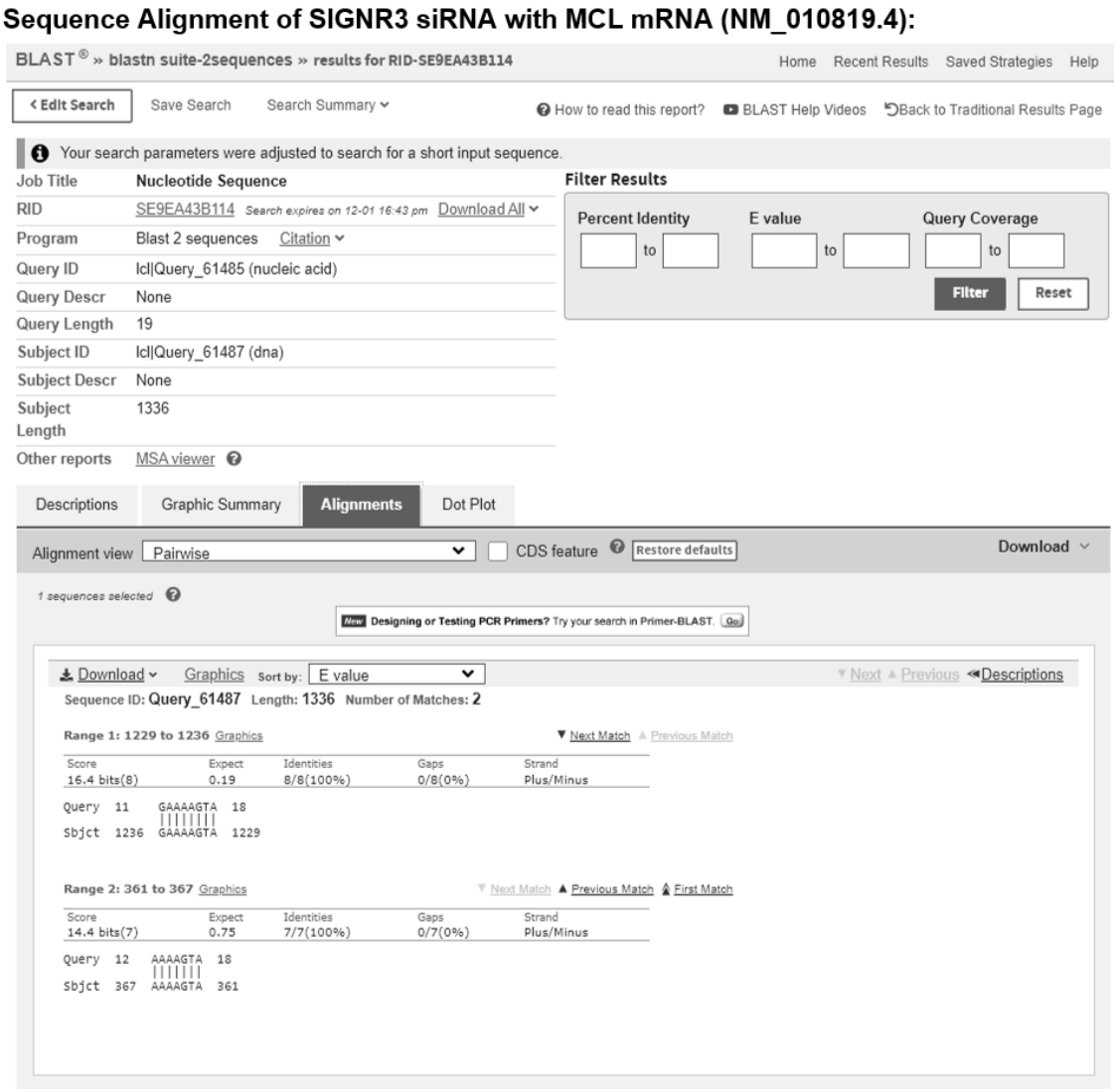

Figure 7.3: Sequence alignment of SIGNR3-specific siRNA with mRNA of MCL. Sequence alignment was performed using the Nucleotide Basic Local Alignment Search Tool (Nucleotide BLAST®, https://blast.ncbi.nlm.nih.gov/Blast.cgi, screenshot of search results optimized for highly similar sequences (megablast)) of the National Library of Medicine (NIH). The guide sequence (5'-TACAGATCCAGAAAAGTAG-3') of the siRNA was set as query and aligned to the respective mRNA. Relevant sequence homologies included full or seed-sequence (nucleotide 2 – 8 of the siRNA) similarities to the respective mRNA in a sense/antisense manner (Query/Subject, Plus/Minus) [283]. Last checked on the 30th of November 2022.

Sequence Alignment of MCL siRNA with SIGNR3 mRNA (NM_130904.2):

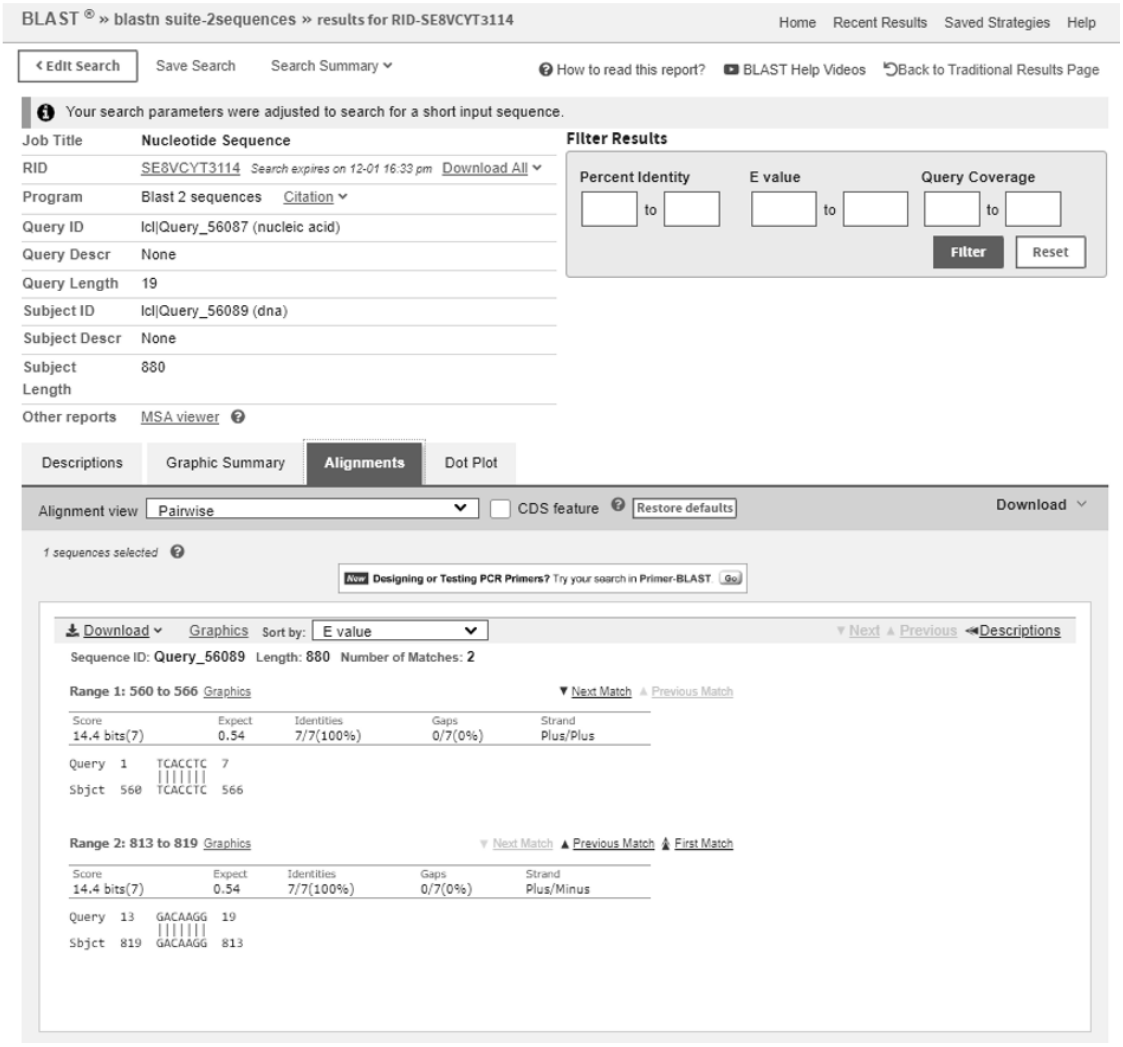

Figure 7.4: Sequence alignment of MCL-specific siRNA with mRNA of SIGNR3. Sequence alignments were performed using the Nucleotide Basic Local Alignment Search Tool (Nucleotide BLAST®, https://blast.ncbi.nlm.nih.gov/Blast.cgi, screenshot of search results optimized for highly similar sequences (megablast)) of the National Library of Medicine (NIH). The guide sequence (5'-TCACCTCAAAGTGACAAGG-3') of the siRNA was set as query and aligned to the respective mRNA. Relevant sequence homologies included full or seed-sequence (nucleotide 2 – 8 of the siRNA) similarities to the respective mRNA in a sense/antisense manner (Query/Subject, Plus/Minus) [283]. Last checked on the 30th of November 2022.

To 4.9 Analysis of the impact of MCG uptake by imDCs on the acute allergic airway inflammation

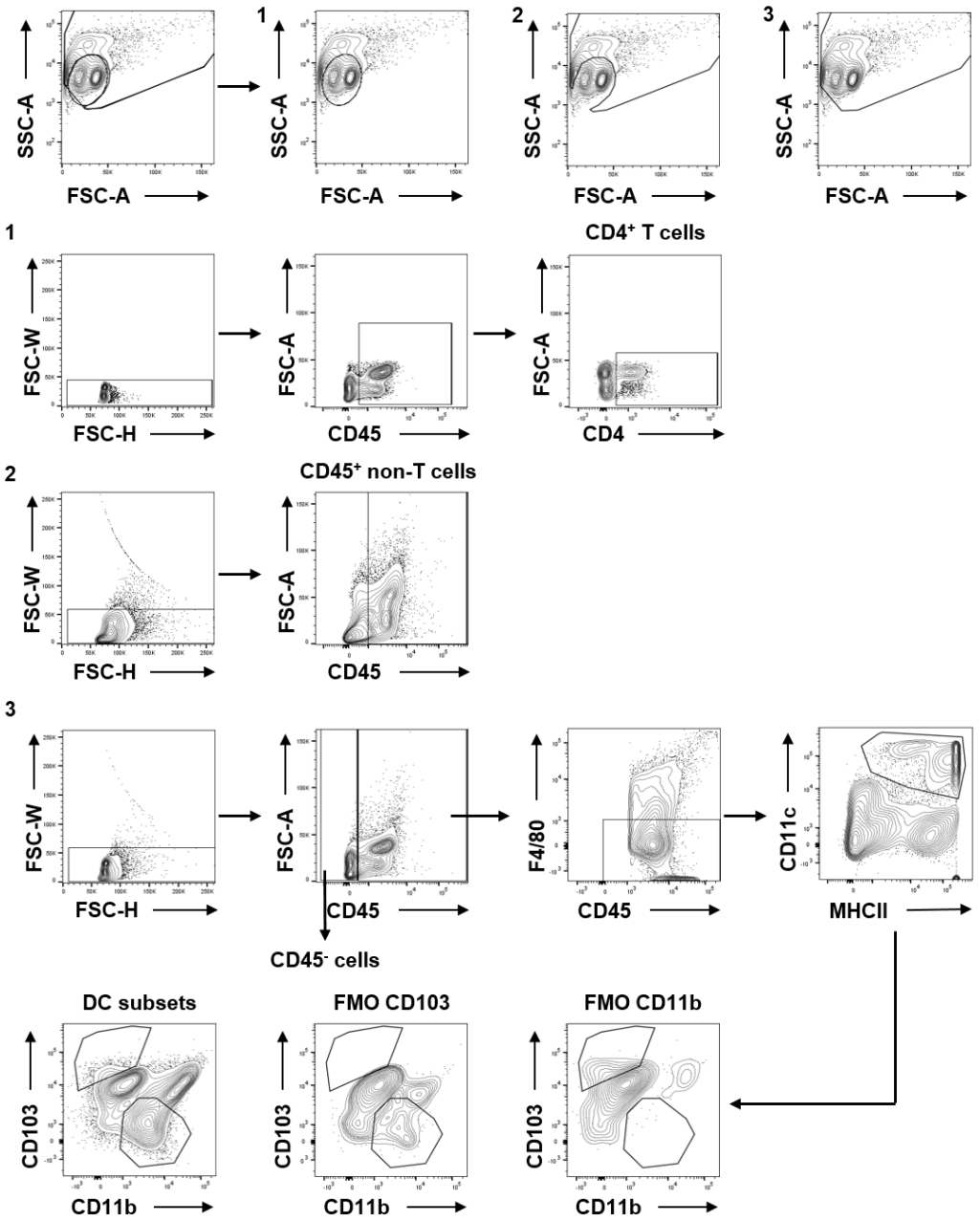

Figure 7.5: Gating strategy upon allergic airway inflammation on the example of lung tissue. Allergic airway inflammation was introduced by HDM extract and lung tissue was analyzed by flow cytometry. First, cell debris was excluded and cells were gated on the lymphocyte population (1), non-lymphocyte population (2) or all cells (3). All populations were subjected to a doublet exclusion and subsequently gated for $CD45^+$ cells (1,2) or $CD45^-$ and $CD45^+$ cells (3). (1) $CD4^+$ T cells were further gated as $CD4^+$ cells out of the lymphocyte$^+$ $CD45^+$ population and subsequently subjected to cytokine analysis (see Figure 7.6). (2) $CD45^+$ non-T cells were futher subjected to cytokine analysis (see Figure 7.6). (3) $CD45^-$ cells were futher subjected to cytokine analysis (see Figure 7.6). DCs were further gated out of the $CD45^+$ population as F4/80$^-$ CD11c$^+$ MHCII$^+$ cells. The gates to define $CD103^+$ cDC1s and $CD11b^+$ cDC2s were set based on FMO controls. Cell populations within LNs were gated equally. See additionally Table 3.6.

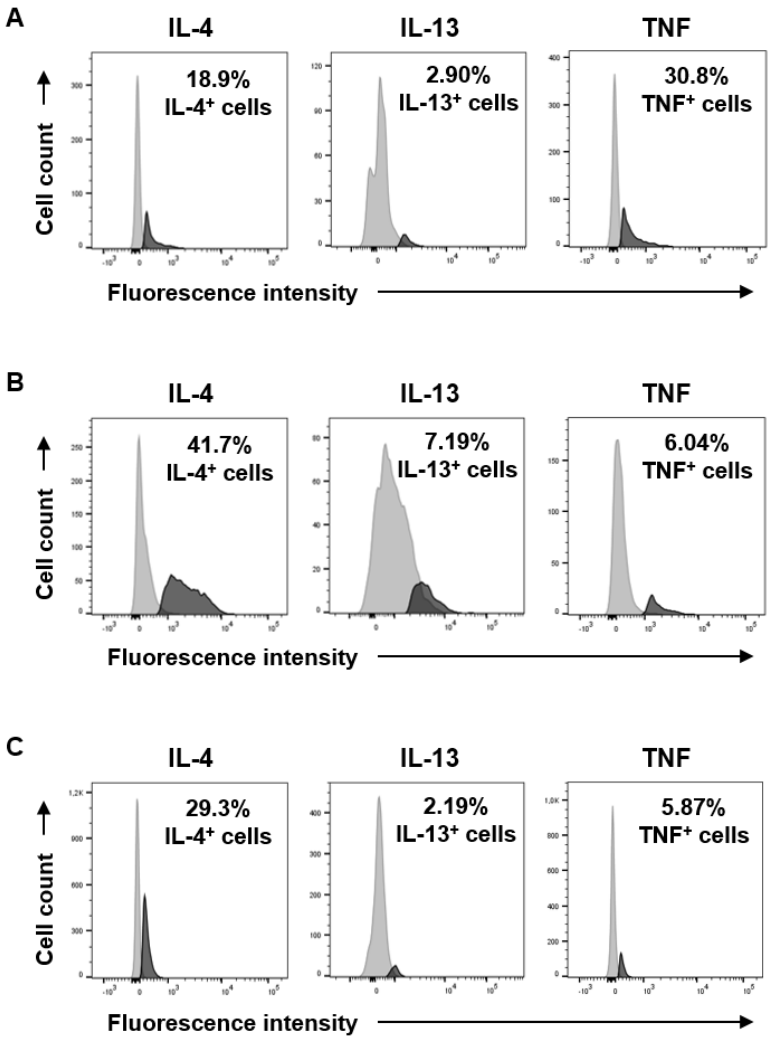

Figure 7.6: Cytokine analyses upon allergic airway inflammation by means of intracellular flow cytometry on the example of lung tissue. Allergic airway inflammation was introduced by HDM extract and lung tissue was analyzed by flow cytometry. $CD4^+$ T cells (A), $CD45^+$ non-T cells (B) and $CD45^-$ cells (C) were gated as described in Figure 7.5. Histograms show cell counts and fluorescence intensities of the indicated cytokine$^+$ cells. Cytokines$^+$ cells (dark grey) were identified based on FMO controls (light grey). Cytokine analyses within LNs were performed equally.

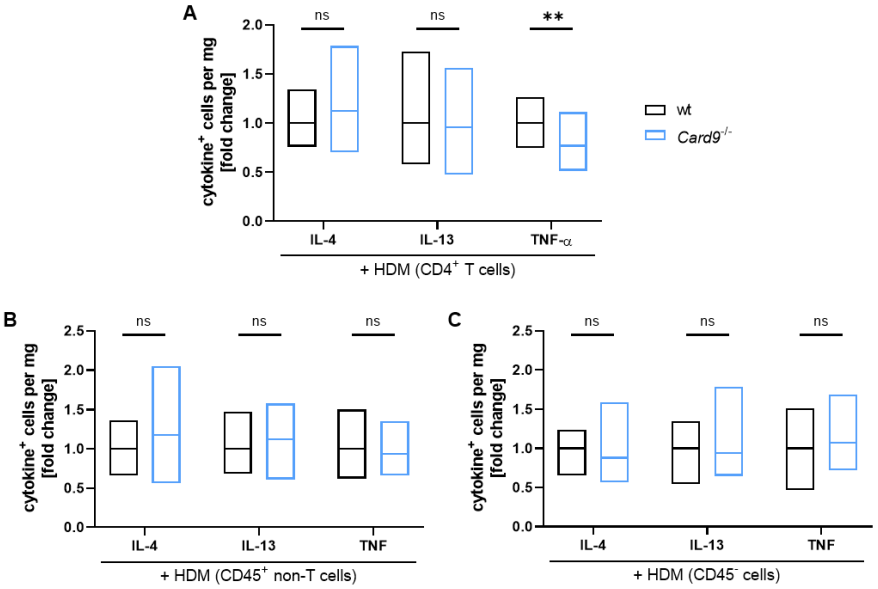

Figure 7.7: Analysis of numbers of cytokine-producing cells within lung tissues of wt and *Card9*$^{-/-}$ mice upon allergic airway inflammation. Allergic airway inflammation was introduced by HDM extract in wt and *Card9*$^{-/-}$ mice and lung tissue was analyzed by flow cytometry. Total cell counts were determined and normalized to the tissue weight for numbers of IL-4-, IL-13- and TNF-producing (A) CD4$^+$ T cells, (B) CD45$^+$ non-T cells and (C) CD45$^-$ cells (N = 9-12). Fold change was calculated setting the mean of cytokine$^+$ wt cells of each data set to 1. *** $p < 0.001$, ** $p < 0.01$, * $p < 0.05$, # $p \leq 0.10$, ns $p > 0.10$.

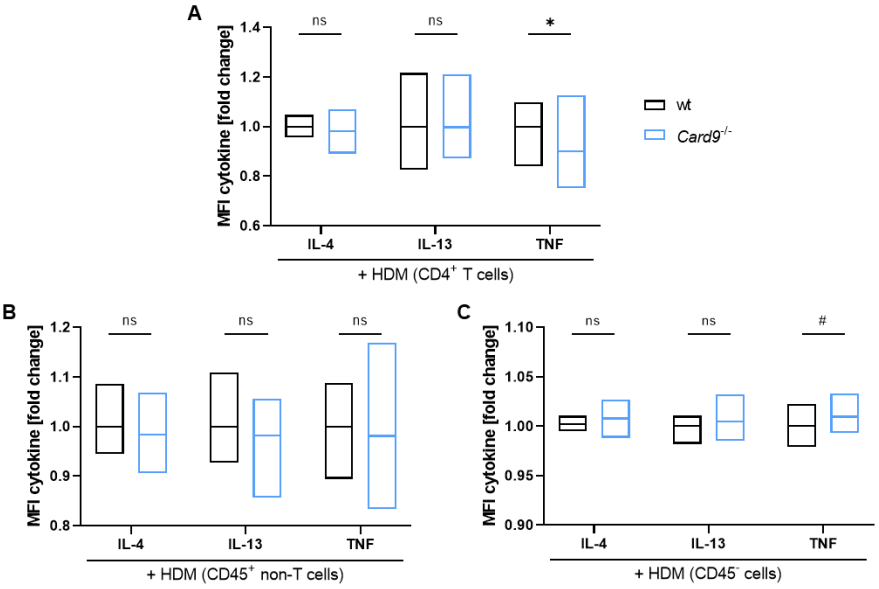

Figure 7.8: Analysis of the cytokine production per cell of wt and *Card9*$^{-/-}$ mice within lung tissues upon allergic airway inflammation. Allergic airway inflammation was introduced by HDM extract in wt and *Card9*$^{-/-}$ mice and lung tissue was analyzed by flow cytometry. Cytokine production per cell was analyzed as MFI of IL-4, IL-13 and TNF per (A) CD4$^+$ T cell, (B) CD45$^+$ non-T cell and (C) CD45$^-$ cell (N = 10-12). Fold change was calculated setting the mean of cytokine production by wt cells of each data set to 1. *** $p < 0.001$, ** $p < 0.01$, * $p < 0.05$, # $p \leq 0.10$, ns $p > 0.10$.

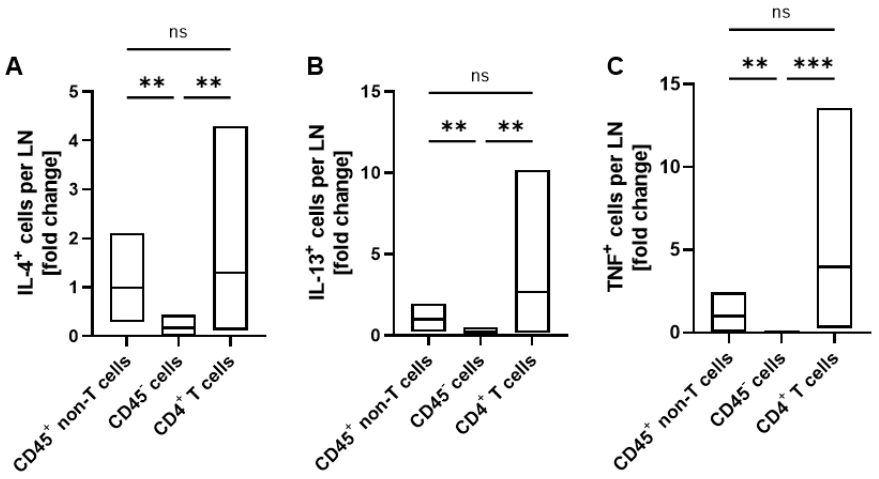

Figure 7.9: Number of cytokine-producing cells within the mediastinal LNs of wt mice upon allergic airway inflammation (introduced in wt/*Card9*$^{-/-}$ mice). Allergic airway inflammation was introduced by HDM extract in wt and *Card9*$^{-/-}$ mice and mediastinal LNs were analyzed by flow cytometry. Total cell counts per LN were determined for (A) IL-4-, (B) IL-13- and (C) TNF-producing wt CD45$^+$ non-T cells, CD45$^-$ cells and CD4$^+$ T cells (N = 9/10). Fold change was calculated setting the mean of cytokine$^+$ CD45$^+$ non-T cells to 1. *** $p < 0.001$, ** $p < 0.01$, * $p < 0.05$, # $p \leq 0.10$, ns $p > 0.10$.

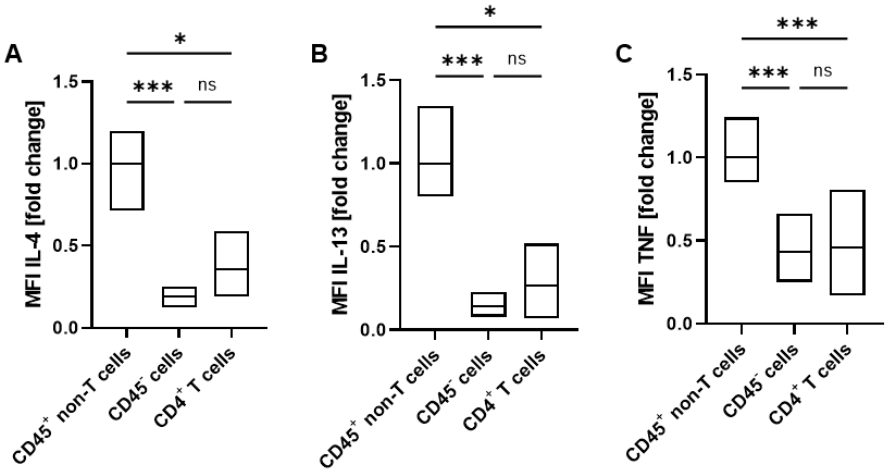

Figure 7.10: Fluorescence intensity of cytokine-producing cells within mediastinal LNs of wt mice upon allergic airway inflammation (introduced in wt/*Card9*$^{-/-}$ mice). Allergic airway inflammation was introduced by HDM extract in wt and *Card9*$^{-/-}$ mice and mediastinal LNs were analyzed by flow cytometry. Cytokine production per cell was analyzed as MFI of (A) IL-4, (B) IL-13 and (C) TNF per wt CD45$^+$ non-T cell, CD45$^-$ cell and CD4$^+$ T cell (N = 10). Fold change was calculated setting the mean of cytokine production by CD45$^+$ non-T cells to 1. *** $p < 0.001$, ** $p < 0.01$, * $p < 0.05$, # $p \leq 0.10$, ns $p > 0.10$.

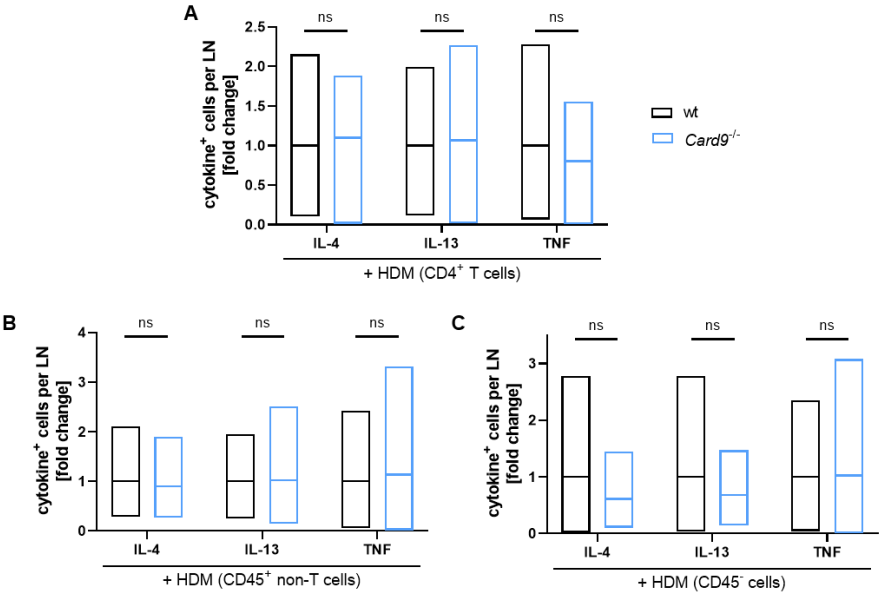

Figure 7.11: Analysis of numbers of cytokine-producing cells within mediastinal LNs of wt and *Card9*$^{-/-}$ mice upon allergic airway inflammation. Allergic airway inflammation was introduced by HDM extract in wt and *Card9*$^{-/-}$ mice and mediastinal LNs were analyzed by flow cytometry. Total cell counts per LN were determined for numbers of IL-4-, IL-13- and TNF-producing (A) CD4$^+$ T cells, (B) CD45$^+$ non-T cells and (C) CD45$^-$ cells (N = 10/11). Fold change was calculated setting the mean of cytokine$^+$ wt cells of each data set to 1. *** $p < 0.001$, ** $p < 0.01$, * $p < 0.05$, # $p \leq 0.10$, ns $p > 0.10$.

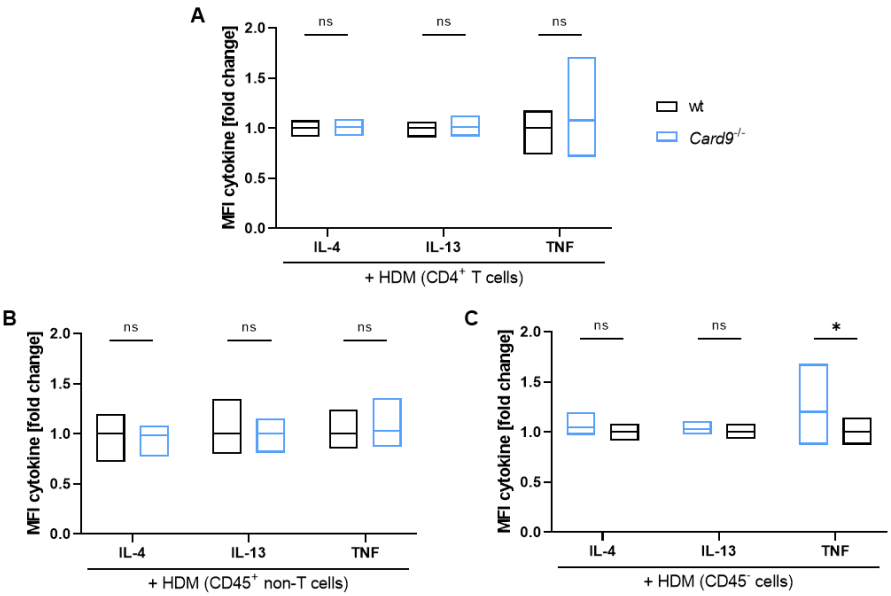

Figure 7.12: Analysis of the cytokine production per cell within mediastinal LNs of wt and *Card9*$^{-/-}$ mice upon allergic airway inflammation. Allergic airway inflammation was introduced by HDM extract in wt and *Card9*$^{-/-}$ mice and mediastinal LNs were analyzed by flow cytometry. Cytokine production per cell was analyzed as MFI of IL-4, IL-13 and TNF per (A) CD4$^+$ T cell, (B) CD45$^+$ non-T cell and (C) CD45$^-$ cell (N = 10/11). Fold change was calculated setting the mean of cytokine production by wt cells of each data set to 1. *** $p < 0.001$, ** $p < 0.01$, * $p < 0.05$, # $p \leq 0.10$, ns $p > 0.10$.

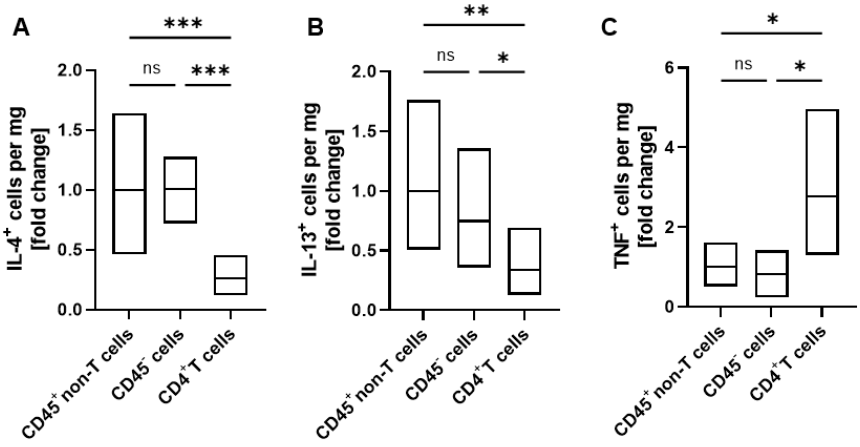

Figure 7.13: Number of cytokine-producing cells within the lung tissue of wt mice upon allergic airway inflammation (introduced in wt/*MCL*$^{-/-}$ *SIGNR3*$^{-/-}$ mice). Allergic airway inflammation was introduced by HDM extract in wt and *MCL*$^{-/-}$ *SIGNR3*$^{-/-}$ mice and lung tissue was analyzed by fow cytometry. Total cell counts were determined and normalized to the tissue weight for (A) IL-4-, (B) IL-13- and (C) TNF-producing wt CD45$^+$ non-T cells, CD45$^-$ cells and CD4$^+$ T cells (N = 7/8). Fold change was calculated setting the mean of cytokine$^+$ CD45$^+$ non-T cells to 1. *** p < 0.001, ** p < 0.01, * p < 0.05, # p ≤ 0.10, ns p > 0.10.

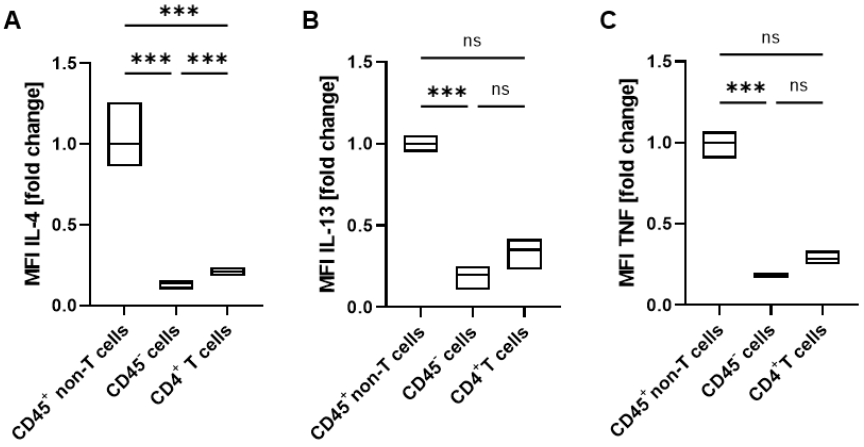

Figure 7.14: Fluorescence intensity of cytokine-producing cells within the lung tissue of wt mice during allergic airway inflammation (introduced in wt/*MCL*$^{-/-}$ *SIGNR3*$^{-/-}$ mice). Allergic airway inflammation was introduced by HDM extract in wt and *MCL*$^{-/-}$ *SIGNR3*$^{-/-}$ mice and lung tissue was analyzed by fow cytometry. Cytokine production per cell was analyzed as MFI of (A) IL-4, (B) IL-13 and (C) TNF per wt CD45$^+$ non-T cell, CD45$^-$ cell and CD4$^+$ T cell (N = 8). Fold change was calculated setting the mean of cytokine production by CD45$^+$ non-T cells to 1. *** p < 0.001, ** p < 0.01, * p < 0.05, # p ≤ 0.10, ns p > 0.10.

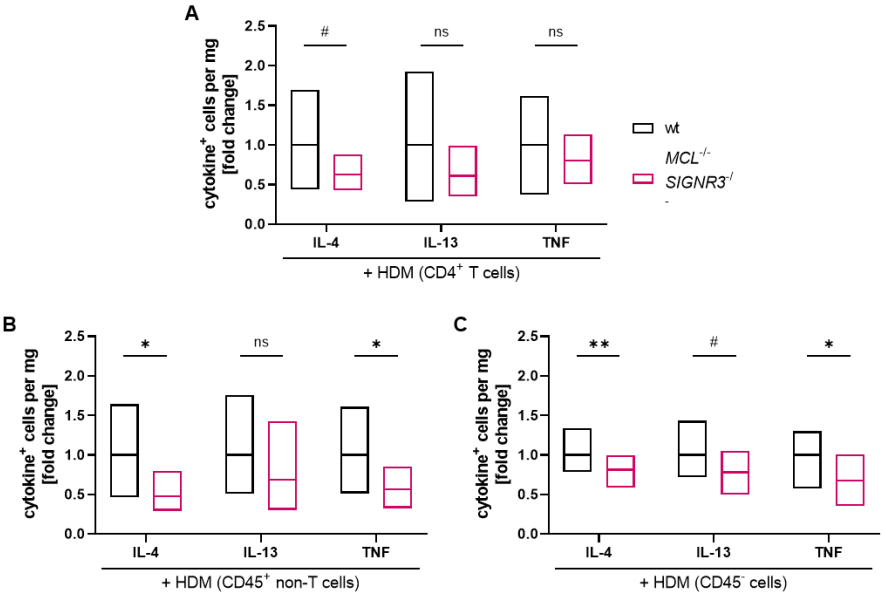

Figure 7.15: Analysis of numbers of cytokine-producing cells within lung tissues of wt and *MCL*$^{-/-}$ *SIGNR3*$^{-/-}$ mice upon allergic airway inflammation. Allergic airway inflammation was introduced by HDM extract in wt and *MCL*$^{-/-}$ *SIGNR3*$^{-/-}$ mice and lung tissue was analyzed by flow cytometry. Total cell counts were determined and normalized to the tissue weight for numbers of IL-4-, IL-13- and TNF-producing (A) CD4^{+} T cells, (B) CD45^{+} non-T cells and (C) CD45^{-} cells (N = 7/8). Fold change was calculated setting the mean of cytokine^{+} wt cells of each data set to 1. *** $p < 0.001$, ** $p < 0.01$, * $p < 0.05$, # $p \leq 0.10$, ns $p > 0.10$.

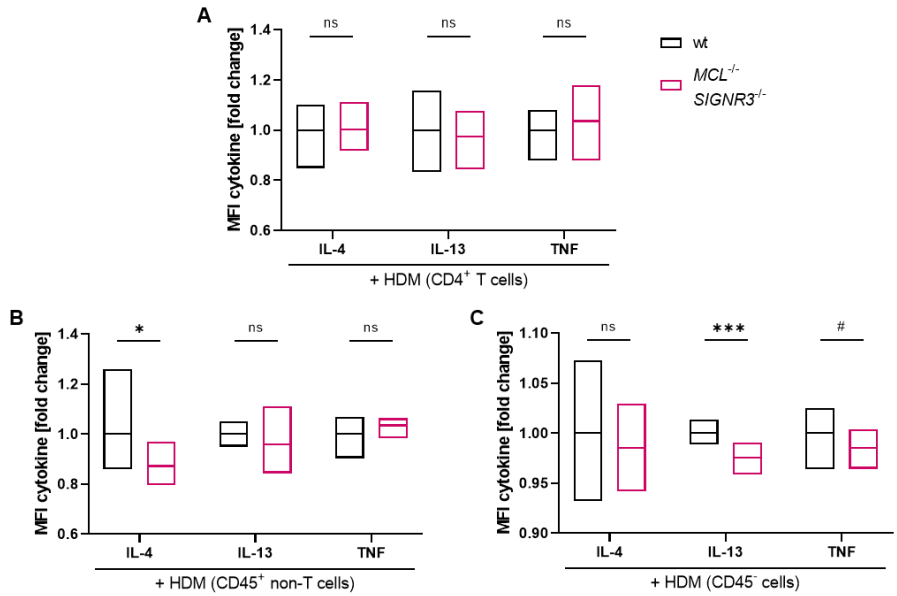

Figure 7.16: Analysis of the cytokine production per cell of wt and *MCL*$^{-/-}$ *SIGNR3*$^{-/-}$ mice within lung tissues upon allergic airway inflammation. Allergic airway inflammation was introduced by HDM extract in wt and *MCL*$^{-/-}$ *SIGNR3*$^{-/-}$ *mice* and lung tissue was analyzed by flow cytometry. Cytokine production per cell was analyzed as MFI of IL-4, IL-13 and TNF per (A) CD4^{+} T cell, (B) CD45^{+} non-T cell and (C) CD45^{-} cell (N = 7/8). Fold change was calculated setting the mean of cytokine production by wt cells of each data set to 1. *** $p < 0.001$, ** $p < 0.01$, * $p < 0.05$, # $p \leq 0.10$, ns $p > 0.10$.

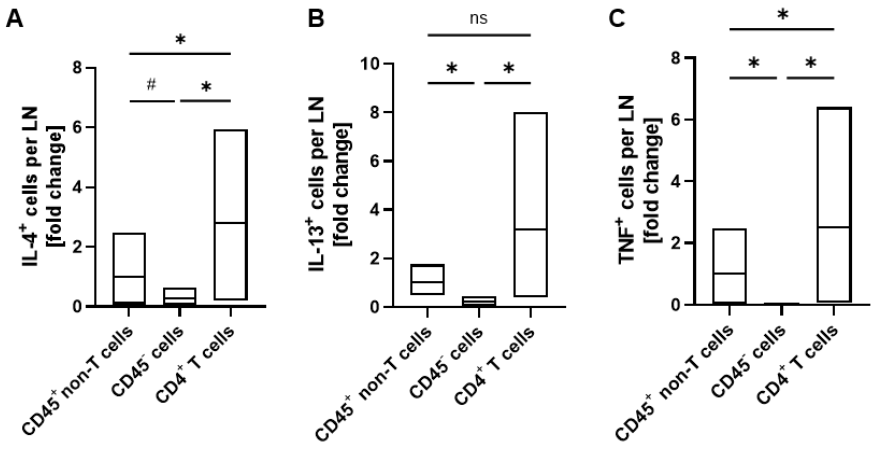

Figure 7.17: Number of cytokine-producing cells within mediastinal LNs of wt mice during allergic airway inflammation (introduced in wt/*MCL*$^{-/-}$ *SIGNR3*$^{-/-}$mice). Allergic airway inflammation was introduced by HDM extract in wt and *MCL*$^{-/-}$ *SIGNR3*$^{-/-}$mice and mediastinal LNs were analyzed by flow cytometry. Total cell counts per LN were determined for (A) IL-4-, (B) IL-13- and (C) TNF-producing wt CD45$^+$ non-T cells, CD45$^-$ cells and CD4$^+$ T cells (N = 8). Fold change was calculated setting the mean of cytokine$^+$ CD45$^+$ non-T cells to 1. *** $p < 0.001$, ** $p < 0.01$, * $p < 0.05$, # $p \leq 0.10$, ns $p > 0.10$.

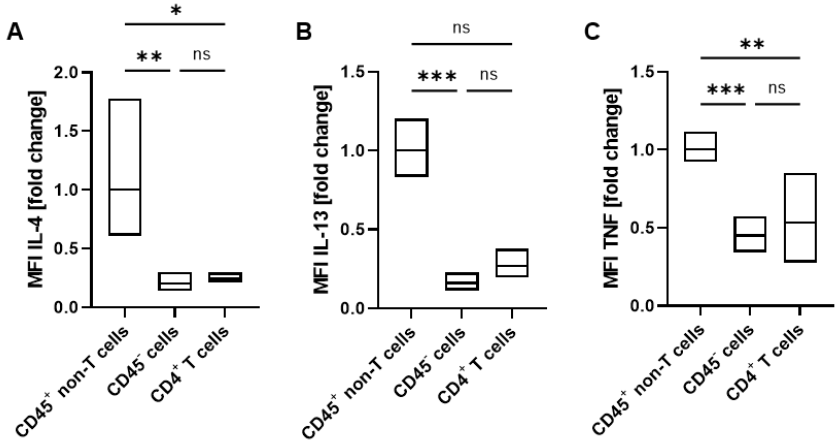

Figure 7.18: Fluorescence intensity of cytokine-producing cells within mediastinal LNs of wt mice during allergic airway inflammation (introduced in wt/*MCL*$^{-/-}$ *SIGNR3*$^{-/-}$mice). Allergic airway inflammation was introduced by HDM extract in wt and *MCL*$^{-/-}$ *SIGNR3*$^{-/-}$mice and mediastinal LNs were analyzed by flow cytometry. Cytokine production per cell was analyzed as MFI of (A) IL-4, (B) IL-13 and (C) TNF per wt CD45$^+$ non-T cell, CD45$^-$ cell and CD4$^+$ T cell (N = 8). Fold change was calculated setting the mean of cytokine production by CD45$^+$ non-T cells to 1. *** $p < 0.001$, ** $p < 0.01$, * $p < 0.05$, # $p \leq 0.10$, ns $p > 0.10$.

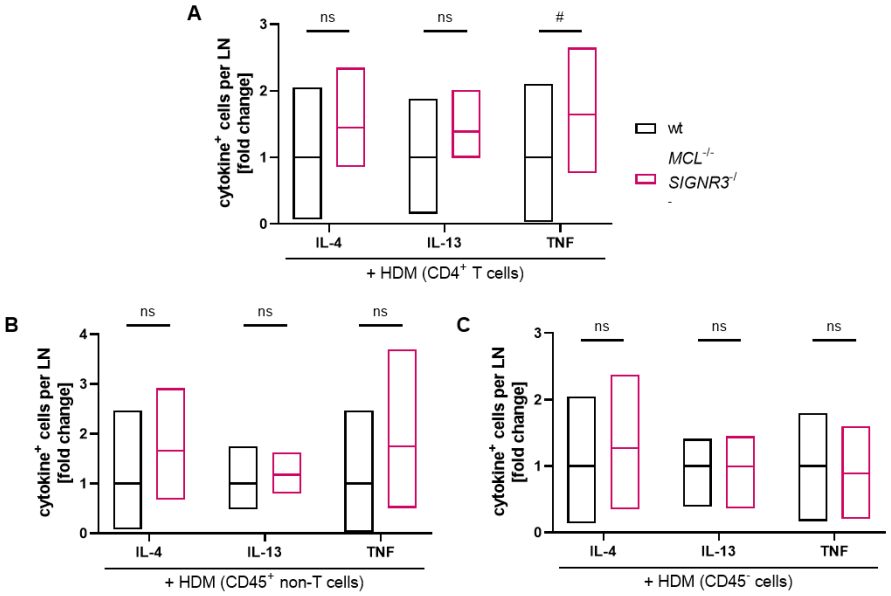

Figure 7.19: Analysis of numbers of cytokine-producing cells within mediastinal LNs of wt and *MCL*$^{-/-}$ *SIGNR3*$^{-/-}$ mice upon allergic airway inflammation. Allergic airway inflammation was introduced by HDM extract in wt and *MCL*$^{-/-}$ *SIGNR3*$^{-/-}$ mice and mediastinal LNs were analyzed by flow cytometry. Total cell counts per LN were determined for numbers of IL-4-, IL-13- and TNF-producing (A) CD4$^+$ T cells, (B) CD45$^+$ non-T cells and (C) CD45$^-$ cells (N = 8). Fold change was calculated setting the mean of cytokine$^+$ wt cells of each data set to 1. *** $p < 0.001$, ** $p < 0.01$, * $p < 0.05$, # $p \leq 0.10$, ns $p > 0.10$.

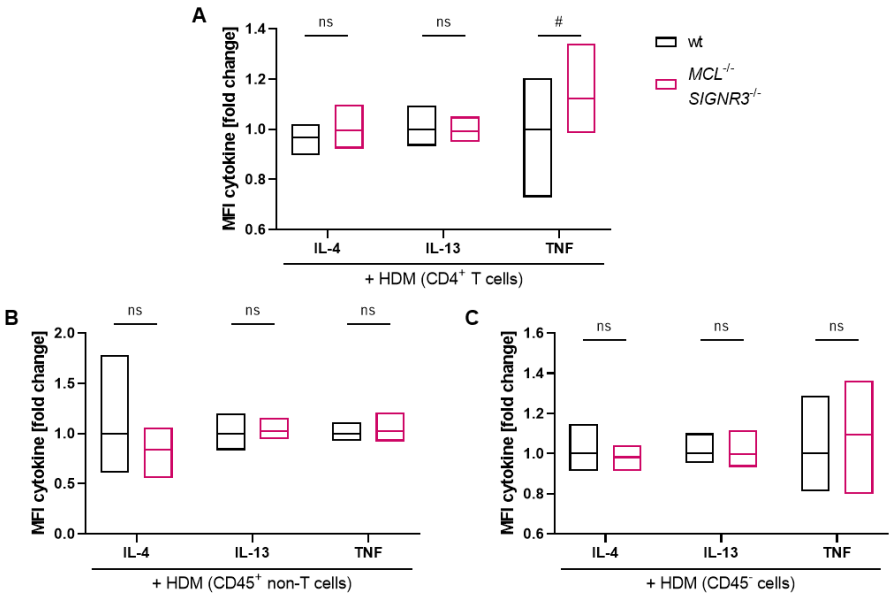

Figure 7.20: Analysis of the cytokine production per cell within mediastinal LNs of wt and *MCL*$^{-/-}$ *SIGNR3*$^{-/-}$ mice upon allergic airway inflammation. Allergic airway inflammation was introduced by HDM extract in wt and *MCL*$^{-/-}$ *SIGNR3*$^{-/-}$ mice and mediastinal LNs were analyzed by flow cytometry. Cytokine production per cell was analyzed as MFI of IL-4, IL-13 and TNF per (A) CD4$^+$ T cell, (B) CD45$^+$ non-T cell and (C) CD45$^-$ cell (N = 7/8). Fold change was calculated setting the mean of cytokine production by wt cells of each data set to 1. *** $p < 0.001$, ** $p < 0.01$, * $p < 0.05$, # $p \leq 0.10$, ns $p > 0.10$.

Declaration of Honor

I hereby declare that I prepared this thesis without impermissible help of third parties and that none other than the indicated tools have been used; all sources of information are clearly marked, including my own publications.

In particular I have not consciously:

- Fabricated data or rejected undesired results
- Misused statistical methods with the aim of drawing other conclusions than those warranted by the available data
- Plagiarized external data or publications
- Presented the results of other researchers in a distorted way

I am aware that violations of copyright may lead to injunction and damage claims of the author and also to prosecution by the law enforcement authorities.
I hereby agree that the thesis may be reviewed for plagiarism by mean of electronic data processing.
This work has not yet been submitted as a doctoral thesis in the same or a similar form in Germany or in any other country. It has not yet been published as a whole.

Magdeburg, 14.09.2023, Johanna Kotrba